TECHNICAL MEMORANDUM 2157

SAFETY ENGINEERING AND PROTECTIVE TECHNOLOGY IN SUPPORT OF ARMY MODERNIZATION PROGRAMS--PICATINNY ARSENAL PAPERS PRESENTED AT THE 16TH ANNUAL EXPLOSIVE SAFETY SEMINAR

FACILITIES AND PROTECTIVE TECHNOLOGY DIVISION
MANUFACTURING TECHNOLOGY DIRECTORATE

AUGUST 1975

PICATINNY ARSENAL
DOVER, NEW JERSEY

The findings in this report are not to be construed as an official Department of the Army Position.

DISPOSITION

Destroy this report when no longer needed. Do not return it to the originator.

UNCLASSIFIED

SECURITY CLASSIFICATION OF THIS PAGE (When Data Entered)

REPORT DOCUMENTATION PAGE		READ INSTRUCTIONS BEFORE COMPLETING FORM
1. REPORT NUMBER Technical Memorandum 2157	2. GOVT ACCESSION NO.	3. RECIPIENT'S CATALOG NUMBER
4. TITLE (and Subtitle) SAFETY ENGINEERING AND PROTECTIVE TECHNOLOGY IN SUPPORT OF ARMY MODERNIZATION PROGRAMS--PICATINNY ARSENAL PAPERS PRESENTED AT THE 16TH ANNUAL EXPLOSIVE SAFETY SEMINAR		5. TYPE OF REPORT & PERIOD COVERED Special Publication 6. PERFORMING ORG. REPORT NUMBER
7. AUTHOR(s) Facilities and Protective Technology Division Manufacturing Technology Directorate		8. CONTRACT OR GRANT NUMBER(s) AMCMS 4932.05.4201/4114
9. PERFORMING ORGANIZATION NAME AND ADDRESS Commander, Picatinny Arsenal ATTN: SARPA-MT-F, Dover, N.J. 07801		10. PROGRAM ELEMENT, PROJECT, TASK AREA & WORK UNIT NUMBERS 54201/54114
11. CONTROLLING OFFICE NAME AND ADDRESS Commander, US Army Armament Command ATTN: AMSAR-PP, Rock Island, IL 61201		12. REPORT DATE AUGUST 1975 13. NUMBER OF PAGES 276
14. MONITORING AGENCY NAME & ADDRESS(if different from Controlling Office) Project Manager for Production Base Modernization and Expansion, ATTN: AMCPM-PBM-L, Dover, N.J. 07801		15. SECURITY CLASS. (of this report) UNCLASSIFIED 15a. DECLASSIFICATION/DOWNGRADING SCHEDULE

16. DISTRIBUTION STATEMENT (of this Report)

Approved for Public Release; Distribution Unlimited

17. DISTRIBUTION STATEMENT (of the abstract entered in Block 20, if different from Report)

18. SUPPLEMENTARY NOTES

19. KEY WORDS (Continue on reverse side if necessary and identify by block number)

Safety Engineering concepts
H.E. Explosions
Secondary fragment impact
TNT equivalency
Primary fragment characteristics
Blast environment
Explosion propagation
Hazardous waste disposal
Fluidized bed incineration

20. ABSTRACT (Continue on reverse side if necessary and identify by block number)

Comprehensive programs of technology development in the safety engineering and pollution abatement fields are being carried out by the US Army. The purpose is to provide support to its munitions production base modernization and expansion program. This report contains nine papers concerning eight selected safety engineering technology development efforts and one on waste explosive and propellant disposal by incineration techniques that provide minimal air and water pollution. These papers were presented at the 16th DOD Explosive Safety Seminar (September 1974).

DD FORM 1 JAN 73 1473 EDITION OF 1 NOV 65 IS OBSOLETE

UNCLASSIFIED

SECURITY CLASSIFICATION OF THIS PAGE (When Data Entered)

The citation in this report of the names of commercial firms or commercially available products or services does not constitute official endorsement or approval of such commercial firms, products, or services by the US Government.

TABLE OF CONTENTS

SUMMARY

The Manufacturing Technology Directorate of Picatinny Arsenal is carrying out a broad-based, comprehensive program of safety engineering and protective technology under the sponsorship of the U. S. Army Armament Command. The purpose for this is to provide technology development support to the design of new munitions manufacturing and load, assemble pack-out facilities. Construction of these modernized Army facilities is under the cognizance of the Army Materiel Command Project Manager for Production Base Modernization and Expansion.

This report is a compilation of Picatinny sponsored papers presented at the DOD 16th Annual Explosives Safety Board Seminar. It is by no means a complete review of the total technology development program. However, the topics covered here were selected as advanced studies of specific interest to the Safety Echelon scientific community. They vary broadly in scope from the more basic work in explosive output, sensitivity and explosion propagation investigations to discussions of the use of pre-engineered buildings and procedures or data for the design of steel structures or to predict the blast environment for vented laced reinforced concrete cubicles. Finally, two papers oriented to final design applications are presented. One focuses attention on a typical major facility project emphasizing safety features embodying recently developed concepts; and the other describes development of incineration systems that are acceptable from a pollution standpoint for the disposal of waste explosives and propellants.

The work was performed both in-house government and by contract to industry. Authors are from Picatinny Arsenal, Ammann and Whitney Consulting Engineers, Research Institute of Illinois Institute of Technology, Civil Engineering Laboratory of the Naval Construction Battalion Center, and Arthur D. Little, Inc.

APPLICATION OF LATEST SAFETY ENGINEERING CONCEPTS TO MUNITION PLANT MODERNIZATION

Irving Forsten

ABSTRACT

A brief review of the magnitude of the Army Plant Modernization Program planned through 1992 is presented. Attention is focused on a typical major facilitization project at Lone Star Army Ammunition Plant entailing modernization of the 105 mm load, assemble and pack line. Emphasis is placed on safety features embodying recently developed concepts. The paper discusses and contains some examples of wall design for close-in blast effects, optimum quantity distance building layouts, safe separation distances of explosive items, buildings designed for far-out blast effects, explosive waste collection, building-access designs to avoid direct line of sight of flying projectiles, and protection afforded by low cost innovations such as earth mounded structures.

Picatinny Arsenal
Dover, New Jersey

INTRODUCTION

The U. S. Army has underway a multi-billion dollar munitions plant modernization program destined to continue beyond the next decade. Although cost effectiveness through automation and advanced process technology are major considerations in the program, the area of personnel safety as affected by an explosive incident or through environmental pollution is receiving primary attention.

The Army's program deals with both explosive and propellant manufacturing facilities as well as load assemble and pack plants. There are 17 plants serving Picatinny Arsenal mission item needs.

In consonance with the subject of this paper, a specific example of a major facility to be built will be presented with attention drawn to major safety considerations using latest technology.

DISCUSSION

GENERAL

The facility to be discussed is the advanced load, assemble and pack facility dealing with the 105 mm HE, M1 projectile to be produced at Lone Star Army Ammunition Plant (LSAAP), Texarkana, Texas. General production characteristics of the round are described by Figure 1. The planned modernized 105 mm projectile LAP facility, Area E at LSAAP is shown in Figure 2. The identity of the building numbers is shown on Figure 3.

PROPAGATION PREVENTION

The one million rounds per month production rate of the Lone Star 105 mm projectile melt/pour facility requires the use of minimum spacing between explosive items to achieve full production. The following is a brief discussion of safe spacing, shielding and/or other means utilized to prevent propagation of an explosion.

Safe Spacing between Boxes and Buckets of Flake Explosive

In the case of bulk explosives, recent separation tests have indicated that when cardboard boxes and/or plastic buckets (with covers) containing 60 pounds of Composition "B" are separated by 12 feet, propagation of an explosion between adjacent items is negated. However, spread

of fire is not prevented. Movement of box explosives in the Lone Star facility is required between the Bulk Explosive Distribution Building (Bldg. E-161) and the Box Opening Building (Bldg. E-174) (Fig 4). In this latter building (Fig 5), the flake explosive is removed from the boxes and placed in 60-pound plastic buckets for movement to the Automatic Explosive Inspection Building (E-125). Passage of the boxes through the ramp connecting Buildings E-161 and E-174 is by means of a belt type conveyor, whereas the plastic buckets are transported on two overhead, power-free conveyors from the Box Opening Building to the Inspection Building. As mentioned, each box on the belt conveyor is separated by 12 feet from a box in front of it and to the rear of it. The two conveyors carrying the plastic buckets are separated by 12 feet. The dual conveyors permit spacing between adjoining buckets on any one conveyor to be greater than 12 feet. This increased spacing can be reduced to 12 feet in the event future expansion (increased production rate) of the facility warrants it. Both ramps connecting the three buildings are furnished with fire retardant systems (water curtains) to prevent the spread of fire in the event of an explosion in one of the ramps or the buildings.

Bucket conveyors containing 60 pounds of explosive are used in other parts of the facility, namely, (1) where the explosive risers are transported between the Funnel Pulling Building and the Riser Melter Building and (2) where the riser flake is transported from the Riser Melter Building to the Inspection Building; however, the spacing between adjoining buckets is larger than the minimum 12-foot in the ramp between the buildings; and therefore, protection against the spread of fire is not required.

Screen Flake on Belt Conveyors

Uncontaminated flake explosive, which has already been inspected for foreign material, is transferred to one of the two melt buildings using a belt conveyor. Here, the flake is spread on the belt approximately one inch thick. By limiting the depth of the explosive to one inch, propagation of an explosion along the conveyor is prevented. Tests demonstrating this retardation of propagation were performed as a part of the Navy's Modernization Program and are reported in the minutes of the 13th Safety Seminar.

Shielding between Explosives

After the empty projectiles are filled, they are transported to the Projectile Cooling Buildings from the Melt/Pour Facility by means of a high speed power-free conveyance system carrying 16 projectiles on each

carrier. Initially, it was planned to separate these carriers by 109 inches which is the separation distance specified for pallets of 32 Composition "B" loaded 105 mm projectiles by AMCR 385-100. However, a series of tests performed by Picatinny Arsenal has indicated that at separation distances as large as 170 inches, propagation of explosion will occur between pallets of 16-105 mm projectiles. Therefore, in order to determine another means to prevent propagation, tests will be made to establish whether structural steel or aluminum shields will be effective substitutes for safe spacing.

If the shields are found effective in negating the propagation of an explosion, then they will be made a part of the conveyance system. Rather than mounting the shields on the carriers, they will be attached to turntables which are used to change direction of the carrier flow.

Figure 6 illustrates the method of utilizing shielding. Here, two aluminum or structural steel plate shields are mounted on a turntable with the stationary shields positioned between the turntable and the protective structure. As a carrier reaches the turntable, it is in an unprotected position. Once the turntable rotates 90 degrees, the shields attached to the table will protect the carrier from the effects of an explosion in an adjoining unprotected carrier and, thereby, eliminate the propagation from one carrier to another all the way down the line. In the illustrative example, after the turntable is in the closed position, the protected carrier can move into the building through the stationary shields and the concrete mazes. This operation is continuously performed with alternately shielded turntables in the open and closed position.

Protective Barriers

If the above shielding is not effective, then an alternate method will be considered in the facility design (Fig 7). The spacing between explosive items in a ramp connecting two buildings need not be limited if, (a) both buildings are protected from an explosion within the ramp with separating protective barriers, and (b) adjoining buildings are separated from the ramp by intra-line distances based upon the larger of the explosive quantities in the ramp or the building.

For the Lone Star AAP, the above principles can be incorporated without significantly modifying the facility.

Maze Concept

For a protective barrier to be effective, it must be provided with a maze or other means to prevent a line of sight between the ramp and the interior of the building. There are two types of mazes, namely, (1) line of sight, and (2) safe zone mazes. Line of sight type of maze is used when the building is located at the end of a ramp where the items within the ramp are spaced at safe separation distances and protection is required primarily from an explosion in an adjoining building. Safe zone maze is used when the ramp having safe separation between ramp items passes in front of the protective barrier or when the building is at the end of the ramp and the ramp items are spaced at less than minimum safe separations. In the latter case, a turntable shield may be used in combination with a line of sight maze to achieve the same protection afforded by a safe zone maze.

For the Lone Star facility, the use of line of sight type of mazes was originally contemplated. However, when safe separation distances could not be established for palletized projectiles, then all mazes were revised to conform to the safe zone arrangement. Here, when an item passes through the maze, it must enter a "safe zone" where it will be shielded from items located at the exterior and interior of the building.

Figure 8 illustrates the passage of explosive items through a "safe zone" maze. Here, in stage No. 1, lot numbers 1, 2 and 3 are located in the interior of the building, within the safe zone and exterior of the building, respectively. In stage No. 2, lot No. 1 will move further into the building with lot No. 2 leaving the safe zone and entering the building. While the first two lots move into the building, the third lot will begin to enter the maze. However, the speeds of the second and the third lots will be adjusted as such to insure that the line of sight between the two lots will not occur. In the third or the final stage, lot No. 2 enters the building, the third lot passes through the safe zone and the first lot enters the maze to repeat the operation.

FACILITY PROTECTION

Overall safety for the facility is provided by various means, such as (1) safe separations between buildings, (2) use of protective construction using barricade walls, strengthened frangible construction and igloo construction, (3) separation of hazardous operations from less hazardous operations, and (4) the use of remote operating procedures for hazardous operations. In general, full protection has been provided for personnel and equipment in buildings with conveyors and ramps, which are assumed to be expendable in the event of an explosion.

Building Separation

The buildings of the bulk explosive receiving and processing portion of the facility are separated as shown in Figure 9. Here, both the Box Opening and the Automatic Inspection Buildings are separated from the Bulk Explosive Receiving Building based on unbarricaded distances corresponding to the explosives in the two former buildings. Also, protective barricades are placed at these two structures. The separations of these buildings differ from the criteria of AMCR 385-100 which require that all separations be based upon the largest quantity of explosive in either building. In this particular case, even though the explosive quantity in the Receiving Building is much larger than that of the other two buildings, the potential hazard is much less.

In order to reduce the length of conveyors and, therefore, the overall operating costs of the facility, a minimum (barricaded intraline) distance is used to separate the Melter Buildings from the adjoining Inspection and Cooling Buildings. The latter two buildings, as well as the Melter Buildings, are remotely operated; and minimizing the building separations does not create a hazard for personnel.

Other hazardous operations, such as cooling, funnel pulling, and facing operations, are performed remotely in earth covered steel arch igloos. Separations between igloo structures conform to earth covered steel arch separation distances of Safety Manual AMCR 385-100.

Protective Structures

As mentioned, where separation distances are barricaded intraline distances, protective barriers are provided to protect the acceptor structures from low flying debris and relatively high reflected pressures associated with the blast pressure output. Because these barriers are required to remain intact in the event the structures containing barriers become donor structures, the protective walls are constructed utilizing laced reinforced concrete as detailed in DA Tech Manual TM5-1300. The process equipment within some of the buildings has laced walls and is relatively tall. In order to limit the thicknesses of the protective barriers, several of the taller buildings, including the Automatic Inspection, Melt/Pour and Riser Melt Buildings, are positioned partly below the ground (Fig 9). In these cases, only the above ground portions of the barriers require laced reinforcement.

At lower pressures, such as those corresponding to unbarricaded intraline distances, protection for personnel and equipment is furnished with use of "Strengthened Frangible Construction." The structural steel buildings provide the necessary strength to afford full protection for personnel from the effects of blast pressures while debris protection is afforded by the distances associated with this type of construction. For distances less than unbarricaded intraline distance, protective barriers, as described above, are used for debris protection.

To illustrate this type of protective structure, let us consider the X-ray Building (Bldg. E-138). As shown in Figure 10, only the west wall of the building is barricaded from an explosion in Building E-168 (X-ray Hold). Here the shortest distance between Building E-138 and E-168 which could be maintained without violating unbarricaded intraline distance based upon the 15,000 pounds of explosive in Building E-132 is intermediate of unbarricaded and barricaded intraline distances based upon the 8,000 pounds of explosive in Building E-168.

To provide the necessary protection, the wall of Building E-138 facing Building E-168 is constructed of laced reinforced concrete; whereas, all other portions of the building are constructed of structural steel (Fig 11). The laced concrete wall was designed to resist the effects of 4,000 pounds of explosive which was distributed at various locations between the X-ray cells and walls. For the charge distribution, as shown in Figure 11, a 5-foot wall thickness is required to sustain structural response for incipient failure. It may be noted that if this same wall were subjected to a single explosive, the capacity of the wall would be such as to resist 9,300 pounds of TNT or a factor 2.3 times the explosive weight of the distributed charge.

Minimized operational space requirements necessitate the use of earth covered steel arch magazine larger than the standard type magazine. Here, the required interior height and the floor width of the structure are 20 feet and 30 feet, respectively. To accommodate these space requirements, a corrugated steel semi-circular arch having a radius of 16 feet is used. The bottom of each end of the arch (spring line) is mounted on a 2-foot thick and 4-foot high concrete side wall. Both end walls of each arch are constructed of laced reinforced concrete. Use of this igloo construction was authorized by cognizant safety officers with the stipulation that the steel plate for the arch will be 3/8-inch thick and that the arch will have a full 180-degree cross-section (Fig 12). The end walls of the arch are designed to resist the effects of an explosion within a ramp exterior of the walls. On the other hand, in the event of an explosion within the igloo, the structure will fail, relieving the explosive effects to the atmosphere.

Separation and Remote Operation of Hazardous Processes

The separation of hazardous operations from other operations, and remote operation of these hazardous processes are interrelated. For Hazard Category II operations, prevention of a propagation is required; whereas complete protection for both the personnel and the equipment must be afforded for Hazard Category III operations. In general, all Hazard Category II and III operations involving large quantities of explosives (greater than approximately 30 pounds) should be located in separated structures. This has been achieved in the Lone Star facility by utilizing igloos and other types of protective construction and by performing high hazard operations (Category II and III) remotely. As may be expected, remote operating of processes will require a surveillance system. This is achieved with the use of complete telemetering and remote visual monitoring (television) systems. All monitoring equipment is located in a centralized control facility, the construction of which provides full protection for operating personnel.

EXPLOSIVE WASTE COLLECTION SYSTEM

The explosive waste collection system used in the proposed 105 mm projectile melt/load facility at LSAAP essentially mixes the waste explosive in water and then transports the mixture to a treatment building where the explosive is removed from the water prior to being sent to an incinerator.

The waste is either passed directly into process scrubbers within the process building where it is generated when the quantity of waste is relatively small. For larger explosive quantities, the waste is transported by pneumatic lines to a wet collector building situated adjacent to the process building (Fig 13). Within the collector building, the waste also enters an air scrubber. When the explosive enters these scrubbers, it passes through a water spray and forms an explosive/water mixture.

The waste in water suspension passes out of the bottom of the scrubbers where the mixture is pumped to a settling-basin reservoir where the explosive waste is initially concentrated. Each building containing an explosive dust generating operation is equipped with both process or equipment air scrubbers and environmental air scrubbers. The latter serve to collect that explosive dust, which leaks past the process air scrubber, and is subsequently distributed thoughout the building. The environmental air scrubbers are sized to reduce the explosive contamination of the air discharged from the buildings to a safe level for personnel, as specified by

the design criteria. As for the process scrubbers, the explosive/water mixture collected in the environmental scrubbers is pumped to the settling basin reservoirs.

A settling basin reservoir (Fig 14) is provided for each building or group of buildings generating explosive waste. Each reservoir is designed to provide a minimum retention time of one hour for the contaminated "pink water" from the scrubbers. Solids carried in the water are collected in "sump pits" which are periodically emptied by pumping a water/solid mixture (approximately 5 to 10 percent solids) to the pink water treatment building storage reservoir where it is held prior to treatment in the treatment building. Clear water overflows a weir to a clear water chamber from which the scrubbers within the process buildings draw their water supply. This recirculation of water between the reservoir and the process building will minimize the amount of pink water that must be treated in the treatment buildings. Sufficient capacity is provided in the settling basins to accommodate the potable water used for washdown of the process buildings during non-production hours. This water is pumped by sump pumps from the building being washed to the treatment building where it is filtered and then transferred to the settling reservoir. This accumulated washdown water serves to "make-up" for a major portion of the evaporation that takes place in the air scrubbing equipment.

For each pneumatic line leading from the process building, two scrubbers are provided in the wet collector building; namely, primary and secondary collector scrubbers. The explosive dust first enters the primary collector where it passes through a water spray similar to the process and environmental scrubbers. Because of the large quantity of explosive waste handled by the wet collection system, a portion of the dust entering the primary collector may escape the water. The "non-captured" dust is exhausted to the secondary collector where the collection process is repeated. The air passing through the secondary collector is exhausted to the atmosphere. The explosive/water mixture from both collectors is pumped directly to the treatment building storage reservoir without passing through a local settling basin reservoir. Water supply for each wet collector building is furnished from the treatment building reservoir.

Piping for the pink water treatment system is divided into four units. Three of these units connect the local collection systems (wet collector buildings and settling reservoirs) to the three treatment buildings. The fourth unit interconnects the three treatment buildings to provide operational flexibility in the event one of the treatment buildings is non-functioning.

The three treatment plants are essentially identical. The water treatment process (Fig 15) is based on the system in use at the Iowa AAP. Contaminated water enters the process through a rotary filter within the building that continuously removes solids in suspension. Explosive waste removed by the filter is discharged into a collection bin where it is retained for disposal in a wetted condition. The maximum quantity of explosive waste accumulated is approximately 600 pounds before it is removed to the incinerator. The filtered water is directed to a storage reservoir immediately adjacent to the treatment building. This reservoir is designed in a manner similar to a local settling reservoir. Explosive waste collected in the reservoir is periodically pumped to the rotary filter for removal.

Water containing dissolved nitro-bodies and solid matter of minute size is drawn from the clear water chamber of the storage reservoir of each treatment building and directed to one of two sets of water purification equipment. The two sets of equipment are arranged in parallel with one another. This will permit dual operation at any one time. Each set of equipment has a treating capacity of 20 gallons per minute for a total capacity of 120 gallons in all three buildings. The treatment requirement is estimated at 90 gallons per minute. This arrangement will permit any one of the six sets of equipment to be inoperable without compromising the facility needs.

Each set of equipment consists of a pair of diatomaceous earth filters arranged in parallel, two "up-flow" carbon adsorption columns, a pre-coat tank and a body feed tank. The water with the nitro-bodies first passes through the diatomaceous earth filters. Prior to being placed into operation, a cleaned filter must be pre-coated with a mixture of diatomaceous earth fibers and water. A small amount of diatomaceous earth (mixed in water) contained in the "body feed" tank must be added to the main stream of the process flow ahead of the filters. The discharge from the earth filters, which essentially contains only dissolved TNT, is directed to the inlet of the first of the two adsorption columns. The second column, which is in series with the first column, may be considered as a "polishing" column. After leaving the polishing column, the clean water can either be discharged from the facility as overflow or returned to the collection system.

Before recharging the carbon columns, the carbon is removed through a drain and then is passed through the rotary filter. The columns are charged hydraulically from a carbon charging vessel. This vessel charges all four columns in any one building.

CONCLUDING REMARKS

The future Lone Star Army Ammunition Plant 105 mm projectile melt/pour modernized facility will encompass many new safety innovations which have stemmed from recent developments.

To achieve full production requirements within allocated land areas, minimum spacing between explosive items is a necessity. In the course of acquiring pre-design safety information, a safe spacing between 60 lb quantities of Comp B for boxes and buckets of 12 feet was established. By limiting the depth of explosive spread on a belt conveyor to one inch, propagation along the length of the conveyor is eliminated.

A problem area has been surfaced in which the AMCR 385-100 specification of 109 inches for 32-105 mm projectiles, loaded with Comp B, was inadequate when applied to a 16 projectile carrier configuration. Further tests with suitable shielding will be made to achieve separation without propagation at reduced distances.

Buildings containing explosive are separated based upon barricaded or unbarricaded interline distances as specified by the safety manual AMCR 385-100. The use of earth-covered igloos for cooling, funnel pulling, and facing operations affords cost saving approaches.

Technical Manual, Army designation TM5-1300, employing proven structural techniques, should be employed for such applications as protecting acceptor structures from low flying debris and high reflective pressures stemming from explosive blast effects. Where applicable, low cost, frangible construction should be employed at the lower pressure environments which would exist at unbarricaded interline distance.

Other safety considerations must include analysis and separation of hazardous processes and use of such aids as TV monitoring systems for remote operations. Collecting explosive waste should stress capturing of explosive or propellant waste particles through filtration and scrubbing systems which can later be recycled into the basic process or destroyed by specially designed incinerators. Explosive wastes in water solution can subjected
to regeneration.

MUNITION

- 105MM HE, M1 PROJECTILE

EXPLOSIVE

- COMPOSITION B

PRODUCTION RATE

- 1,000,000 SHELL / MONTH

SHIFT SCHEDULE

- 500 HOURS PER MONTH

EFFECTIVE TIME PER SHIFT

- 350 MINUTES

SHELL PER SHIFT

- PRESENT – 9524
- PROPOSED – 15,876

BULK EXPLOSIVE

- 175,000 LBS

MELT/POUR CAPACITY (PER UNIT)

- 9000 LBS/HR

Fig 1 General production characteristics

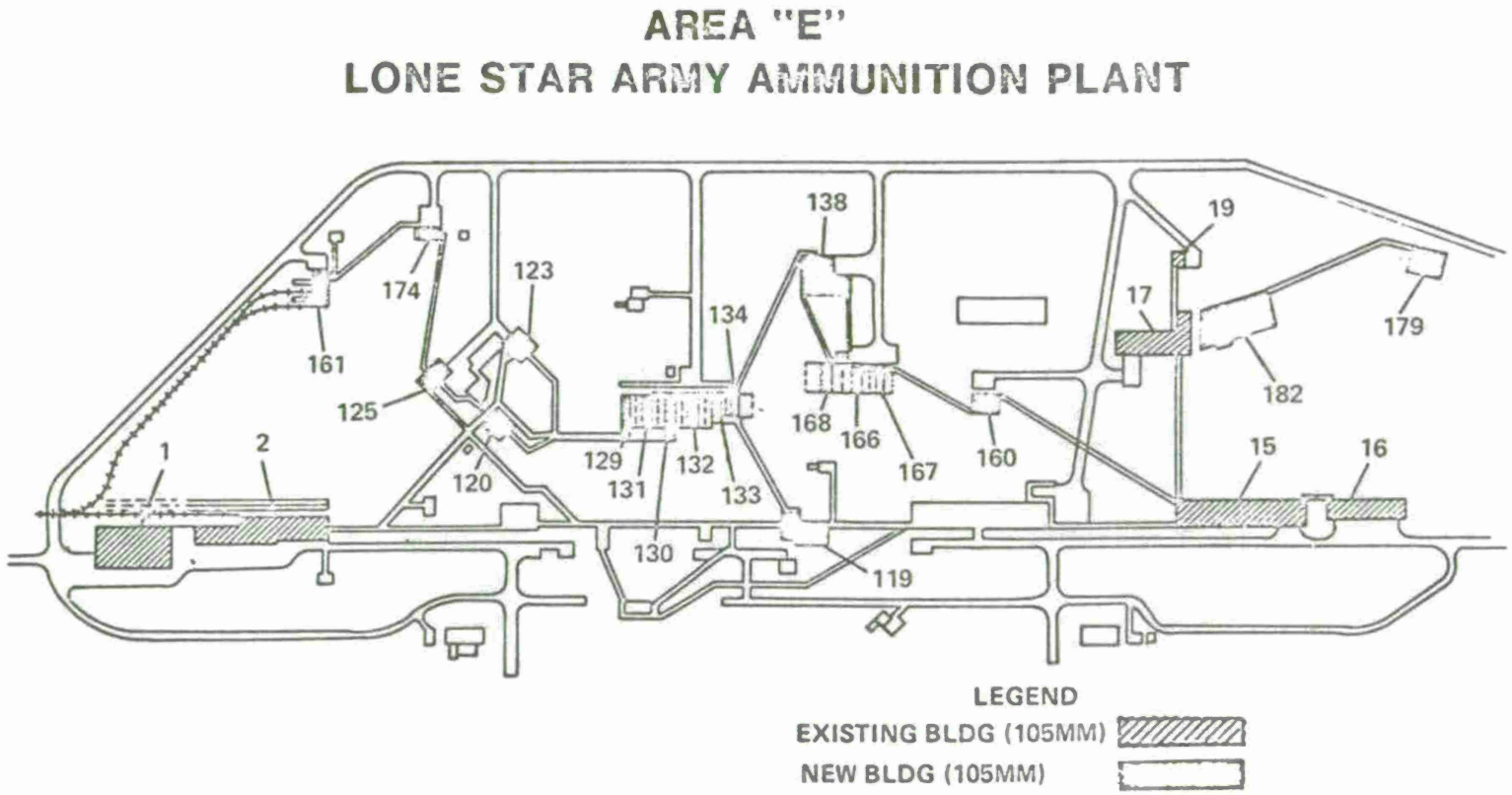

Fig 2 Modernized 105 mm projectile LAP facility

LONESTAR AAP - 105MM HE, M1 LAP LINE
PROJECT NO 5752626

BLDG NO	TITLE	FLOOR SPACE SQ FT
161	BULK EXPLOSIVE RECEIVING	6100
174	BOX OPENING	3200
125	AUTOMATIC EXPLOSIVE INSPECTION	5210
120	MELT POUR	4680
123	MELT POUR	4680
129	COOLING IGLOO	2700
130	COOLING IGLOO	2700
131	COOLING HOLD	2190
132	COOLING HOLD	2190
133	FUNNEL PULLING	1200
134	FUNNEL PULLING	1200

Fig 3 Major building nomenclature

LONESTAR AAP - 105MM HE, M1 LAP LINE
PROJECT NO 5752626

BLDG NO	TITLE	FLOOR SPACE SQ FT
138	PROCESS ASSEMBLY (X-RAY)	14676
168	PROCESS X-RAY HOLD	2190
166	FACING AND THREAD CLEANING	1800
167	FACING AND THREAD CLEANING	1800
160	LINER INSERTION	4800
15	ASSEMBLY AND PACKOUT	25400
119	PROCESS RISER MELT	11100
163	RISER FLAKE EXPLOSIVE DISTRIBUTION	1500
2	METAL PARTS PREPARATION (INERT WAREHOUSE)	20000

Fig 3 (cont'd)

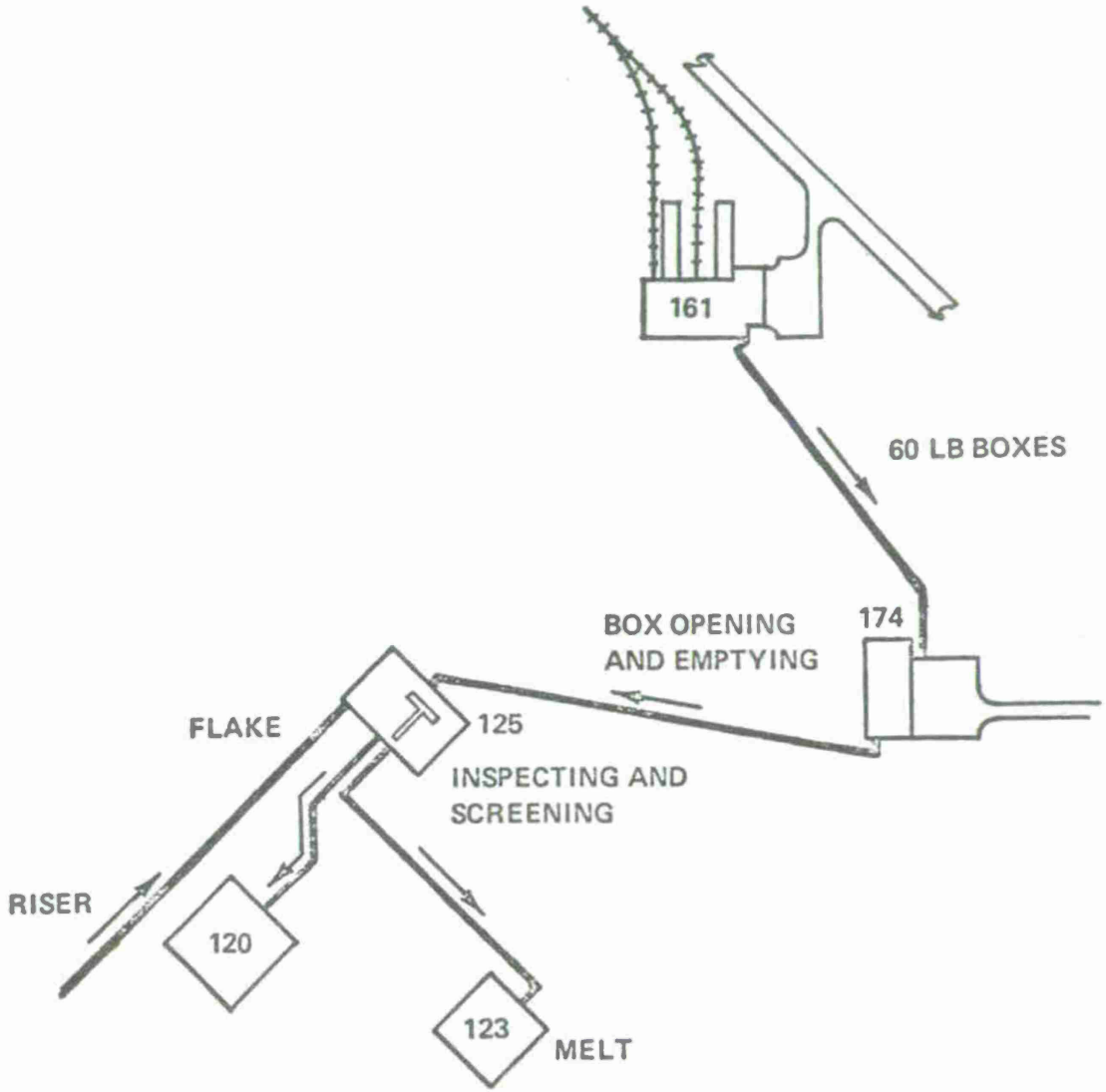

Fig 4 Explosive transfer and building layout

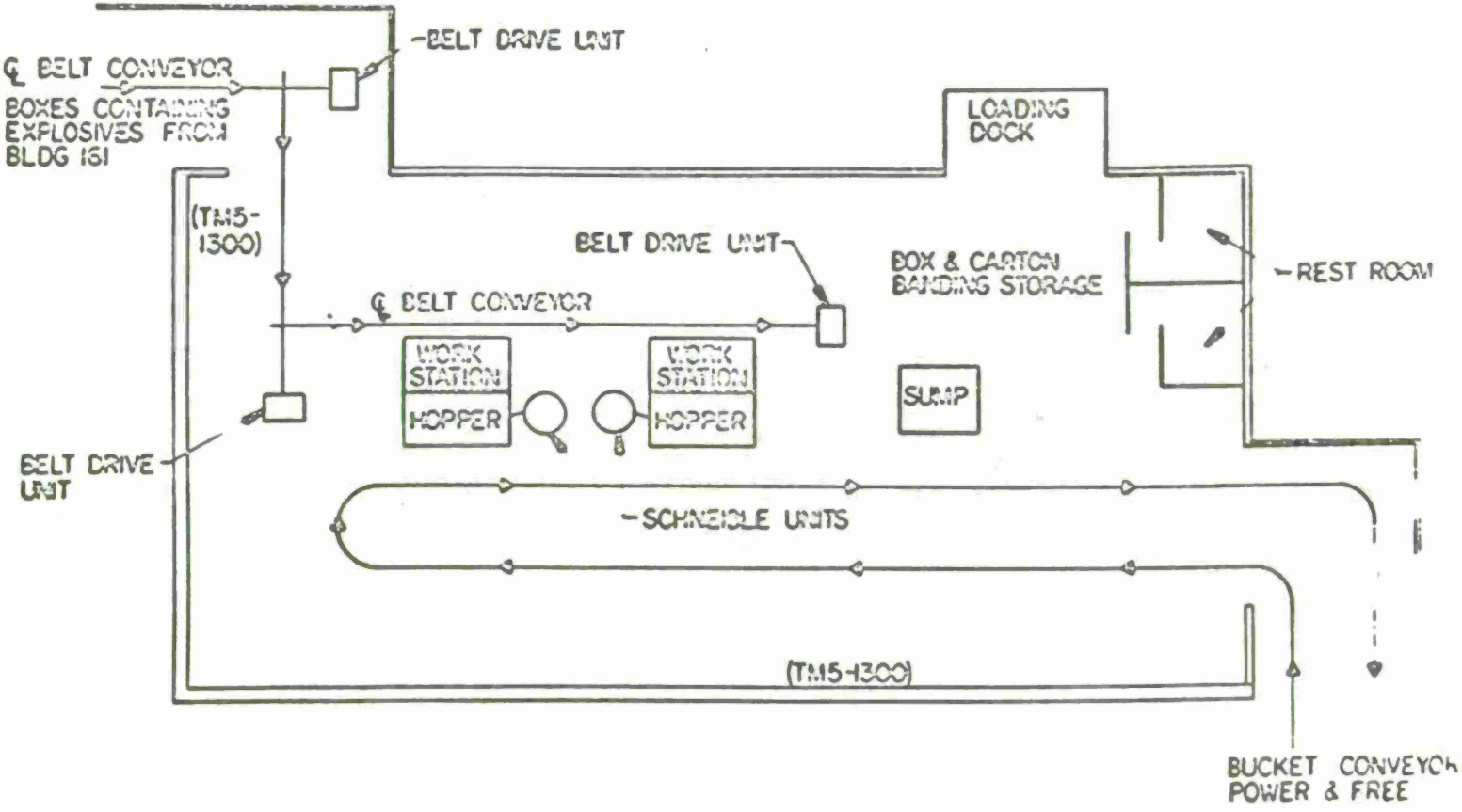

Fig 5 Box opening building E-174

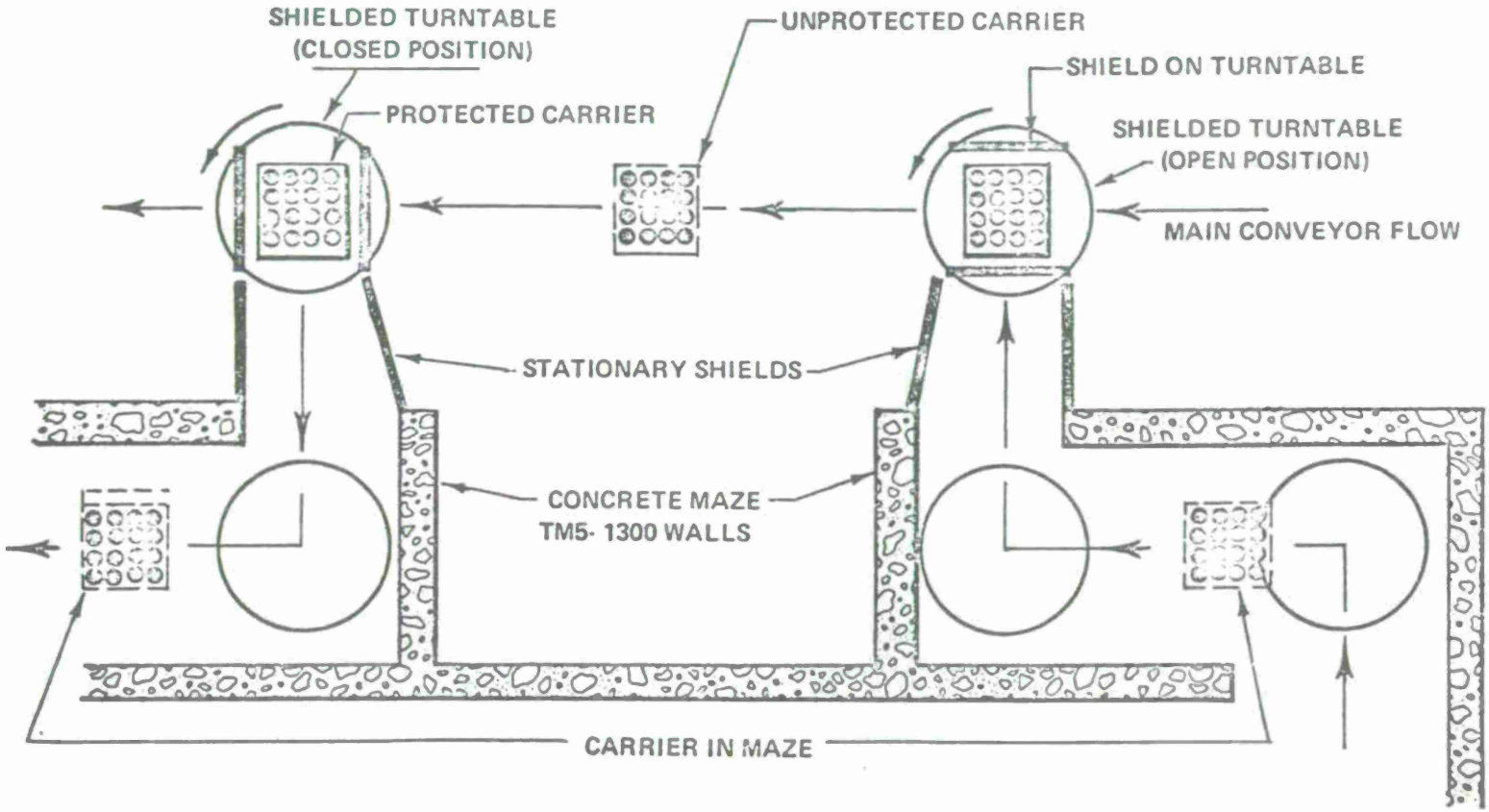

Fig 6 Pallet protection near buildings

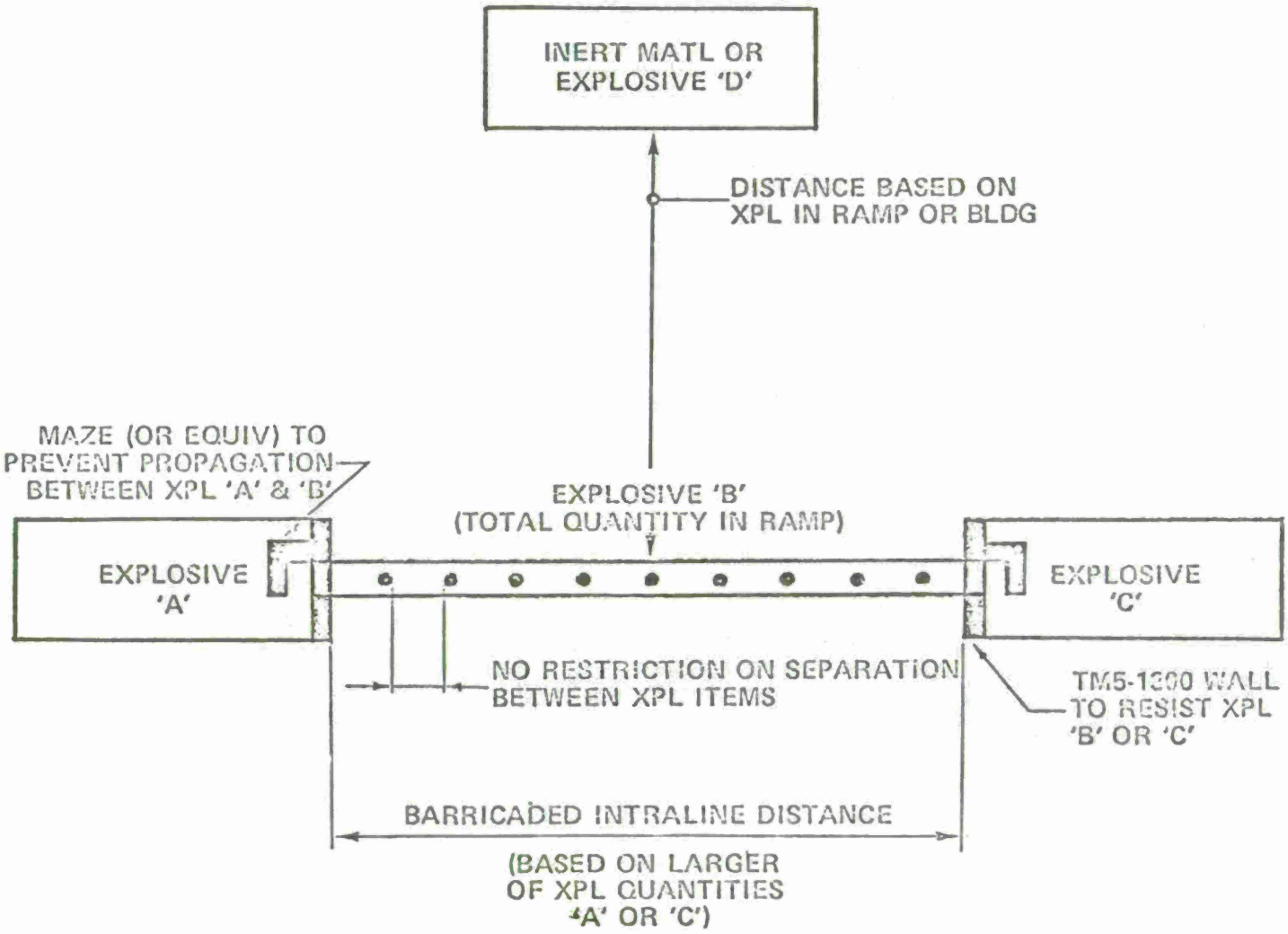

Fig 7 Transfer arrangement No. 1

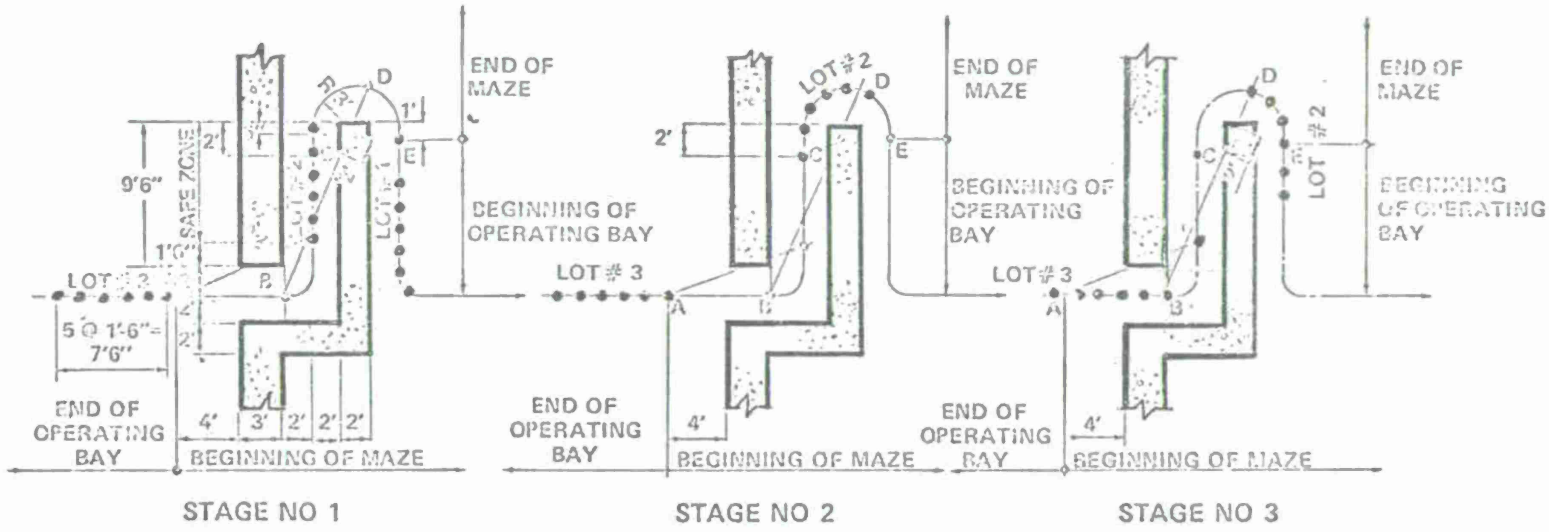

Fig 8 Inter-bay projectile transfer

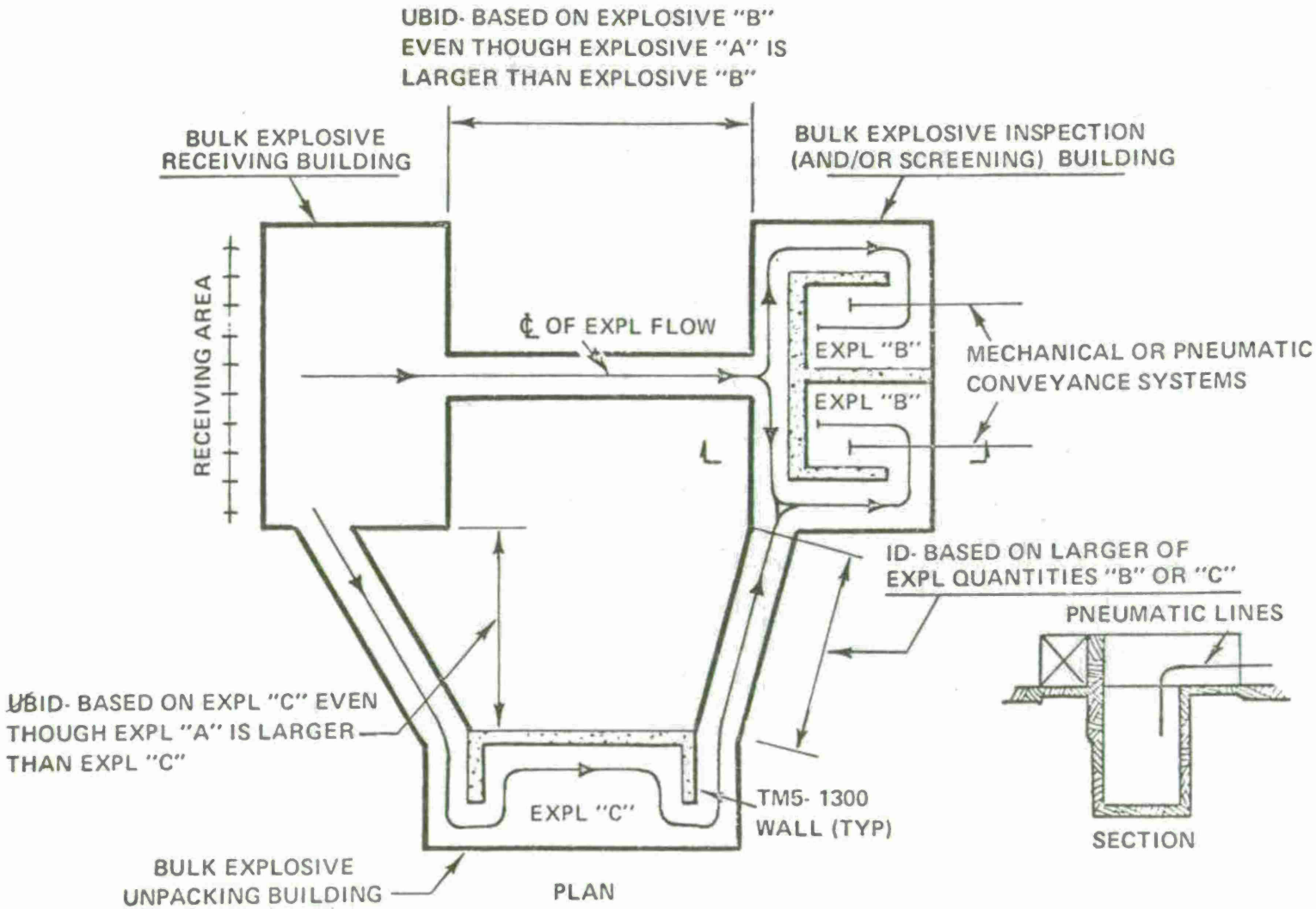

Fig 9 Bulk explosive receiving and processing

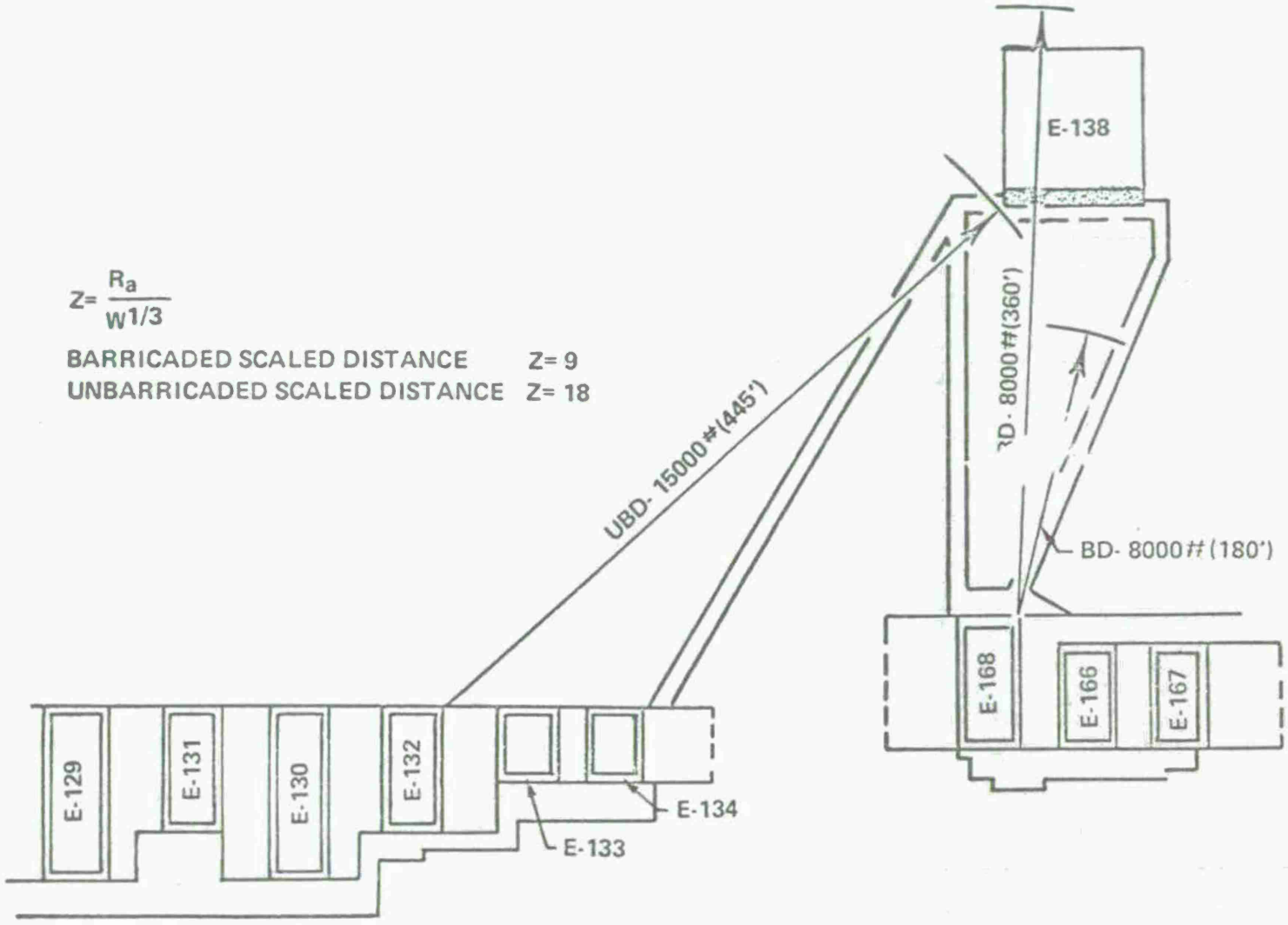

Fig 10 X-ray building quantity/distance spacing

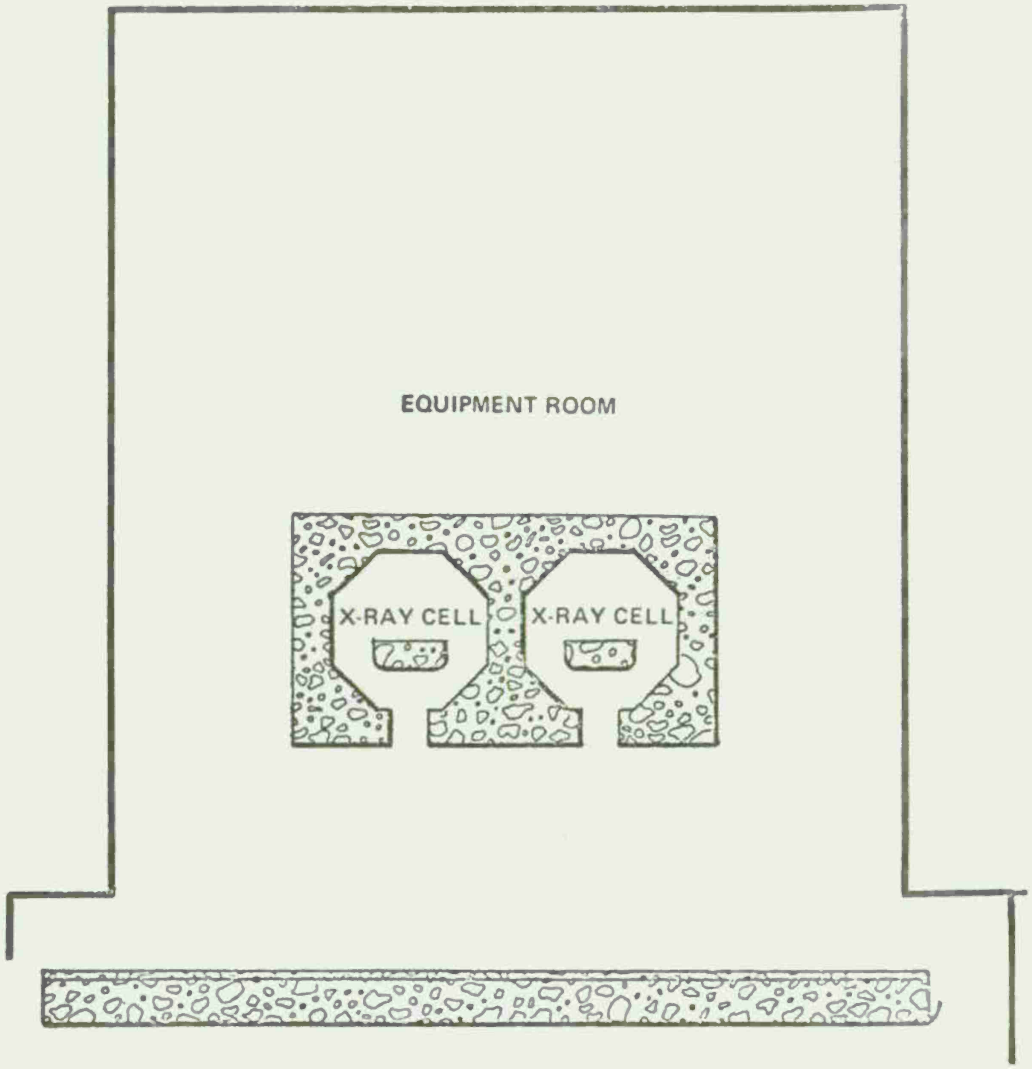

Fig 11 X-ray building floor plan

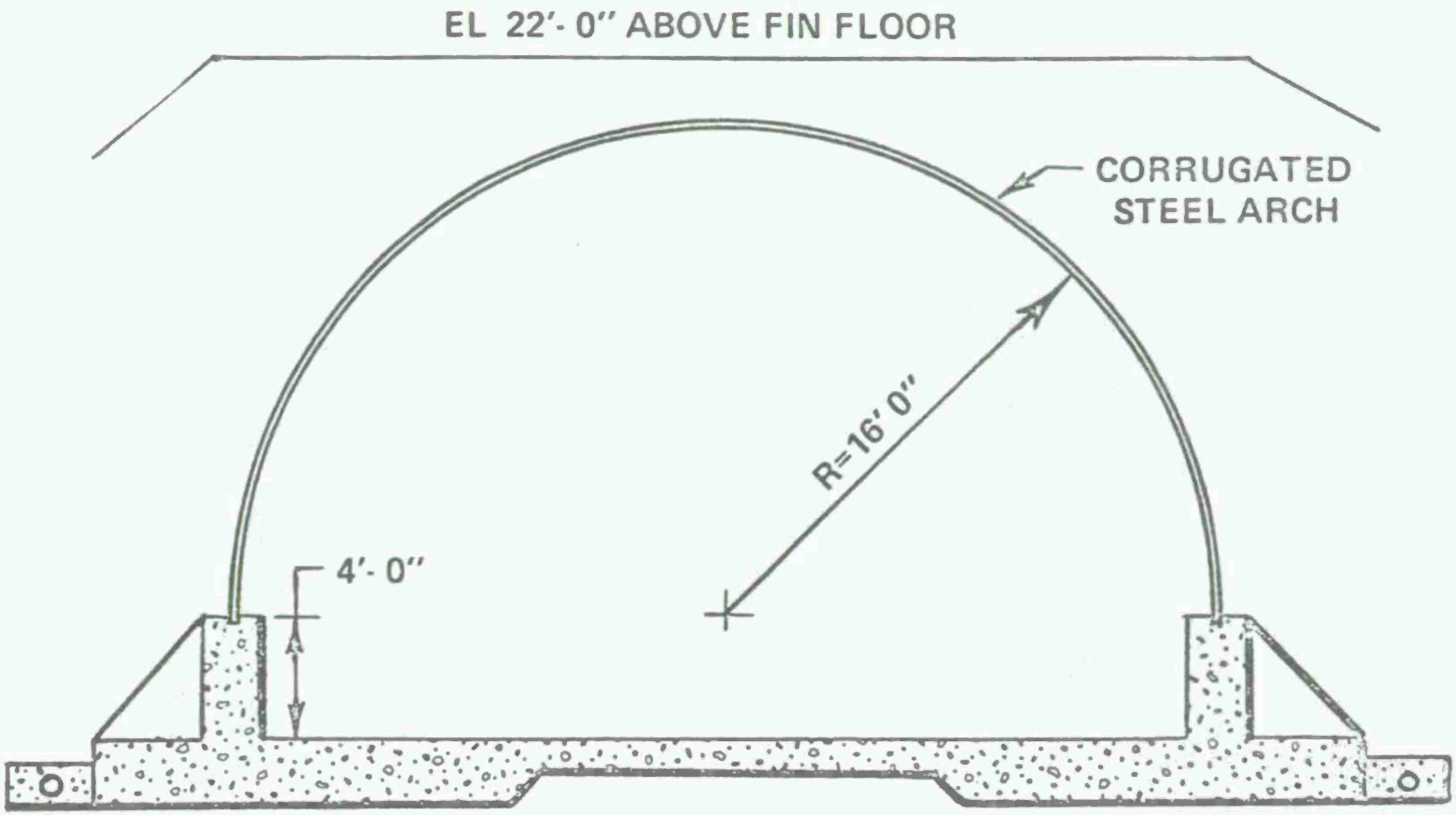

Fig 12 Steel arch igloo

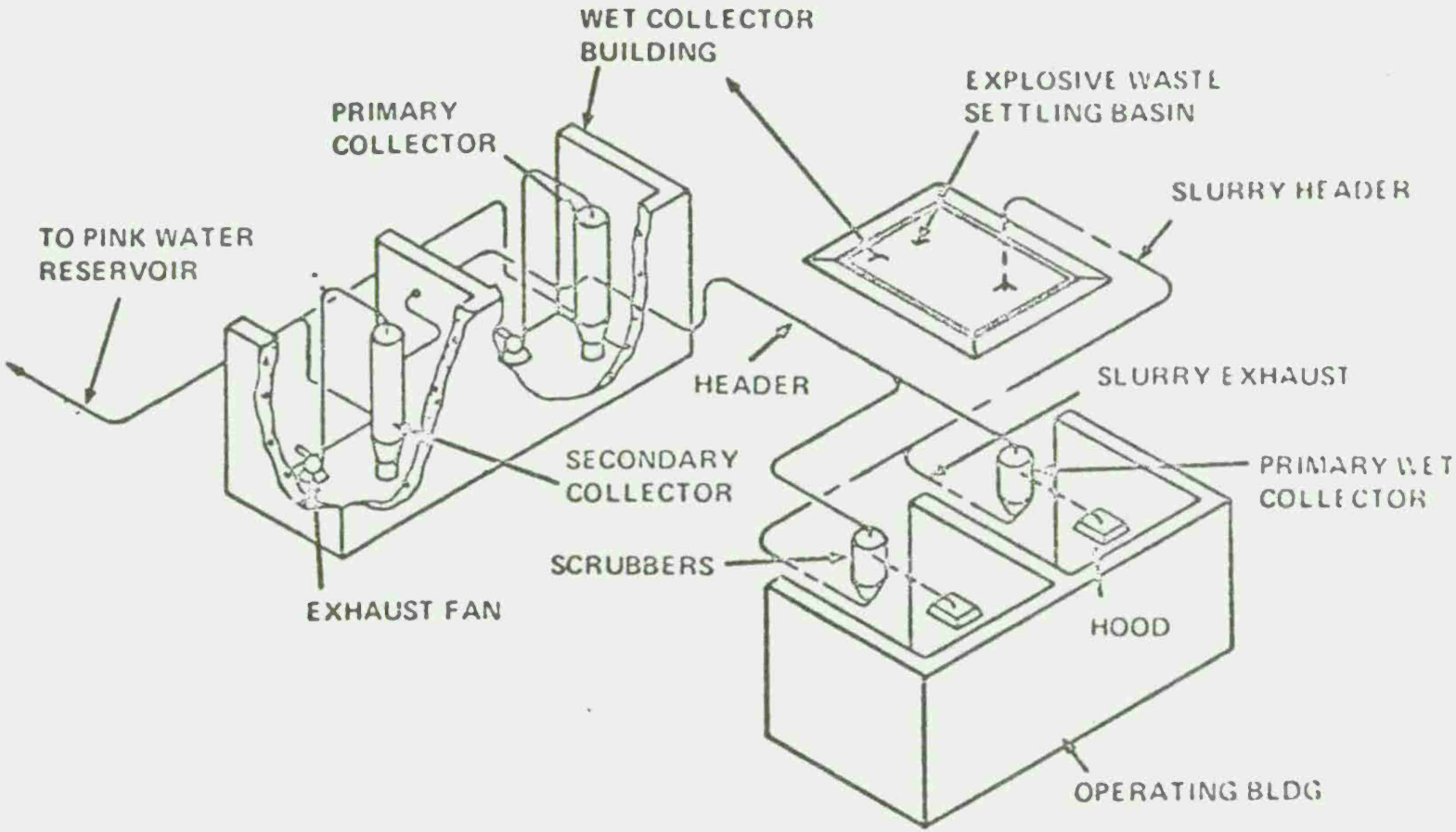

Fig 13 Schematic of typical explosive waste collection system

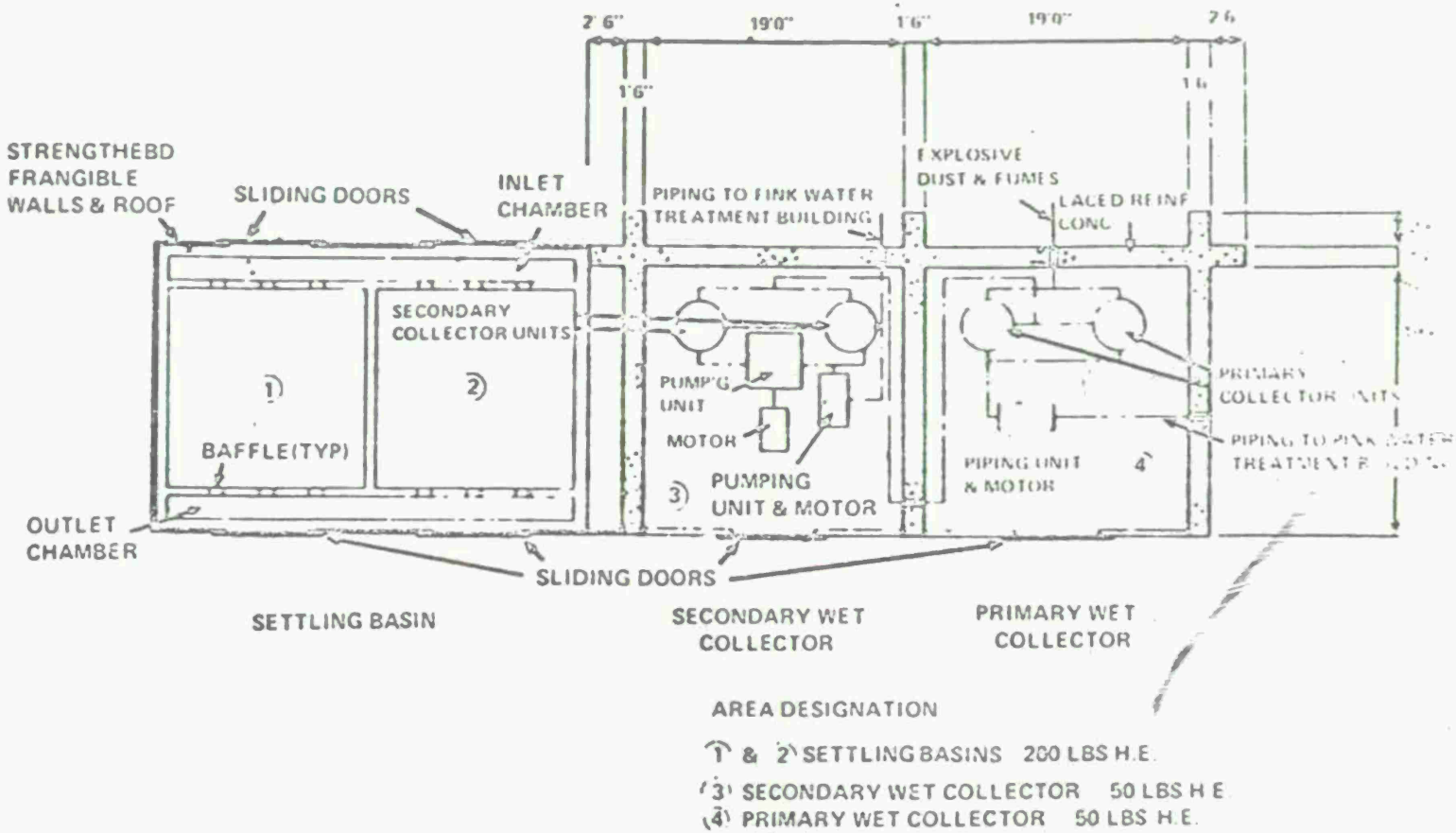

Fig 14 Settling basin and wet collector building

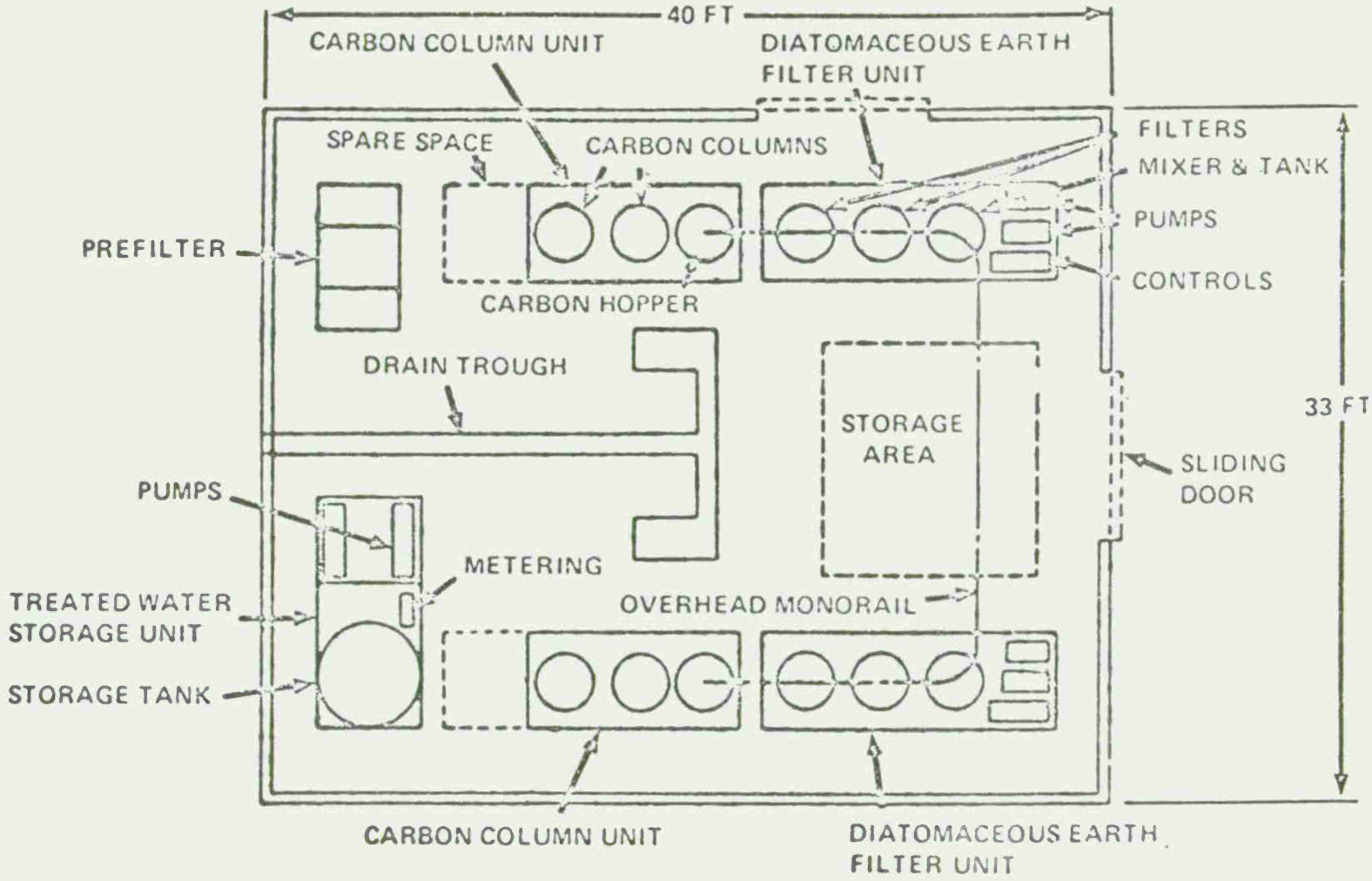

Fig 15 Pink water treatment and collection reservoir

STEEL STRUCTURES TO RESIST THE EFFECTS OF H. E. EXPLOSIONS

Paul Price, Picatinny Arsenal
Norval Dobbs, Ammann & Whitney

ABSTRACT

This paper summarizes the recent Picatinny Arsenal reports which delineate procedures for the design of steel structures to resist the effects of high explosive detonations. The data presented herein is similar to that for reinforced concrete structures in TM 5-1300

A discussion of the use of pre-engineered buildings, as well as procedures used in the design of "Strengthened Frangible Construction," is included. Also discussed are the use of structural steel for both close-in and far range blast effects, and economical factors to be considered at various design levels.

INTRODUCTION

In conjunction with the design of new and modified Army Ammunition Manufacturing Facilities, a broad requirement for structures which must provide personnel and/or expensive equipment protection in the event of an accidental explosion has been identified.

At the present time, procedures are available for the design of protective structures for close-in and far-range effects, in the tri-service design manual "Structures to Resist the Effects of Accidental Explosions" (Ref 1). However, this manual is devoted primarily to the design requirements for reinforced concrete structures, the utilization of which, at distances away from an explosion (far-range), may result in an uneconomical design.

To remedy this situation the Manufacturing Technology Directorate of Picatinny Arsenal, as a part of its Supporting Studies Program for the U. S. Armament Command (ARMCOM), is in the process of developing design criteria for other materials such as structural steel, brick, clay tile, block, and precast concrete. This paper is devoted primarily to the application of structural steel for protective construction. A discussion of the effectiveness of current construction techniques and application of new techniques is presented. Also included is a cursory description of design procedures along with economical considerations related to the use of structural steel.

PRESENT DAY CONSTRUCTION EFFECTIVENESS

Most existing buildings at explosive loading and/or manufacturing facilities which are located relative to potential explosions at unbarricaded intraline distances or greater are either wooden structures from the 1942 era or pre-engineered buildings built within the last 10 to 15 years (Fig 1). Both building types provide less than a marginal degree of protection for the personnel and equipment at unbarricaded intraline distance, with damage to both types of structures approaching collapse.

At inhabited building distances, which correspond to blast incident overpressure of approximately 1.2 psi, the wood building frames and sidings will resist the blast pressures without significant damage. However, the doors and windows, which are numerous in the wood buildings (Fig 2), will fail, producing debris hazards for the building occupants.

On the other hand, failure of the doors and windows permits pressure flow into the structure. This internal pressure, in combination with the increased resistance provided by the relatively more massive timber members, helps to relieve the blast loads on the building exteriors and, therefore, minimizes the damage to the structure as a whole.

It may be well to consider the current practice under which standard pre-engineered buildings are supplied by the various manufacturers. The practice results in efficient and economical structures but does not readily lend itself to meeting the increased requirements of blast protective buildings. In general, a procedure for obtaining such a pre-engineered building is as follows. The designer shows the size and layout of the building and specifies the wind, snow, and earthquake loadings based on the location where the building is to be constructed. The manufacturer then uses this information as input to a design analysis which calculates the size of his standardized building member components, i.e., wall panels, roofing, purlins, frames, etc. These standard size components are either precut or fabricated through an automated or semi-automated manufacturing system. Under this procedure, only the foundation and architectural designs are required by the architect/engineer to furnish a pre-engineered building.

However, the conventional loadings and the standard component sizes do not cover the range of loads and component sizes required for blast protection. Also, the blast load parameters cannot be given as input for the manufacturer's analysis without extensive modification of his current programs and fabricating procedure. Based upon the maximum wind, live and earthquake loads used for the various parts of the country, an estimate of the blast incident overpressure at which the building can be reusable is in the order of 0.2 psi, while an upper limit for the capacity of non-reusable structures is approximately 0.5 to 0.7 psi. The upper limit capacity is a function of the number of doors and windows which will fail and thereby relieve the external blast on the structure. It should be noted that the upper limit of pre-engineered buildings is less than 1.2 psi, or less than the overpressure associated with inhabited building distances.

To illustrate the vulnerability of the use of pre-engineered buildings for blast resistant construction, consider a recent explosive incident where a pre-engineered structure was subjected to a long duration (80 to 100 milliseconds) blast load having an incident overpressure equal to approximately 2.5 psi. The building was approximately 100 feet long by 50 feet wide and with a roof height varying from 16 feet at the edge of the building

to 24 feet at the center. These heights were measured above a concrete floor slab which in turn was positioned four feet over the ground. Framework consisted of four interior, 50-foot long rigid frames spaced at 20 feet on center. The transverse end wall framework utilized columns and beams with diagonal bracing. The siding and roofing were constructed of corrugated aluminum panels connected to the girts and purlins by 1/4-inch screws. A transverse 8-inch concrete block wall was located at the second and fifth frame from the front (side facing the blast) of the building. Equipment and personnel access doors were located within the side wall of the building.

Figure 3 is a plan layout of the building.

The damage to the building was severe (Fig 4), and was of a magnitude which would produce injury to personnel. The south wall (wall facing the blast), west and north walls, and roof failed, producing large holes in these surfaces of the structure. The east wall sustained damage but did not fail because of the failure of the doors in this surface which afforded relief for the exterior blast loads. The block wall near the front of the structure remained intact. The pressures penetrated the west wall at the rear of the block wall and relieved the pressures which had penetrated the front wall of the building. On the other hand, relief was not afforded for the rear of the second block wall and the pressures which entered the west side of the building failed this wall. Flying blocks, in addition to the blast pressure, penetrated and deformed the rear wall of the building. Although little damage was sustained by the frames, some of the purlins and girts yielded and buckled. The siding and roof that remained were highly deformed with deflections approaching those that would be formed if the siding acted as a catenary. The minimum damage to the frame was due to the roof failure which considerably reduced the blast loads acting on the framing.

Another pre-engineered building, which was closer to the explosion than the above structure, sustained more severe damage than the first structure. The front of this structure was subjected to an overpressure of 3.5 psi which corresponds to that produced at unbarricaded intraline distance. Here, about 50 percent of the siding and roofing were either dislodged or near dislodgement (Fig 5). It may be noted in Figure 6 that another open ended corrugated steel structure which also was located at the 3.5 psi overpressure level was virtually undamaged. In this case, both the front (side facing the detonation) and rear of the structure were open. The blast wave passing through the interior of the structure equalized the external blast loads.

DESIGN MANUAL

The manual for the design of steel structures to resist the effects of H.E. explosions is contained in two Picatinny Arsenal reports (Ref 2, 3) which will be published in the near future. The first report, titled "Use of Structural Steel in the Design of Structures to Resist the Effects of H.E. Explosions," deals primarily with the analysis of steel elements which can be analyzed as a single-degree-of-freedom system while the methods given in the second report are used for the performance of multi-degree-of-freedom system analyses. The latter report, which is applicable to both structural steel and reinforced concrete, is titled "Analysis of Frame Structures Subjected to Blast Overpressures."

Included in the first report are the procedures for structural steel design which are similar to the information given for reinforced concrete in TM 5-1300 (Ref 1). Procedures are given for the determination of ultimate strengths of wide flange and standard I - sections, channel elements, structural steel plates, and corrugated metal sections (Fig 8). Also contained in this report are static and dynamic properties of steel columns and beams; as well as recommended types of steels and details to be used for blast load design and structural response. In the latter case, permissible deflections of elements are specified for buildings which are either reusable or non-reusable.

In addition to the above, the first report contains a series of charts to simplify the design of beam elements including purlins, spandrels and girts. Here, required member sizes are specified for various span lengths, spacings and peak blast loads, and durations. The charts include solutions for simply supported, fixed, and multi-span elements. The charts have been developed for both reusable and non-reusable structural response conditions.

Figure 9 illustrates a typical design chart. The data presented in the first report is so arranged that it supplements (does not repeat) the data given in References 1 and 4.

The second report describes the solution for performing nonlinear dynamic analysis of one- or two-dimensional rigid frames. The method of analysis, which has been programmed for solution on a CDC 6600 computer, utilizes a lumped parameter method to represent the masses and stiffnesses of a frame. Solution of the equations of motion is accomplished by

a direct integration using the linear acceleration procedure. Nonlinear behavior of the frame is accomplished by using a bilinear stress-strain diagram and by the formation of plastic hinges at the points of maximum moments having values equal to the plastic moments for the cross-section of the member at these points. The combined effects of axial loads and bending are considered to define points of hinge formation or material yielding.

The computer program is capable of analyzing multi-bay and/or multi-story frames and has the following features:

1. The application of dynamic loads in the horizontal and vertical directions, either in combination or separately.

2. The use of either pinned or fixed end conditions for both the beams and the columns.

3. The interaction between axial loads and displacements.

The computer program input data includes the modulus of elasticity of the material of construction, structural geometry (member length, slope, etc), type of support connection and capacity at yield (axial load and moment) of individual elements and applied loads (time-history relationships). The output data for individual elements includes:

1. Time history of joint and member displacements, accelerations, and velocities.

2. Time history of end shears and moments, and middle span moments.

3. Maximum and minimum displacements.

4. Maximum tensile and compressive axial loads, and associated bending moments and shears.

5. Maximum positive and negative bending moments and associated axial loads and shears.

Call out of the individual output data is optional depending upon the needs of the designer. The above output can be used in combination with the data given in Reference 2 for the design of individual elements of a frame.

APPLICATION OF STEEL DESIGN

As may be expected, structural steel elements designed to resist blast overpressure will be stronger and heavier than steel elements designed to sustain conventional loads. However, in the event of an explosion within the steel building, the structure will fail with resulting fragments. Therefore, the mass of structural steel elements should be kept to a minimum. Because steel structures must exhibit strength rather than mass, this type of construction is referred to as "Strengthened Frangible Construction" i.e., construction done by materials used for conventional loads which have been strengthened to resist blast loads. Use of strengthened frangible construction is usually practical up to blast overpressure level of approximately 10 psi. At higher pressure levels, the use of reinforced concrete begins to be economical. To illustrate the use of strengthened frangible material consider the following three case studies.

Case Study I (Line Office)

Line offices for many munition manufacturing facilities are located away from the main production line. For the case at hand, the line office is situated at approximately inhabited building distance from the nearest building containing explosive. Therefore, in the event of an explosion, the line office would be subjected to an incident overpressure of 1.2 psi with the responding reflected pressure of 2.5 psi.

For this case study, the line office is 62 feet long and 30 feet wide (Fig 10) and has an overall height of approximately 12 feet. Basically, the building is constructed of seven rigid portal frames each of which spans in the short direction of the building (Fig 11). Each member of the portal is 12 W 31.

Exterior walls of the building are constructed of 8-inch concrete blocks. Each horizontal course of the block walls is reinforced with extra heavy Dur-O-Wal, thereby furnishing the necessary strength for the walls to span between the columns of the rigid frames. It may be noted that the 10 ft-0 inch spacing between the adjacent frames was predetermined by the ultimate strength of the walls. To prevent the walls from collapsing either as a result of rebound and/or negative overpressures, the block walls are connected to the column supports by anchor straps. Corners of two intersecting block walls are provided with reinforcement to insure continuity between the walls at the corners.

Access into the building is through a series of blast doors constructed of light metal frame and cover plate. Blast doors are discussed later in this paper.

Roof of the building (Fig 12) is constructed of 18 gage corrugated (top hat section with backup plate) metal decking which spans between the spandrels of the adjoining frames. The decking is supported and bolted to spandrel beams of the rigid frames. The bolts provide the continuity for the decking to resist both the positive and negative pressures. The top hat section (with backup plate) metal roof has been selected because of its unique characteristics where the flat (backup) plate portion of the decking provides the necessary lateral restraint to prevent the corrugated portion of the decking from collapsing intermediate of its support as a result of the impingement of the blast loads. It may be noted that in this case the tie-down bolts are located in the valleys of the corrugation to permit placement of insulation and standard roofing over the metal decking.

Case Study II (Process Building)

The amount of structural steel required for buildings designed for blast overpressures will exceed that required for conventional loads. An evaluation of this increased amount of steel is illustrated by this case study.

Plan dimensions of the building are 59 feet long by 46 feet wide. The two shorter end walls are constructed of reinforced concrete. A third reinforced concrete wall positioned parallel to but intermediate of the end walls divides the building into two separate areas. The remainder of the exterior surfaces (two walls and the roof) is constructed of structural steel.

Initially, the steel portion of the building was designed for wind and earthquake loads. The resulting members consisted of light tubular columns and beams which supported a light metal roof decking and wall paneling (Fig 13). The original steel design did not consider the effects of blast loads.

Because the building which will contain personnel is considered vulnerable to a potential explosion in an adjoining building whose operation has been automated, the structural steel portion of the building has been redesigned to resist a blast overpressure in the order of 4.4 psi (both roof and walls). Although the resulting increased cost of the steel was in

the order of 325 percent of that of the conventionally designed steel, the overall cost increase of the structural portion of the building was only approximately 33 percent. Here, the major structural cost was due to the concrete (walls and foundation slab) portion of the building.

Figure 13 illustrates the variation in members required to change from conventional (frangible) construction to strengthened frangible construction.

Case Study III (Process Building)

As may be expected, the cost of construction of blast resistant structures will vary with the magnitude of the blast overpressures. To illustrate this variation, consider the following building layout as given in Figure 14.

This Process Building is 87 feet long, 68 feet wide, and has a height of 15 feet. The construction consists of structural steel rigid frame supported on a reinforced concrete mat foundation slab. The roof and walls are covered with structural steel decking. Entrances into and exits from the building are through a series of blast doors.

Figure 15 illustrates the variation in cost as a function of the incident blast overpressure for both the structural steel or "hardened" portion of the building and the overall cost. This latter cost, in addition to the structural steel cost, includes the architectural, HVAC, piping, electrical, and the reinforced concrete floor slab and foundation costs.

The percent increase in the cost of the structural steel portion of the building decreases with an increase in the overpressure level as shown below.

Overpressure (psi)	Percent Increase (%)
0 to 0.5	80
0.5 to 1.0	22
1.0 to 1.5	13
1.5 to 2.0	11
2.0 to 2.5	10

The largest percentage cost increase of the structural steel is realized in the lower pressure range, i.e. between 0 and 0.5 psi. Here, the major cost difference is attributed to the change from conventional construction to the blast resistant construction. Above the 0.5 psi level, the cost increase with pressure level decreases rapidly, with the percent increase leveling off to 10 percent at the 2.5 psi overpressure level. At unbarricaded intraline distances (pressure level of approximately 3.5 psi), the cost increase is estimated to be about 10 percent above that for the 2.5 psi level.

Although the above cost variation is typical, the overall cost of structural steel at pressure levels corresponding to unbarricaded intraline distance is three times as high as compared to the cost for conventional construction. However, the overall cost of the blast resistant structure is approximately 33 percent above that of a similar conventional building.

BLAST DOOR

Type of blast doors may be classified based upon the blast pressure levels and fragment environment involved. For relatively high pressure levels and/or where high speed fragmentation will result due to a blast, steel blast doors should be constructed from heavy steel plates. At lower pressure levels (50 psi and less), built-up steel door construction may be used.

The use of steel plate construction is usually applicable where protection is required from the "close-in" effects of relatively small explosive quantities, i.e. in order of several hundred pounds of explosives. Use of structural steel for larger quantities usually will not be cost-effective.

One such arrangement for steel plate doors is illustrated in Figure 16. Here, the direct load produced by the blast will be transmitted from the door to its support by bearing, whereas reversal action of the door and effects of negative pressures are transmitted to the door supports by a series of reversal bolts. Bolts are provided on both vertical sides of the door in order to eliminate the need for transmitting reversal action through the door hinges. For wider doors, the reversal bolts are used at the top and bottom of the door to insure two way action of the plate. The reversal mechanism of steel plate doors should be strong to resist 100 percent of reversal effects.

As previously mentioned, where fragments are not involved and low blast pressures exist, the more conventional built-up door construction may be used. Nevertheless, at low pressures where fragments may occur, plate doors are needed.

A typical layout of a built-up steel door is illustrated in Figure 16, where the frame of the door consists of a series of channel sections with other channel sections serving as intermediate supports for the "skin" plate of the door. All other sections and the plate are welded together. For personnel doors (3'-0" x 1'-0"), minimum size channels (3 inches in depth) may be used. The thickness of the skin plate will be 1/4 inch or less.

Reversal mechanisms for built-up doors are similar to those used for plate doors except that hinges usually can be designed to serve as the reversal mechanism for one side of the doors.

REFERENCES

1. Structures to Resist the Effects of Accidental Explosions, Department of the Army and the Navy and the Air Force Technical Manual TM 5-1300, June 1969

2. *Use of Structural Steel in the Design of Structures to Resist the Effects of H.E. Explosions*, Picatinny Arsenal Technical Report, Draft

3. *Nonlinear Analysis of Frame Structures Subjected to Blast Overpressures*, Picatinny Arsenal Technical Report, Draft

4. Manual of Steel Construction, Seventh Edition, American Institute of Steel Construction, Inc., New York, N.Y.

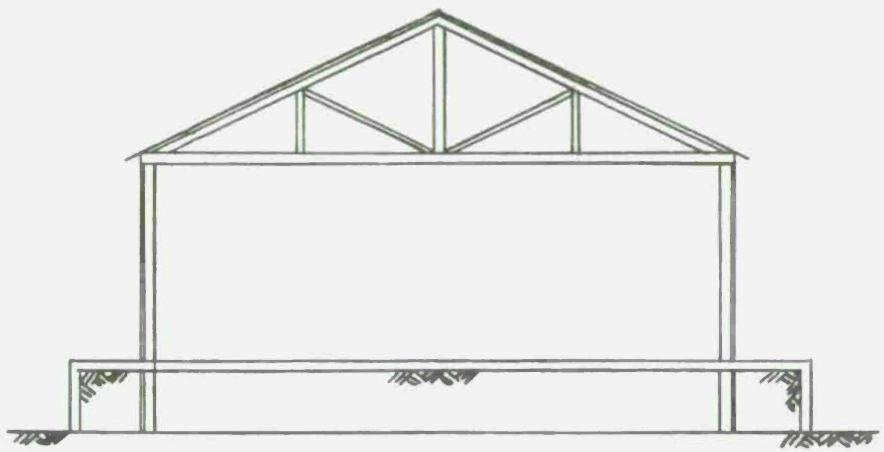

WOOD OR CLAY TILE CONSTRUCTION
(1942 ERA)

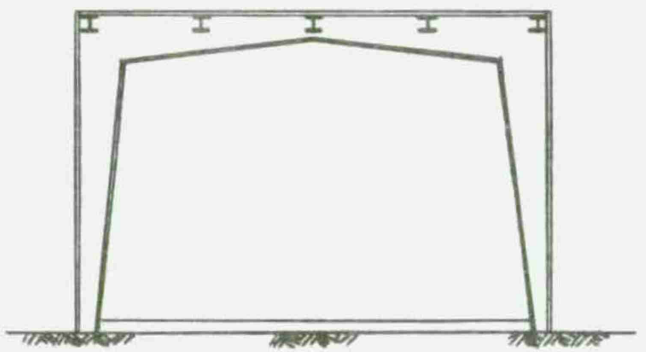

PRE-ENGINEERED BUILDING
(PRESENT TIME)

Fig 1 Existing construction

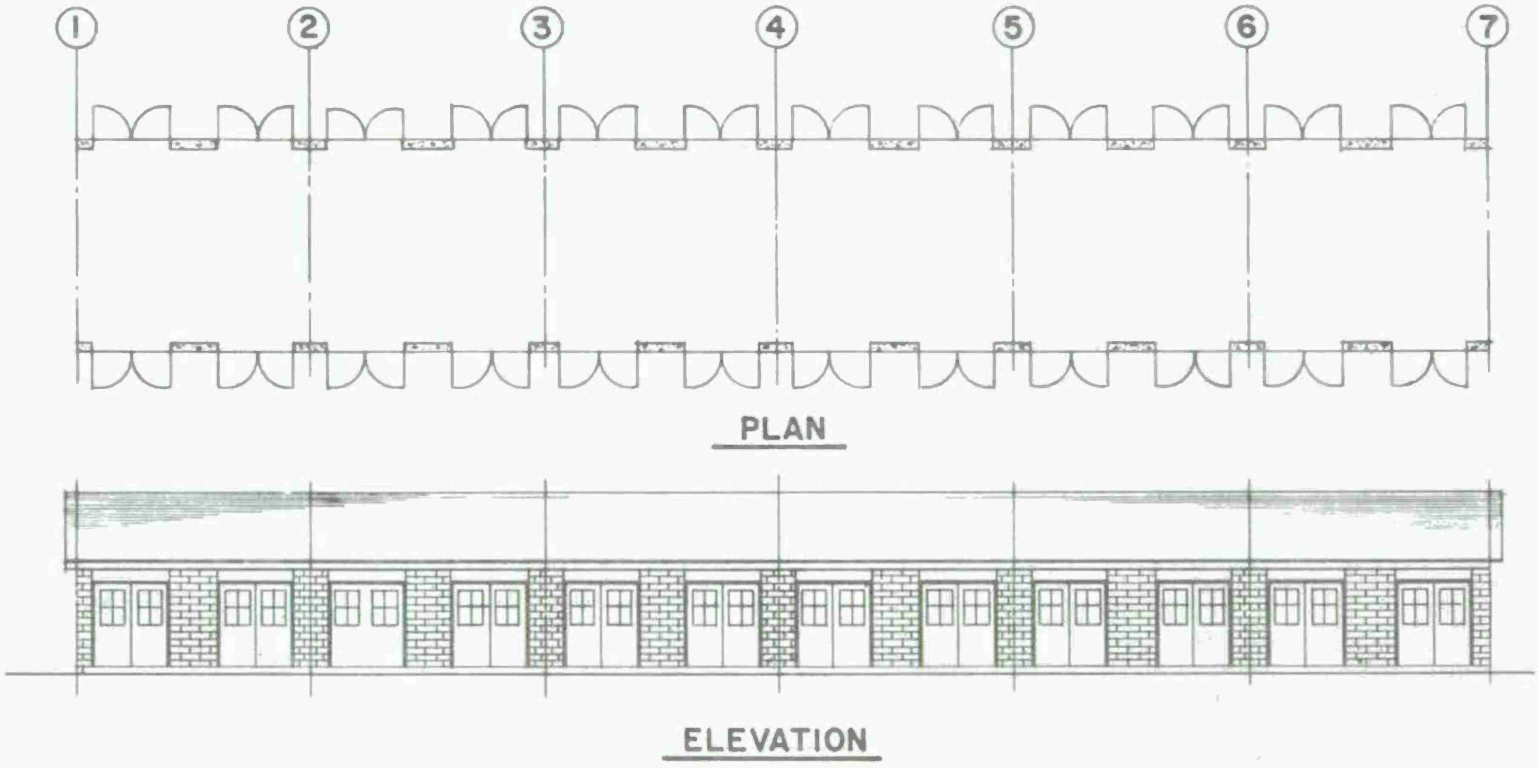

Fig 2 Typical wooden building

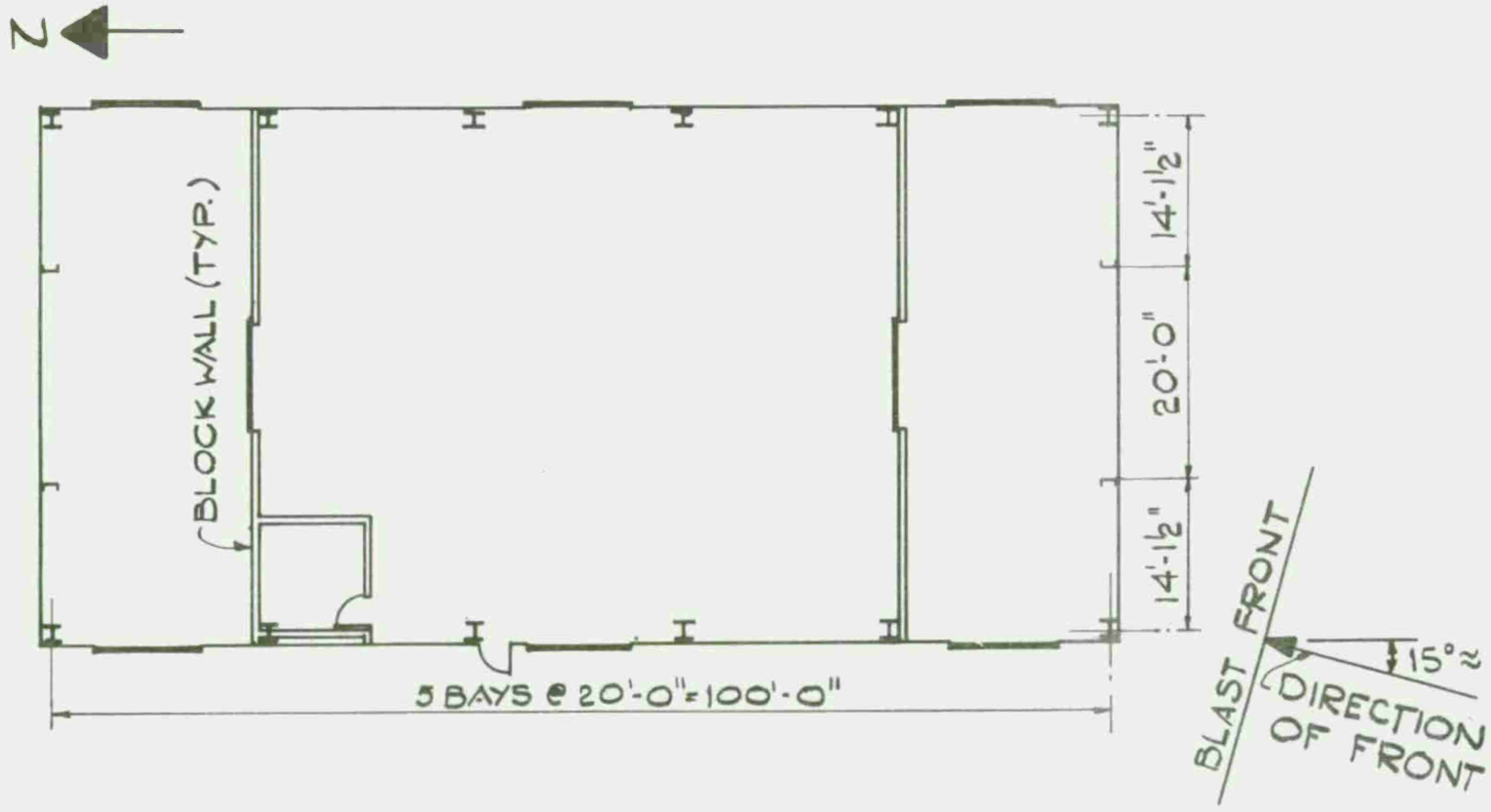

Fig 3 Layout of building No. 1

Fig 4A Front wall of building No. 1 (exterior view)
(Pso ≈ 25 psi)

Fig 4B Rear wall of building No. 1 (interior view)
(Pso ≈ 2.5 psi)

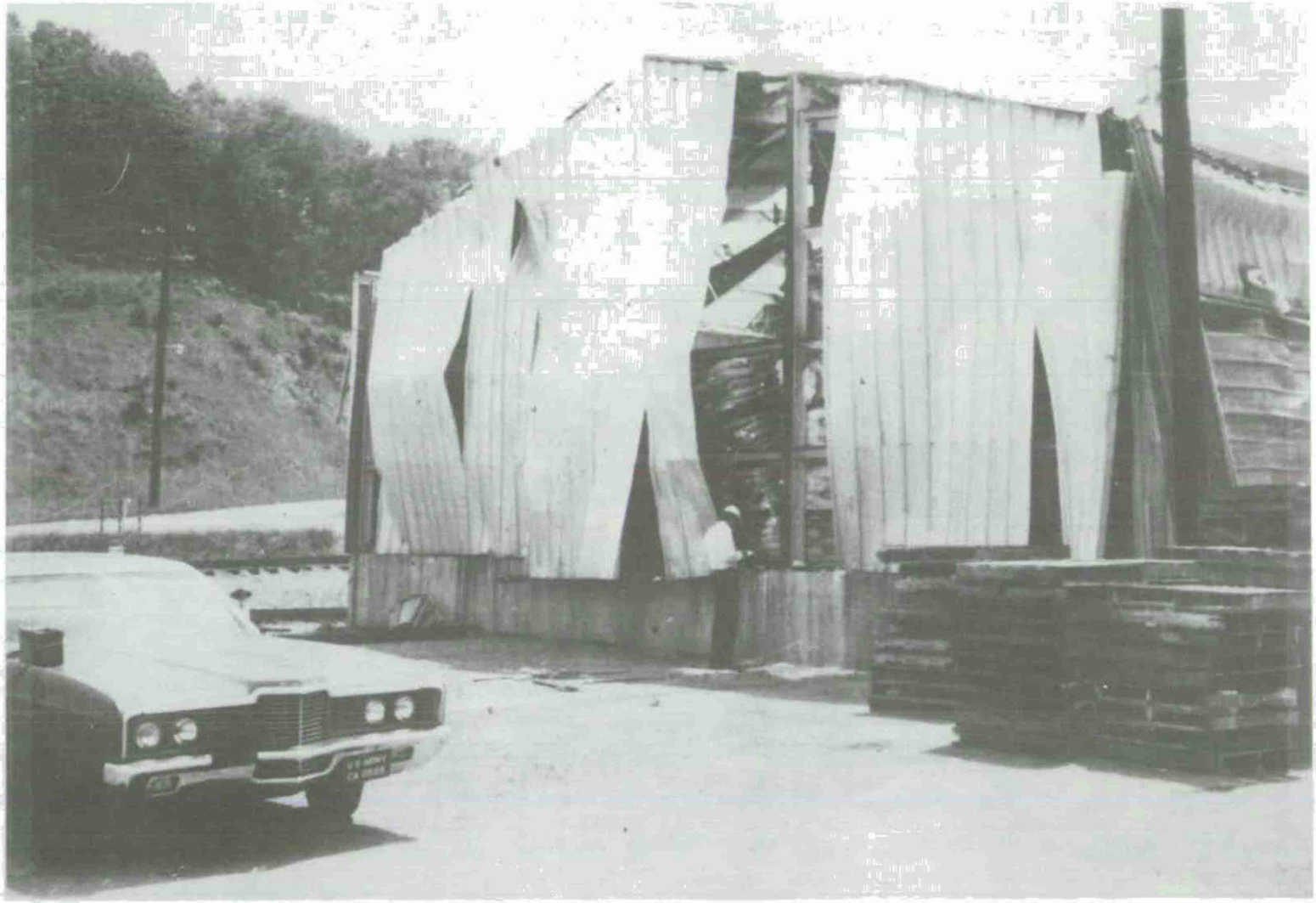

Fig 4C Rear wall of building No. 1 (exterior view)
(Pso ≈ 2.5 psi)

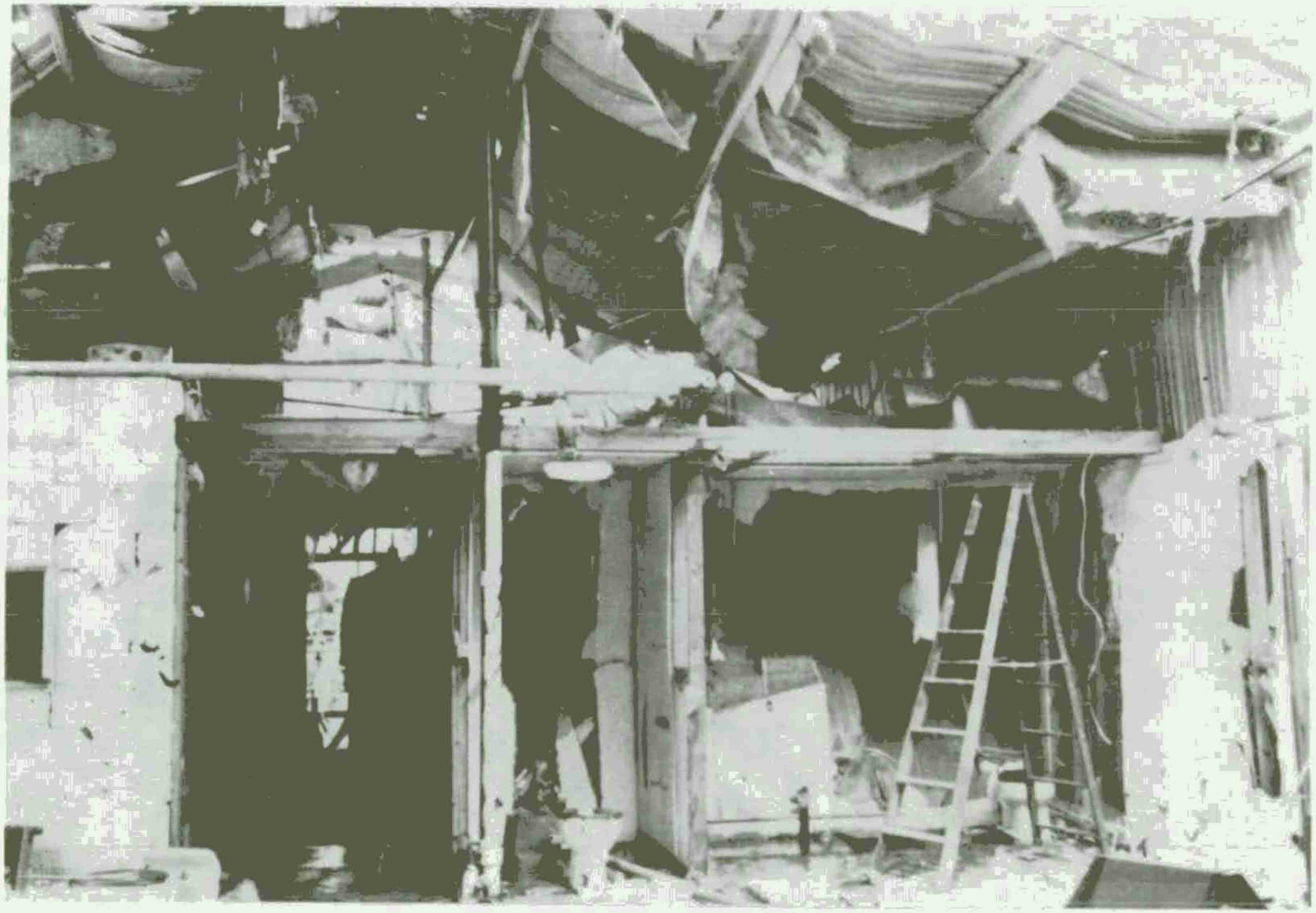

Fig 5A Interior view of building No. 2
(Pso ≈ 3.5 psi)

Fig 5B Side wall of building No. 1 (exterior view)
(Pso ≈ 3.5 psi)

Fig 5C Side wall of building No. 2 (exterior view)
(Pso ≈ 3.5 psi)

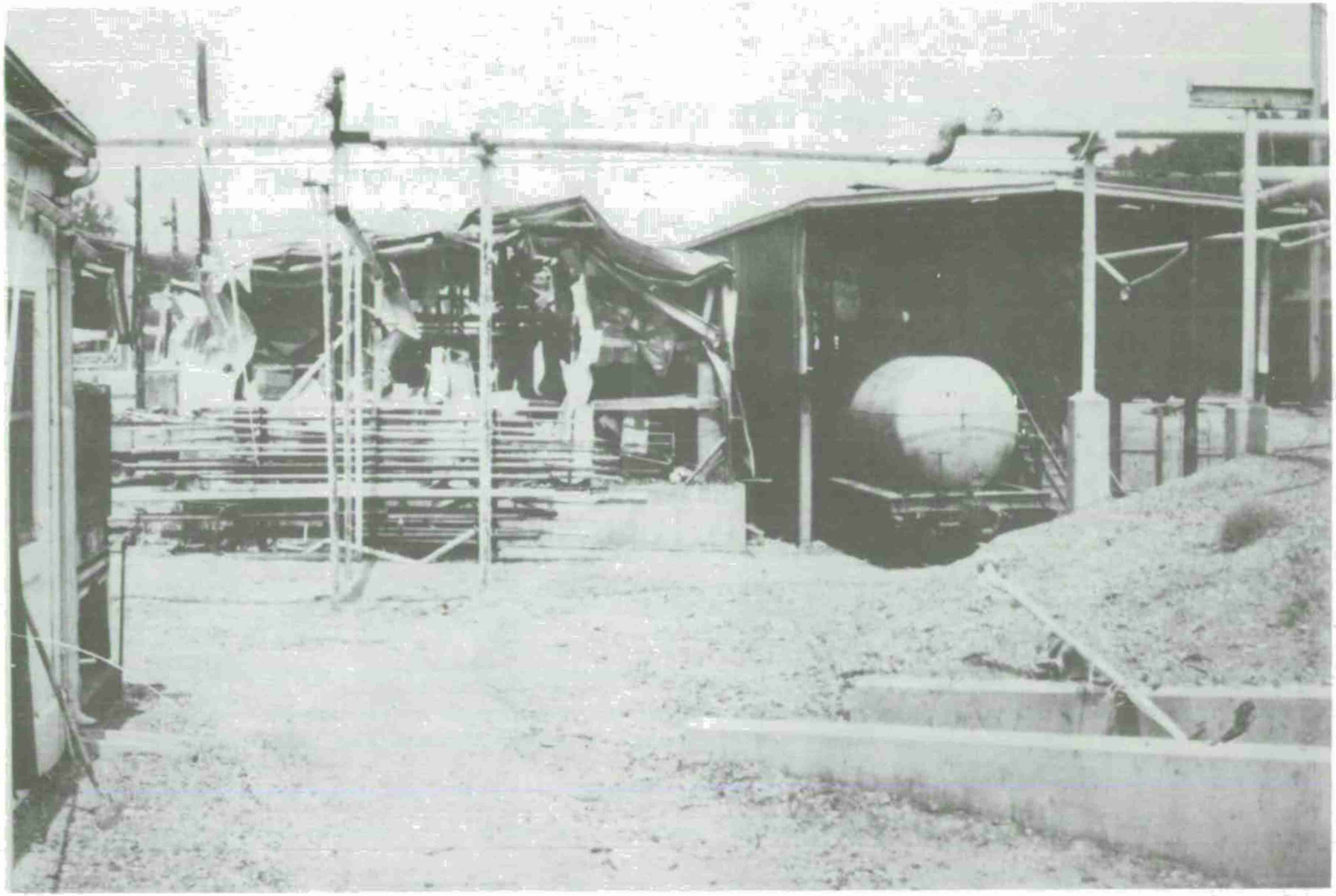

Fig 6 Undamaged building adjacent to building No. 2
(Pso ≈ 3.5 psi)

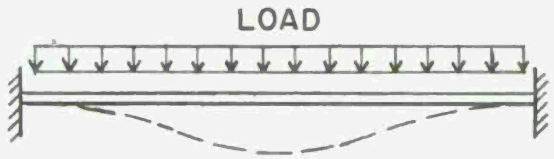

SINGLE DEGREE OF FREEDOM SYSTEM

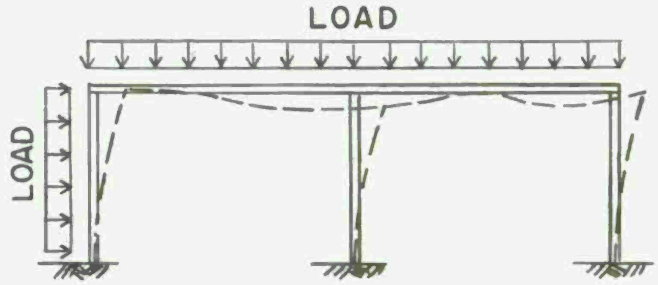

MULTI DEGREE OF FREEDOM SYSTEM

REPORT NO. 1

USE OF STRUCTURAL STEEL
FOR THE DESIGN OF
STRUCTURES TO RESIST THE EFFECTS
OF H.E. EXPLOSIONS

REPORT NO. 2

ANALYSIS OF FRAME STRUCTURES
SUBJECTED TO
BLAST OVER PRESSURES

Fig 7 Design manual

1. Ultimate Strength
2. Static and Dynamic Properties
3. Recommended Steel Type and Detailing
4. Deflection Criteria for Reusable and Nonreusable Structures

Fig 8 Typical structural shapes

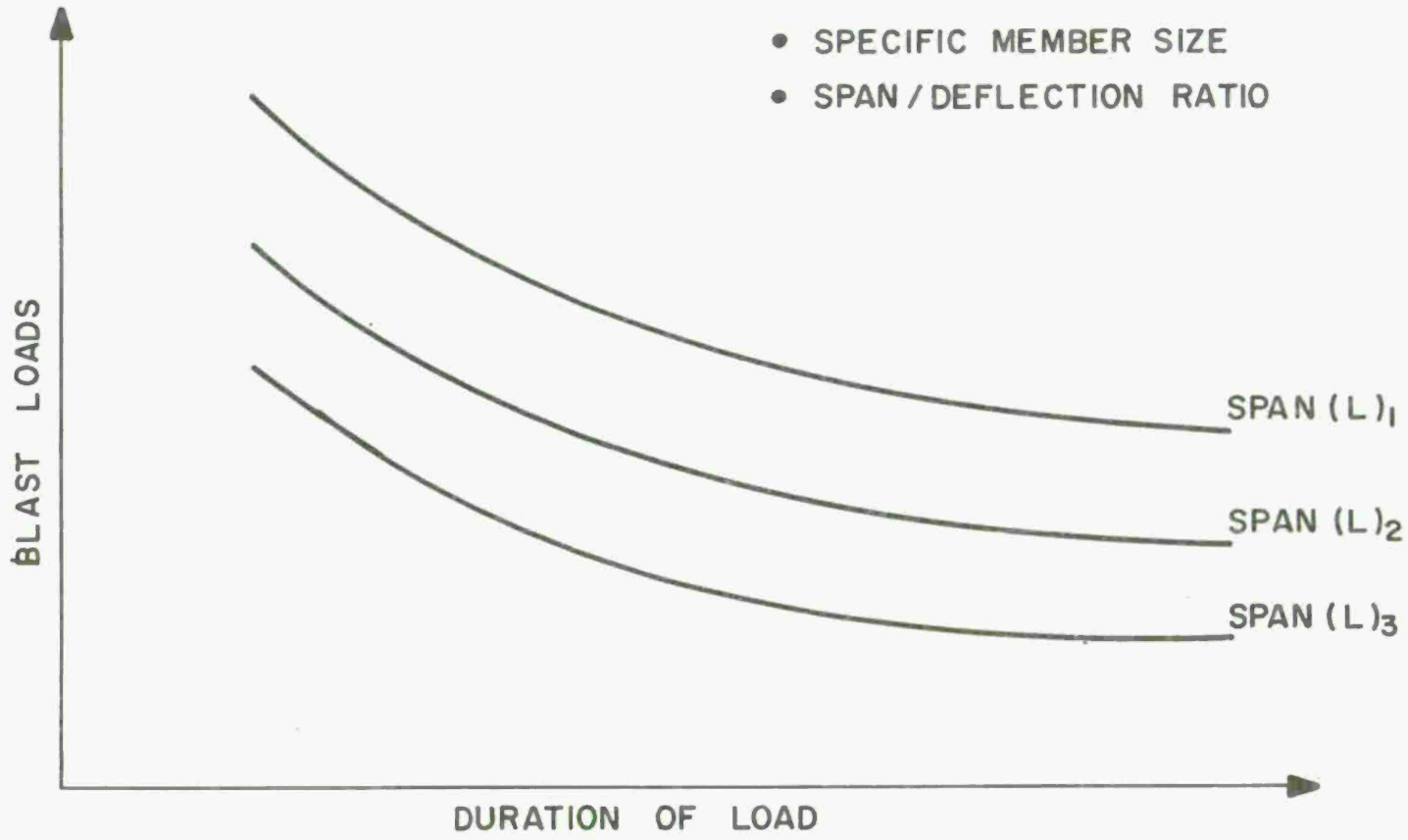

Fig 9 Typical design charts

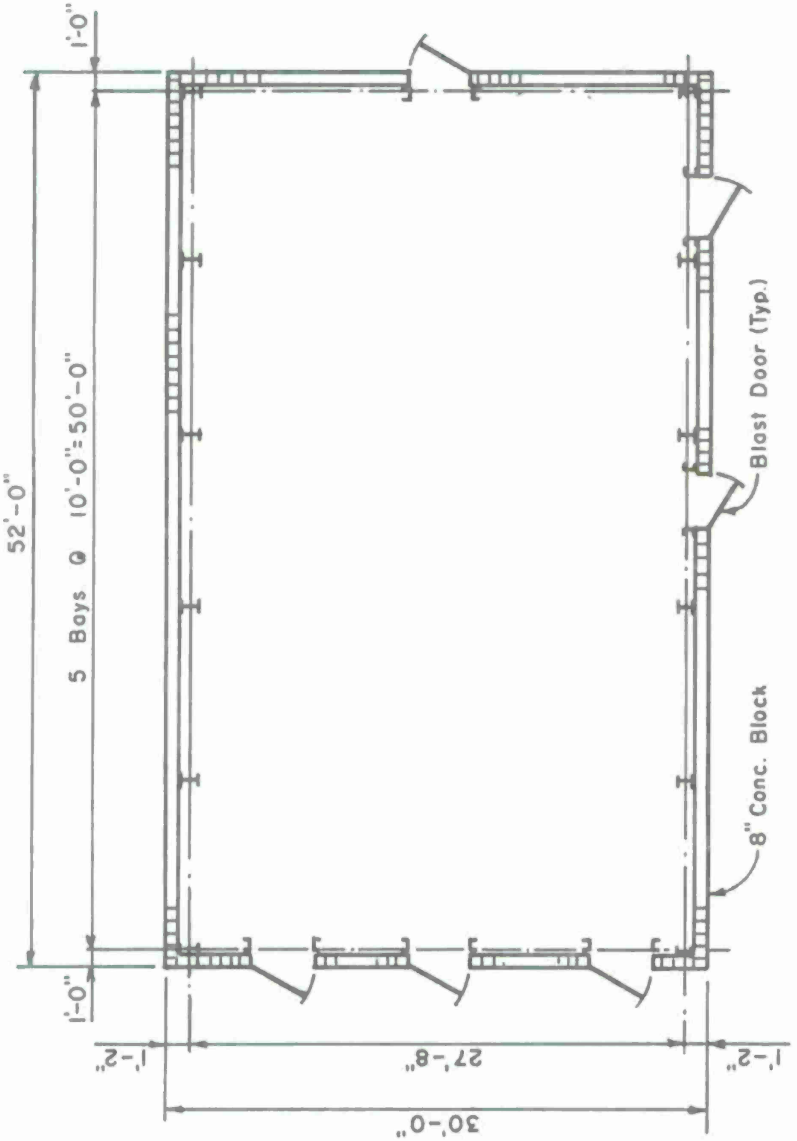

Fig 10 Office building

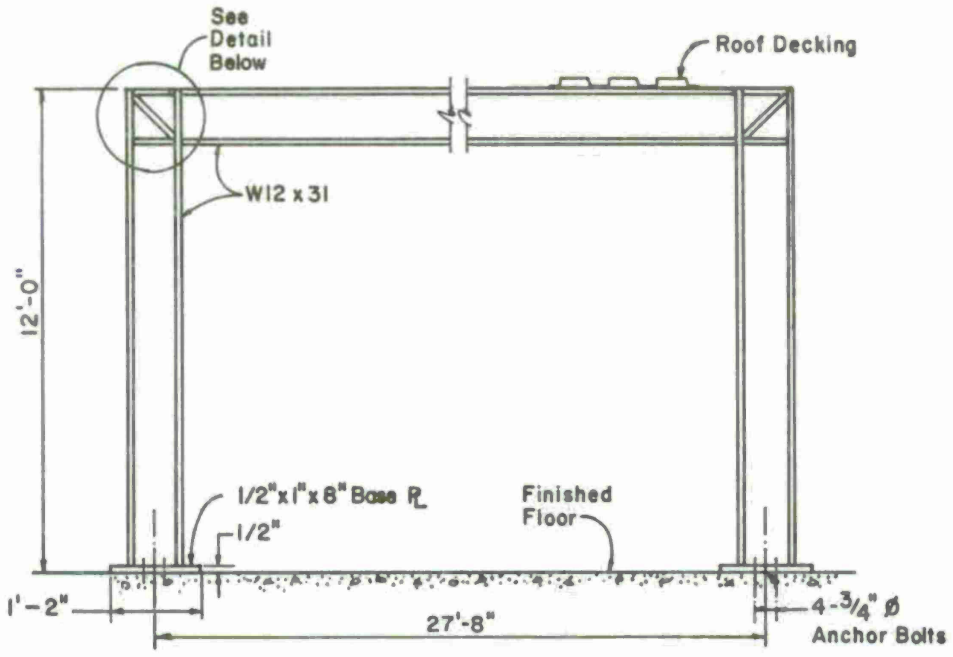

RIGID FRAME

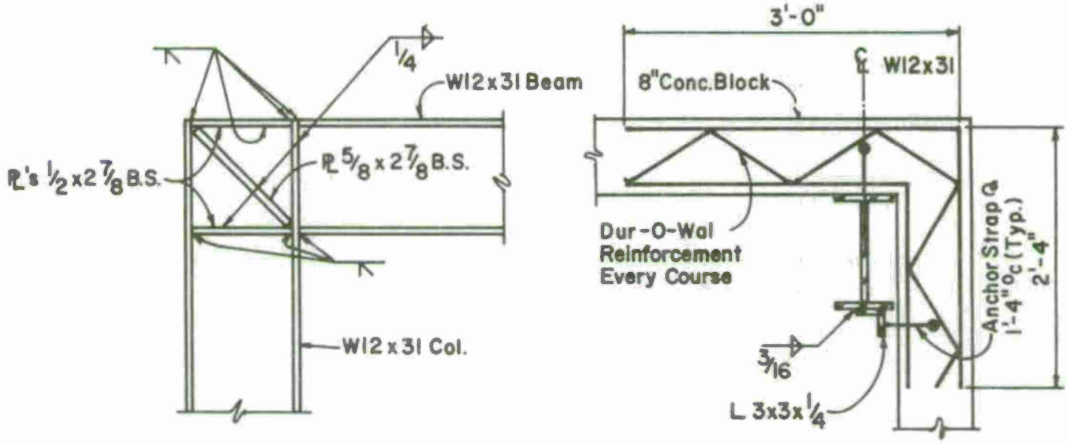

DETAIL

MASONRY CORNER DETAIL

Fig 11 Rigid frame details

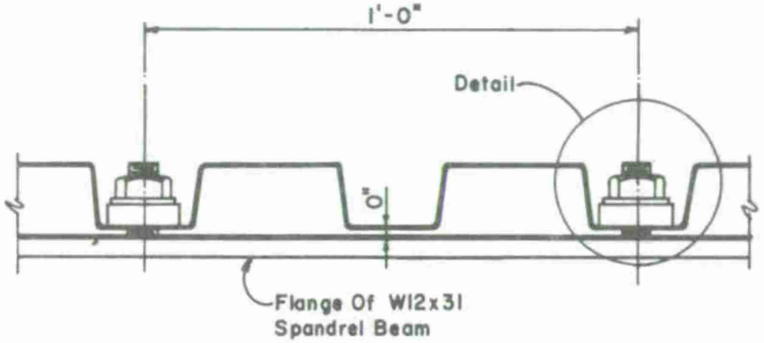

ROOF DECKING

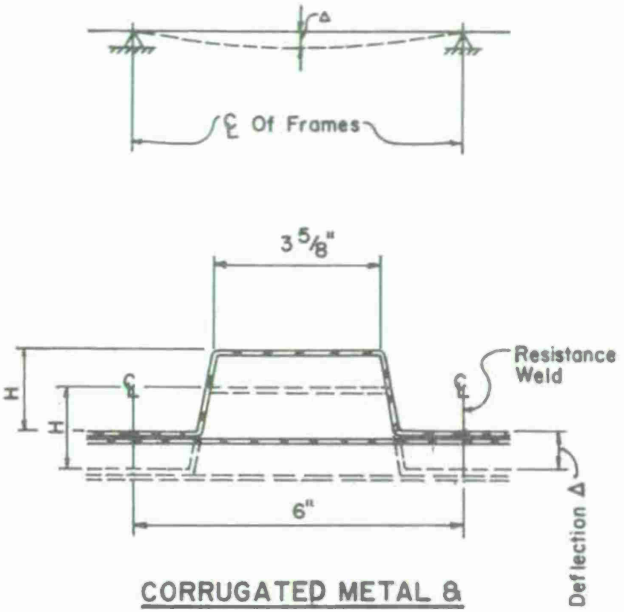

CORRUGATED METAL & BACK-UP PLATE

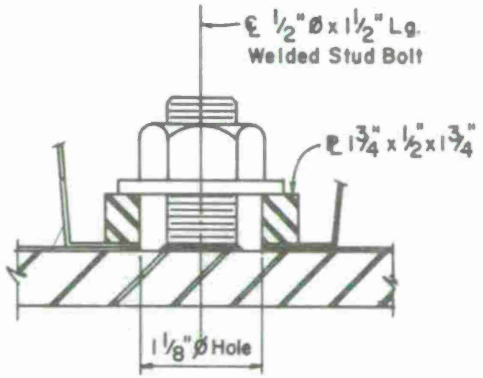

DETAIL

CORRUGATED PLATE WITHOUT BACK-UP PLATE

Fig 12 Corrugated metal roof details

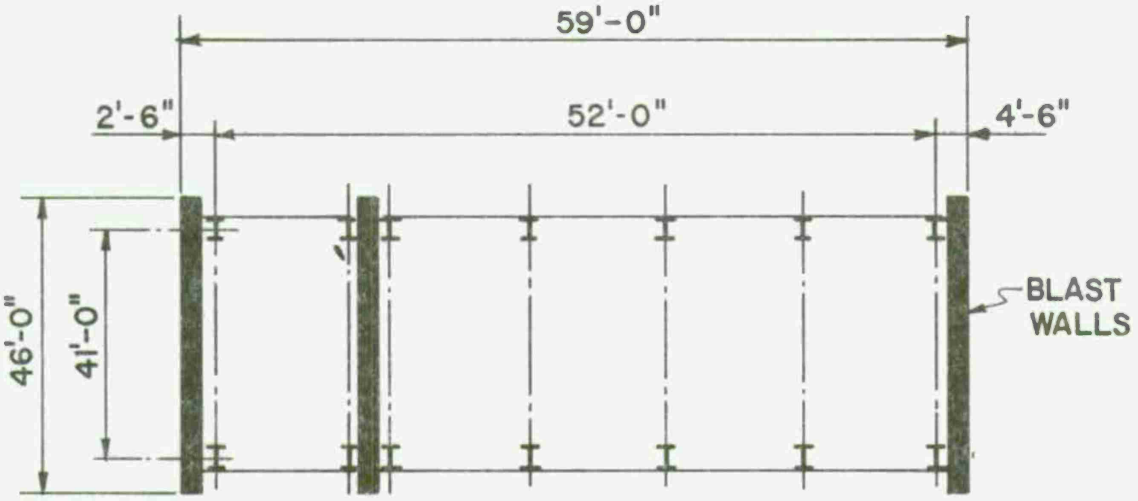

ELEMENTS	STEEL DESIGN	
	CONVENTIONAL (P=0.0 psi)	BLAST (P=4.4 psi)
WALL PANELS	20 GA. (2.2 psf.)	UKX-18/18 (4.8 psf.)
ROOF PANELS	DC 4.5 - 18/18 (5.4 psf.)	UKX-18/18 (4.8 psf.)
GIRTS (WALLS)	TS4x6x1/2(12'-9") (15 lbs/Ft)	W8x28(4'-6") (28 lbs/Ft.)
PURLINS (ROOF)	TS4x6x1/4(7'-0") (15 lbs/Ft.)	W8x28(4'-6") (28 lbs/Ft.)
COLUMNS	TS 6x6x1/2 (35 lbs/Ft.)	W18 x 105 (105 lbs/Ft.)
GIRDERS	TS 6x8x1/2 (41 lbs/Ft.)	W24 x 100 (100 lbs/Ft.)

Fig 13 Variation of member size (conventional & blast design)

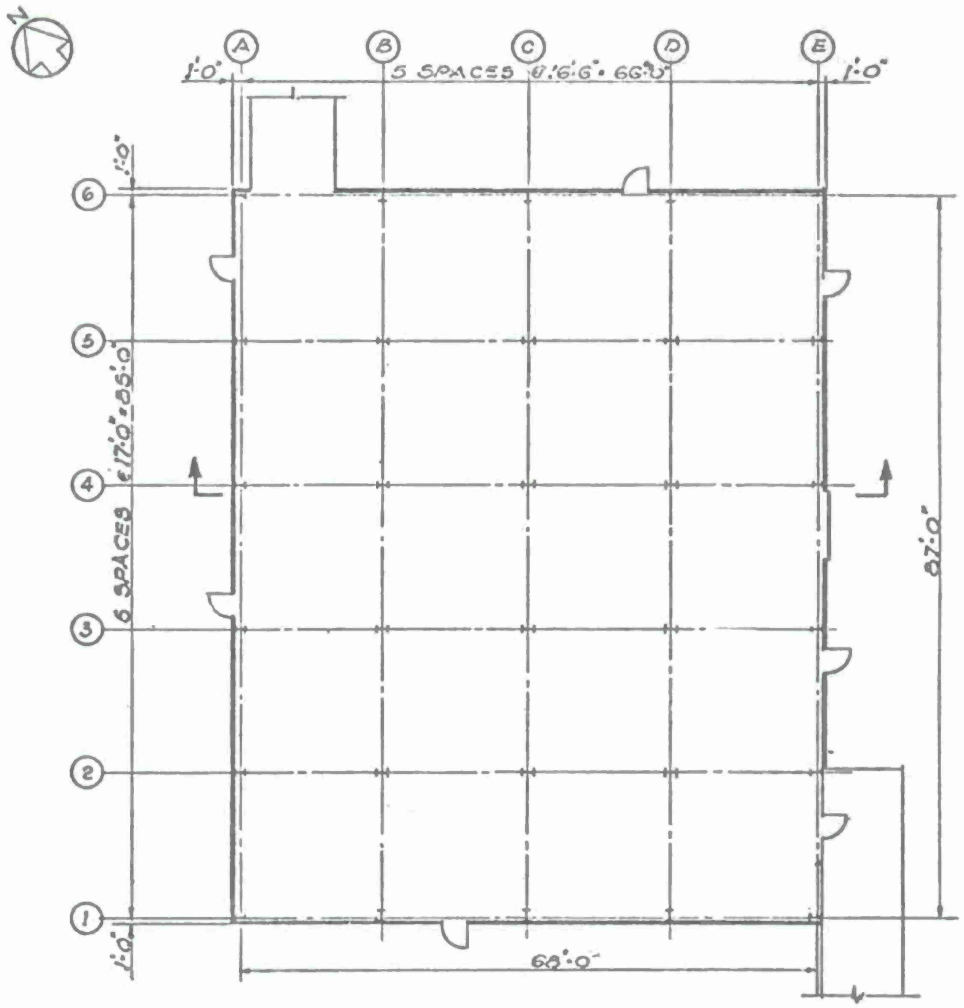

PLAN

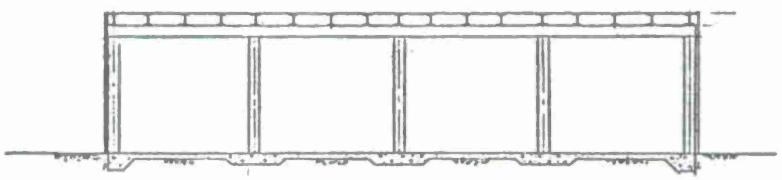

SECTION

Fig 14 Process building (case study III)

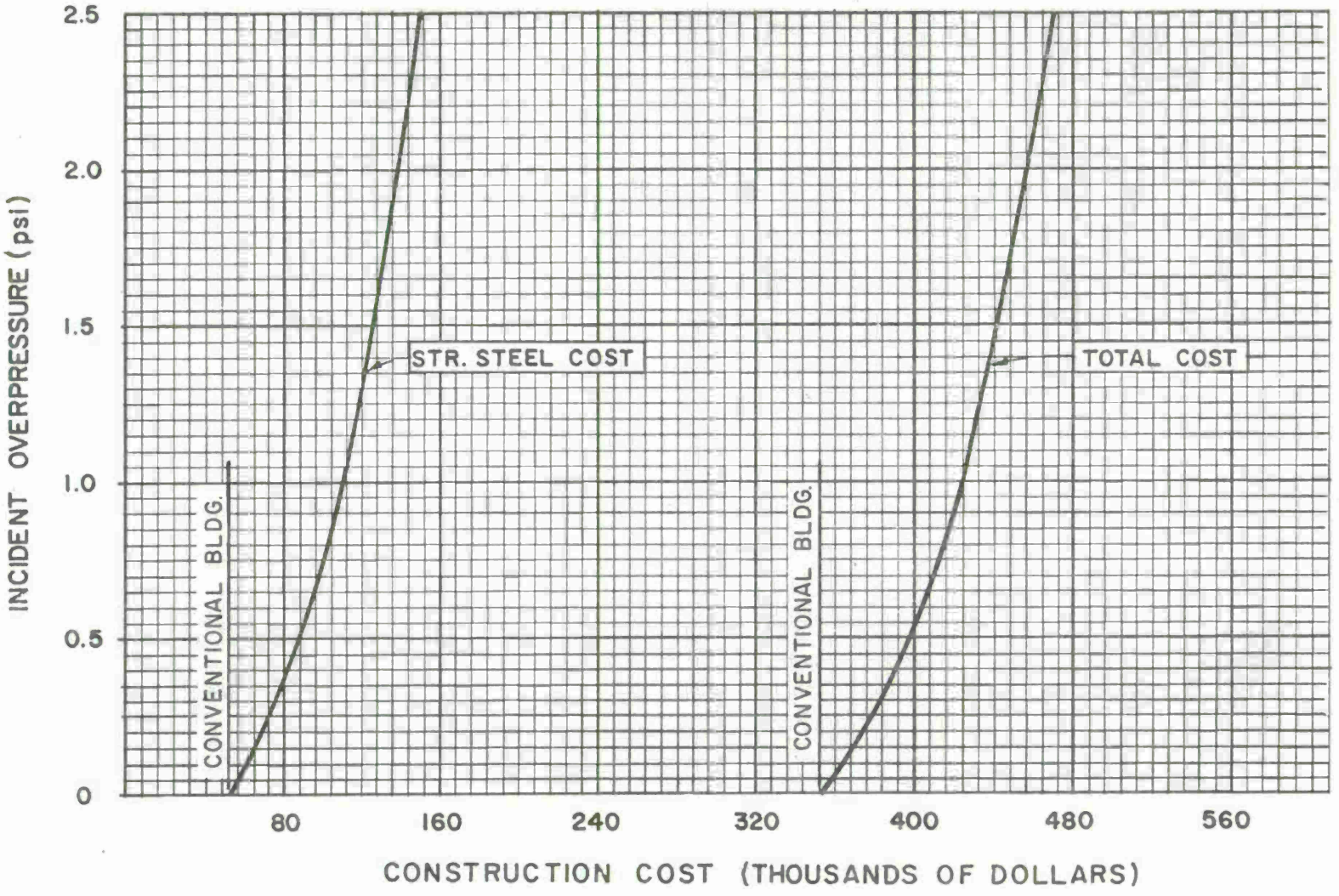

Fig 15 Construction cost vs incident overpressure (str steel bldg)

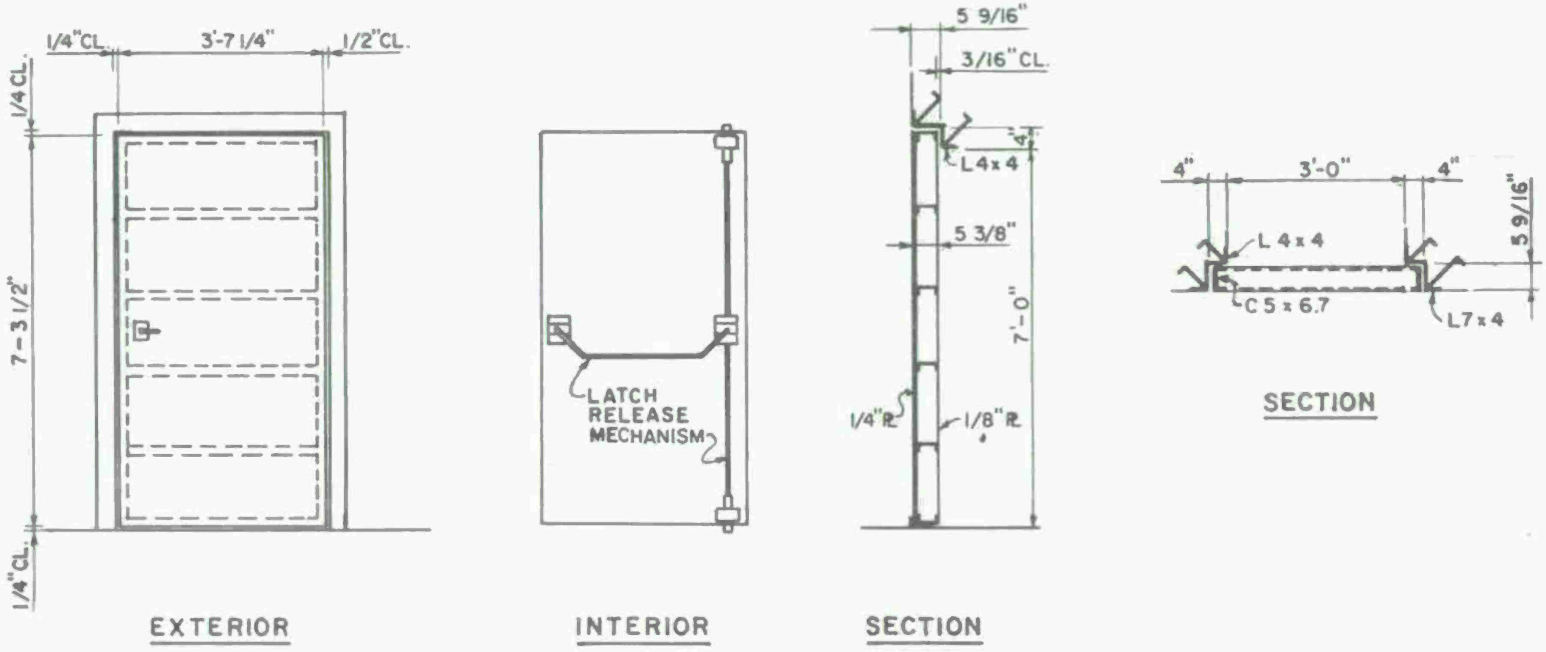

FIGURE - 16A

BUILT - UP BLAST DOORS

Fig 16A Built-up blast doors

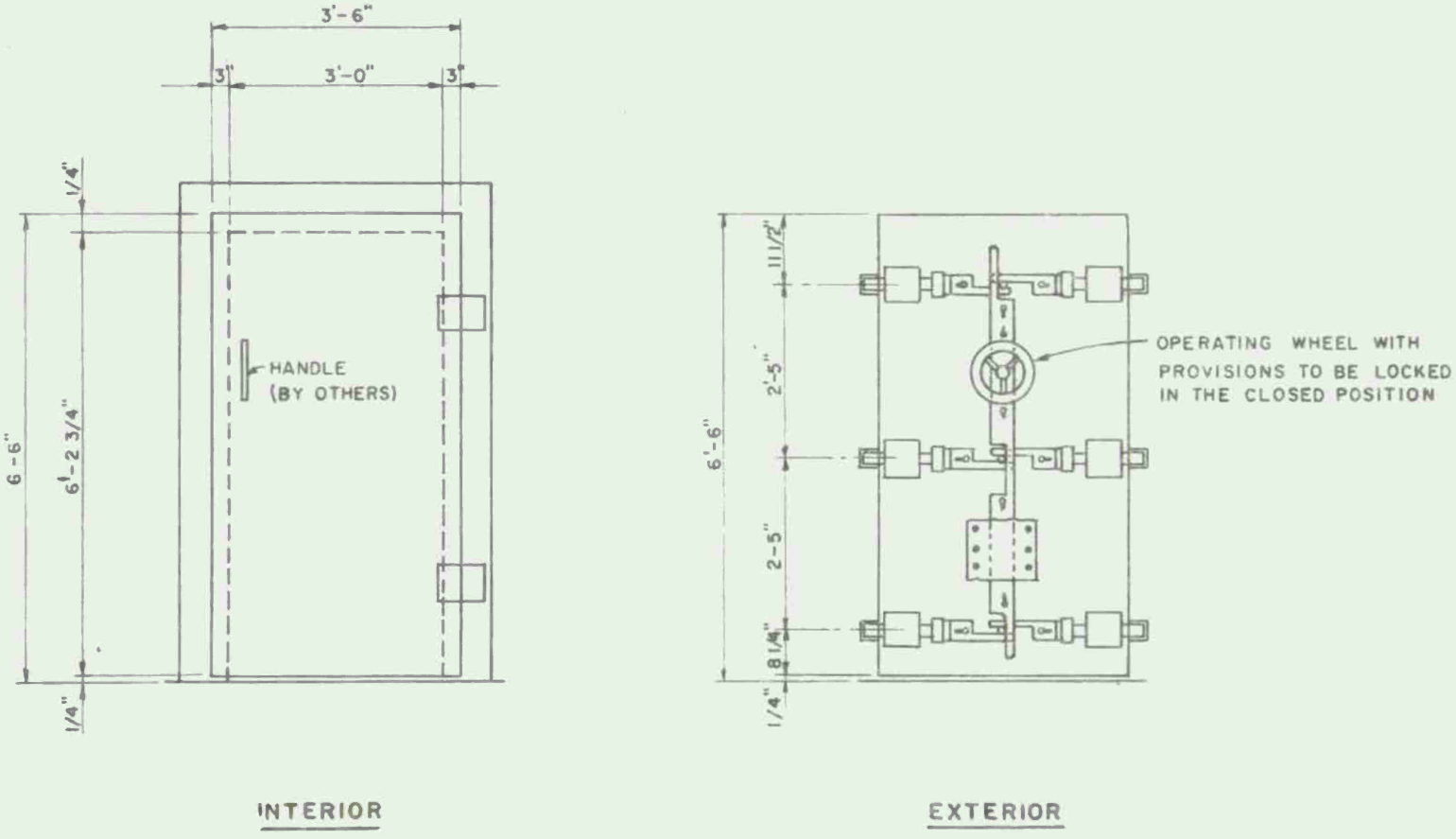

Fig 16B Steel plate blast doors

SAFE SEPARATION AND SECONDARY FRAGMENT IMPACT STUDIES

Richard M. Rindner
Robert S. Kukuvka

Manufacturing Technology Directorate
Picatinny Arsenal
Dover, N.J.

SUMMARY

A continuing experimental program on explosives sensitivity is underway as part of the Picatinny Arsenal Safety Engineering Project. This program provides support to the Modernization of the Army Munition Manufacturing Facilities. Its purpose is:

a. To determine the safe separation distance for ammunition end-items and in-process explosive materials at various stages of their manufacture.

b. To determine the sensitivity of explosives and explosive end-items to impact by secondary fragments (such as concrete pieces) in order to establish the mass-velocity relationship below which no detonation propagation will occur under any realistic condition.

The safe separation distances with or without shielding on a conveyor which were established for several end-items were: 155 mm Comp B loaded projectiles, 1.75" Rockets and M18A1 Mines (presented at the 14th Safety Seminar) as well as 81 mm projectiles and HE cartridges. Also, safe separation distances were established for 55 lb TNT boxes, 60 lb Comp B boxes and buckets, and 35 and 50 lb Comp C4 buckets. Other tests which will have a major bearing on the plant modernization program (and which are discussed in this paper) are presently underway.

Explosive sensitivity tests using secondary (concrete) fragments were performed in which 155 mm projectiles, RDX slurry and Black Powder were impacted with concrete fragments of various sizes at different velocities. No reaction occurred with 155 mm projectiles and RDX slurry and thus it appears that they are insensitive to impact by concrete fragments. A series of go/no-go situations resulted from the experiments with Black Powder and, therefore, a sensitivity profile (weight/velocity combination) was established for Black Powder. At present work is in progress to establish impact sensitivity of molten Comp B in shells and in the melt-kettle.

INTRODUCTION

The modernization of its munition manufacturing facilities and load, assemble and pack operations is of prime importance to the Army. The installation of new, complex systems including processes, handling equipment, buildings, and barricading requires an ultimate effort in safety engineering technology.

Picatinny Arsenal, with Army Materiel Command guidance and under the direction of the U. S. Armament Command, is providing this technology. Under its broad project titled, "Safety Engineering in Support of Ammunition Plants," Picatinny is rendering safer, more economic and realistic design data in support of the Modernization Program. This information is provided to the Government owned, contractor operated plants, the Corps of Engineers and others actively engaged in design and construction of the new munitions facilities.

A segment of the overall "Safety Engineering Project" includes the testing and analysis dealing with the sensitivity of explosives and explosive end-items. The information presented in this paper deals with this subject.

The objectives of the explosives sensitivity task are two-fold, Figure 1:

1. Determination of the safe separation distance (non-propagating) of ammunition end-items and of explosive materials at various stages of their manufacture (in-process conditions).

2. Establish the mass-velocity relationship below which no detonation propagation will occur to explosives and explosive end-items when impacted by secondary fragments (concrete pieces).

It should be stressed at this point that the work already completed to date has resulted in either major savings in space requirements or in establishing the minimum distance for separation that is safe between ammunition items where this information was not covered by present safety regulations. As the work has progressed, it has become obvious that a great deal remains to be done as a result of previous limited testing carried out in this area and the Army has reinforced its efforts in this regard. The ultimate goal of the results achieved by these test programs will be supplementation and/or modification of the present Safety Manual AMCR 385-100.

SAFE SEPARATION DISTANCE TESTS

General

The purpose of these tests was to determine spacing and/or shielding requirements to prevent propagation between ammunition items and explosives being transported on a conveyor.

Several ammunition end-items individually and on pallets as well as in-process explosive materials were tested at the Tooele Army Depot, Sierra Army Depot and Dugway Proving Grounds and are presented in Table 1.

The test series consisted basically of three parts (although not all of them were applied to each item tested).

Part 1 dealt with establishment of safe separation distances (without shields) on a conveyor.

Part 2 dealt with the establishment of safe separation distances using some kind of a shield between the donor and acceptors.

Part 3 dealt with performing confirmatory tests at the acceptable confidence level and reliability based on results produced in Parts 1 and 2.

Several test results which resulted in establishment of safe separation distances for ammunition end-items and explosive in-process materials such as individual 155 mm Comp B projectiles, 2.75" rockets, M18A1 mines and 55# TNT boxes were discussed during the 14th Explosive Safety Seminar and are shown in Table 1.

Test Set-up

81 mm Projectile & HE Cartridge Tests

Tests with 81 mm projectiles and 81 mm HE Cartridges were performed to confirm previously established distances (8.8") between the rounds with interrupters simulating the facing operation which is considered to be the most hazardous operation during the projectile assembly.

In this test, simulated drill fixtures were inserted in the acceptor's fuze well cavity. The transfer pallets were mounted on standard roller-type conveyors approximately 36" from the ground. Figure 2 illustrates the test arrangement, the center projectile being the donor, with the acceptor projectiles each containing drill fixtures for these tests.

60 lb Comp B Boxes

The 60 lb Comp B boxes test set-up was similar to the previously conducted tests with 55 lb TNT boxes. Three boxes were placed in a straight line on salvaged sections of roller conveyors (see Fig 3). The center box was the donor while the end boxes simulated the acceptors. The test items were supported by wooden stools at the height of 30 inches, which simulates the approximate height of a conveyor used in production lines. The entire assembly was then enclosed with three 10-ft long 24-guage aluminum hoods. These covers are analogous to those existing in an actual production line and will be used in future conveying systems.

60 lb Comp B Buckets

The 60 lb Comp B bucket tests simulated buckets being transported through a tunnel via an overhead pendant-type conveyor.

The buckets were suspended from a 3 x 2 3/8" steel "I" beam and oriented longitudinally within the tunnel at a distance of five feet from the ground as shown in Figure 4. The tunnels were fabricated from welded 2 x 2 x ¼" structural steel angle and covered with 24-gauge corrugated steel sheeting in order to closely simulate the actual plant conditions. The buckets used in the test were 1/8" molded phenolformaldehyde plastic and were 16" in dia x 14" deep.

35 lb and 50 lb Comp C4 Buckets

This test series was conducted to simulate a material handling system for extruder operations.

The test set-up for this test series is shown in Figure 5. The tunnels were fabricated from 2 x 4 lumber and covered with 26-gauge corrugated steel sheeting. They were eight feet wide by 10 ft high. The total length of each tunnel was approximately 56 ft. The aluminum buckets (containing Comp C4) were suspended longitudinally from the roof structure at a distance of seven feet from the ground. The same size buckets (14" dia x 20" deep) were used for both 35 lb and 50 lb Comp C4 separation tests.

105 mm M1 Comp B Projectiles on Conveyor Carriages

The purpose of this test program, which has been recently initiated and is presently underway, is to establish safe separation distances between carriages containing 16 105 mm Comp B loaded projectiles on a conveyor. This test series is being performed in support of several GOCO plant modernization programs.

Sixteen projectiles spaced approximately 1" apart on a carriage will be transported by conveyor within and out of the melt-pour area. Preliminary tests have been performed with and without pouring funnel and with and without blast interrupter bars. The fixtures and carriages used in these tests (aluminum alloy 6061-T6) are comparable to those used in actual operating conditions (see Fig 6).

Two carriages (one serving as a donor, the other as an acceptor), each containing 16 vertically oriented projectiles, were placed on 18" x 5 ft long sections of salvaged steel roller conveyor and spaced apart at various distances from each other. These assemblies were supported by wooden horses at 33" above the ground, which simulates the approximate height of plant conveyor systems.

Test Results

Except for the 105 mm carriage test, all tests discussed above were completed. After performing exploratory type tests in order to establish a minimum safe distance and/or shielding between the donor and acceptors, confirmatory tests were conducted at which no detonation propagation occurred.

81 mm Projectile and HE Cartridges

In the case of the 81 mm projectile tests, although cracking and splitting did occur to the acceptor projectile, no penetration of the acceptor projectiles was caused by primary fragments emitted from the donor. Since the prime objective of the test was to determine the effectiveness of the shield in preventing detonation propagation, the degree of indentation and cracking was not considered relevant.

105 mm Projectiles in Pallets

The preliminary tests with 16 105 mm projectiles on a transfer carriage (pallets) indicated, however, that the present regulations concerning safe spacing of these pallets are grossly inadequate.

These tests, which will be continued shortly, indicated that a total propagation between pallets occurred at a clear separation distance of 170 in. As of now, no safe separation distance was established between the pallets. Present regulations, however, (as spelled out in Safety Manual AMCR 385-100) call for 109" separation between pallets containing 32 projectiles.

A summary of the results of all safe separation tests with explosive end items, discussed in this paper and planned shortly, is presented in Table 2.

Comp B Boxes

Tests performed with Comp B boxes indicated that no propagation occurred at a clear separation distance of nine feet.

In view of the above, 25 confirmatory tests involving 50 acceptors were performed at 12 ft clear separation between the donor and the acceptors. No detonation propagation took place in any of these tests. However, burning of both acceptors in some tests was observed.

Comp B Buckets

Ten tests (20 acceptors) performed at 12 ft separation distance with Comp B buckets resulted in no propagation into the acceptor buckets. Although the steel angle frame and the tunnel sections were severely damaged, no fragments were emitted by the steel framing or "I" beam (see Fig 7). All acceptor buckets were torn apart and Comp B was scattered to within 100 ft from its original location. No burning of the plastic bucket debris was evident. Only one small Comp B acceptor fire was observed and this was attributed to a burning piece of wood from a tunnel base support.

Comp C4 Buckets

A total of 20 tests were performed (10 each) with 50 lb and 35 lb buckets containing Comp C4 . The safe separation distance of 35 lb and 50 lb buckets was established at 20 ft and 25 ft, respectively. In all

tests conducted, no propagation into the acceptor bucket occurred (see Fig 8). The steel corrugated sheeting was torn apart or deformed and strewn about the test site. In all cases the acceptor buckets sustained only minor deformation with no penetration. No fires were produced in the acceptors.

Table 3 summarizes the test set-up and results of all tests conducted to date and planned for the near future with the explosive in-process materials.

SECONDARY FRAGMENT IMPACT TESTS

A series of experiments were conducted at the IIT Research Institute Test Facility to determine explosive sensitivity to impact by concrete fragments. Figure 9 simulates a situation where wall fragments resulting from donor detonation impact the acceptors.

The concrete used in this program was launched from a 12 in. air gun facility (Fig 10). The gun is capable of launching a wide range of missile weights at varying velocities.

These tests utilized two types of concrete fragments:

a. Solid concrete cylinder

b. Containers filled with concrete rubble.

To prevent scoring of the air gun barrel, it was necessary to place the concrete fragments in some type of soft container. The container had to be strong enough to support the weight of the fragment, yet have minimal influence on the impact of the projectile with the target (see Fig 11).

155 mm Projectile Experiments

Twenty experiments were performed on 155 mm Comp B loaded projectiles subjected to impact by concrete fragments. Of these, 12 shots were made using solid concrete projectiles with weights ranging from 55 - 480 lb. Eight experiments used concrete rubble filled containers weighing from 125-250 lb. High speed and normal speed cameras recorded the results. The direction of fragment impact in all experiments was approximately normal to the 155 mm projectile axis. The 155 mm projectiles were

placed on steel witness plates and then positioned such that the projectile's axis was normal to the expected line of flight of the concrete fragment (see Fig 12).

Post test inspection of the 155 mm projectiles showed a varying degree of deformation to the projectile casing. In several tests, the lifting eyebolt ring was sheared from the projectile assembly. None of the tests resulted in any Comp B reaction. A summary of the test results is given in Table 4.

RDX Slurry Experiments

Fourteen experiments were conducted employing RDX Slurry as the target. The RDX was type B1 Class E. For these experiments, the same type of fragments as described before in this paper were employed. The experimental configurations, along with the weight of the slurry and its mode of confinement, are given in Figure 13. The direction of impact between the concrete projectile and the target was approximately 75 degrees.

Failure of the slurry to react to impact necessitated the number of different experiment configurations. As each configuration was tried, and failure to produce a reaction occurred, a new set up was instituted.

Sixteen additional experiments were performed by firing 30 caliber bullets from a rifle into RDX slurry. The purpose of these experiments was to observe if a reaction to the RDX slurry by bullet impact would occur. Both armor piercing and copper ball bullets were used. For both types of bullets, the target velocity was approximately 2,500 ft/sec. In each of these experiments, where a five gallon container was used as the target, the canister was either badly damaged or destroyed by the kinetic energy of the projectile. The water tanks employed as the environment for the slurry container were split apart at the seams. In every case, RDX slurry was scattered about the test area.

Table 5 summarizes the results of these experiments. The fragment velocities ranged from 200-1,270 ft/sec. The projectile weights ranged from 55-480 lb. In none of these experiments, regardless of fragment size or velocity, did an explosion-type reaction occur.

No reaction of the slurry was produced in the series of slurry bullet experiments. However, the box containing RDX slurry had been blown away from the area of impact.

Black Powder Experiments

For this series of 20 experiments, in which Black Powder was subjected to fragment impact, a single configuration was maintained (see Fig 14). A single 25 lb cylindrical metal shipping container of Black Powder was placed on a steel witness plate with the length of the container in line with the line-of-flight of the fragment. Impact direction was approximately 15 degrees off normal to the side of the container. The witness plate was placed on hard packed soil. The shipping container had a thickness of 0.013 in.

The same type concrete fragments were used as before and are described in Table 6. Only one out of 20 experiments used concrete rubble. The size of fragments ranged from 55-480 lb, their velocities from 100-1055 ft/sec.

The results of this test series are presented in Table 6. The magnitude of the reaction varied from no reaction, to slow burning, to intense reactions with accompanying fireball. Since no instruments were used in this series, no measurements of the degree of reaction (explosion) were possible. Where the shot resulted in no reaction, a post test survey showed Black Powder to be scattered about the test area. In each test (except one), the target canister was destroyed. Based on the test data obtained, an attempt was made to plot a go/no go profile of confined Black Powder as a function of projectile velocity and its weight. Figure 15 is a graphical presentation of these data.

Because only camera coverage of these tests was used as the basis for determining reaction intensity level, it is anticipated that a limited number of tests will be conducted in the future using airblast measuring devices. This will provide a quantitative assessment of the reaction intensity level.

CURRENT AND FUTURE WORK ON FRAGMENT IMPACT

Currently, we are determining the impact sensitivity of molten Comp B and TNT in various in-process stations of the production of the 155 mm shell. Specifically, sensitivity of the following configurations is being evaluated:

1. The melter-kettle, which will hold 40 lb of either Comp B or TNT in a molten state.

2. The Comp B filled 155 mm shell with the explosive at approximately 155°F (its temperature during the facing operation).

3. The Comp B 155 mm shell--"just filled condition", i.e. with the loading funnel in place and the explosive at approximately 200°F.

Work has started in evaluating these configurations. Preliminary results indicate that the Comp B at elevated temperature is significantly more sensitive to impact by secondary fragments. The fragments (both rubble and solid concrete) ranged in weight from 40-500 lb and impacted at the target at velocities from 360 to over 1000 ft/sec.

Figure 16 is a summary of the work either in progress or planned in the near future.

CONCLUSIONS

The safe separation tests conducted to date and currently in progress have demonstrated the following:

1. The present requirements and direction for safe separation of explosive end-items and in-process materials are inadequate.

2. Major savings in space requirements and safe separation distances on a conveyor can be achieved.

3. An urgent need exists for additional work in this field in order to accomplish effective facility design.

The outcome of the secondary fragment impact testing may result in less stringent design requirements for dividing wall construction in new facilities and thus, a cost savings. Experiments of this type could also make the redesign of existing walls in many instances unnecessary. Utilization of the air gun technique in simulating wall fragment impact of explosive munitions appears to be quite effective.

- SAFE SEPARATION DISTANCE
  - END ITEMS
  - IN-PROCESS MATERIALS
- SECONDARY CONCRETE FRAGMENT IMPACT

Fig 1 Sensitivity studies

Table 1

Sensitivity results

ITEM	SAFE SEPARATION DISTANCE
155MM, M107 PROJECTILE	18 INCHES WITH SHIELDING ROD– (½ IN. STEEL OR 1 IN. ALUMINUM)
2.75 IN. ROCKET WARHEAD	9 IN. CTR TO CTR, WITH 2 IN STEEL ROD
M18A1 MINE	10 INCHES
COMP C4 BLOCKS	10 INCHES
COMP C4 BUCKETS	35 LBS – 20 FEET 50 LBS – 25 FEET
50 LBS TNT BOXES 60 LBS COMP B BOXES	12 FEET 12 FEET
81MM HE M374A2E1 CARTRIDGE	8.8 IN. (WITH ¼ IN. THICK X 6 IN. HIGH LEXAN SHIELD)
81MM HE M374 PROJECTILE	8.8 IN. (WITH 2 IN. X 4 IN. X 14 IN. ALUM BAR

Fig 2 Propagation test 81 m/m M374A2E1 fixture M-913-200

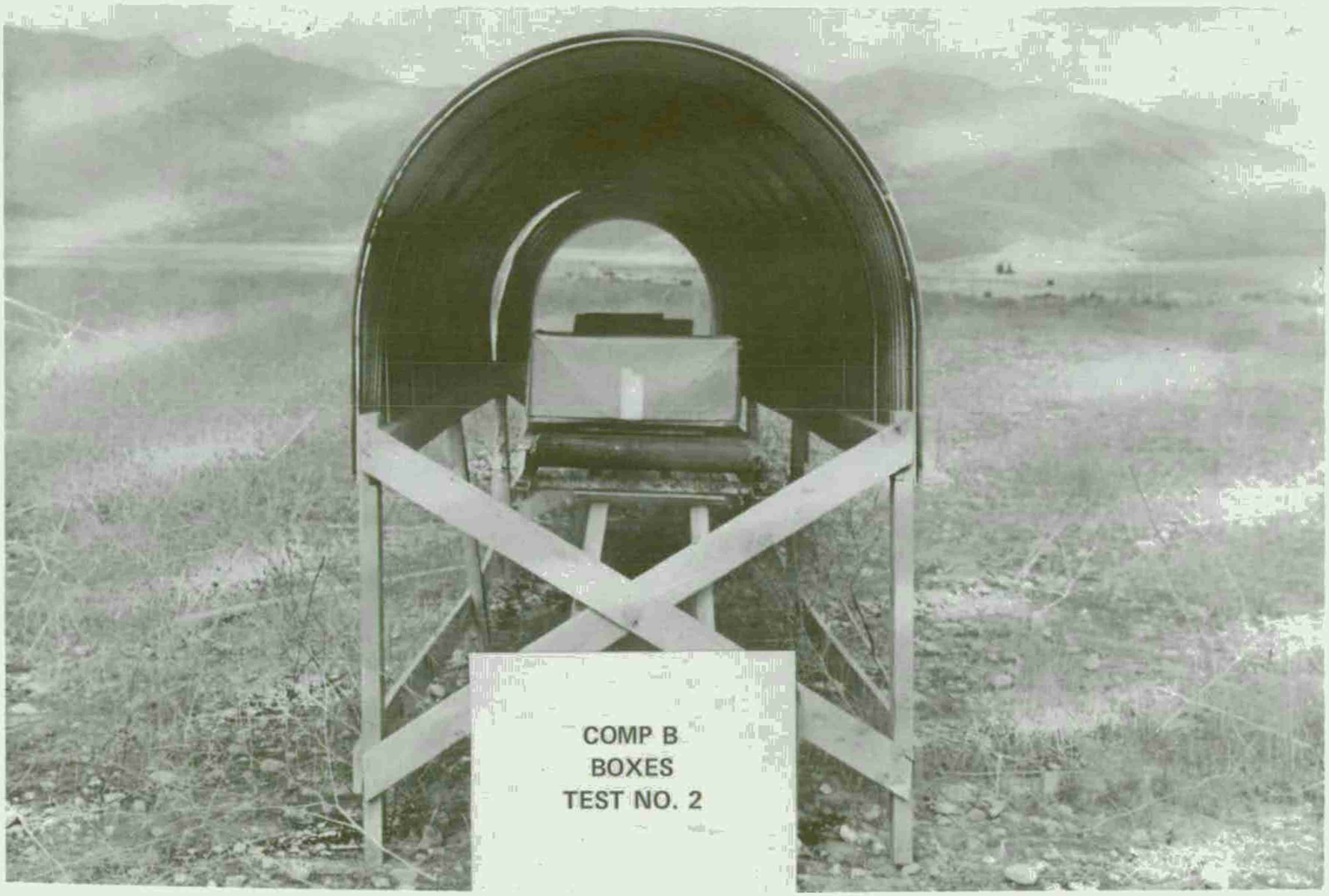

Fig 3 Test setup, 60 lb comp B boxes

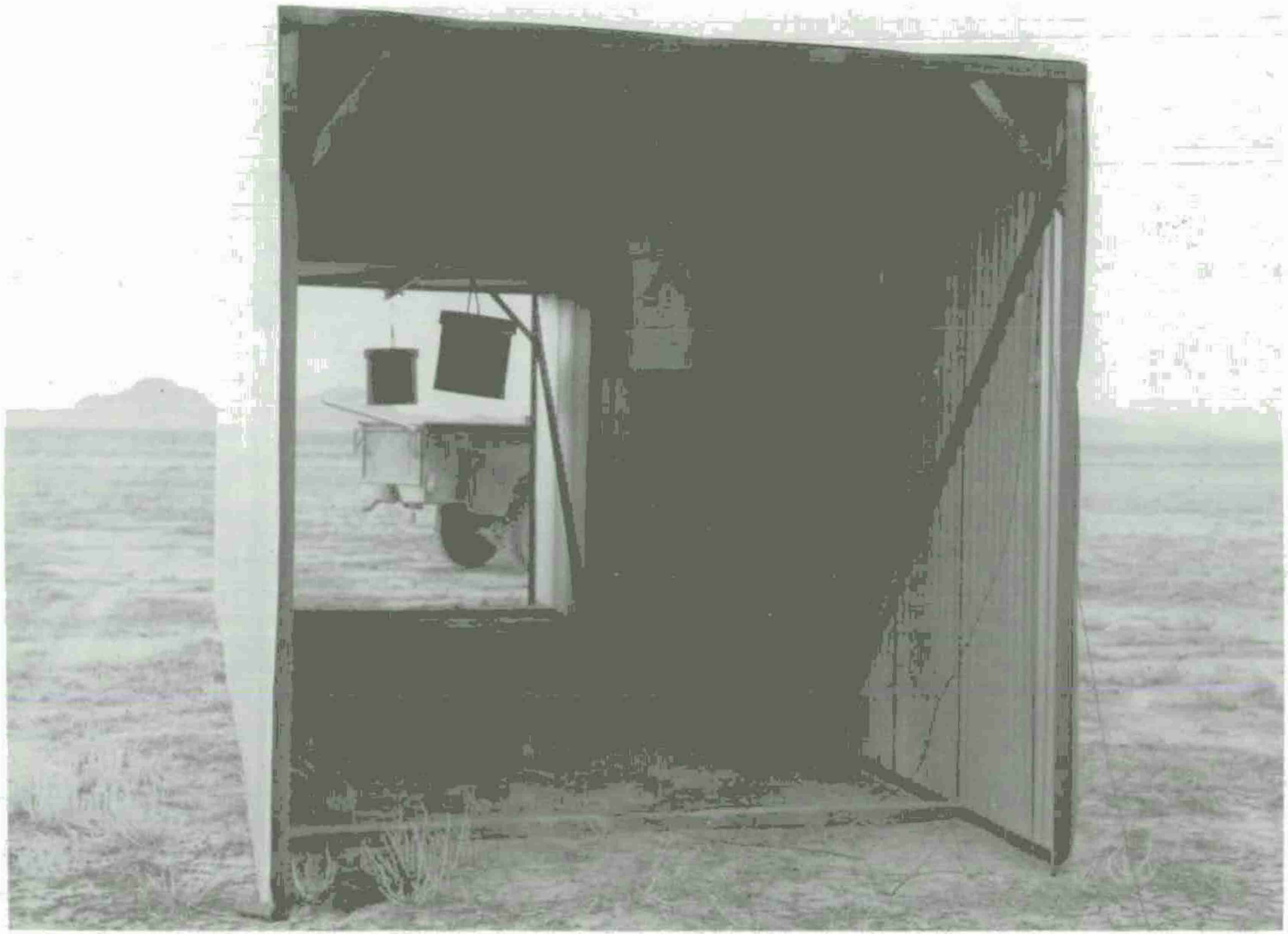

Fig 4 Test setup, 60 lb comp B buckets

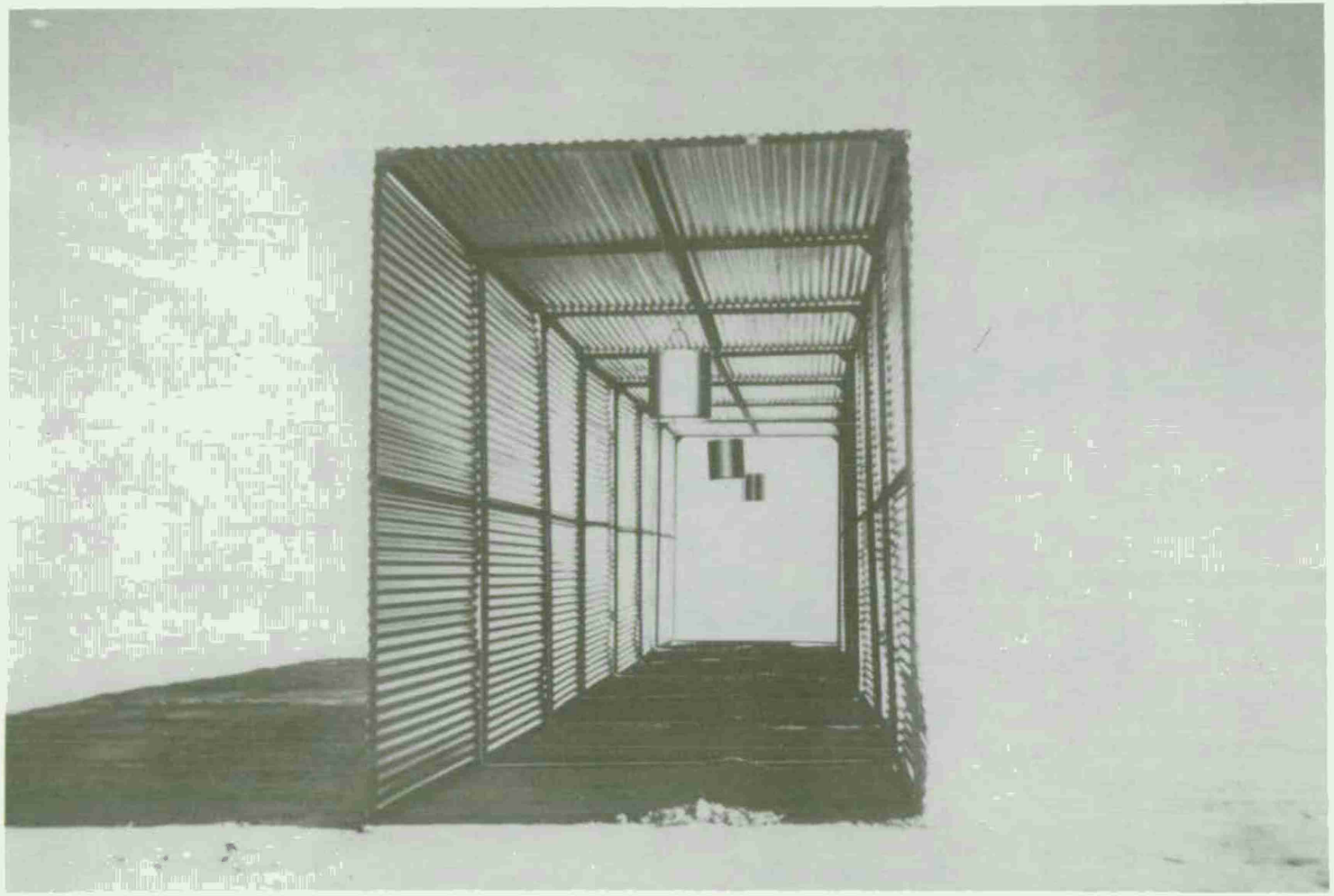

Fig 5 Test setup, comp C4 buckets

Fig 6 Test No. 4, 105 mm M1 comp B projectile

Table 2

Safe separation distance tests, end items

(STORAGE & IN PROCESS)

ITEM	TEST SETUP (ON CONVEYOR)	RESULTS/STATUS
81MM MORTAR a. HE M374 PROJECTILE b. HE M374A2E1 CARTRIDGE	2"x4"x14" ALUM PLT ¼"x6" LEXAN SHIELD ON HOUSING	COMPLETED. 8.8" SAFE DISTANCE ESTABLISHED. REPORT BEING FINALIZED
105MM (M1) PROJECTILE	16 ITEMS/CARRIAGE W & W/O FUNNELS & W & W/O BLAST SHIELDS	IN PROGRESS. INITIAL RESULTS INDICATE EXCESSIVE SAFE DISTANCES
155MM PROJECTILE M107 & M549	SINGLE ITEMS W & W/O FUNNELS & W & W/O BLAST SHIELDS & 4/ CARRIAGE	PRELIM TESTS CONDUCTED. ADDITIONAL TESTS PLANNED
8" PROJECTILE (M106) TNT & COMP B	SINGLE ITEMS	PRELIM TESTS CONDUCTED. ADDITIONAL TESTS PLANNED
155MM PROJECTILE (M107)	24 ITEMS/PALLET	PLANNED

Fig 7 Test result, 60 lb comp B buckets

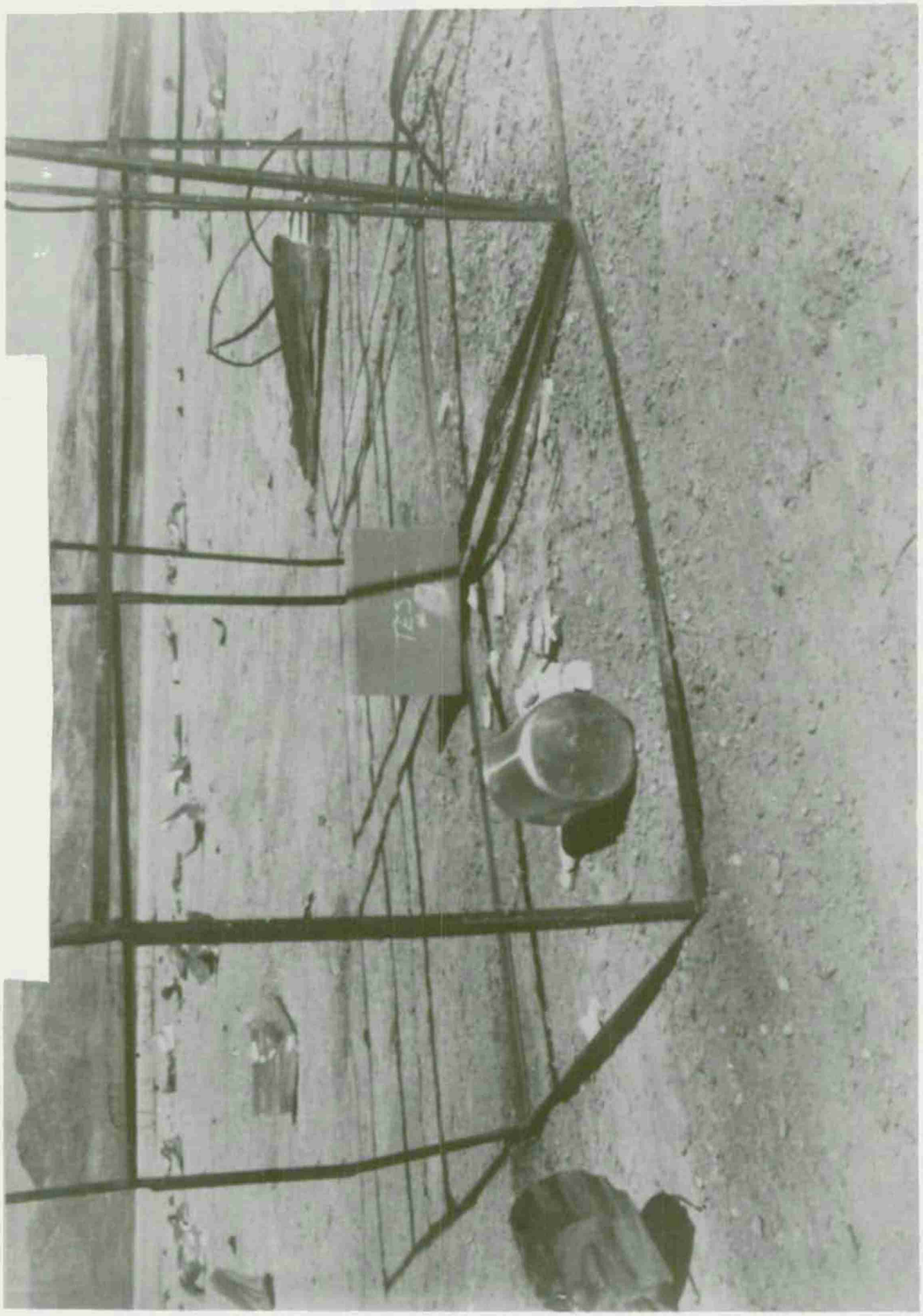

Fig 8 Test result, comp C4 buckets

Table 3

Safe separation distance tests in process explosives

MATERIAL	TEST SETUP	RESULTS/STATUS
COMP B (60 LB BOXES)	ON CONVEYOR IN TUNNEL	COMPLETED. 12' SAFE DISTANCE ESTABLISHED. TR4622 DISTRIBUTED
COMP B (60 LB BUCKETS)	PENDENT CONVEYOR IN TUNNEL	COMPLETED. 12' SAFE DISTANCE ESTABLISHED
COMP C4 a. 35 LB BUCKETS b. 50 LB BUCKETS	PENDENT CONVEYOR IN TUNNEL	COMPLETED { 20' SAFE DISTANCE 25' SAFE DISTANCE
COMP A7 (165 LB TOTE BIN)	ON CONVEYOR IN TUNNEL	IN PROGRESS
COMP B (FLAKE)	ON CONVEYOR	PLANNED

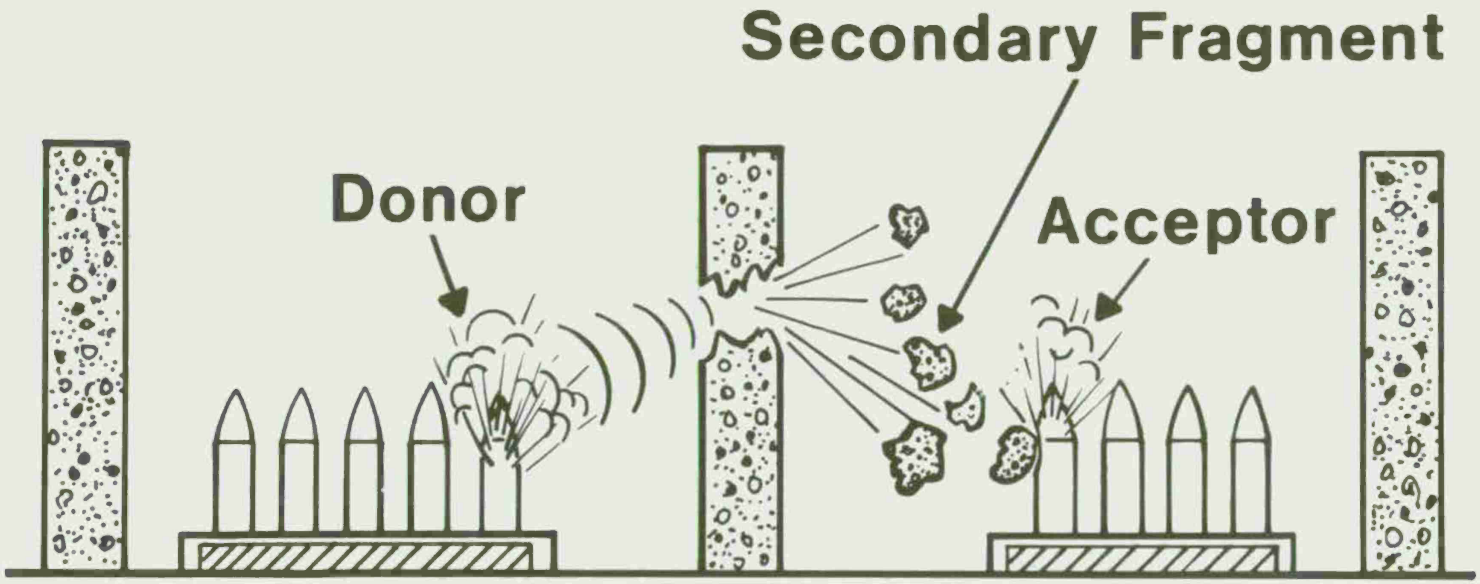

Fig 9 Secondary fragment effect

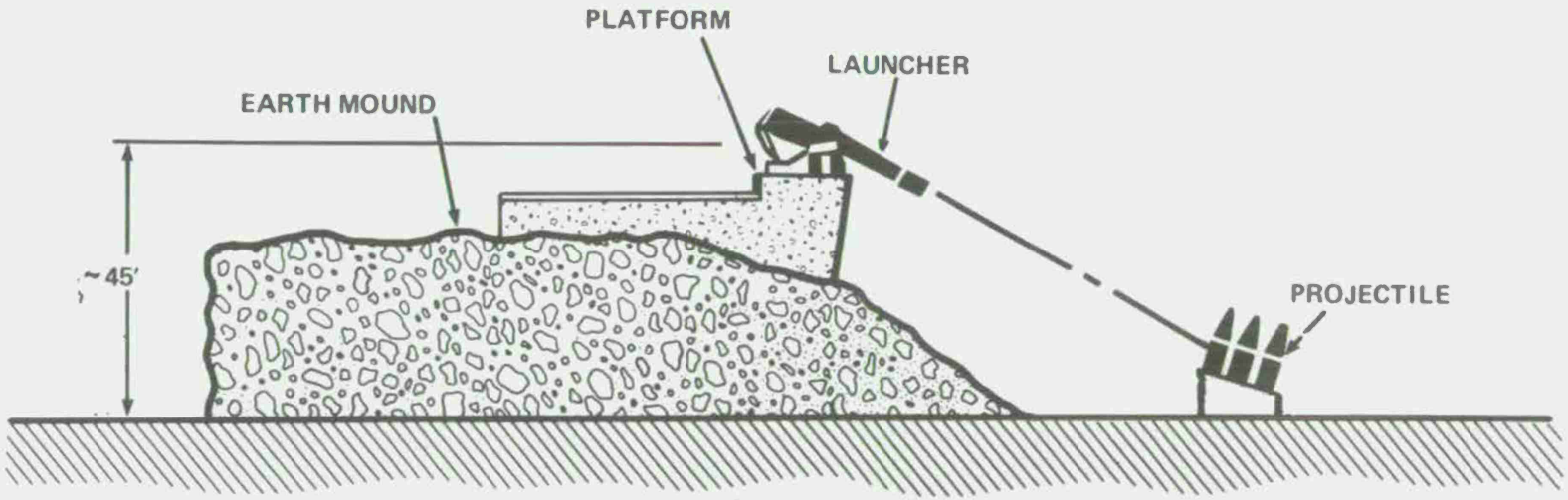

Fig 10 Secondary fragments impact test against 155 mm projectile

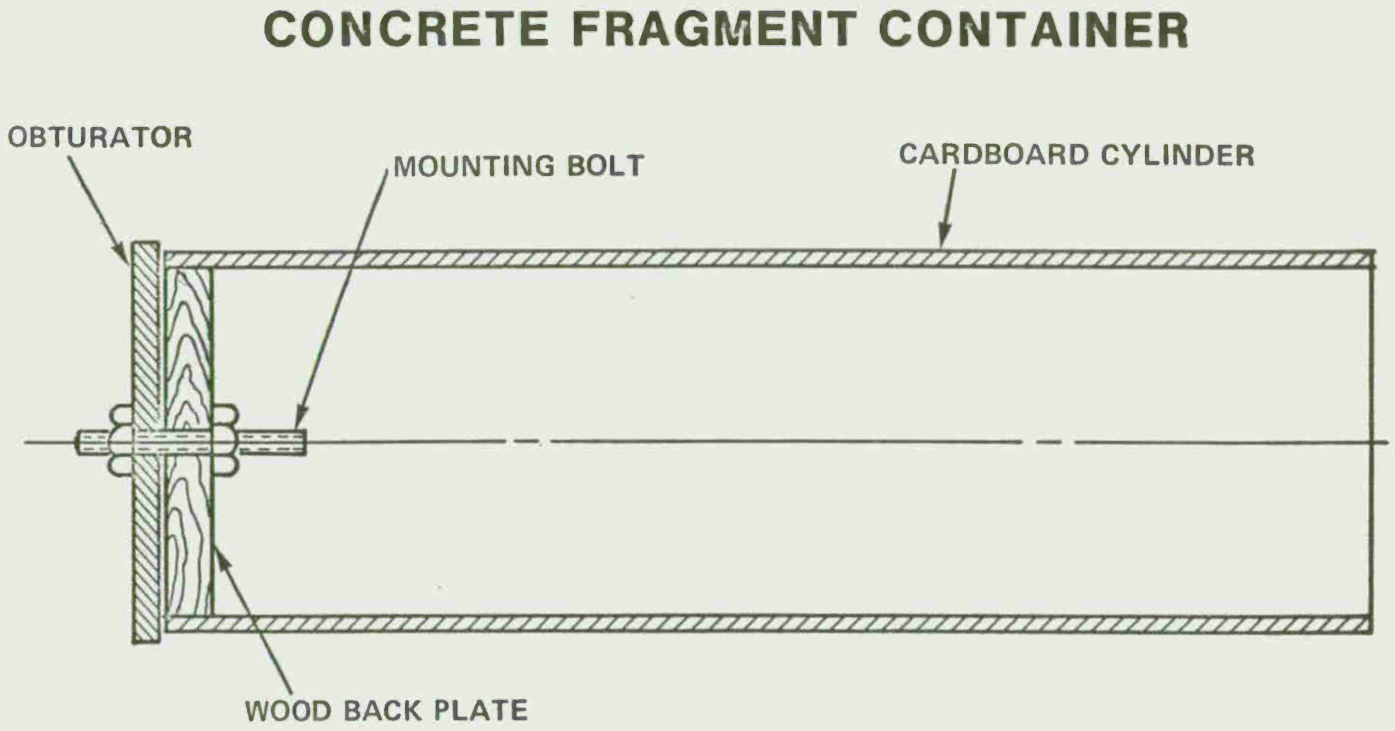

Fig 11 Concrete fragment container

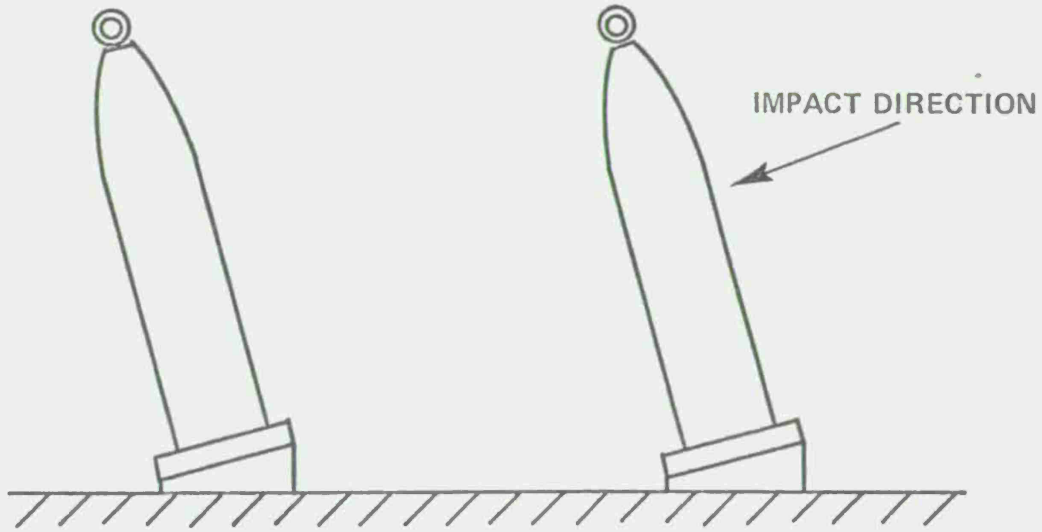

Fig 12 Initial 155 mm projectile configuration

Table 4

155 mm projectile results

Test No.	L/D	Projectile Description Type	Weight (lb	Velocity (fps)	Results
S-1	4	Solid	380	500	Glancing impact - no visible damage
S-2	4	Solid	380	425	No damage
S-3	2	Solid	180	560	No damage
S-4	2	Solid	180	555	Small deformation of projectile case
S-5	2	Solid	188	560	Small deformation of case
S-6	1/2	Solid	55	1170	Deformation of casing
S-7	1/2	Solid	55	1170	Deformation of casing
S-8	4	Solid	380	545	Slight damage
S-9	4	Solid	380	550	Slight damage
R-1	4	Rubble	250	600	Small crack in casing near lifting eye
R-2[a]	4	Rubble	250	540	Slight damage to casing
R-3[a]	2	Rubble	125	675	Slight damage to casing
R-4[a]	2	Rubble	125	680	Sheared off the lifting ring
R-5[a]	3	Rubble	190	525	Slight damage to casing
R-6[a]	3	Rubble	190	540	Sheared off the eyebolt
R-7[a]	3	Rubble	190	560	Slight damage to casing
R-8[a]	3	Rubble	190	570	Slight damage to casing
S-10[a]	5	Solid	480	350	Dented casing
S-11[a]	5	Solid	480	360	Sheared off the eyebolt
S-12[a]	5	Solid	480	350	Sheared off the eyebolt

[a]Witness plate placed on concrete pad

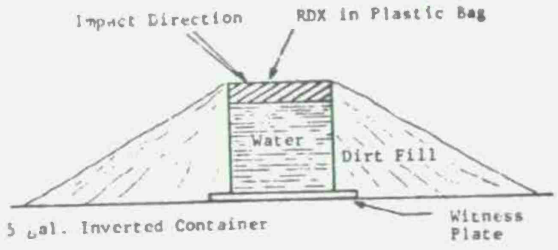

15 lb RDX

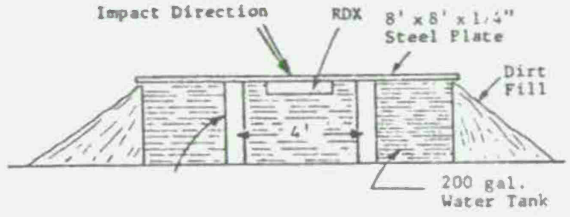

23 lb RDX

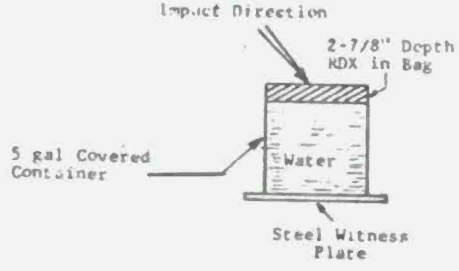

15 lb RDX

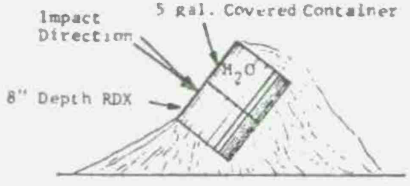

35.5 lb RDX

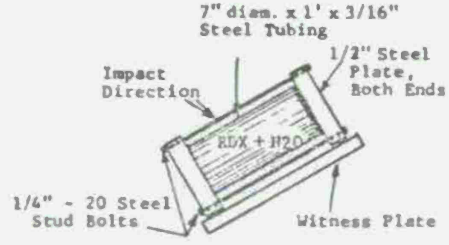

17 lb RDX
17.25 lb RDX
17 lb RDX
18 lb RDX
17 lb RDX

Fig 13 RDX slurry experiment configurations

Table 5

RDX slurry results

Test No.	Projectile Description L/D	Type	Weight (lb)	Velocity (fps)	Results
X-1	5	Solid	480	370	No reaction. Tank split at riveted seams. RDX scattered over area
X-2	5	Solid	480	370	No reaction. Canister split at seam. Bottom found in crater
X-3	0.5	Solid	55	1220	No reaction. Top and bottom of can in good condition. RDX found in area posttest
X-4	0.5	Solid	55	1270	No reaction. RDX found in area after test
X-5	0.5	Solid	55	1270	No reaction. RDX in area posttest. Canister was split
X-6	0.5	Solid	55		No reaction. RDX scattered about area
X-7	5	Solid	480	470	No reaction. RDX strewn over area. Two feet of projectile left in one piece
X-8	0.5	Solid	55	1200	Miss. Nicked lower corner. Pipe found in area after test
X-9	0.5	Solid	55	1230	No reaction. Pipe split apart. Most of pipe recovered in test area. Projectile completely smashed
X-10	5	Solid	480	470	No reaction. Pipe split apart. Recovered two pieces of pipe with RDX trapped between them. 18 inches of projectile recovered. RDX scattered about area
X-11	5	Solid	480	200	No reaction. RDX scattered over area. 3 feet of projectile left in one piece
X-12	0.5	Solid	55	500	No reaction. Recovered tube flattened out. RDX scattered over area and on tube
X-13	5	Solid	480	200	No reaction. Hit top of tube. Most of tube found in one piece
X-14		Rubble	135	850	No reaction. Some bolts and nuts found in hole. RDX scattered about area

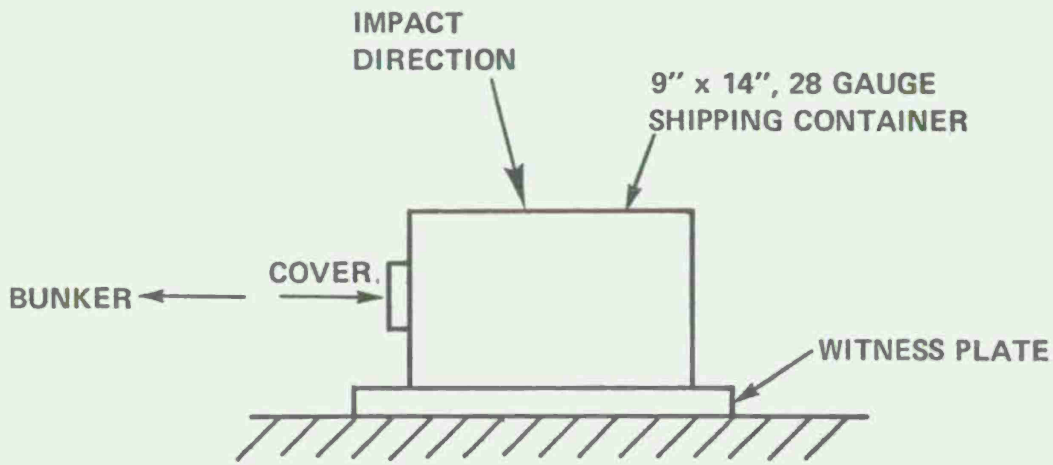

Fig 14 Black powder experiment configuration

Table 6

Black powder results

Test No.	Projectile Description L/D	Type	Weight (lbs)	Velocity (fps)	Results
BP-1[a]	0.5	Solid	55	1055	Reaction. Small fragments of container found
BP-2[a]	0.5	Solid	55	621	Reaction. Recovered most of container in three pieces
BP-3	0.5	Solid	55	606	Reaction. Container destroyed. Pieces of container recovered
BP-4	0.5	Solid	55	377	No reaction. Recovered container in four pieces. Black powder strewn over area. Projectile in one piece
BP-5	0.5	Solid	55	538	Reaction. Most of container recovered in one piece. Projectile broken up
BP-6	0.5	Solid	55	514	Reaction. Container split at seams. Projectile broken up
BP-7	0.5	Solid	55	434	No reaction. Container recovered. Black powder strewn about
BP-8	5	Solid	480	185	Reaction. Small pieces of container recovered Projectile broken into three pieces. Impact end slightly damaged. Projectile fragments found in area
BP-9	5	Solid	480	114	Reaction. Fireball. Most of container found in hole after test. Projectile found almost intact
BP-10	5	Solid	480	100	No reaction. Impact with container doubtful
BP-11	5	Solid	480	100	No reaction. Container impaled on end of projectile. Black powder strewn about area

[a]Class 6, all other experiments are for Class 1 Black Powder

Table 6 (Cont'd)

Test No.	Projectile Description L/D	Type	Weight (lbs)	Velocity (fps)	Results
BP-12	2	Solid	175	187	Slow burn. Container split apart at seams. Burn marks on projectile cover
BP-13	0.5	Solid	55	365	No reaction. Container recovered in part with top torn away. No visible damage to concrete projectile
BP-14	2	Solid	190	150	Reaction. Container recovered in five pieces Projectile in one piece
BP-15	2	Solid	205	125	No reaction. Projectile hit end of container. Black powder crushed inside container. Projectile broken into many small fragments
BP-16	3	Solid	300	154	No reaction. Container split apart. Black powder strewn about area. Projectile not broken
BP-17	3	Solid	300	201	Reaction. Parts of container found in area posttest. Concrete projectile broken up
BP-18	1	Solid	100	336	Reaction. Fragments of container found in area. Projectile found basically in one piece
BP-19	0.5	Rubble	40	266	Reaction. Container split apart and found in area posttest. Black powder found in area. Rubble strewn about
BP-20	1	Solid	110	173	No reaction. Black powder strewn over area. Projectile in one piece

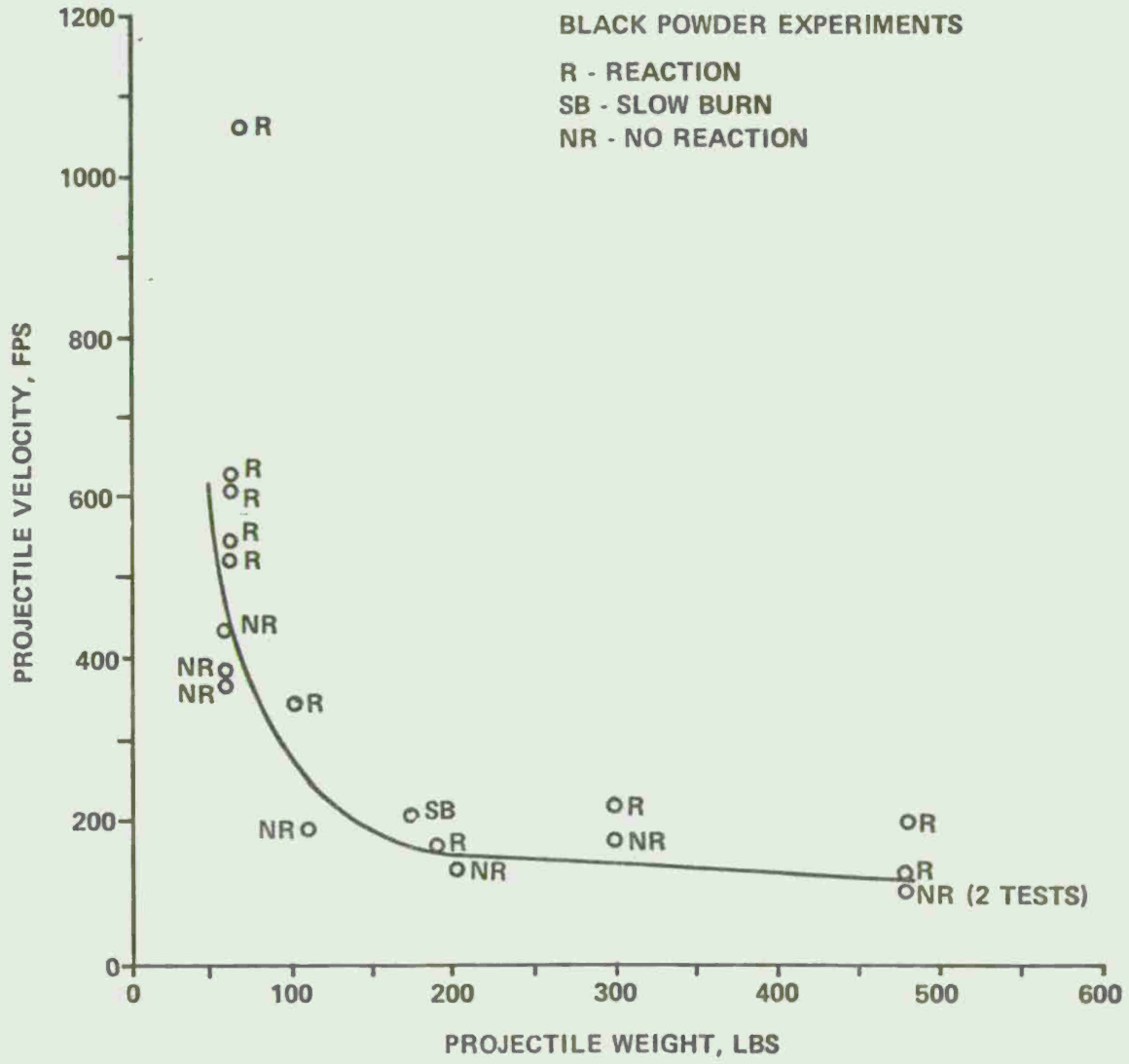

Fig 15 Go/no-go regions as a function of projectile velocity and projectile weight

- 155MM PROJECTILES WITH FUNNEL (SIMULATING COOLING BAY)
- SIMULATED MELT KETTLE-COMP B & TNT
- 105MM PROJECTILES
- 81MM PROJECTILE

END ITEM & IN-PROCESS

Fig 16 Future work (secondary fragments)

TNT EQUIVALENCY INVESTIGATIONS

H. S. Napadensky
IIT Research Institute, Chicago, Illinois

L. Jablansky
Manufacturing Technology Directorate
Picatinny Arsenal, Dover, New Jersey

ABSTRACT

As part of the Army's plant modernization program, an effort is currently under way to generate airblast data for explosives and propellants. The purpose is to provide realistic data in support of structural designs. In this work, peak pressure, impulse, and other blast wave characteristics are compared to similar parameters obtained from a hemispherical surface burst of TNT. The results are reduced to a TNT equivalency value, which is defined as the weight ratio of TNT to test-material for given output conditions. Various factors influence the magnitude of TNT equivalency. These include: charge geometry, critical mass/dimensions, confinement, distance from charge burst, and method of initiation. This paper discusses the effects of the different variables from experimental and analytical viewpoints. It also introduces new inferences about high energy materials drawn from the shapes of TNT equivalency curves, and discusses initiation sources in terms of critical energy considerations.

1. INTRODUCTION

The airblast parameters such as peak overpressure, positive impulse, positive phase duration, etc, are being determined for explosives, propellants, and pyrotechnics in their in-process and final product forms. The data obtained from these experimental investigations are being applied, by the Manufacturing Technology Directorate of Picatinny Arsenal, to designs of new manufacturing facilities as part of the Army's Ammunition Plant Modernization Program.

If building construction and quantity-distance siting are based on evaluations of the maximum airblast output that an energetic material is capable of achieving, then the cost of new manufacturing facilities may be

reduced and/or safety can be improved. When building construction and siting are based on maximum output, changes in the manufacturing process can be implemented or new equipment may be used without concern that the facility would not survive an accidental explosion.

The measured airblast parameters for a material of interest is often viewed on a relative basis; that is, it is compared with the airblast produced by a hemisphere or sphere of TNT. The convention that is most frequently used in defining TNT equivalency is that it is the ratio of the weight of a hemisphere of TNT to the weight of the test material that will give the same peak pressure, or impulse, at the same distance. The ratio is multiplied by 100 so that the TNT equivalency is expressed as a percentage.* The reason that TNT equivalency is most often defined with respect to a hemispherical surface burst, as the reference shape, is because the most extensively documented data on the blast wave parameters for TNT have been obtained for the hemispherical shape (Ref 1).

It is well established for explosives that the values of the airblast parameters at a given distance will depend upon charge geometries. It is occasionally suggested that the TNT equivalency should be defined, or referenced, with respect to the same geometry as the test material (i.e. a propellant cylinder of L/D=1 should be compared with a TNT cylinder of L/D=1, etc). However, this suggestion is not practical for investigations in support of facilities modernization because, it would require that TNT be evaluated in geometric shapes that are the same as that of the test material (hoppers, pipes, etc), or that all tests be done on spheres or hemispheres of the test material. Either suggestion is impractical for at least two reasons: it would be too costly to evaluate both TNT and the test material in the various shapes in which in-process materials are found; and secondly, if only hemispheres were evaluated, it would not allow us to take into account the significant effect of charge geometry on the amplitude of the blast wave.

In order for meaningful comparisons to be made between the material being tested and TNT, the blast wave shapes must be similar (Fig 1). It is not necessary that rigorous requirements of similarity (dynamic and kinematic) be met; only that a sharp rise in pressure and exponential decay

*For example, suppose a 1 lb TNT hemisphere gives the same peak pressure at a given distance as a 10 lb cylindrical propellant charge. The TNT equivalency of the propellant is considered to be 10 percent, 1/10 x 100, at that distance.

of the wave be obtained. Pressure-distance and impulse-distance curves for the test sample may or may not be parallel to the TNT curve. Whether or not they are parallel will depend on composition, which depends upon energy density, oxygen balance, and other factors. In any event, much can be gleaned from the curve shapes derived from such studies, and these will be analyzed with respect to the TNT equivalency phenomenon.

This paper is primarily concerned with a discussion of the factors that affect the blast output. Results of experiments on a variety of energetic materials will be used to illustrate how variables such as charge size, geometry, confinement, initiation method, etc, influence the blast wave, and hence, TNT equivalency. Based on results of experiments, we will also show that materials can be divided into two broad categories which we call high explosives and marginal explosives. The category into which a material is placed is determined by the shape of its TNT equivalency curve. In other words, it depends upon the extent to which the pressure-distance and impulse-distance curves for the test material are parallel to or deviate from the TNT pressure and impulse curves. An understanding of the factors affecting airblast output is important in planning experiments, interpreting their results, and in the intelligent use of experimental data.

2. FACTORS AFFECTING BLAST OUTPUT

For all materials, the airblast output decreases with an increase in distance.* The degree or extent of that decrement depends primarily upon two factors. One has to do with kinetics of the reaction (a characteristic of the explosive or propellant composition), the other concerns charge geometry. These, and other conditions which affect the decay of the blast wave with distance, will be discussed in the following sections.

2.1 Properties of the Material

If the pressure vs scaled distance and scaled impulse vs scaled distance curves for TNT and the test material were parallel, then a single value for TNT pressure equivalency and a single value for TNT impulse equivalency would exist. However, the curves for the two materials would be parallel only if the blast waves were completely similar (i.e. met the rigorous definitions of kinematic and dynamic similarity). If TNT and the

*There is evidence to the contrary, for impulses at scaled distances less than 2.5 (see Ref 1).

test material had the same geometry, and approximately the same energy density (energy release per unit volume), and the same oxygen balance, we would expect complete similarity of the blast wave and the curves would be parallel.

However, in the applications discussed in this paper, involving primary explosives, secondary explosives, propellants and pyrotechnics, the materials have widely different energy densities. The overpressures, produced by materials of lower energy densities than TNT, are lower close to the source and higher at large distances. The opposite is true for the higher energy density materials. They have higher initial overpressures, but lower overpressures at large distances from the charge. This is primarily because energy is dissipated at a much higher rate in shock fronts of higher overpressure.

The oxygen balance of the material being evaluated is also important. If a composition has a negative oxygen balance, i.e. deficient in oxygen, the detonation products can react with the oxygen in the air, in a process called afterburning which results in a greater blast effect.

These effects are illustrated in Figure 2, which shows the results of tests on nitroglycerin (Ref 2) and N-5 paste propellant (Ref 3) containing 10 percent process water. Both materials are in a cylindrical container, L/D=1. The energy density, as measured by the heat of detonation, is 1590 cal/gm for nitroglycerin and for N-5 propellant it is approximately 1200 cal/gm. Thus, in comparing nitroglycerin with N-5 propellant, we see that close to the charge the pressure is much higher for the material with the higher heat of detonation, but as the distance from the charge increases, the differences between the two materials decreases. At larger scaled distances than shown here, we would expect the N-5 curve to approach and finally cross the nitroglycerin curve.

2.2 Geometric Effects

It is well established that for high explosives, (Ref 4, 5, 6) the blast wave shape and the airblast parameters of nonspherical charges differ significantly from spherical charges. These differences are most pronounced close to the charge. As the distance from the charge increases, the blast wave tends toward sphericity and the blast wave parameters approach that of a point source.

The geometric shapes evaluated in our investigations were shapes that simulated actual process or shipping container configurations. Hence, no spherical or hemispherical configurations were evaluated (with the exception of a single test on 4500 lb of Black Powder (Ref 7) and the routine calibration tests on hemispheres of C4 explosive). The effect of charge geometry on the peak overpressure can be illustrated by considering test results for nitroglycerin, tested in cylindrical containers of L/D=1, with the peak pressure distance curve for a hemisphere of TNT (Fig 3). The difference in the heat of detonation between TNT and nitroglycerin is about 13 percent (1400 and 1590 cal/gm, respectively). The differences in the two curves are attributable to geometry.

Another comparison can be made between N-5 propellant and M-1 propellant (Fig 4, 5). The M-1 propellant is packaged as the M-1 propelling charge (Ref 8) in a cylindrical container, L/D=6, while the N-5 has an L/D=1. The heat of detonation of M-1 propellant is almost identical to that of N-5 propellant. Thus, we should only expect to see the effects of geometry. Close to the explosions, the pressures are higher for L/D=6 than the L/D=1 as expected. Other work done on the effect of geometry on blast output (Ref 4) shows that close to the charge an increase in L/D results in an increase in peak pressure. There is some evidence (Ref 4) that this effect peaks at L/D=6.

2.3 Confinement Effects

The degree of confinement, as characterized by the weight ratio of the explosive to that of the confining material, is an important factor that can affect the blast output. For high explosives, it has been shown that a very small amount of confinement results in a higher blast output over that of a bare high explosive charge (Ref 9). This may be due to some spalling of the bare charge from the precursor shock wave. As the amount of confinement increases, the blast output decreases below that obtained with a bare charge. This effect of confinement is somewhat different for materials that are not high explosive. In particular, Black Powder showed that as confinement increased the blast output increased. Figure 6 shows qualitatively how the confinement affects the peak pressure. In all experiments, particular attention is paid to ensuring that the amount of confinement is properly scaled so that the experiment simulates the actual system that is modelled.

2.4 Effect of Mass and Critical Dimension

In order to determine maximum airblast output, the dimensions of the test material must be above some critical size. If the size is too small, a detonation will not propagate. The kinetics of the reaction is a dominant factor in establishing the critical size of an energetic material. Because kinetic data is not available for most of the materials of interest, experimental approaches must be used. For high explosives, there is no problem in testing above its critical mass (and dimensions) since these values are quite small. That is, detonation of high explosives can occur in charges weighing grams or less, and sizes that are smaller than a centimeter. Propellants and pyrotechnics generally have large critical dimensions, from several inches in diameter to many feet.* Thus it is important to ensure that tests are carried out above the critical diameter and/or mass. This is accomplished in our studies by testing at several different charge sizes to assess the dimensions above which the results are independent of charge size. In this way, it is experimentally determined if the results on a small scale can be applied to full scale systems. An example of the dependence of TNT pressure and impulse equivalency on the weight of Black Powder is shown in Figure 7. Other materials also exhibit similar behavior. Thus, as a necessary part of TNT equivalency studies, we must determine the critical diameter or mass of the material for the type of confinement that exists under the process conditions that are being simulated. To ascertain if the critical diameter and/or mass have been achieved, it is necessary to: (a) determine the size scaling relationships experimentally, i.e., to find the weight beyond which the curve for TNT equivalency versus weight (at selected distances) is flat, and (b) determine if the value of the experimentally determined equivalency is consistent with the order of magnitude that is expected based on the heat of detonation and oxygen balance of the material. The latter two parameters are only indicators of what the magnitude of blast output should be, i.e., "high" or "low." They are insufficient in themselves to be used reliably as a quantitative predictive tool.

Scaling techniques of the sort briefly described above must be used, since the cost of full scale testing for every material would be prohibitive. However, if scaled tests (weights of less than 100 lb) show low or no blast output, then, depending upon the physical variables, tests may have to be carried out for sizes that may approach full scale to insure that maximum output has been reached.

*The critical diameter of a typical composite solid propellant is between 60 and 72 in. (Ref 10).

2.5 Initiation Method

Secondary high explosives are readily detonated with small booster explosives. Primary explosives, being more sensitive, can be detonated by means of a hot wire, a blasting cap, or a detonator. However, propellants and pyrotechnics are most readily or conveniently driven to a detonation by means of an explosive booster whose detonation pressure is higher than the detonation pressure of the test material. In this work, we do not attempt to determine the minimum stimulus required for detonation because this involves sensitivity investigation. We are only concerned with whether or not the initiator is adequate to cause the material to achieve its maximum possible energy release. Of course, the initiator must not be so large that it makes a significant contribution to the airblast output. The contribution of the booster is, nevertheless, taken into account in the calculations of equivalency. For many materials, an increase in airblast output may be achieved by increasing the booster size. Thus, several size boosters are usually evaluated in a test program to ensure that maximum output is obtained. An example of this is shown in Figure 8, for M-1 propellant, which shows the effect of booster size on TNT equivalency.

Initiation methods other than using high explosive boosters can be used to initiate a detonation. This subject will be discussed in detail in Section 3.

3. INFLUENCES AND INTERPRETATIONS OF BLAST DATA

3.1 Initiation Method and Critical Initiation Energy

Under manufacturing plant, storage, and transportation conditions, the most likely initial initiation stimulus is a heat source, causing burning of the material to occur. The fire or deflagration reaction may transit to a detonation. The conditions under which this can occur depend upon many factors, including the mass of material, the amount of confinement, its initial temperature, the rate of temperature rise, the details of the ignition source, and the way in which the deflagration spreads. It is much more expensive to carry out experiments where a transition to a detonation can be achieved, than it is to initiate a detonation by means of a shock wave from a booster explosive. Although a detonation that occurs as a result of the deflagration to detonation transition is a more realistic situation, the end result, when compared to a booster explosive initiation, is the same, i.e., detonation of the material.

The objective of TNT equivalency studies is to determine the maximum output; it is not essential to determine all the ways in which a detonation can occur. It is sufficient to show that a certain magnitude reaction can be achieved.

There are several factors that affect the initiation of an energetic material by a shock wave. They are: the peak pressure of the disturbance, its duration, and the surface area of the initiation source that has a direct action on the test material. The shock wave can be produced by a high explosive booster, by impact of a foil, or by a thick plate impact. If the foil and plate are of the same material and velocity, then the pressure at the acceptor face is the same, but the duration is much smaller for the foil than it is for the thick plate. Similarly, we can increase the duration of the shock wave produced by an explosive booster, by increasing the weight of the booster, where the booster is in contact with the acceptor material. It has been shown for three different explosive materials, using test results of a number of investigations, that the shock sensitivity of an explosive can be characterized by a critical energy for initiation, i.e. peak pressure and duration of pulse (Ref 11). Conceptually, this relationship is seen in Figure 9. This curve has been well defined for the region between no reaction and ignition threshold, curve B. In Figure 9 we see that in the region between curves A and B there is a continuum of ever-increasing reaction intensity levels, as we increase the pulse width for a given pressure.

In our work, the peak pressure of the donor charge was constant (C4 boosters were used in the majority of the tests). The durations, or pulse widths, were increased by using a range of booster weights. Figure 8 shows the TNT equivalency for a number of booster sizes. As booster size (pulse duration) increases, the TNT equivalency or reaction intensity level increases, until a large enough booster is used that no longer produces an increase in blast output in the test material.

The same results could have been obtained by using a booster with a lower peak pressure, but longer pulse duration. By using lower pressure boosters or impact of flyer plates, we would still be able to map out the possible reaction intensity levels that the test materials achieve. This would be the same as already achieved with C4 boosters.

In a study of pyrotechnic materials (Ref 12), we achieved a wide range of pressure and pulse widths (durations) by using the gaseous products of the detonation of an explosive booster to fill a large, heavily

confined air cavity (Fig 10), adjacent to the pyrotechnic mix (50 lb). Essentially, the sequence of events was as follows. The explosive is detonated in a few microseconds and the reaction products expand into the air cavity. The resulting transient pressure rapidly decays and a relatively quiescent state is achieved in the air cavity. The initial pressure within the cavity will depend upon the volume of the cavity and the quantity and type of explosive used. A series of gas dynamic calculations were performed to determine the test parameters that would produce pulse durations, of the order of a millisecond, using explosives weighing approximately one pound. The air cavity experiments gave at least as large an airblast output as experiments where the booster was placed inside the pyrotechnic charge. The same airblast output (TNT equivalency) was also achieved when the explosive booster was separated from the pyrotechnic charge by an air space (Fig 11). In these tests the booster explosive was supported by a heavy walled cardboard tube, which provided the stand-off distance, as well as a means for preventing the booster explosion's gaseous products from venting to the atmosphere at the time of detonation. Thus, in the above mentioned air gap experiments, the peak pressure was lower and duration of the shock wave was greater then if the booster explosive were inside the pyrotechnic material; yet, the airblast output from pyrotechnics initiated by these two methods was the same.

3.2 Categorizing Energetic Materials

On the basis of experimental data on a variety of explosives, propellants, and pyrotechnics, we have observed that these materials fall into two categories which can be described in terms of the shapes of their TNT equivalency curves. The two categories are characterized as marginal explosives and high explosives. The shape of the equivalency-distance curves for materials that we call marginal explosives can be seen in Figure 12. The TNT equivalency increases with scaled distance and reaches a maximum at a scaled distance in the neighborhood of 10 ft/lb and then decreases. In these cases, the maximum value of TNT equivalency is well below 100 percent. Materials that we have evaluated thus far that can be categorized as marginal explosives are: an in-process form of N-5 propellant containing 30 percent process water, black powder, guanidine nitrate (less than 150 lb charges), tetracene, lead azide and two illuminant pyrotechnic compositions.

This listing contains a diverse range of compositions and it is necessary to remember that energetic materials should be viewed in terms of both their sensitivity and explosive output. A material such as lead

azide is very sensitive, but has a low explosive output. On the other hand, TNT is a relatively insensitive composition that has a relatively high explosive output.

Materials that we classify as high explosives have TNT equivalency vs distance curves that decrease with distance, or are constant with distance (depending upon factors such as charge geometry). Materials that we have evaluated that fall into the category of materials that behave like high explosives, in addition to the secondary high explosives, are M-1 propellant, N-5 paste propellant with 10 percent process water, M-30 propellant, and lead styphnate. Typical equivalency curves are shown in Figure 5.

4. CONCLUSIONS

We have shown in this paper that the airblast output and the TNT equivalency of explosives, propellants and pyrotechnic materials depend upon many factors. In order to design meaningful experiments and for the resulting data to be intelligently applied, it is important that the many factors and parameters that affect the airblast be recognized, and that the data be used in the context in which they were derived. In line with this, it would seem reasonable to assign a more descriptive term for TNT equivalency which would more suitably reflect the influence of these variables and would be more useful to the engineer for structural design purposes. Such a term could be designated as "TNT Equivalency Profile" and would constitute a family of curves showing Impulse and Pressure Equivalency versus Scaled Distance, as well as Pressure versus Time and Distance for various systems.

REFERENCES

1. Kingery, C.N., *Airblast Parameters Versus Distance for Hemispherical Surface Bursts,* BRL Report No. 1344 (Sep 1966)

2. Swatosh, J.J. and Napadensky, H.S., *TNT Equivalency of Nitroglycerin,* IITRI Final Report J6312 (Sep 1973)

3. Swatosh, J.J. and Napadensky, H.S., *TNT Equivalence of N-5 Slurry and Paste,* IITRI Report J6278 for Badger Army Ammunition Plant (Sep 1972)

4. Wisotski, J. and Snyer, W.H., *Characteristics of Blast Waves Obtained from Cylindrical High Explosive Charges,* DRI-2286, AD367625 (Nov 1965)

5. Stoner, R.G. and Bleakney, W., "The Attenuation of Spherical Shock Waves in Air," J. Appl. Physics 19, p 670-678 (1948)

6. Adams, C.L., et al., *Comparisons of Blast from Explosive Charges of Different Shapes,* BRL-681 (Jan 1949)

7. Napadensky, H.S. and Swatosh, J.J., *TNT Equivalency of Large Charges of Black Powder,* IITRI Final Report J6289-4 (Feb 1974)

8. Napadensky, H.S. and Swatosh, J.J., *Explosive Hazards Classification of the M1 Propelling Charge in its Container I II,* IITRI Report J6265-2 for Indiana Army Ammunition Plant (Apr 3, 1972)

9. Filler, W.S., *The Effect of a Case on Airblast Measurements, Part 1: Friable Inert Cases,* NOLTR 74-62 (Apr 9, 1974)

10. Elwell, R.B., et al., *Solid Propellant Explosive Test Program - Project SOPHY I II,* AFRPL-TR-67-211 (Aug 1967)

11. Walker, R.E. and Wasley, R.J., "Critical Energy for Shock Initiation of Heterogeneous Explosives," Explosivstoffe 1 (1969)

12. Napadensky, H.S., et al., *TNT Equivalency of Three Pyrotechnic Compositions,* Picatinny Arsenal Technical Report 4628 (June 1974)

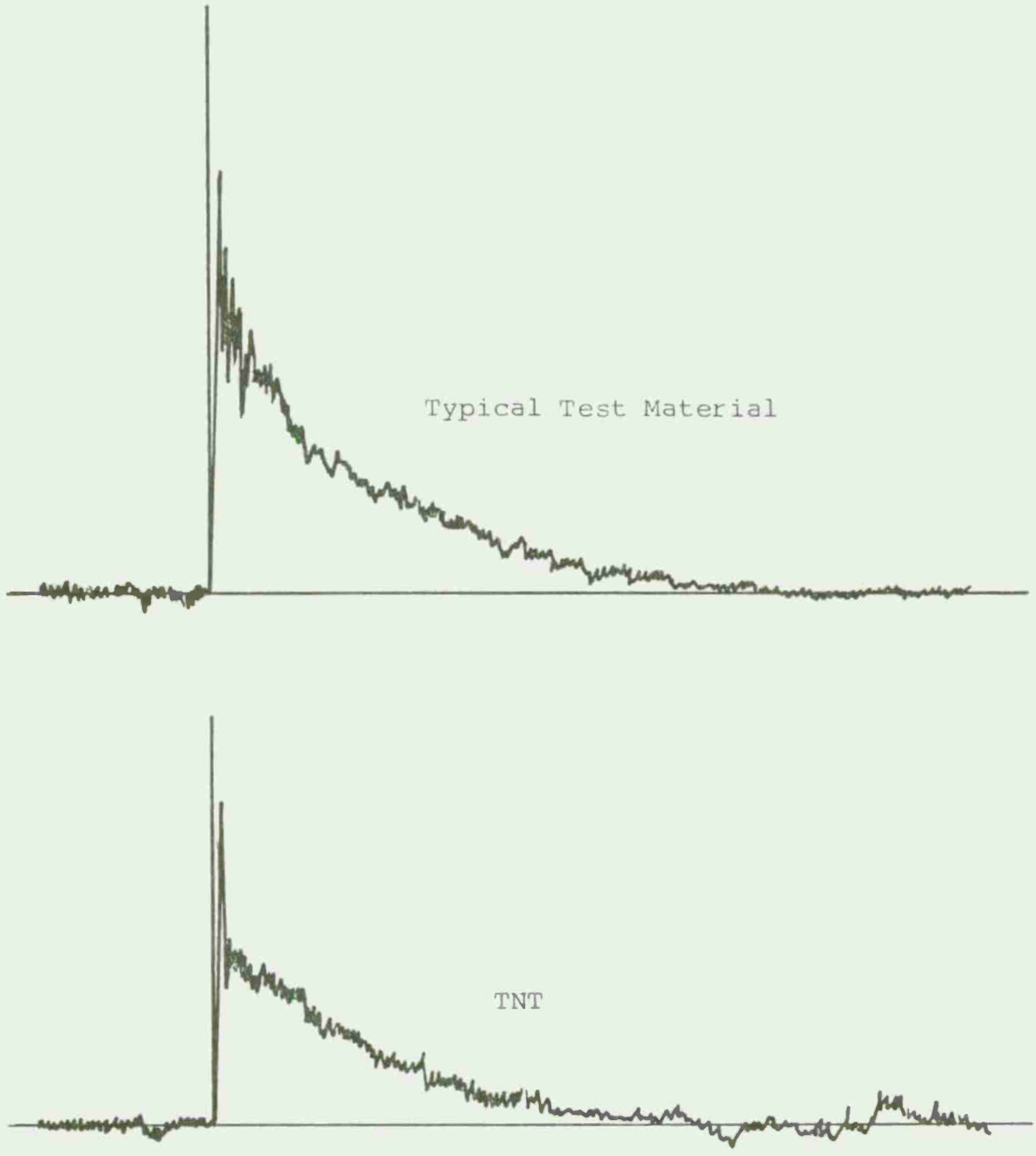

Fig 1 Pressure-time records

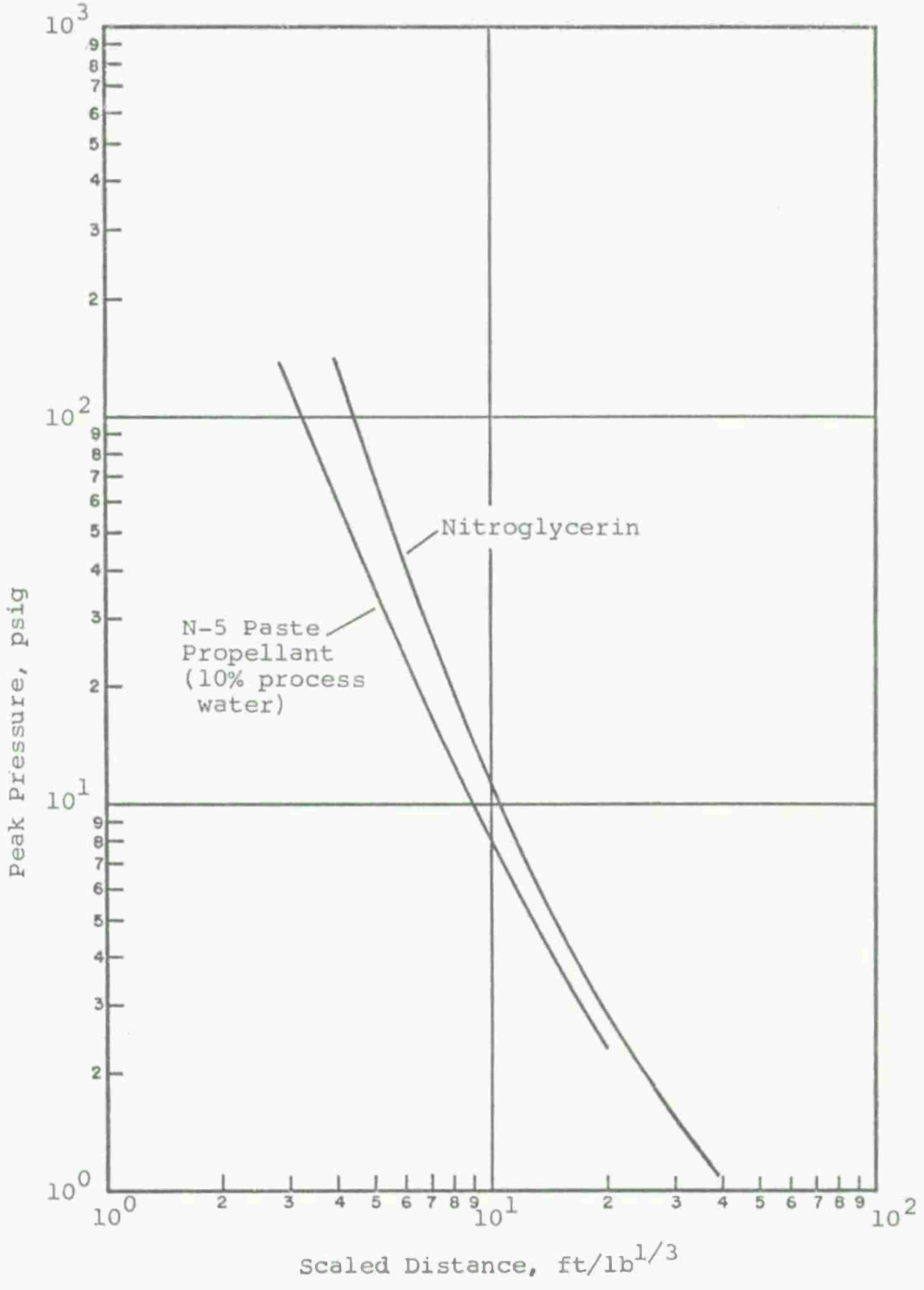

Fig 2 Blast output comparison, effect of energy density

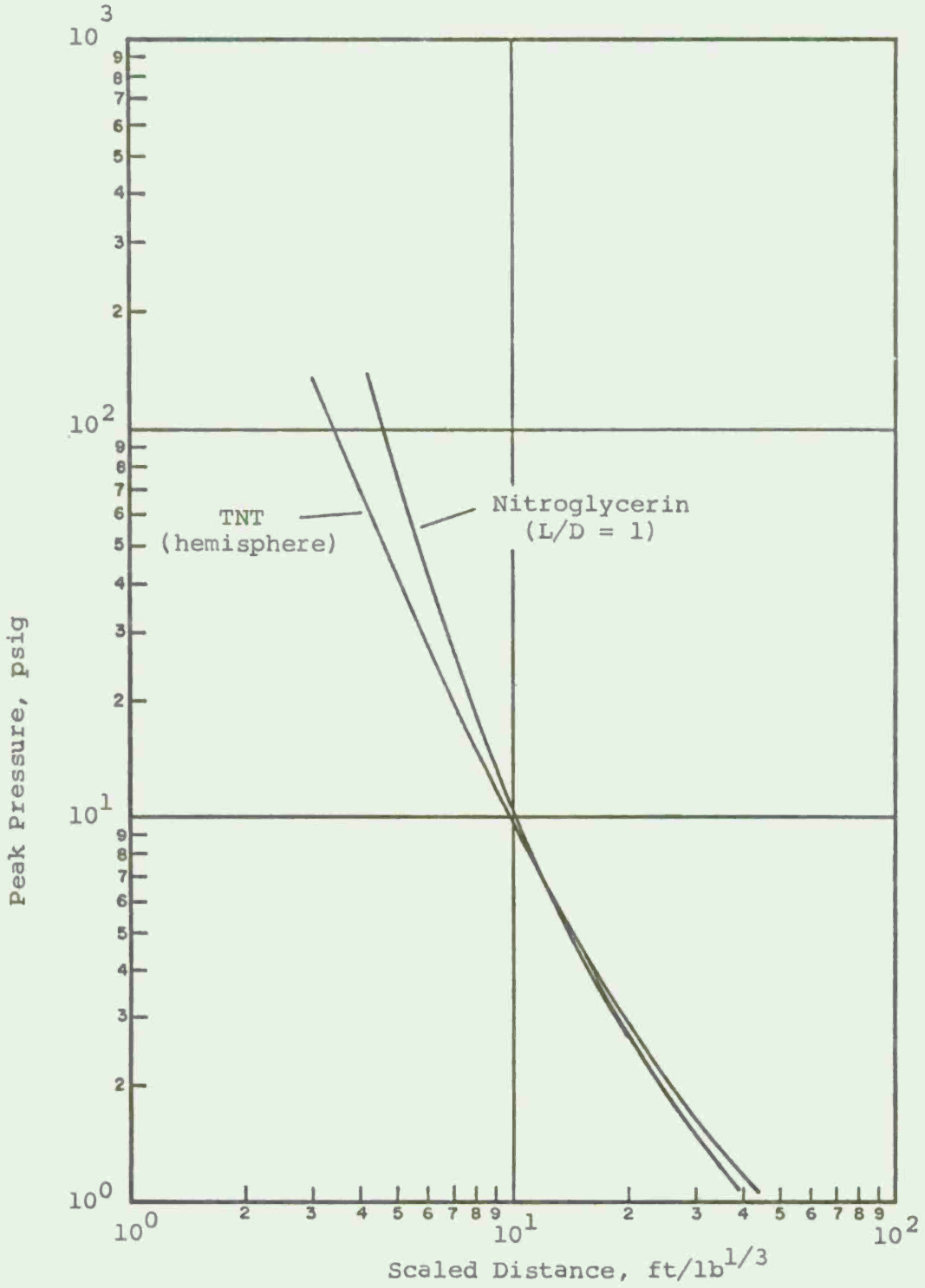

Fig 3 Blast output comparison, geometry effects

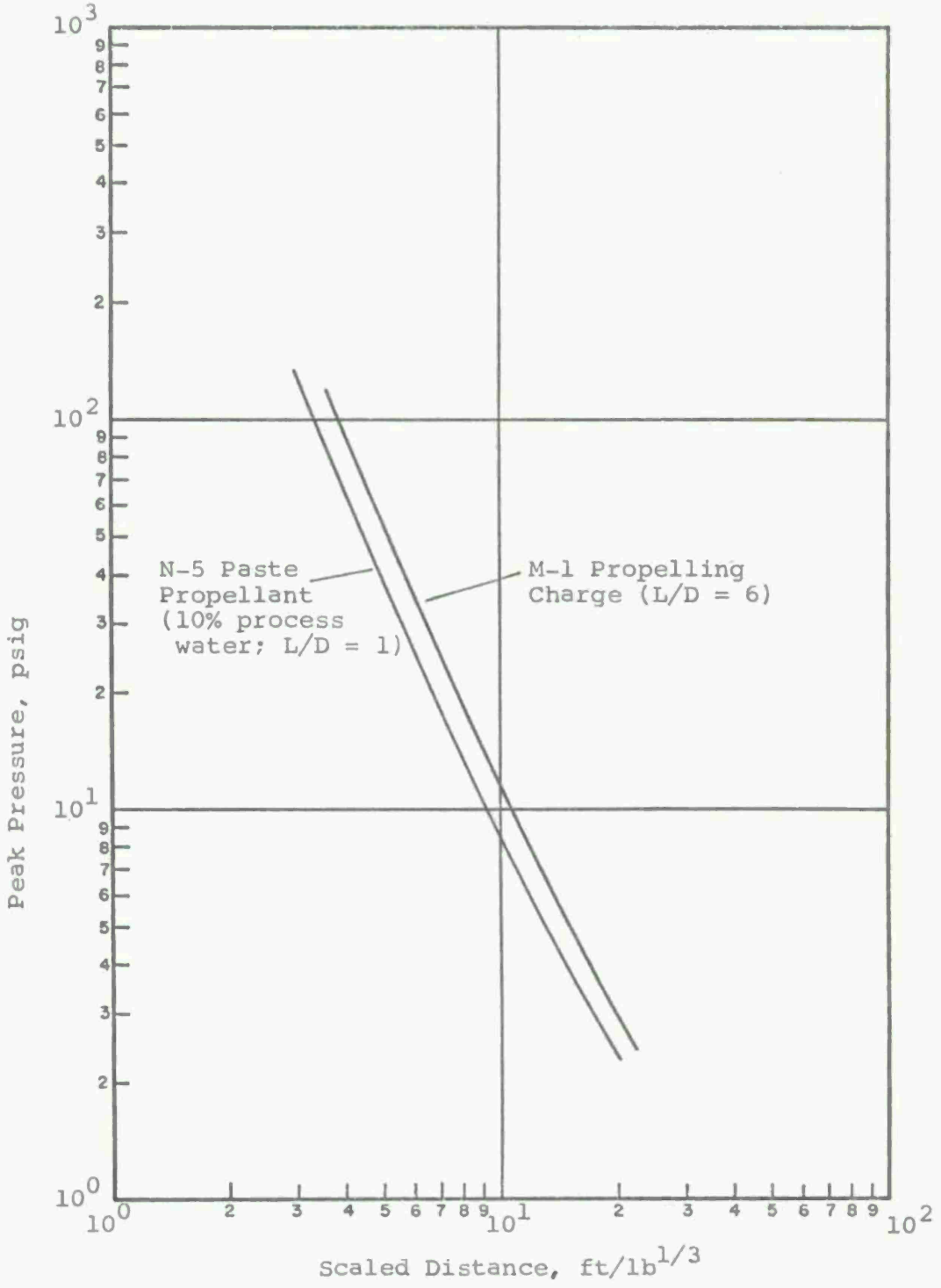

Fig 4 Blast output comparison, geometry effects

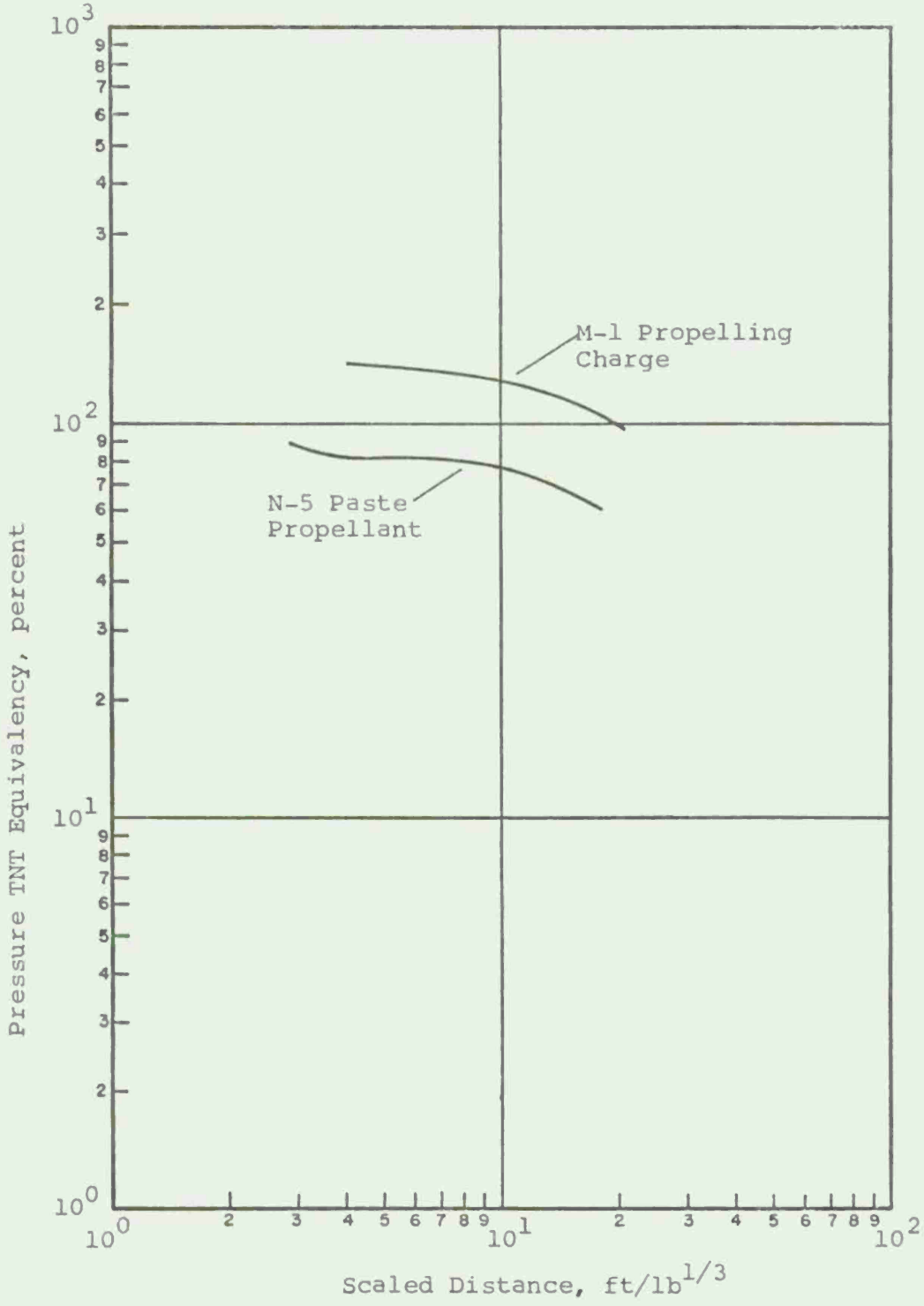

Fig 5 Equivalency comparison

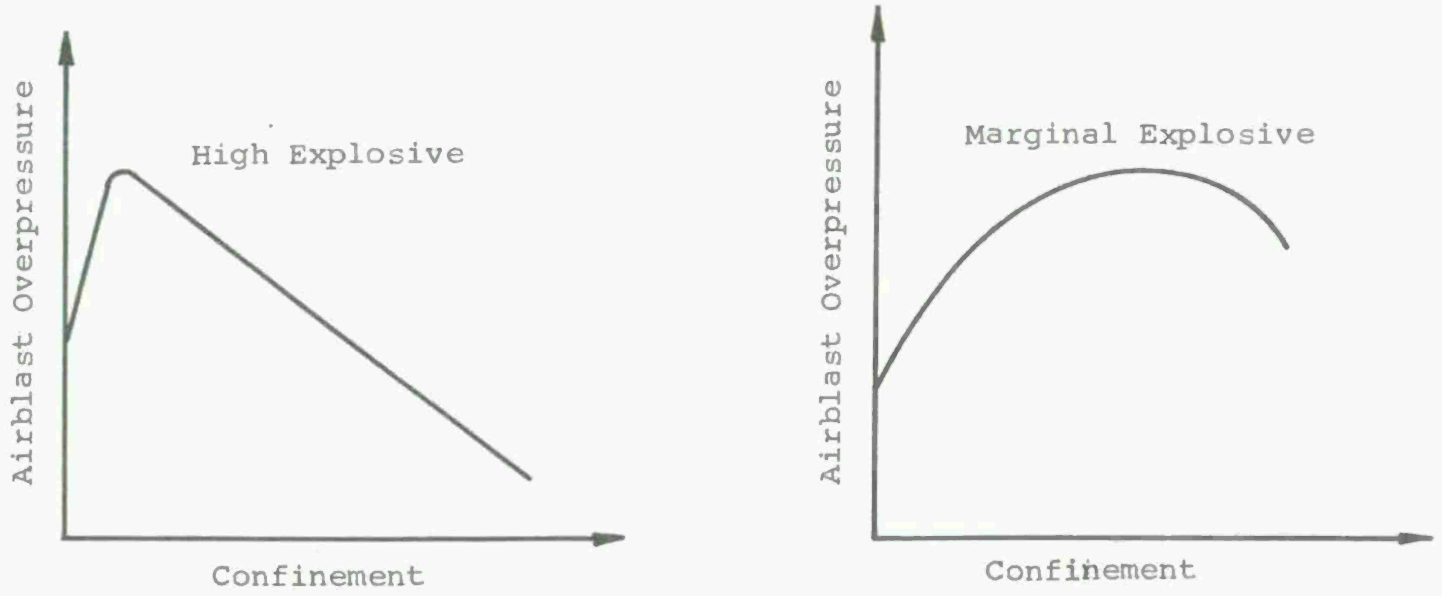

Fig 6 Effect of confinement on blast output

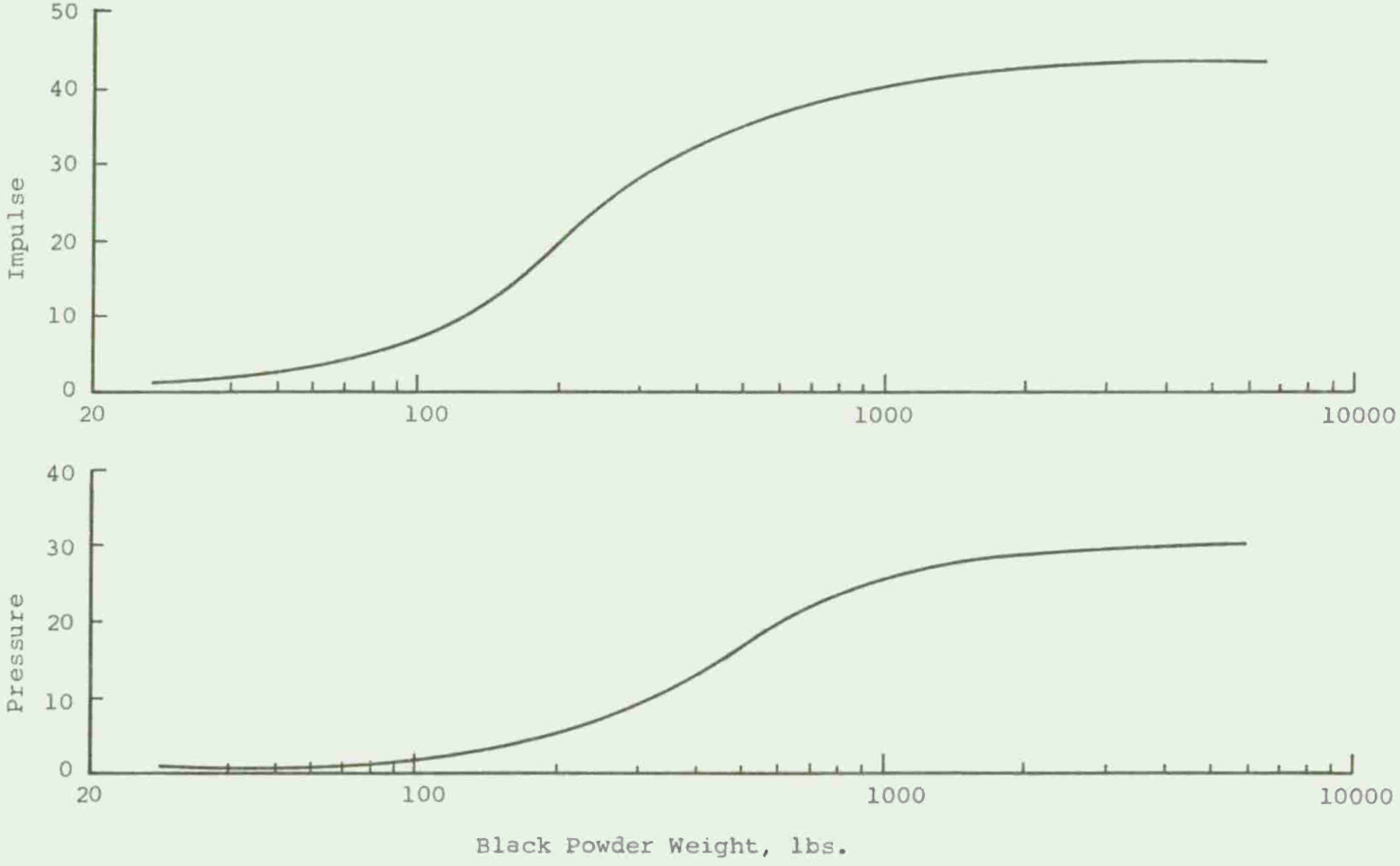

Fig 7 Effect of weight change on equivalency

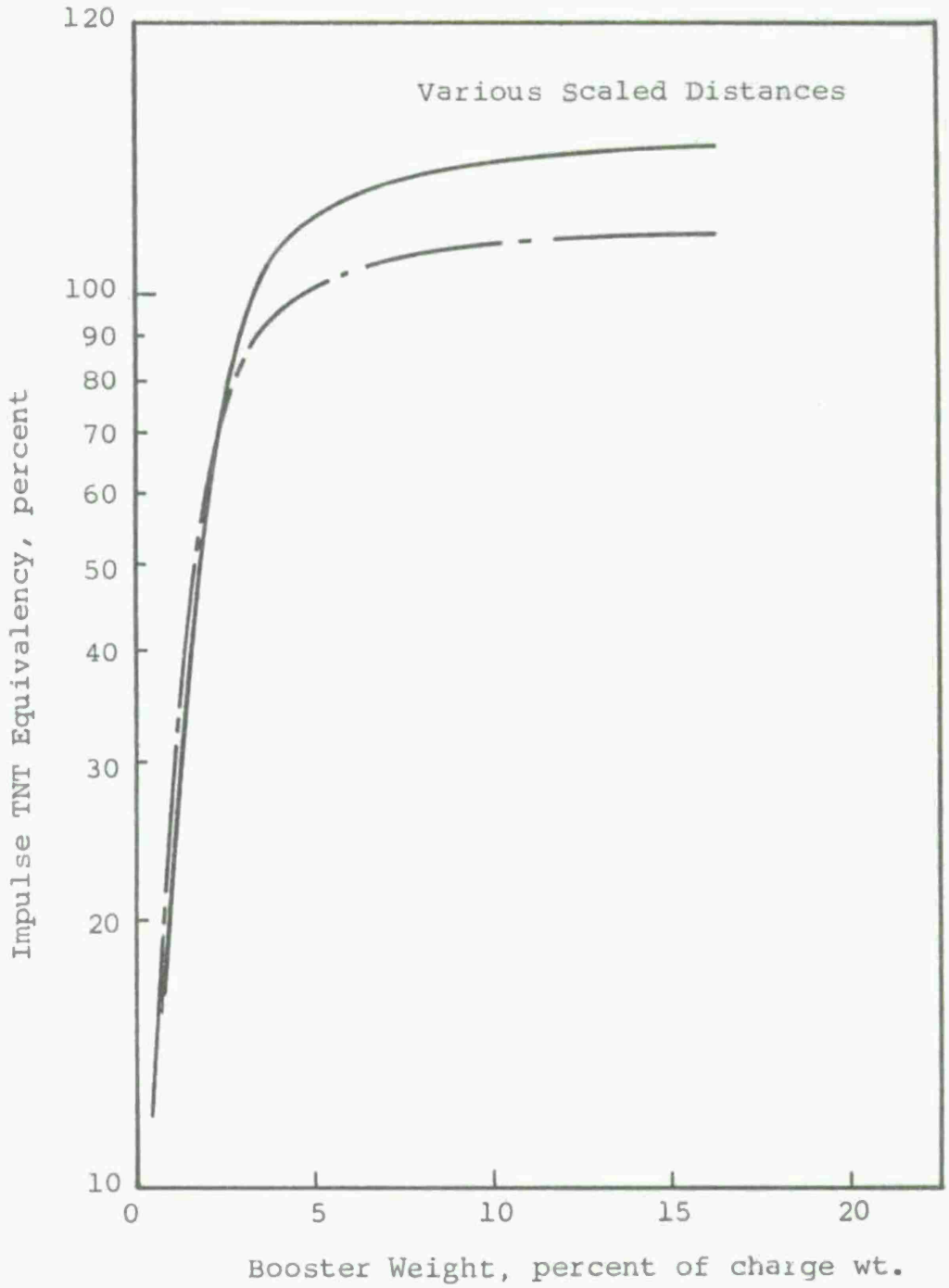

Fig 8 Effect of booster size for M-1 propelling charges

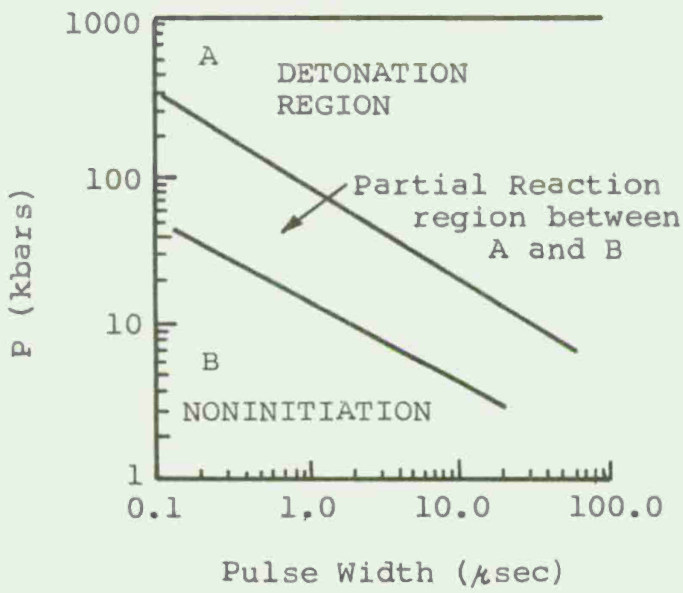

Fig 9 Boundary for shock initiation of reactive materials (not scale)

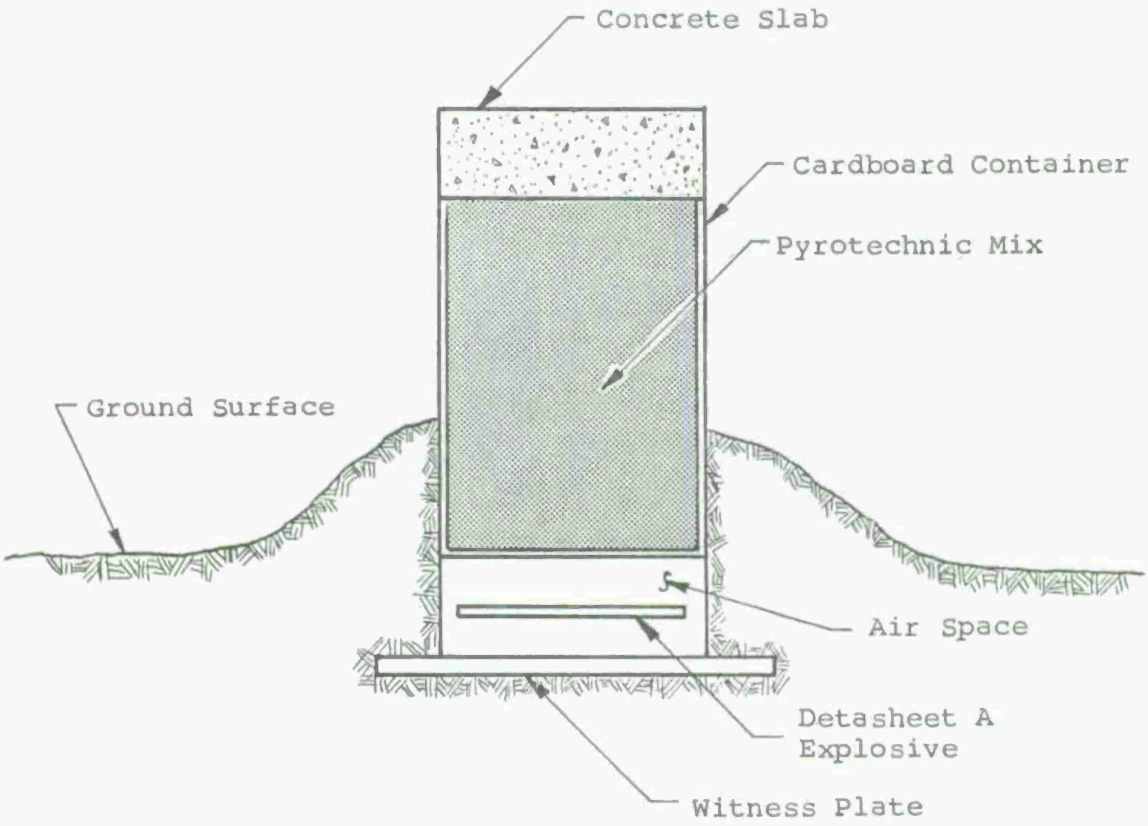

Fig 10 Air cavity configuration

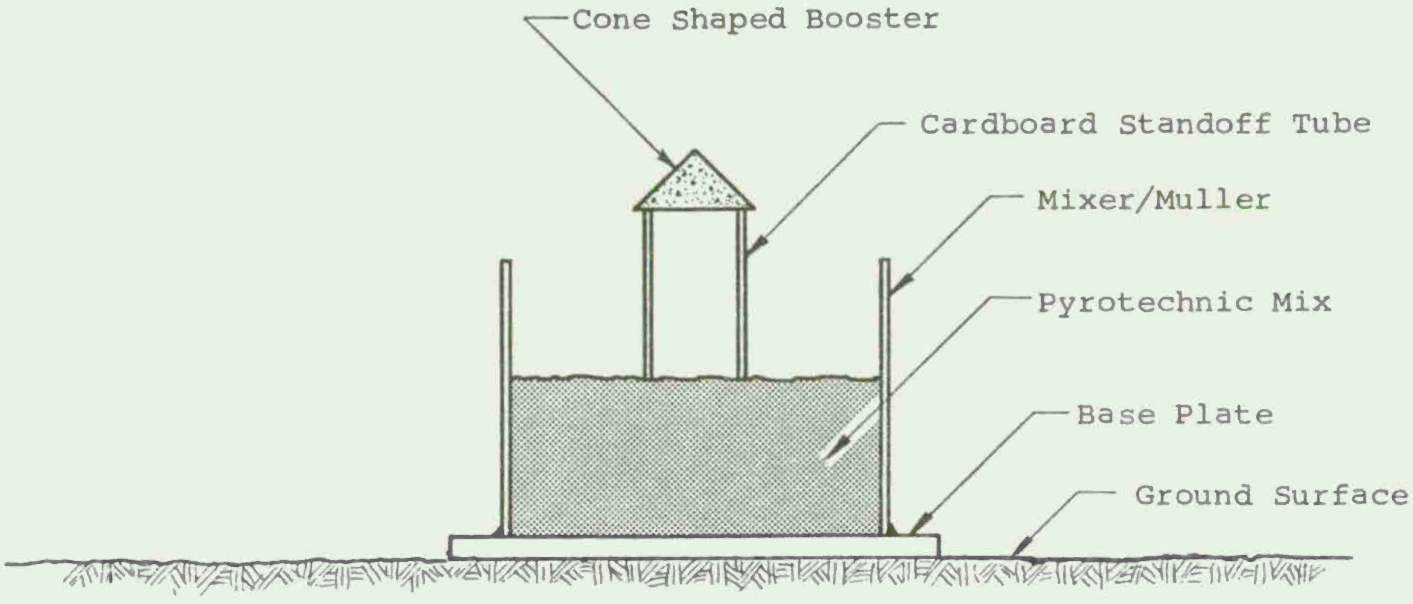

Fig 11 Mixer/muller configuration

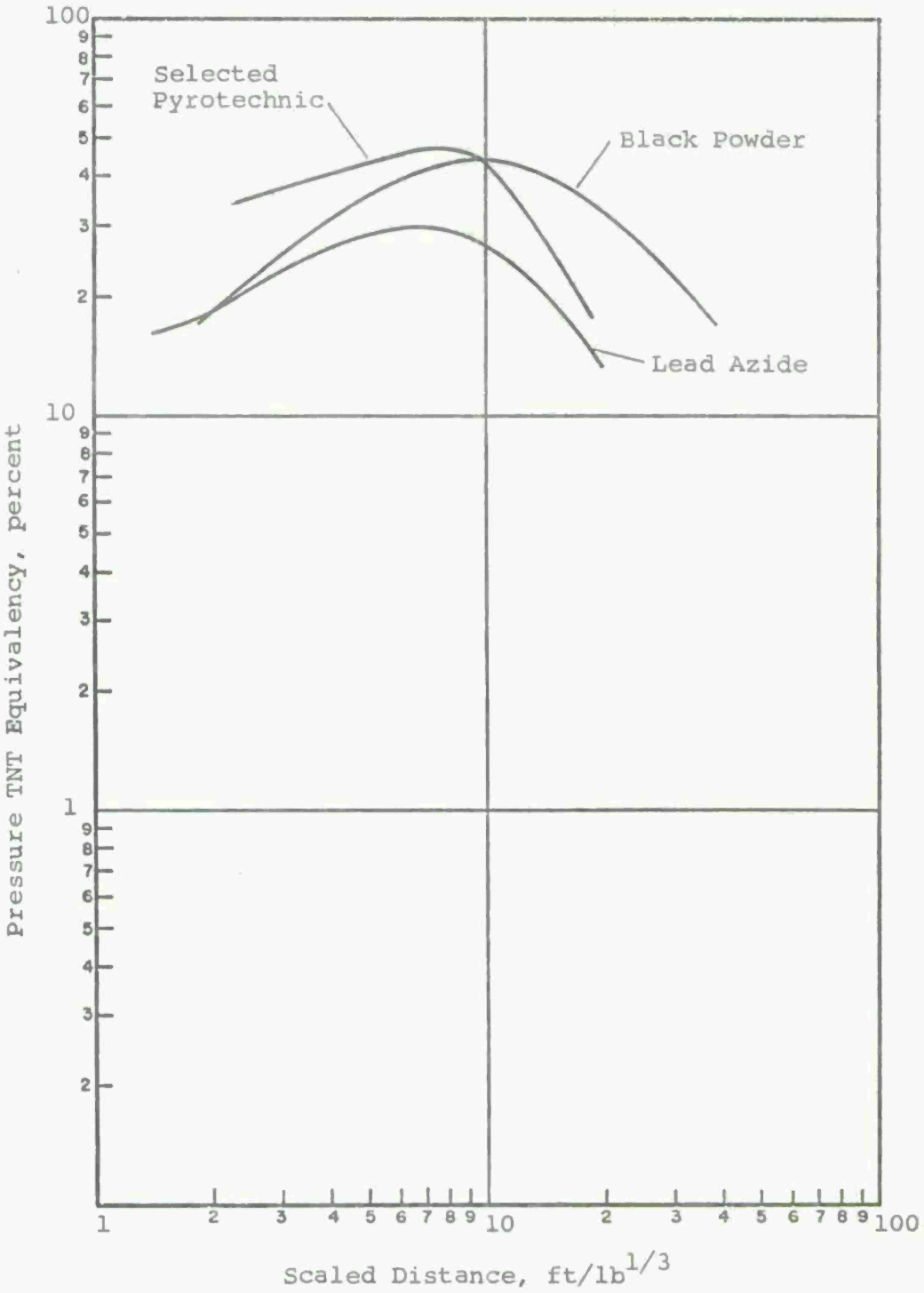

Fig 12 Pressure equivalency for some marginal explosives

PRIMARY FRAGMENT CHARACTERISTICS AND IMPACT EFFECTS IN PROTECTIVE DESIGN

John J. Healey and Samuel Weissman
Ammann & Whitney, Consulting Engineers
New York, N.Y.

ABSTRACT

Based upon a comprehensive review and critical analysis of available information, the material on primary fragment characteristics and fragment impact effects in the tri-service design manual, "Structures to Resist the Effects of Accidental Explosions" (TM 5-1300) has been updated and expanded. This paper summarizes the results of the study in the areas of fragment design parameters and the effect of fragment impact upon concrete barriers and steel plates. Charts developed to facilitate design calculations are included.

INTRODUCTION

An important consideration in the design of structures for accidental explosions is impact by primary fragments, the relatively small, high velocity fragments produced from the casing of a detonated explosive container. The tri-service design manual, "Structures to Resist the Effects of Accidental Explosions", TM 5-1300, (Ref 1) contains procedures for treating the phenomena of fragmentation and fragment impact into concrete and composite barriers as they relate to protective structure design.

As part of its overall Engineering Support Program for the U. S. Army Armament Command (ARMCOM), the Manufacturing Technology Directorate of Picatinny Arsenal with the assistance of Ammann & Whitney has undertaken a study to update these design procedures and to expand the treatment to include other structural materials. In order to accomplish this objective, a detailed review and critical analysis of existing data and analytical approaches was performed. Based upon this review, revised and expanded design procedures for protective structures have been developed. The background for and the development of this material are described in Reference 2. In addition, this reference contains design charts, tables and detailed example problems. The objective of this paper is to summarize the material in two areas, the determination of primary fragment design characteristics and the effect of primary fragment impact on concrete barriers and steel plates.

FRAGMENT CHARACTERISTICS

General

Design for fragment penetration effects requires a complete definition of the probable characteristics of a critical design fragment at its point of impact with the structure. The known data consists of a given explosive in a container of known geometry and material properties at a specified distance from the protective structure. The principal fragment characteristics are random values and include the total number of fragments released and the distribution of their weights, the initial fragment velocity and other physical and geometrical characteristics.

Fragment Weight Distribution

Upon detonation of an explosive container, the casing breaks up into a large number of high velocity fragments with varying weights. Design calculations require that the weight of a so-called critical fragment

be defined. A basic equation defining the weight distribution of released fragments has been provided by Mott (Ref 3), i.e.,

$$\ln N_x = \ln(C'M_A) - M/M_A \qquad (1)$$

where

N_x = the number of fragments with weight greater than the fragment weight, W_F

C' = fragment distribution constant = $C/2M_A^3)$

C = total casing weight (ounces)

$M = (W_F)^{1/2}$

M_A = fragment distribution parameter

$= Bt_i^{5/6} d_i^{1/3} [1 + t_i/d_i]$

t_i = average casing thickness (inches)

d_i = average inside diameter of casing (inches)

B = explosive constant (Table 1).

The Mott equation assumes that the fragments result from the high-order detonation of a uniform thickness cylindrical casing filled with evenly distributed explosive. Since no procedure is available for a more general configuration, actual explosive containers are usually treated as one or more equivalent cylinders meeting the required conditions.

Equation (1) was derived assuming that the fragmentation process can be described as the two-dimensional break-up of a thin-walled casing. Although there is some evidence that the fragmentation of thick casings ($t_i > 0.6$ in.) should be considered as a three-dimensional process, the Mott equation has been shown to produce estimates of fragment numbers and weights in substantial agreement with experimental results.

In order to refine the treatment in Reference 1, formulas were developed, based on Equation (1), for the total number of released fragments, for the average fragment weight and for the design fragment weight in terms of a specified design probability or design confidence level.

The Mott equation can be expressed in the following form:

$$N_x = \frac{C\ e^{-\sqrt{W_F}/M_A}}{2M_A^2} \qquad (2)$$

Hence, the total number of fragments is

$$N_T = \frac{C}{2M_A^2} \qquad (3)$$

and the average fragment weight can be founr

$$\overline{W}_F = 2M_A^2 \qquad (4)$$

The ratic N_x/N_T represents that fraction of the total number of fragments which have a weight greater than W_F. It is interesting to observe that 75.7 percent of all primary fragments generated by the detonation have a weight less than that of the average fragment weight. Hence, the Mott equation predicts the release of a continuous distribution of fragments ranging in size from a large number of lightweight particles to a small number of very heavy casing fragments.

The probability, $1 - N_x/N_T$, that weight W_F is the largest weight fragment released is defined as the design confidence level, CL, and can be expressed as follows:

$$CL = 1 - N_x/N_T = 1 - e^{-\sqrt{W_F}/M_A} \qquad (5)$$

Equation (5) can then be rearranged to express the design fragment weight W_F as a function of the prescribed probability or design confidence level:

$$W_F = M_A^2\, 1n^2(1 - CL) \qquad (6)$$

It should be recognized that the Mott equation yields values of W_F exceeding the total casing weight C for values of CL extremely close to one. Although an adjusted equation for W_F was derived which takes into account the finite upper limit of W_F, comparison of this equation with Equation (6) shows that the results are virtually identical except for CL values of the order of 0.9999 and greater. Hence, Equation (6) is recommended for use in all practical design cases.

In order to illustrate the implementation of these relationships in practical design, a step-wise procedure is outlined below. Design charts (Fig 1, 2, and 3) have been developed to reduce the amount of necessary calculations.

The problem statement and solution can be summarized as follows.

GIVEN: A cylindrical casing filled with a specific explosive, inside diameter of cylinder = d_i (in.), cylinder wall thickness = t_i (in.), total casing weight = C (oz), design confidence level = CL.

FIND: Fragment design weight, W_F. Also, calculate the number of fragments with weight greater than W_F.

SOLUTION: (1) From Fig 1, determine M_A/B for known values of d_i and t_i. With value of B from Table 1 corresponding to given explosive, determine fragment distribution parameter, M_A.

(2) From Fig 2 determine design fragment weight, W_F, for prescribed CL value and previously determined M_A.

(3) From Fig 3, determine quantity B_2N_T/C for known d_i and t_i. Calculate the total number of particles, N_T, for known casing weight C and explosive constant B.

(4) Calculate N_x, the number of particles with weight greater than the design fragment weight from the following relationship:

$$N_x = N_T(1 - CL)$$

Initial Fragment Velocity

The initial velocity of primary fragments resulting from the detonation of cased explosives is a function of the ratio of explosive charge to casing weight and of the explosive output of the explosive. Gurney (Ref 4) was able to derive, on a theoretical basis, expressions for the initial velocity of some specific container/explosive configurations. Assuming an even distribution of explosive charge and a uniform casing wall thickness, the following expression was developed for the initial fragment velocity resulting from the detonation of a cylindrical container:

$$v_o = (2E')^{1/2}\left[\frac{E/C}{1 + 0.5E/C}\right]^{1/2} \qquad (7)$$

where $(2E')^{1/2}$ = Gurney explosive energy constant (fps) (Table 1)

E = weight of explosive (in design calculations, E = 1.2 times the actual explosive weight)

C = weight of casing

V_o = initial fragment velocity (fps)

Figure 4 shows the variation of the normalized quantity $V_o/(2E')^{1/2}$ with E/C for this case. Expressions for the initial velocity for other configurations are summarized in Reference 1.

Although the calculated velocity actually corresponds only to the smaller fragments, the variation of velocity with fragment weight is not well defined and hence is not considered in design calculations. Instead, the conservative assumption is made that all fragments generated by the detonation travel at the velocity calculated from the Gurney equation.

An alternate fragment velocity expression derived by Mott (Ref 3) for a cylindrical casing is:

$$V_o = [(E/C)kf]^{1/2} \qquad (8)$$

where V_o = initial fragment velocity (fps)

E/C = ratio of explosive weight to casing weight

k = explosive output constant (Table 1)

f = factor defined as follows:

$f = -0.682 \log_{10} E/C + 0.80$ for $E/C > 0.509$

$f = 1.00$ for $E/C \leq 0.509$

Comparison of calculated initial velocities from Equation (7) with those from Equation (8) shows that consistently higher values are obtained with the Gurney velocity equation. An expression can be developed for the ratio of the Gurney velocity to the Mott velocity as a function of E/C:

$$V_G/V_M = \frac{\sqrt{2E'}}{\sqrt{k}} \left[\frac{1}{(1 + 0.5E/C)f} \right]^{1/2} \qquad (9)$$

Plotting this velocity ratio relationship for TNT (Fig 5) shows that for high values of the E/C ratio, the calculated velocity ratio is consistently greater than one; e.g., for TNT, V_G/V_M equals 1.37 for E/C equal to 10. Therefore, for design purposes, it is conservative to base initial velocity calculations upon the Gurney equation. It should be possible to resolve this discrepancy by examining the basic assumptions and ranges of applicability of the two velocity prediction equations.

In addition, the source of variations in measured Gurney constants should be investigated. Reported values of the constant $\sqrt{2E'}$ for a given explosive show variations of up to 12 percent.

Variation of Fragment Velocity with Distance

Since the fragment velocity of interest is the velocity of the fragment when it strikes the protective barrier, the decay in fragment velocity with distance is considered for distances greater than about 20 feet. The variation in velocity is a function not only of the distance but also of the area to weight relationship for the fragment [$A/W_F = 0.78/(W_F)^{1/3}$ for random steel fragments], the drag coefficient ($C_D = 0.6$) and the air density (Ref 5). The resulting expression for the striking velocity is

$$V_s = V_o e^{-0.004R/W_F^{1/3}} \qquad (10)$$

where V_s = fragment velocity at distance R from detonation (kfps)

V_o = initial fragment velocity (kfps)

R = distance (ft) from detonation to the protective barrier

W_F = fragment weight (oz).

The variation of the ratio V_s/V_o over a range of fragment weights for various distances R is shown in Figure 6.

Primary Fragments - Caliber Density, Shape and Impact Angle

The randomness in fragment characteristics applies not only to their weight and velocity but also to the nature of the fragment surface which strikes the barrier, the relation between weight and diameter and the angle of impact. For design calculations, it is necessary to specify standard fragment characteristics.

The total weight/diameter relationship is usually defined as the caliber density of the fragment

$$D = W_F/d^3 \qquad (11)$$

where W_F = fragment weight (lb) and d = fragment diameter (in.). The nose shape factor, N, is defined as

$$N = 0.72 + 0.25\sqrt{n - 0.25} \qquad (12)$$

where n = the caliber radius of the tangent ogive of the assumed fragment nose.

Two possible fragment shapes with their corresponding caliber densities and nose factors are shown in Figure 7. The shape in Figure 7(a), the "blunt" fragment, is considered as the "standard fragment" in the penetration design charts presented in the following section. While this fragment shape has a milder nose shape than the alternate shape, it is felt to be appropriate considering the small number of fragments which will strike the structure nose-on and the small fraction of these which will have a more severe nose shape than the standard fragment. Moreover, the length to diameter ratio of these fragments is felt to be more representative of an average fragment configuration.

The angle of obliquity is defined as the angle between the path of the fragment and a normal to the surface of the barrier. In order to design for the most severe condition, normal impact, i.e., an obliquity angle of zero degree, is usually assumed in penetration calculations.

FRAGMENT IMPACT EFFECTS

General

A number of different phenomena are associated with primary fragment impact having different consequences with regard to personnel safety, damage to sensitive equipment and the detonation of additional explosive containers. Since a primary fragment can generally be categorized as a high-speed particle with a mass much smaller than the barrier or target which it strikes, the interaction between local penetration effects and any overall structural response engendered by the impact is not significant. The effects of impact can then be broadly grouped into two classes, namely (1) "front face" effects which include deformation of the missile upon striking the surface, possible shatter or ricochet of the missile, spalling around the point of impact in a more or less conical crater and penetration of the missile into the barrier wall, and (2) "back face" effects including the possible formation of a back face crater with spalling and/or perforation, wherein the missile completely penetrates the barriers and exits with a known residual velocity.

The intent herein is to treat those effects which have a critical bearing on the structural design of protective facilities, e.g., depth of penetration, the prediction of residual fragment velocity in the event that perforation occurs and the prediction of spalling of concrete barriers. The emphasis is upon the development of design data rather than a complete description of all the phenomena involved.

The two basic factors affecting the damage inflicted upon the barrier are the characteristics of the fragment (as defined previously) and the properties of the barrier material. The basic equation underlying all penetration formulations is Newton's Second Law of Motion. The case of "mass penetration" wherein the penetration process is treated as the rectilinear motion of a nondeforming fragment through a thick homogeneous material serves as a baseline for which a good deal of test data is available and for which an analytical approach can at least be formulated. However, even for this somewhat simplified case, a complete analytical solution is not available due mainly to a lack of understanding of the exact manner in

which the resisting force representing the interaction between the penetrating mass and the barrier varies as the penetrator travels through the barrier.

As a result, missile penetration, which has been under serious study since the mid-eighteenth century, has remained predominantly an empirical field. This fact is evidenced in the comprehensive review by Robertson of the significant work in this area prior to World War II (Ref 6), in the summary of the extensive research programs conducted during the war (Ref 7), and by the orientation of most of the research activity since that time. Empirical study of this subject is also quite difficult due to the degree of scatter exhibited by experimental penetration data and the difficulty involved in comparing experimental data generated by different investigators.

Concrete Penetration

In the development of a design equation for concrete penetration, the "massive penetration" case is considered, i.e., the following conditions are assumed: (a) the angles of obliquity and yaw are zero, i.e., both the path of the missile and the missile axis are coincident with the normal to the surface of the barrier; (b) the missile is an inert non-deforming armor-piercing (AP) projectile or fragment; (c) the barrier or wall constitutes a uniform target of sufficient thickness that this finite dimension does not influence the penetration, i.e., it is assumed initially that back-face phenomena do not influence penetration; and (d) the loss of fragment mass during penetration is not considered. In order to avoid complications introduced by missile and plate hardness effects and non-normal impact, these topics are treated separately as modifications to the basic penetration case.

Under these conditions, the penetration problem essentially involves the one-dimensional motion of a particle with given initial conditions into a target medium which resists the motion. According to the separable force law postulated by Beth (Ref 8), the force on a penetrator at a given instant is a function of both its current velocity and its current depth of penetration. Adopting this assumption, the basic equation of motion can be solved for the maximum caliber penetration. By including the values of the empirical constants which provide a good representation of observed penetration data (Ref 8) and by establishing a weighted average value $(6.53/\sqrt{f'_c})$ for the concrete penetrability constant (K), the following

semi-empirical concrete penetration equation was obtained:

$$G(Z) = \frac{6.53}{\sqrt{f'_c}} NDd^{0.2}V^{1.8} \qquad (13)$$

where $G(Z) = \frac{1Z^2}{4}$ for $Z \leq 2$

$= Z - 1$ for $Z > 2$

and, to summarize

N = nose shape factor

D = caliber density of the missile, W/d^3 (lb/in.^{3})

W = missile weight (lb)

d = diameter of missile (in.)

V = striking velocity (kfps)

Z = caliber penetration, s/d

x = depth of penetration (in.)

f'_c = concrete compressive strength (ksi).

As shown, this equation accounts for the missile nose shape, N, the missile caliber density, D, the effect of the concrete compressive strength, and the scale effect for penetration into concrete, i.e., the observed increase in maximum caliber penetration with increase in projectile caliber for otherwise similar projectiles.

Equation (13) can also be rearranged in terms of the maximum depth of penetration.

For $x \leq 2d$,

$$x = 2\sqrt{KND}\ d^{1.1}V^{0.9} \qquad (14)$$

and for $x > 2d$,

$$x = KND\, d^{1.2} V^{1.8} + d \qquad (15)$$

These equations were compared with other formulations and experimental data for the normal penetration of reinforced concrete by armor-piercing missiles. Figure 8 shows the variation of maximum caliber penetration with striking velocity corresponding to Equation (13) and to concrete penetration formulas from References 1 and 9. Also shown are the results of tests on concrete slabs as reported in Reference 7. The resuits indicate the following: the penetration equation in Reference 4 underestimates the experimental data at low striking velocities and overestimates the results at higher velocities. In general, the equations in Reference 9 and Equation 13 agree quite closely and give conservative estimates vs the test data. It should be noted that the penetration equation from Reference 9 does not account for nose factors different from 1.0 and, as the striking velocity approaches zero, the caliber penetration approaches a finite value of 0.5, indicating that the equation gives overly conservative results at low striking velocities. Finally, Figure 9 shows an excellent correlation between Equation (13) and a series of test results on concrete slabs described in Reference 10.

It can be concluded from these comparisons that Equation (13) provides reliable estimates of massive penetration by armor-piercing projectiles into reinforced concrete.

Equations (14) and (15) can be expressed in more convenient form for design against impact by the standard design fragment shown in Figure 7(a) by substituting the N and D values for the standard shape and assigning the value of 5 ksi to f'_c. The resulting penetration equations in terms of the fragment weight, W_F (oz), are therefore:

For $x \leq 2d$,

$$x = 0.91 W_F^{0.37} V^{0.9} \qquad (16)$$

For $x > 2d$,

$$x = 0.30 W_F^{0.40} V^{1.8} + 0.575 W_F^{0.33} \qquad (17)$$

Depth of concrete penetration according to these equations for a range of velocities and fragment weights was developed to facilitate design calculations as shown in Figure 10.

Equations (16) and (17) and Figure 10 apply to the penetration of 5 ksi concrete by an armor-piercing steel primary fragment. The results can be adjusted for a different f'_c by multiplying by the square root of the ratio of 5 ksi to the f'_c of the concrete in question.

Steel Penetration

In developing a prediction equation for the penetration and perforation of steel plates, it is important to recognize some qualitative differences between failure mechanisms in steel and concrete barriers. The failure mode of primary concern in mild to medium hard homogeneous steel plates subjected to normal impact is ductile failure. In this mode, as the missile penetrates the plate, plastically deformed material is pushed aside and petals or lips are formed on both the front and back faces with no material being ejected from the plate. For plates with Brinell hardness values above about 350, the likelihood of failure by "plugging" increases. In this mode of failure, a plug of material is formed ahead of the penetrating missile and is ejected from the back side of the plate. A third mode of failure is disking or flaking in which circular disks or irregular flakes are thrown from the back face. This type of failure is mainly of concern with plates of inferior quality and should not therefore be a common problem in the design of protective structures.

An empirical design formula was developed considering the ductile failure mode and subject to the conditions summarized above for massive penetration, i.e., normal impact, non-deforming projectile, etc. An important difference with steel penetration is that penetration and perforation are treated simultaneously since back face phenomena do not influence the depth of penetration as was the case with concrete. For this reason, most of the steel test data are from perforation tests. The usual criteria of failure considered in such tests are the so-called Navy limit in which the missile completely passes through the plate and emerges with zero velocity and the protection limit criteria in which the missile emerges with sufficient velocity to pierce a thin sheet located a short distance behind the plate. At normal incidence, any differences attributable to these alternate definitions of plate failure are within acceptable limits for the purposes of this study.

Various empirical formulas valid for certain limited ranges and various sources of experimental data are available in the literature. A conservative prediction equation will be determined from these results by evaluating the coefficients in the following semi-empirical equation

$$Z = C_1 DV^{C_2} \tag{18}$$

This equation is similar in form to the concrete equation but does not explicitly consider the influence of the missile nose factor or the scale effect since these factors are not significant for steel penetration. It is recognized that due to the relative hardness of the missile and the barrier in the case of steel/steel impact, the likelihood of missile shatter and ricochet is higher than with concrete/steel impact. However, for simplicity and conservatism, these effects are not considered in this design equation.

Steel penetration results from a number of sources (Ref 7, 11, 12, and 13) were plotted together (Fig 11) and compared for the assumed condition of penetration of an armor-piercing missile into mild steel. In order to convert the available results to these conditions of missile and plate hardness, it was necessary to develop conversion factors as summarized in the next section of this paper.

A good deal of scatter is apparent in these results. The main source of this scatter is the sensitivity of steel penetration to the relative hardness of the penetrator and the barrier material due to variations in test specimen material properties from their nominal values. To some extent, differences in definition of plate failure, different nose shapes and the scale effect due to the range of projectiles which these results represent may also be responsible for some of the spread in the plotted results.

The extensive data from the THOR Project essentially represents an upper bound to the results illustrated in Figure 11. Consequently, in order to provide conservative equations for use in protective design, the empirical coefficients in Equation (18) were essentially determined on the basis of these upper bound results. The following penetration equations were developed:

for AP steel missiles penetrating mild steel plate,

$$Z = 2.33 DV^{1.22} \tag{19}$$

for mild steel missiles penetrating mild steel plate,

$$Z = 1.63 DV^{1.22} \tag{20}$$

In order to facilitate the use of these steel penetration equations in design for primary fragment impact, they can be expressed in the following simplified forms:

for AP steel fragments into mild steel plate,

$$x = 0.30 W_F^{0.33} V^{1.22} \tag{21}$$

for mild steel fragments into mild steel plate,

$$x = 0.21 W_F^{0.33} V^{1.22} \tag{22}$$

where W_F = fragment weight (oz), V = striking velocity (kfps).

A design chart for steel penetration by primary fragments according to Equation (21) is presented in Figure 12.

Other Influences on Penetration Depth

A. Missile Material

Since most penetration tests and penetration equations apply to steel and particularly to armor-piercing (AP) steel missiles, conversion factors are used to account for the effect of material properties of the given missile according to the following relation:

$$X_{\text{non-AP}} = k_p X_{\text{AP}} \tag{23}$$

where $X_{\text{non-AP}}$ = penetration achieved by a non-armor piercing steel missile

X_{AP} = penetration achieved by identical armor-piercing steel missile.

The k_p factors are determined based on the assumption that the relative penetration achieved by a missile of other than armor-piercing steel can be related to the material density and Brinell hardness number. The k_p factors developed in Reference 2 and summarized in Table 2 are

essentially identical to those found in TM 5-1300 with the exception of aluminum for which the k_p value has been reduced from 0.25 to 0.15. It should be noted that since the projectile material has a reduced effect on penetration at hypervelocities (> 5 kfps), these relative penetrability factors are not strictly applicable and their use in such cases may be conservative.

B. Steel Plate Hardness

In general, the resistance to penetration of a steel plate increases with increasing Brinell hardness to the point where brittle fracture or plugging type failures occur. In Reference 11, the penetrations were found to be proportional to the following empirical factor:

$$f_h = \frac{1}{e^{\varepsilon B^2 + \omega B}} \qquad (24)$$

where B = Brinell hardness number

$\omega = 5.41 \times 10^{-3}$

$\varepsilon = 8.77 \times 10^{-6}$

This function has a minimum value at a Brinell hardness of $-\omega/2\varepsilon$ or about 310 for steel. The function, as shown in Figure 13, is relatively flat in the region of this minimum. In order to convert data for penetration into steel with a given Brinell hardness to the corresponding penetration into a different type of steel, the following conversion formula can be used:

$$X_{B2} = \frac{f_{h2}}{f_{h1}} X_{b1} \qquad (25)$$

where X_{b1} = depth of penetration into steel plate with Brinell hardness B_1

X_{B2} = depth of penetration into steel plate with Brinell hardness B_2

f_{h1}, f_{h2} = plate hardness factors from Figure 13.

Since the required thickness to provide protection with a plate with a very high Brinell hardness (> 400) may actually exceed the thickness required for a milder steel plate due to the ejection of a plug before the plate is perforated, the use of more ductile plates is advised where deep penetrations are anticipated.

C. Obliquity

It is possible to make a conservative estimate of the effective normal penetration of a missile impacting a target with other than normal incidence. The following relationship provides an upper bound to the penetration achieved normal to the surface of the plate, X_θ:

$$X_\theta = X\cos^n\theta \qquad (26)$$

where

X = penetration for missile with striking velocity V_s and zero obliquity

V_s = striking velocity

θ = angle of obliquity

n = 2 for $V_s \leqq 2.5$ kfps

n = 1 for $V_s > 2.5$ kfps.

Concrete Spalling

Upon impact of a high velocity fragment with a concrete wall, large compressive stresses are developed and a region of high stress expands spherically toward the back face. When the compressive stress waves reach this free surface, they are reflected and travel back as tension waves. If this disturbance exceeds some critical level, pieces of concrete become separated from and fly away from the back face of the wall, i.e., spalling occurs. Spalling is a factor in protective design in two significant respects:

a. The release of secondary concrete fragments with significant mass and velocity represents a danger to personnel, equipment or explosives on the back side of the wall;

b. The spalling of material in the path of the penetrating fragment causes the plate thickness perforated by a given fragment to exceed the equivalent depth of penetration into a massive plate.

The primary approaches to minimizing the effects of spalling are to provide a wall with sufficient thickness such that spalling will not occur or to add steel spall plates to prevent the release of the spalled particles.

Empirical spalling equations for certain test series are available from References 7 and 14. These equations along with some data from Reference 7 are shown in Figure 14. The following single expression was developed from these expressions:

$$t_{sp} = 1.22Zd^{1.1} + 2.12d \qquad (27)$$

Thus, upon calculating the caliber penetration into a massive concrete slab for a missile with diameter d, the slab thickness corresponding to the first occurrence of spalling, t_{sp}, can be determined from Equation 27.

Perforation and Residual Velocity

The most critical effect of fragment impact upon a protective barrier is complete penetration or perforation. This criticality is due to the sympathetic detonation of explosives on the rear side of the wall or the serious damage to personnel and equipment which may result if the fragment emerges from the back face with sufficient residual velocity. The basic massive penetration equations are used here also to predict the occurrence of perforation and in the calculation of the residual fragment velocity upon perforation.

Since spalling is not a consideration for penetration into metallic barriers, the penetration equations can be used directly to determine if a finite thickness of plate will be completely perforated. With concrete, however, spalling has a significant influence upon the slab thickness which will be perforated by a given fragment. The perforation thickness can also be related to the equivalent massive penetration based upon the results from References 7 and 14 and as shown in Figure 15. Based upon this data, the following perforation prediction equation was developed:

$$t_{pf} = 1.13Zd^{1.1} + 1.31d \qquad (28)$$

Thus, the thickness, t_{pf}, of a concrete barrier which will be perforated by a given fragment can be determined based upon the caliber penetration of the fragment into a massive concrete slab.

In cases where a barrier is perforated, it is necessary to calculate the residual fragment velocity in order to evaluate possible effects upon items located behind the barrier.

At the onset of the calculation, the known information will generally consist of the following:

For steel, the calculated fragment penetration, x, is found to be greater than the actual plate thickness, t;

For concrete, the perforation thickness, t_{pf}, exceeds the barrier thickness, t.

In both cases, an expression is needed for the residual velocity, V_r, in terms of the plate thickness, the stricking velocity, V_s and x or t_{pf}.

The basic relationships for determining residual velocity were obtained by relating the velocity value at an intermediate depth of penetration to the striking velocity for the general case of massive penetration.

For concrete penetration, the following residual velocity relationships were developed in this manner:

$$(V_r/V_s) = [1 - (t/t_{pf})^2]^{0.555} \text{ for } x \leq 2d \qquad (29)$$

and

$$(V_r/V_s) = [1 - t/t_{pf})]^{0.555} \text{ for } x > 2d \qquad (30)$$

For steel penetration, the resulting residual velocity equation is:

$$(V_r/V_s) = (1 - t/x)^{0.82} \qquad (31)$$

Equations 29, 30, and 31 are presented in non-dimensional form in Figures 16, 17, and 18.

REFERENCES

1. *Structures to Resist the Effects of Accidental Explosions (with Addenda)*, Department of the Army, Technical Manual TM 5-1300, Washington, D.C., June 1969

2. *Primary Fragment Characteristics and Penetration of Steel, Concrete and Other Materials*, Picatinny Arsenal, Technical Report, Draft

3. Mott, R.I., *A Theory of Fragmentation*, Army Operational Research Group Memo, 113-AC-3642, Great Britain, 1943

4. Gurney, R.W., *The Initial Velocities of Fragments from Bombs, Shells and Grenades*, Report No. 405, Ballistic Research Laboratories, Aberdeen Proving Ground, Maryland, September 1943

5. Thomas, L.H., *Computing the Effect of Distance on Damage by Fragments* Report No. 468, Ballistic Research Laboratories, Aberdeen Proving Ground, Maryland, 1944

6. Robertson, H.P., *Terminal Ballistics*, Preliminary Report, Committee on Passive Protection Against Bombing, National Research Council, January 1941

7. *Effects of Impact and Explosion*, Volume 1, Office of Scientific Research and Development, National Defense Research Committee, Washington, D.C., 1946

8. Beth, R.A., *Final Report on Concrete Penetration*, Report No. A-388, National Defense Research Committee, Office of Scientific Research and Development, March 1946

9. *Fundamentals of Protective Design (Non-Nuclear)*, Department of the Army, Technical Manual TM 5-855-1, Washington, D.C., July 1975

10. Stipe, J.G., et al, *Ballistic Tests on Small Concrete Slabs*, Interim Report No. 28, Committee on Fortification Design, National Research Council, June 1944

11. *The Resistance of Various Metallic Materials to Perforation by Steel Fragments: Empirical Relationships for Fragment Residual Velocity and Residual Weight*, Project THOR Technical Report No. 47, Ballistic Research Laboratories, Aberdeen Proving Ground, Maryland, April 1961

12. Johnson, C. and Moseley, J.W., *Preliminary Warhead Terminal Ballistic Handbook. Part 1: Terminal Ballistic Effects*, NAVWEPS Report No. 7673, U. S. Naval Weapons Laboratory, Dahlgren, Virginia, March 1964

13. Ipson, T. W., *Deformation and Reduction in Weight of Compact Steel Fragments Perforating Thin, Mild Steel Plates*, NWC TP 4553, Naval Weapons Center, January 1968

14. *Industrial Engineering Study to Establish Safety Design Criteria for Use in Engineering of Explosive Facilities and Operations*, Ammann & Whitney, Consulting Engineers, New York, N.Y., Report for Picatinny Arsenal, Dover, New Jersey, April 1963

Table 1

Explosive constants

Explosive Material	Gurney Energy Constant $\sqrt{2E'}$, (fps)	B (Eq 1) ($oz^{\frac{1}{2}}/in.^{7/6}$)	Output Constant (Eq 8) k
Amatol	6190	0.35	2.7×10^7
Comp B	7880	-	4.4×10^7
H-6	7710	0.28	-
Hexanite	6850	0.32	3.3×10^7
Pentolite	7550	0.25	-
RDX/TNT (75/25)	7850	-	-
RDX/TNT (70/30)	8380	-	-
RDX/TNT (60/40)	7880	0.27	4.4×10^7
TNT	6940	0.30	3.6×10^7
Tetryl	7460	0.24	5.2×10^7
Torpex	7450	-	-

Table 2

Relative penetrability coefficient, k_p

Missile Material	Density ($lb/in.^3$)	Brinell Hardness Number (BHN)	Penetrability Coefficient k_p
AP Steel	0.283	285	1.0
Mild Steel	0.283	140	0.7
Lead	0.385	10	0.5
Aluminum	0.098	32	0.15

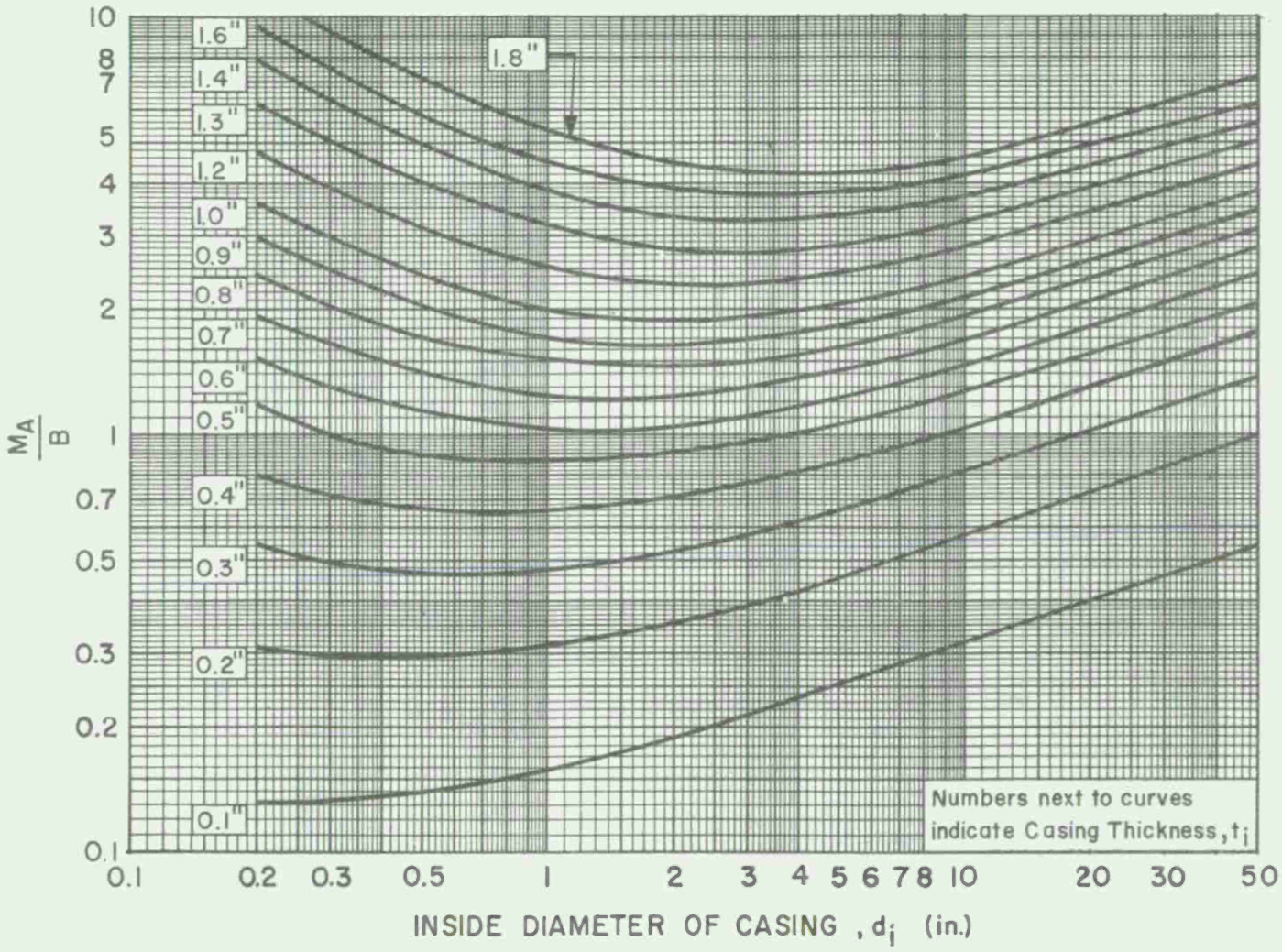

Fig 1 $\frac{M_A}{B}$ versus casing geometry

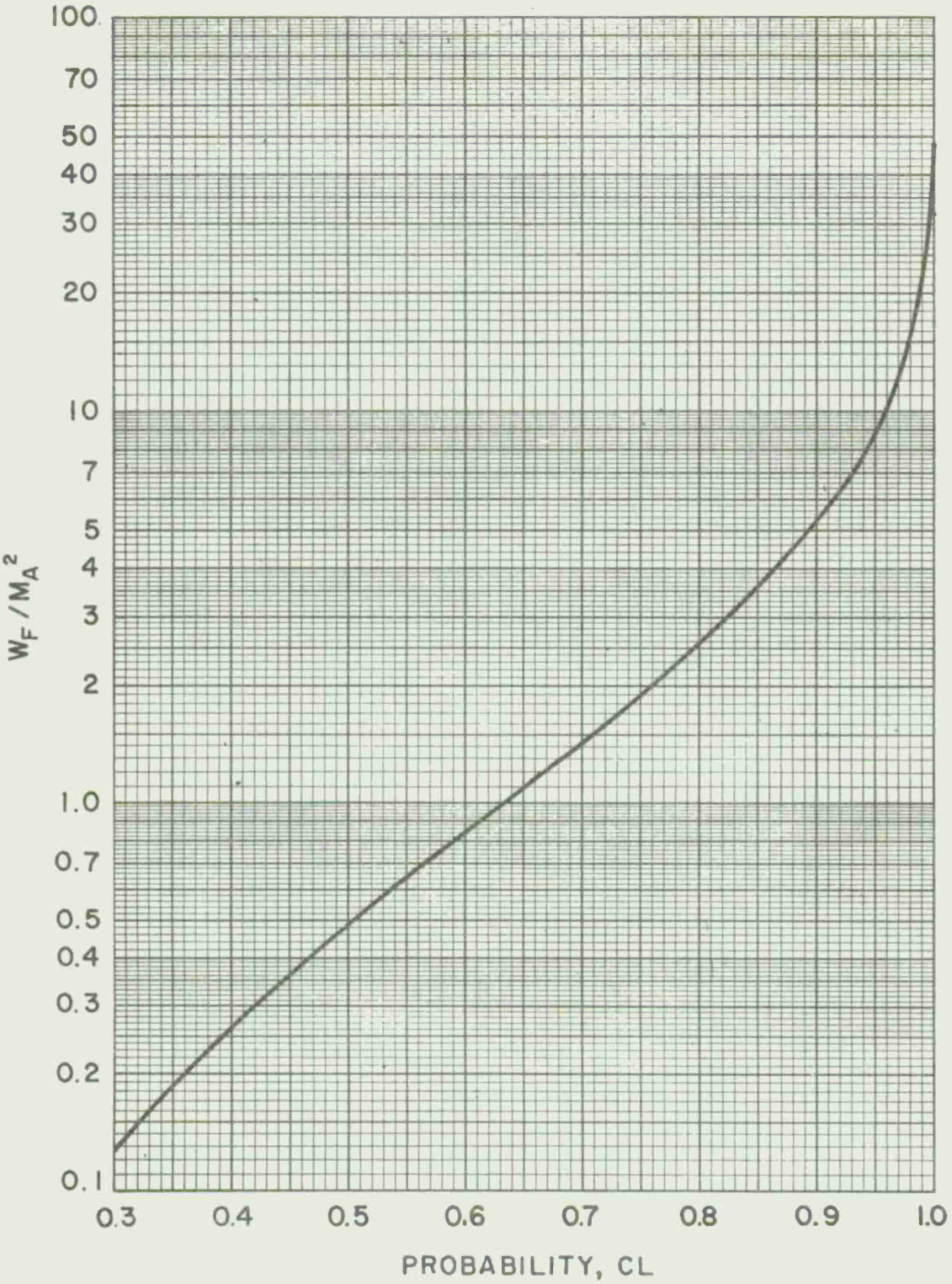

Fig 2(a) Design fragment weight vs design confidence level

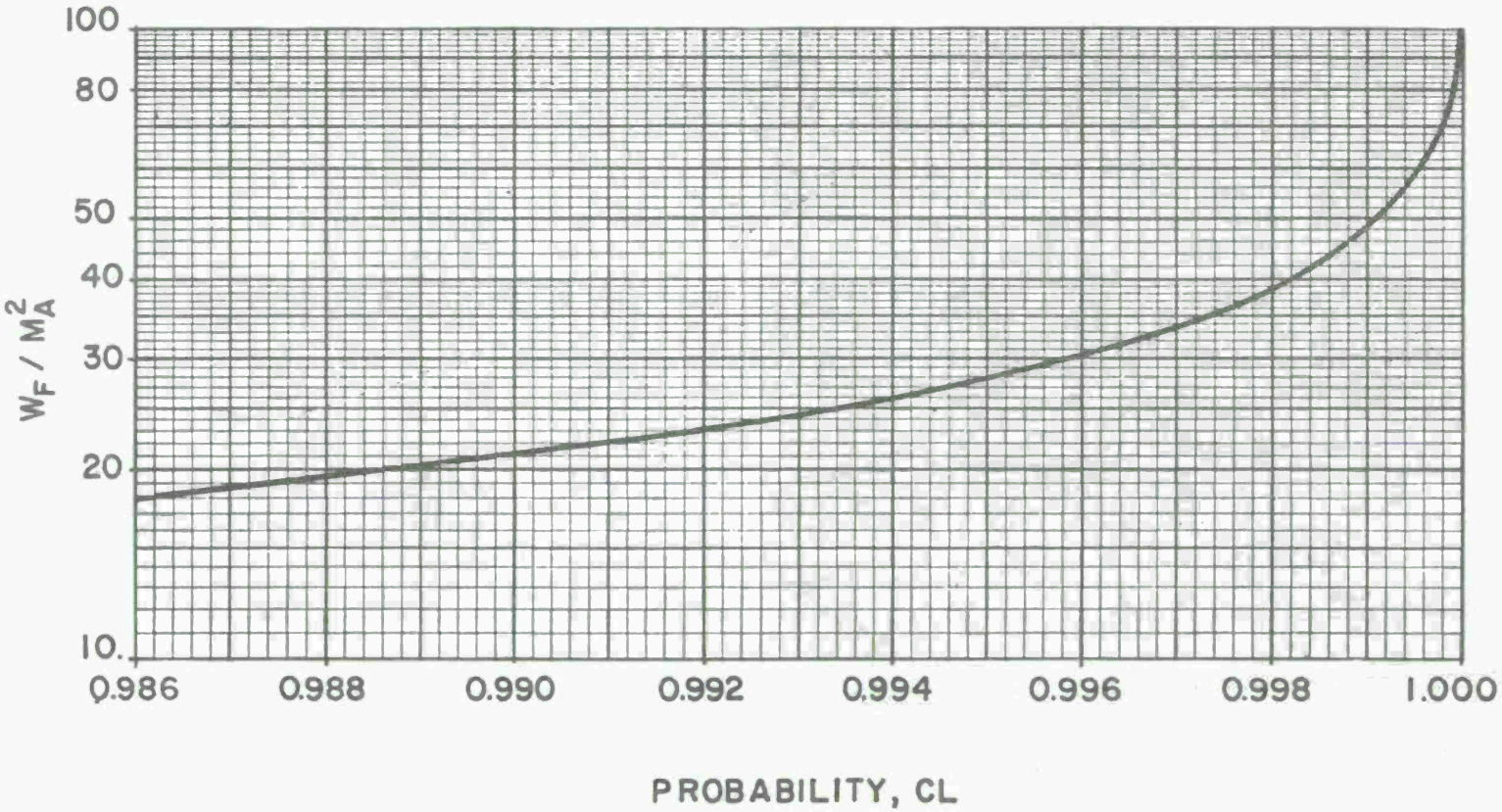

Fig 2 (b) Design fragment weight vs design confidence level

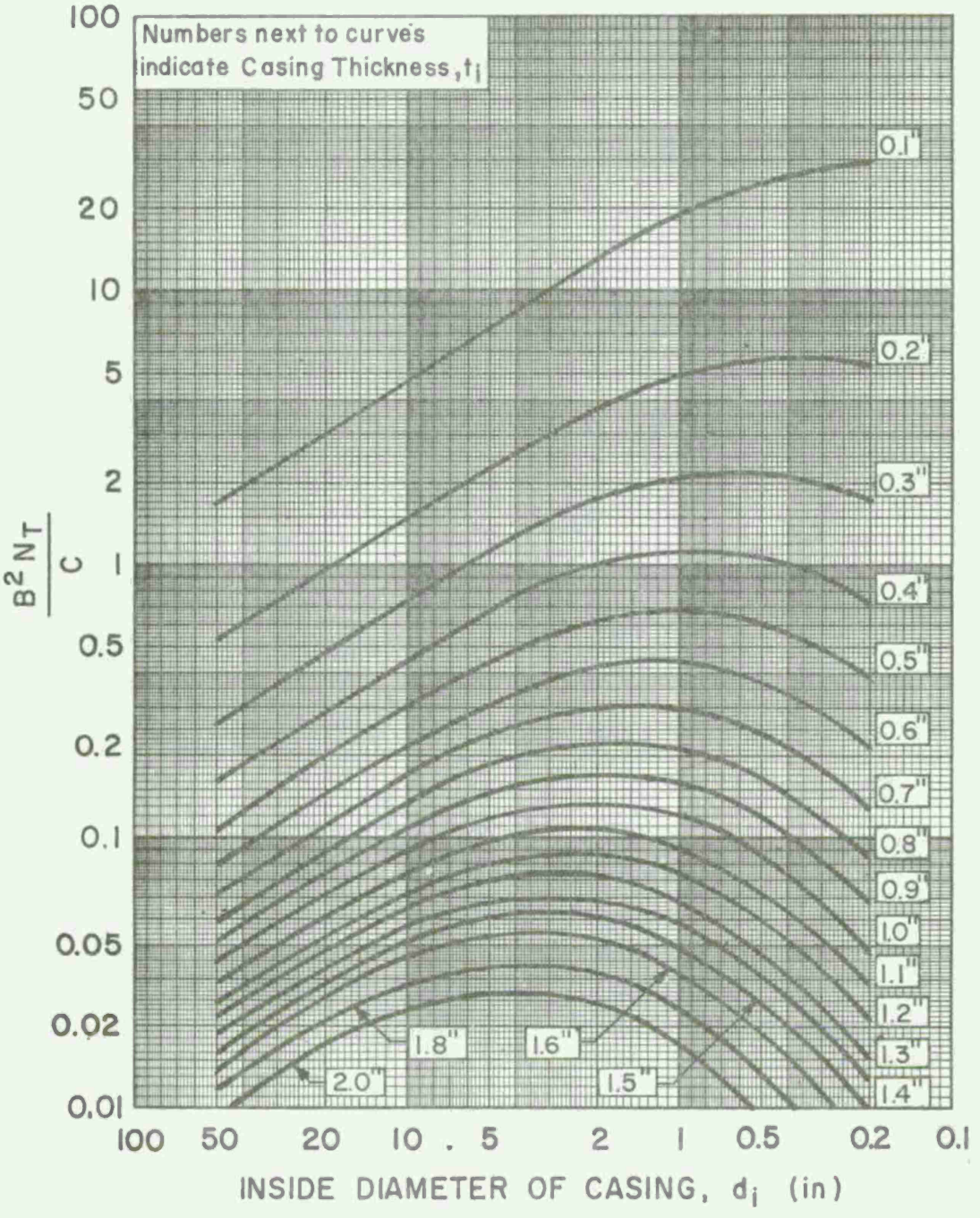

Fig 3 $\frac{B^2 N_T}{C}$ vs casing geometry

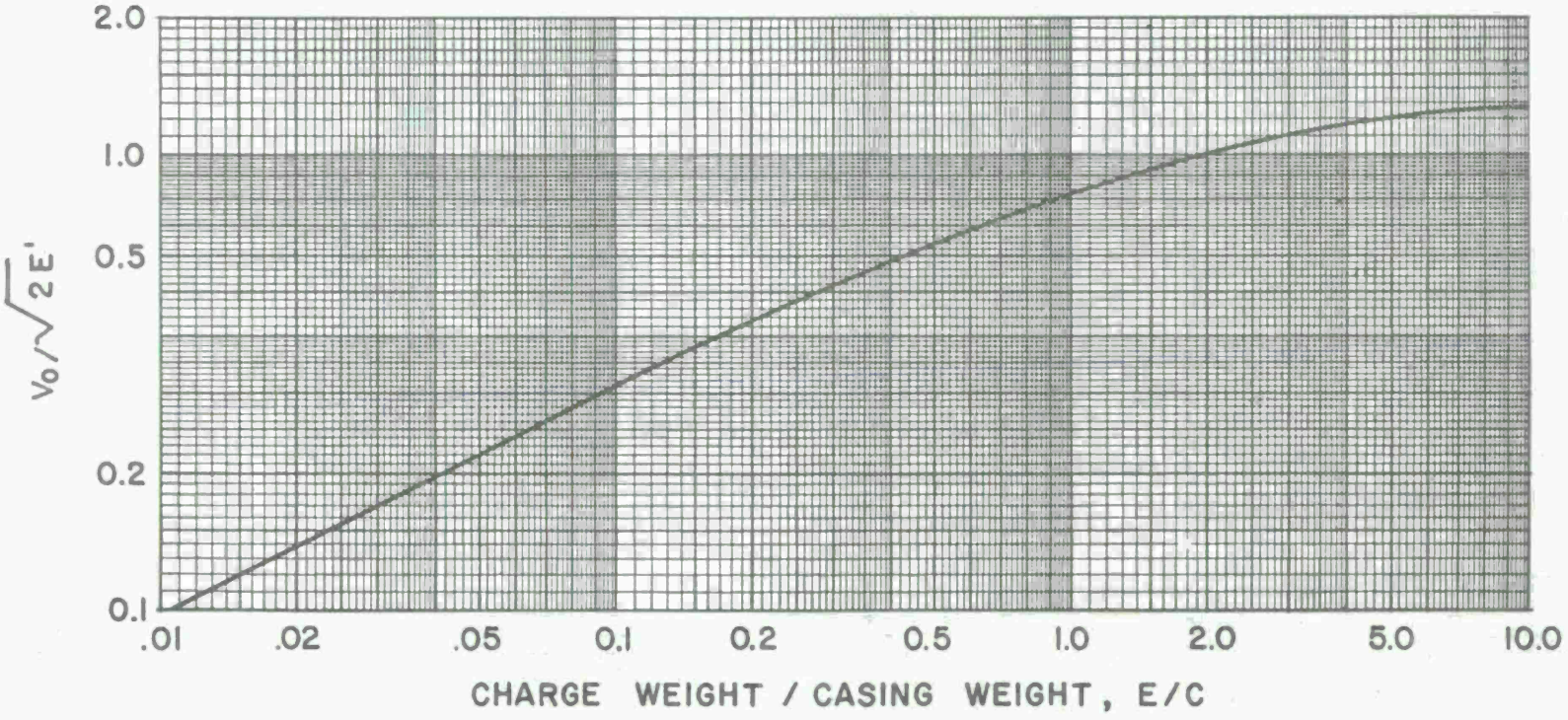

Fig 4 Initial velocity of primary fragments, cylindrical casing

Fig 5 Ratio of calculated initial velocities vs E/C

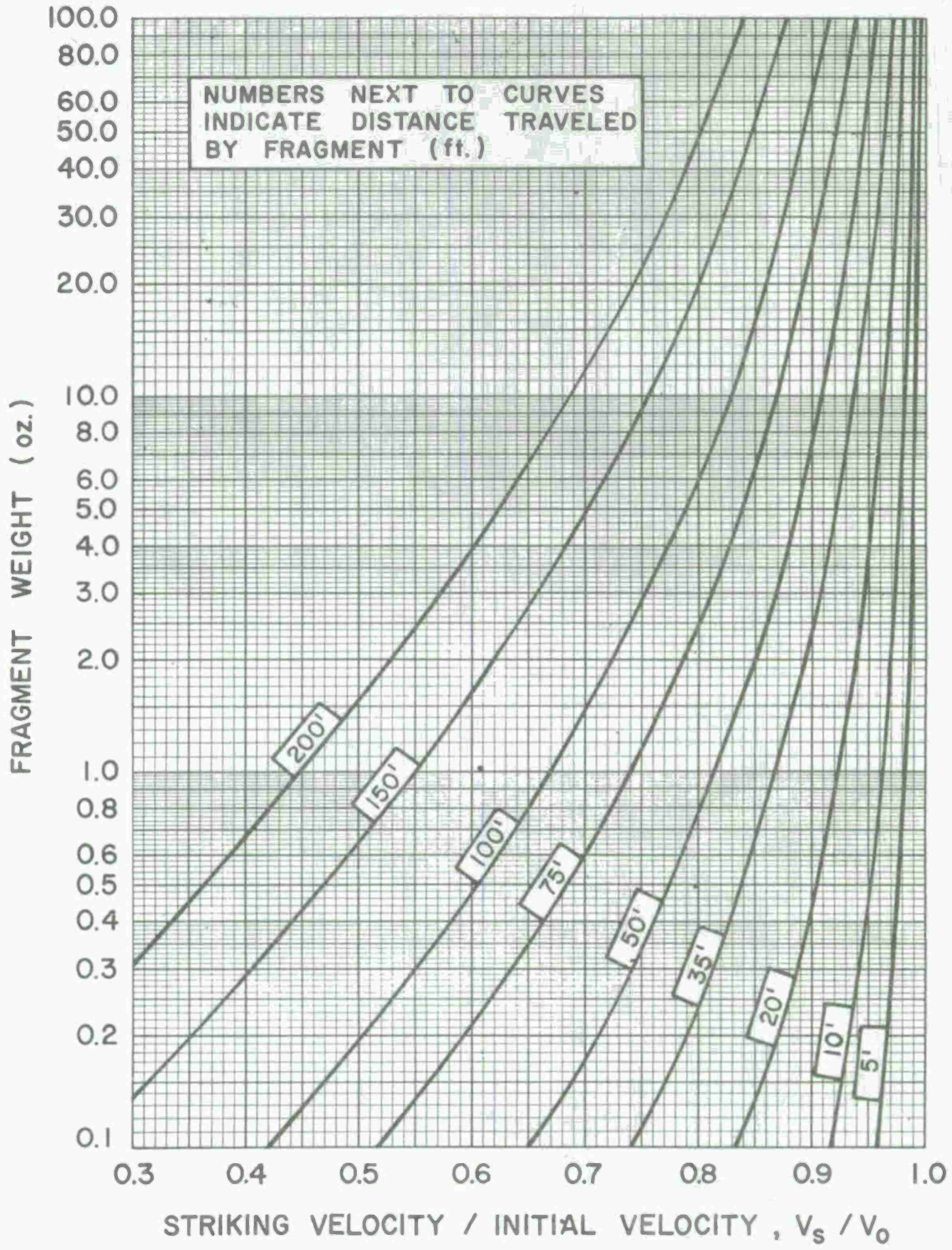

Fig 6 Variation of primary fragment velocity with distance

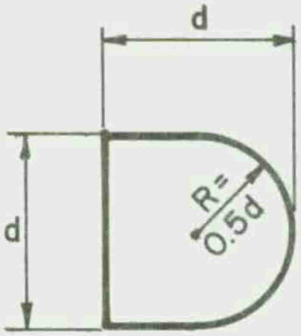

$n = R/d = 0.5$
$N = 0.845$
Volume $= 0.654d^3$
Weight $= 0.654d^3\gamma = 0.186d^3$
$D = 0.186$ lb./in.^{3}

7(a) STANDARD FRAGMENT SHAPE

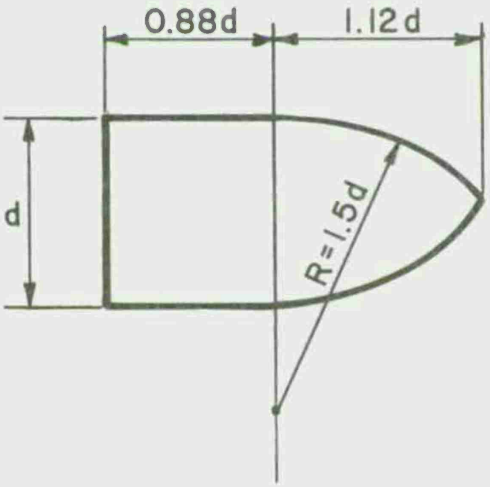

$n = R/d = 1.5$
$N = 1.00$
Volume $= 1.2d^3$
Weight $= 1.2d^3\gamma = 0.34d^3$
$D = 0.34$ lb./in.^{3}

7(b) ALTERNATE FRAGMENT SHAPE

Fig 7 Primary fragment shapes

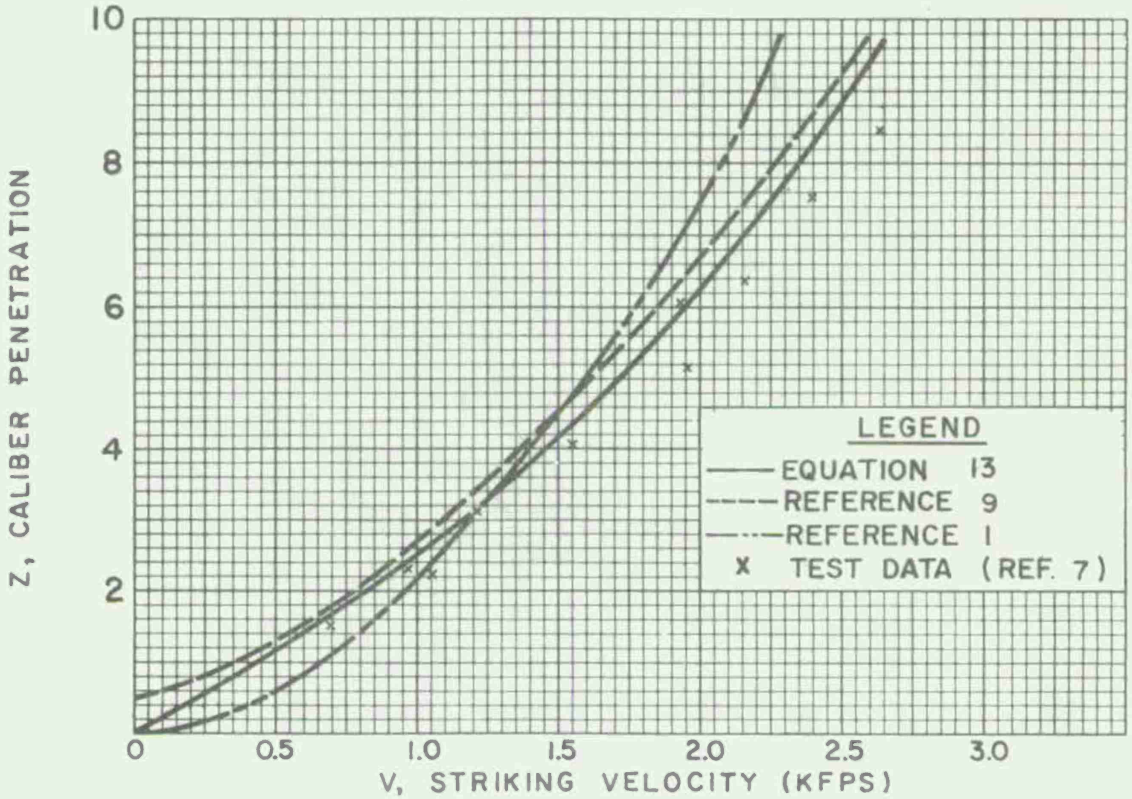

Fig 8 Concrete penetration empirical equations vs test data

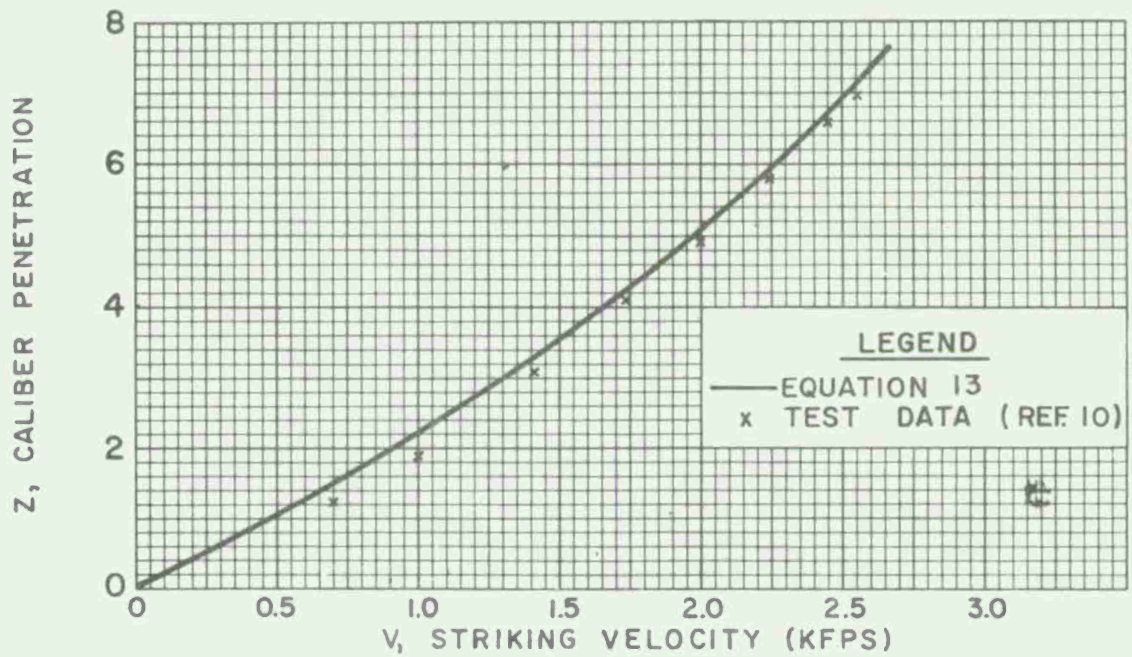

Fig 9 Concrete penetration empirical equation vs test data

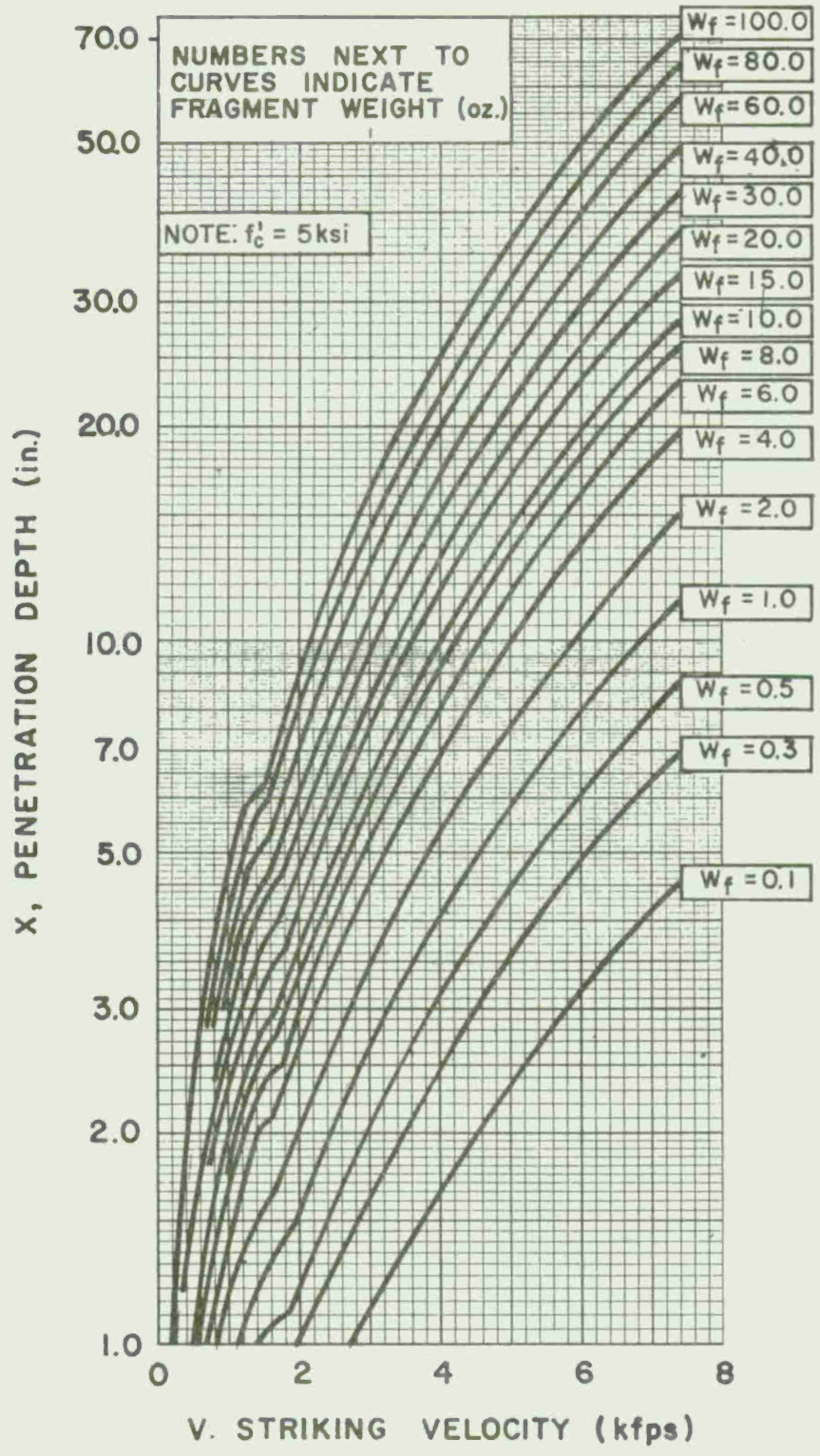

Fig 10 Concrete penetration chart (AP steel fragment)

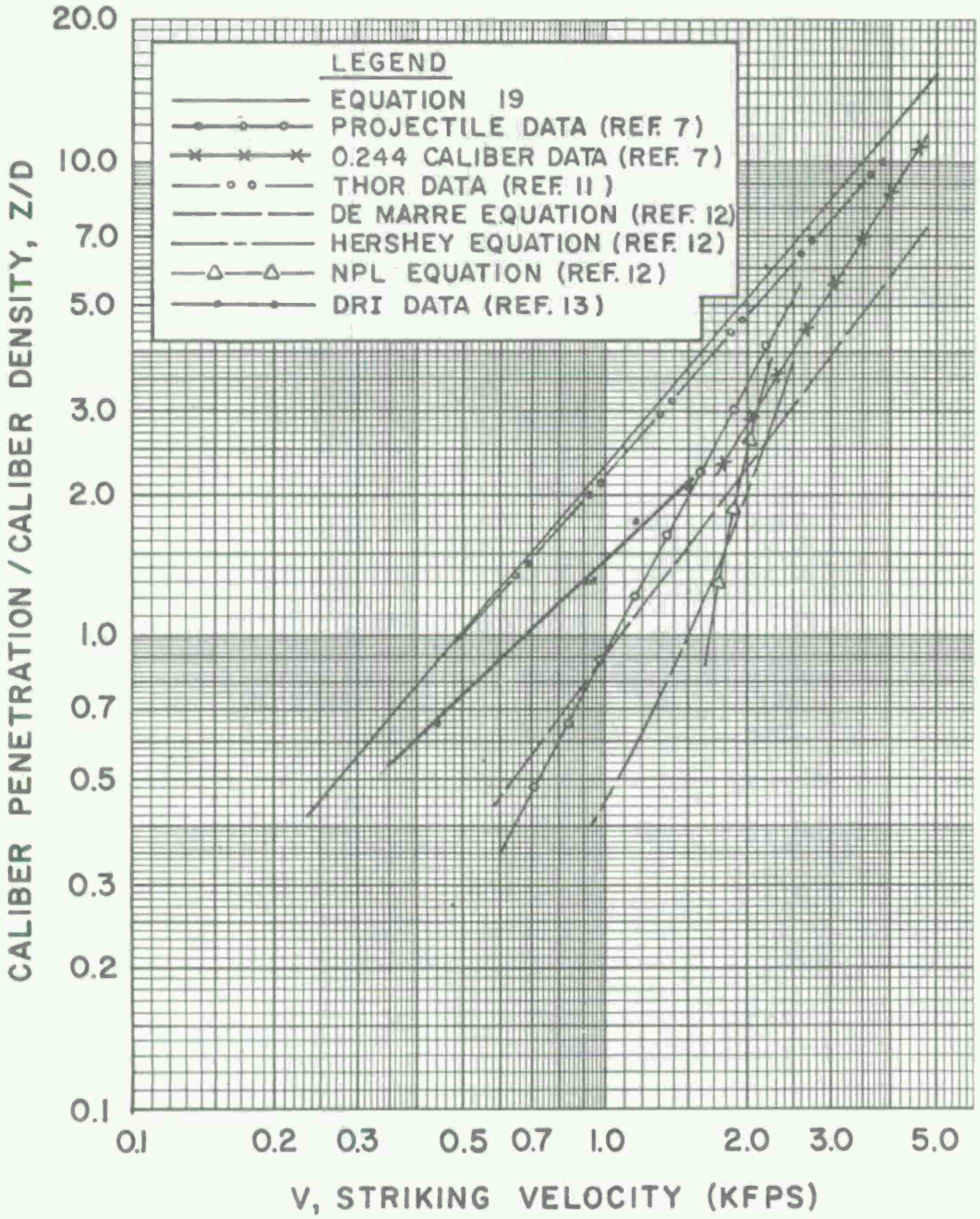

Fig 11 Steel penetration empirical equations
AP fragments into mild steel plate

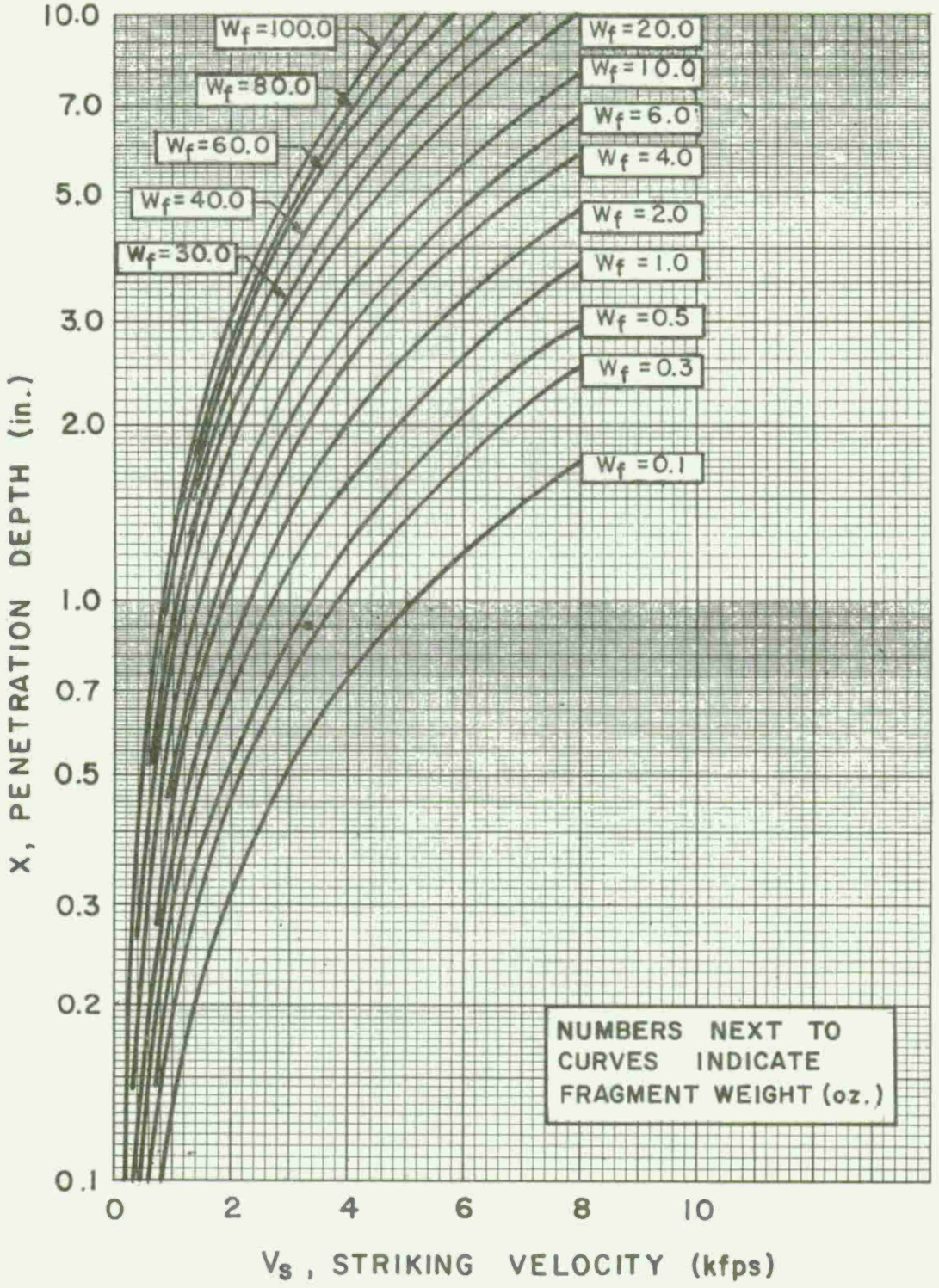

Fig 12 Steel penetration design chart
AP steel fragment, mild steel plate

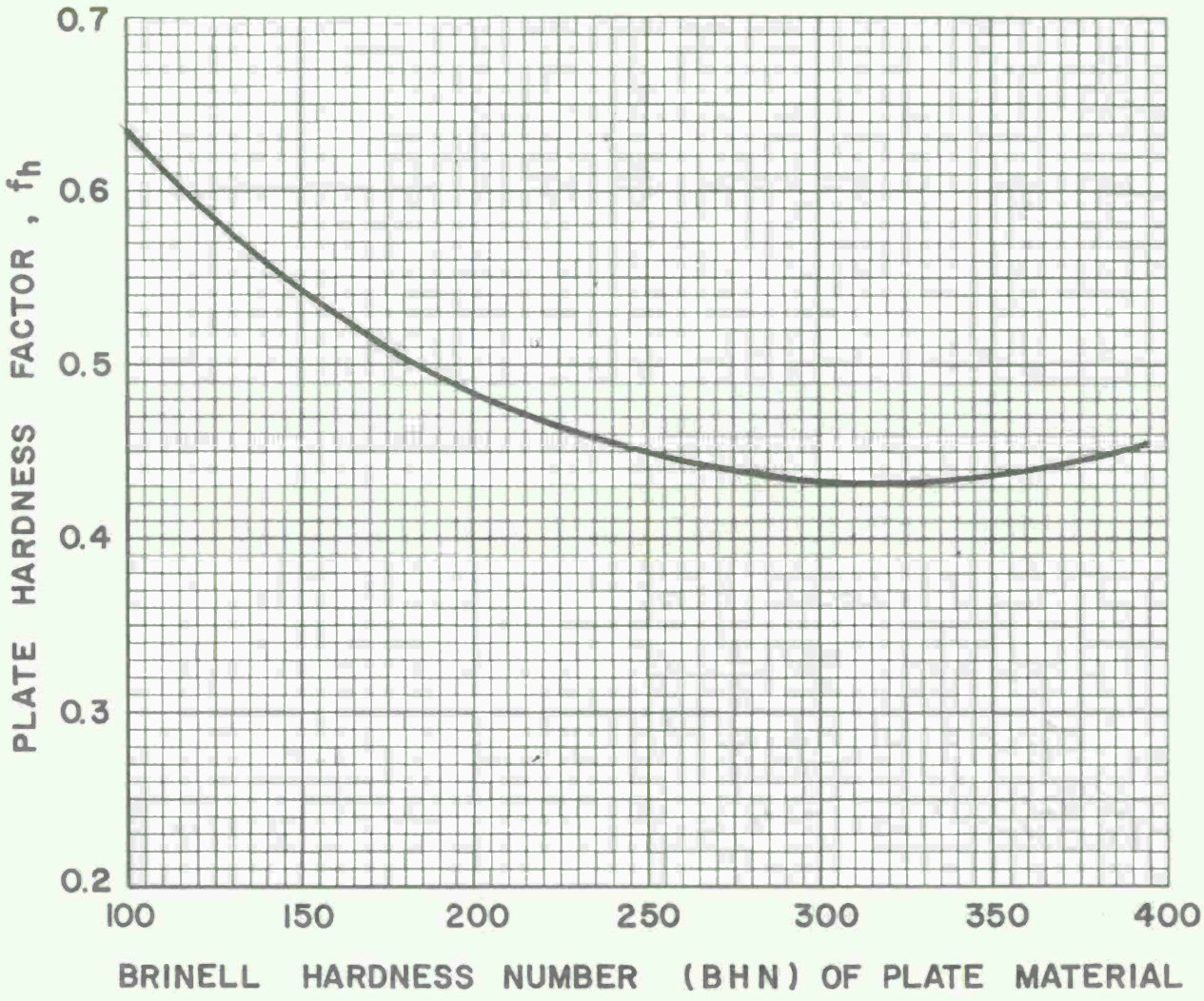

Fig 13 Plate hardness factor

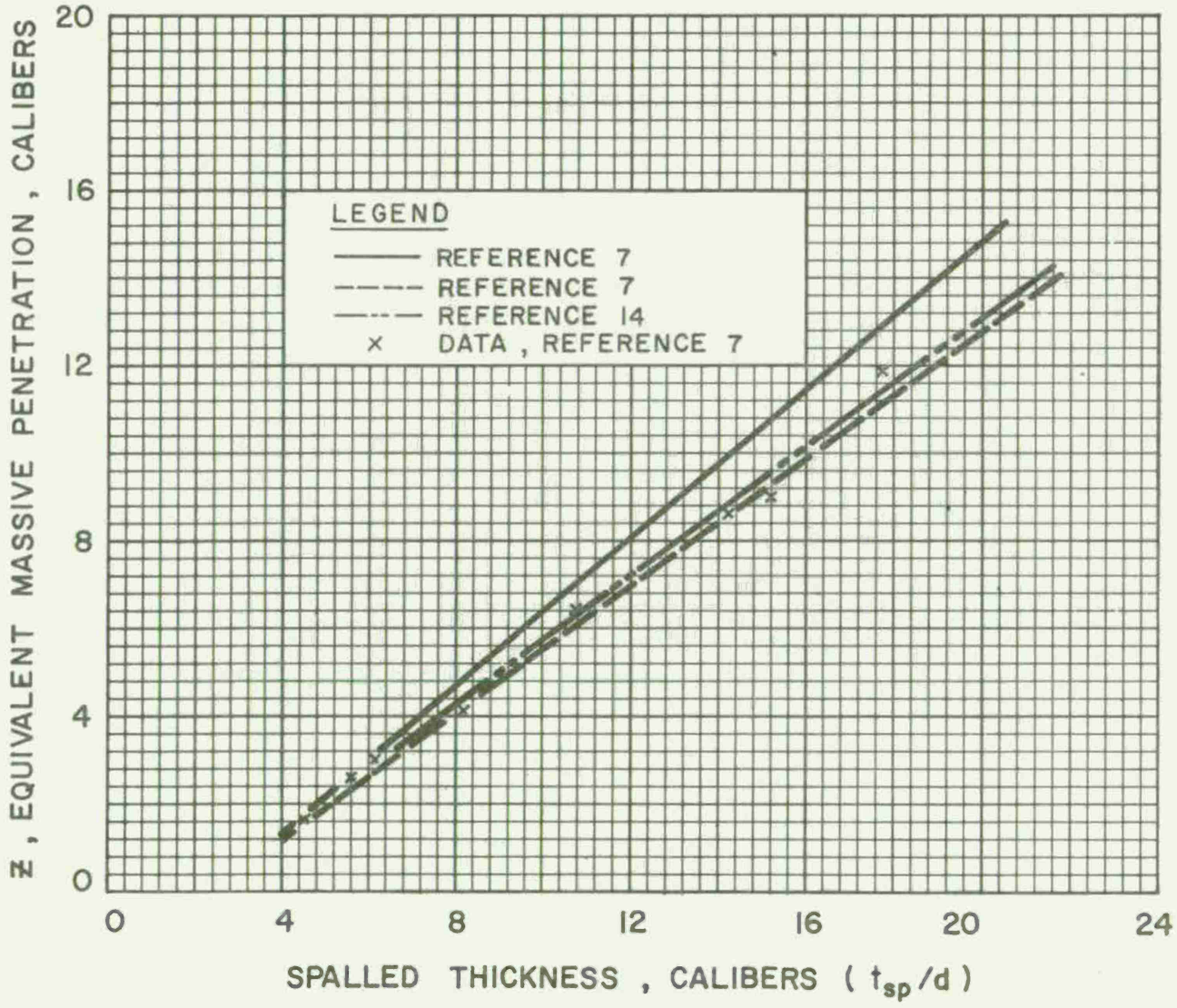

Fig 14 Spalling prediction equations

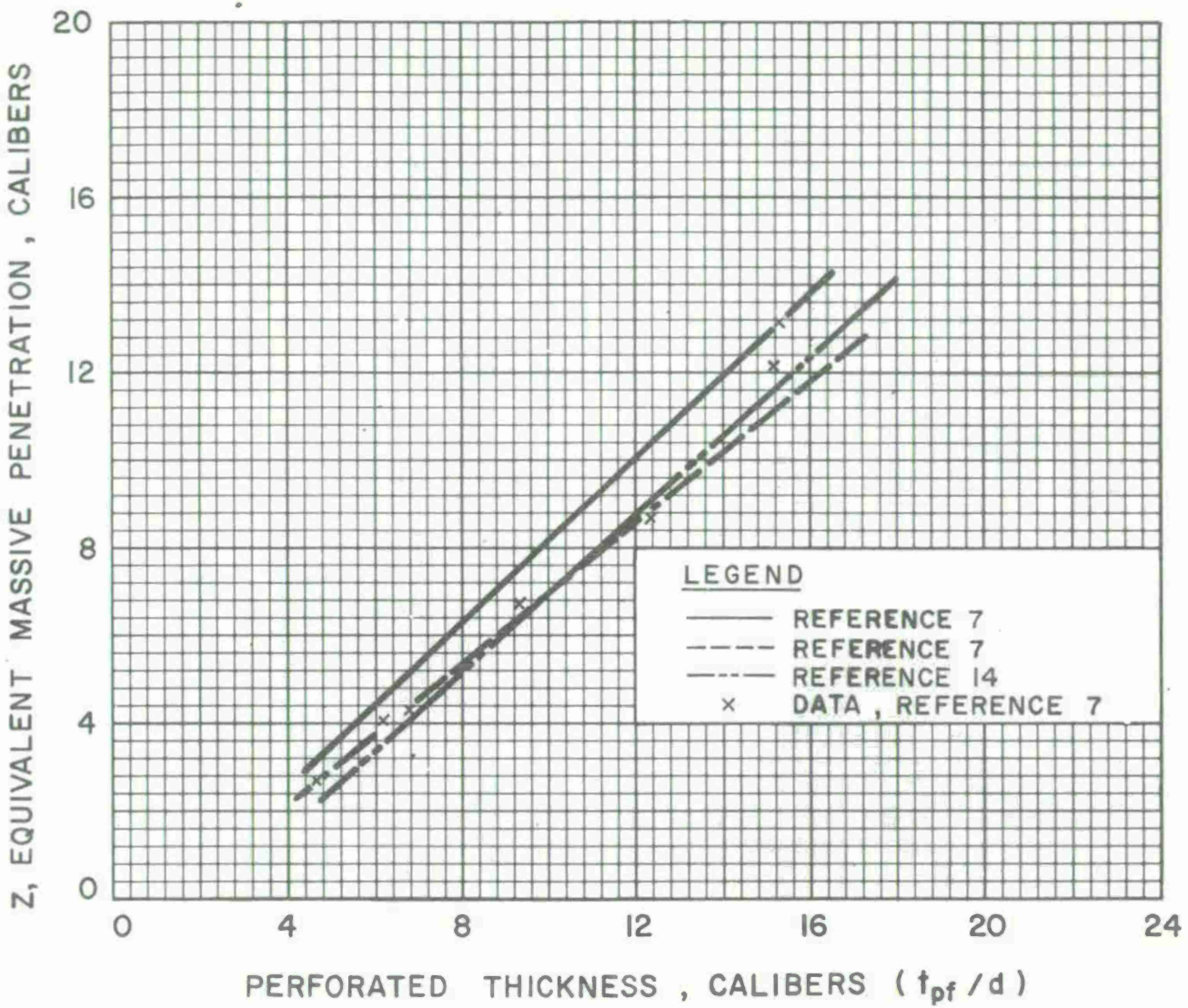

Fig 15 Perforation prediction equations

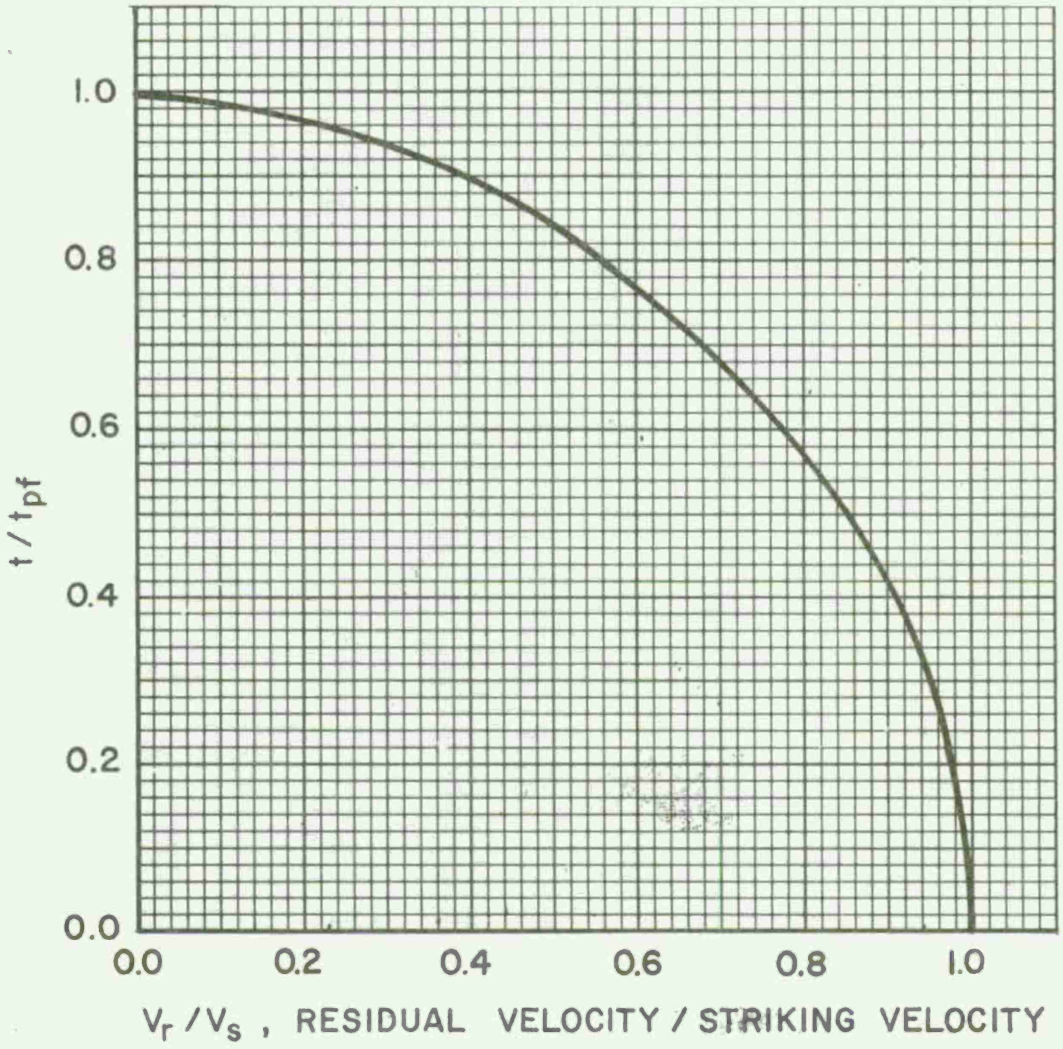

Fig 16 Residual fragment velocity upon perforation of concrete barriers (for cases where $X \leq 2d$)

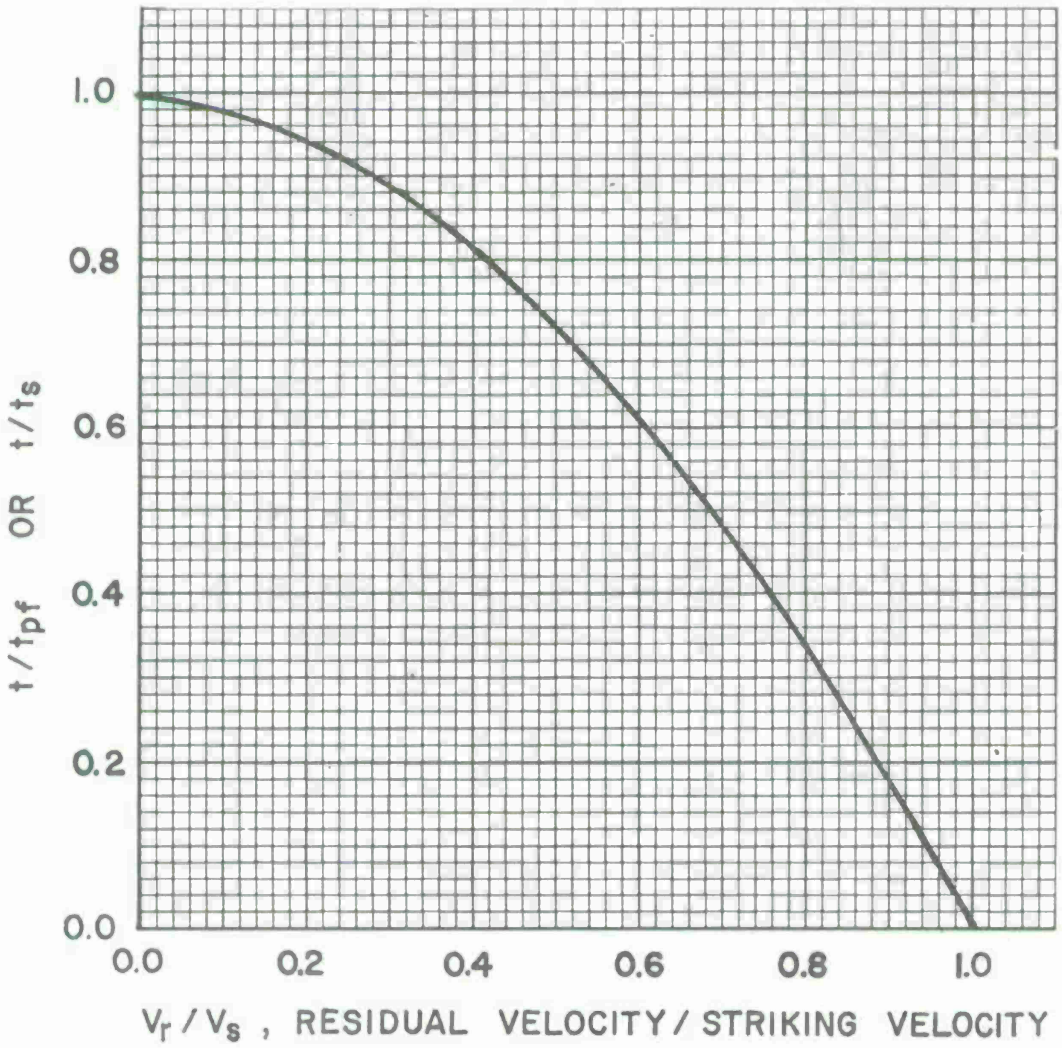

Fig 17 Residual fragment velocity upon perforation of concrete barriers (for cases where $X \geq 2d$)

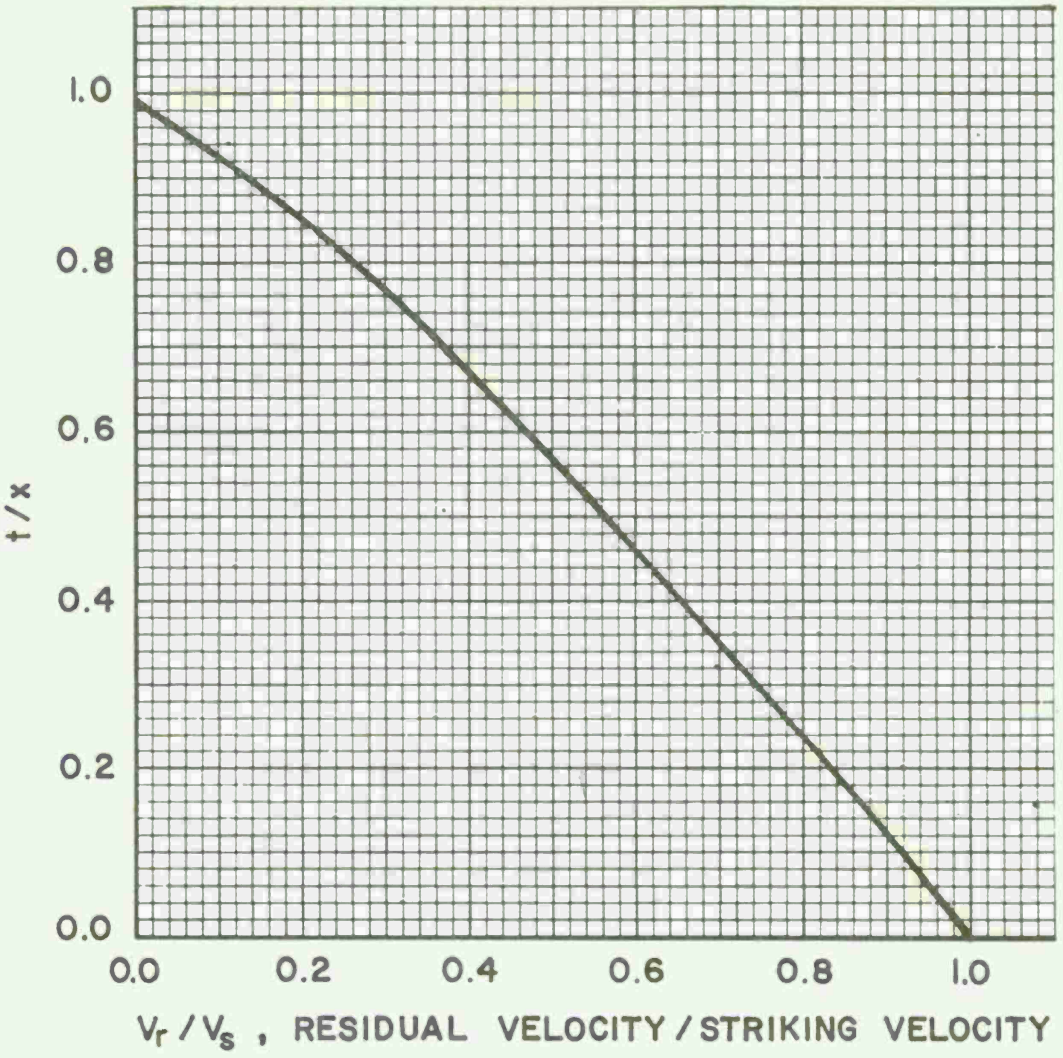

FIGURE 18 – RESIDUAL FRAGMENT VELOCITY UPON PERFORATION OF STEEL PLATE MATERIAL.

Fig 18 Residual fragment velocity upon perforation of steel plate material

BLAST ENVIRONMENT FROM FULLY AND PARTIALLY VENTED EXPLOSIONS IN CUBICLES

Sixteenth Annual Explosives Safety Seminar
Hollywood, Florida
24-26 September 1974

W. A. Keenan
J. E. Tancreto

CIVIL ENGINEERING LABORATORY
Naval Construction Battalion Center
Port Hueneme, California 93043

INTRODUCTION

The U. S. Army Armament Command (ARMCOM) is modernizing ammunition facilities, including equipment and protective structures, used in the manufacture, processing and storage of conventional munitions. Structures which serve to prevent explosion propagation, damage to material, or injury to personnel are being designed to comply with the Army TM5-1300 (Navy NAVFAC P-397) Manual, "Structures to Resist the Effects of Accidental Explosions." [1]. The manual contains methods and criteria to establish the output from an explosion in its environment and its effect on that environment in terms of blast, fragments and structural response.

In the plant modernization program it was found that the TM5-1300 manual lacks complete information in chapter 4 on the blast environment from partially confined explosions, i.e., explosions in an air space confined by one or more walls, such as cubicles which serve to direct and control the output from an accidental explosion. Consequently, Picatinny Arsenal (Manufacturing Technology Directorate) sponsored experiments at CEL (Civil Engineering Laboratory) to develop methods and criteria for predicting the blast environment in and around cubicles. Ammann and Whitney, Consulting Structural Engineers, New York, under contract to Picatinny Arsenal, provided technical guidance throughout the study.

The CEL experiments involved exploding a range of charge weights inside several small-scale cubicles representing various sizes, shapes, vent areas and charge densities. A four-wall cubicle was tested with a restricted roof opening of various sizes to provide data on partially vented cubicles.* Two three-wall cubicles, each with and without a roof, were tested to collect data on fully vented cubicles.* The charge weight (W) varied from 0.50 to 3.00 pounds of Composition B explosive, charge density (W/V) from 0.009 to 0.375 lb/ft^3, and the degree of venting (A/V) from 0.010 to 1.00 ft^2/ft^3. The blast pressure history was measured inside the cubicle and outside at scaled distances ($R/W^{1/3}$) from 1.42 to 63.0 $ft/lb^{1/3}$. The blast environment was related to scaled parameters, involving A, V, W and R, in the form of design charts and equations to aid the designer in predicting the positive and negative pressures, duration and impulse outside

*Distinction between full and partial venting depends on the duration of gas pressures generated inside the cubicle compared to the average duration of shock pressures acting on the cubicle walls. If the gas duration exceeds the shock duration, the partially confined explosion is classified as a partially vented explosion.

fully and partially vented cubicles and the peak gas pressure, impulse, and duration inside partially vented cubicles. A detailed description of the experiments and analysis of the results is contained in Reference 2.

This paper presents and discusses some significant findings from the CEL study, including a series of design charts for predicting the blast environment in and around fully and partially vented cubicles, sample problem solutions which illustrate applications of the design charts, and the influence of cubicle and charge parameters on safe-separation distance requirements for those cases where blast environment, not fragments, dictate safety requirements.

CONFINED EXPLOSIONS

Explosions generate pressures from shock waves produced by the detonation. If the explosion is confined inside an enclosed or partially vented cubicle, gaseous by-products of the explosion generate gas pressures, in addition to the shock pressures. The initial shock wave strikes the walls of the cubicle and is reflected. The reflected waves produce extremely high blast pressures on the walls. The blast pressures rapidly decay as the energy in the shock wave rapidly dissipates.

In the same time period, the gas pressures rise inside the cubicle to some peak value and then gradually decay as gas temperatures drop and gas pressures are vented from the cubicle. The peak gas pressure is characteristically low compared to the peak blast pressure. However, when the vent area is small, the duration of the gas pressure can be many times greater than the duration of the blast pressure. If the vent area is increased, the duration of the gas pressure will decrease. At some critical vent area, the duration of the gas pressure will equal the duration of the blast pressure. This critical vent area can define the division between fully and partially vented explosions.

In terms of structural response, the gas pressure pulse can be far more damaging than the shock pulse, depending on the duration of the gas pulse, t_g, relative to the duration of the shock pulse, t_o. If $t_g/t_o < 1$, the explosion is classified as a fully vented explosion and the gas pulse, if any, can be neglected in the design of the cubicle. Figure 1b is typical of the pressure pulse inside a fully vented cubicle. For $t_g/t_o > 1$, the explosion is classified as a partially vented explosion and both the gas and shock pulses must be considered in the design of the cubicle. Figure 1a is typical

of the pressure pulse inside a partially vented cubicle. The importance of the gas impulse increases with t_g/t_o until at some large value of t_g/t_o, the shock pulse can be neglected since its energy is insignificant compared to that in the gas pulse. Therefore, in presenting methods and criteria for blast environment in and around cubicles, it is useful for design purposes to delineate between fully and partially vented explosions.

PARTIALLY VENTED EXPLOSIONS

Definition

The scaled duration of positive pressure measured inside the cubicles is plotted in Figure 2 as a function of the scaled vent area, $A/W^{2/3}$. The unshaded data points denote cases where $t_g > t_o$. The shaded points denote cases where it appeared that $t_g < t_o$.

The family of lines shown in Figure 2 connect data points representing the same value of W/V. The solid lines are straight, parallel and connect all data points corresponding to $t_g > t_o$. The dashed lines connect the data points believed to correspond to $t_g < t_o$. The dashed lines are also straight and parallel but their slopes are greater.

Between the ends of the solid and dashed lines is a zone which defines the transition from $t_g > t_o$ (partially vented cubicle) to $t_g < t_o$ (fully vented cubicle). There is insufficient experimental data to exactly define the transition zone but the zone can be bounded. It was discovered that a line which falls just "below" all unshaded data points is described by

$$A/V^{2/3} = 0.21 \qquad (1)$$

Equation 1 is considered a reasonable upper bound to the transition zone corresponding to $t_g = t_o$. Similarly, a line which falls just "above" all shaded data points is described by

$$A/V^{2/3} = 0.60 \qquad (2)$$

Equation 2 is considered a reasonable lower bound to the transition zone corresponding to $t_g = t_o$. In other words, the parameter $A/V^{2/3}$, with a

value somewhere between $0.21 < A/V^{2/3} < 0.60$, defines the division between a fully and partially vented explosion, at least for the range of test parameters. Note that $A/V^{2/3}$ is independent of charge weight and a dimensionless parameter and, therefore, independent of the physical size of the cubicle and charge.

To be conservative, it is recommended for design purposes that a cubicle be considered partially vented if $A/V^{2/3} < 0.60$. This criterion implies, as illustrated in Figure 2, that the practical sizes of three-wall cubicles with and without a roof and four-wall cubicles without a roof are fully vented cubicles ($A/V^{2/3} > 0.60$).

Blast Environment Inside Cubicle

Peak Gas Pressure

The peak gas pressure, p_g, measured inside the test cubicles is plotted as a function of W/V in Figure 3. The figure includes experimental data reported in Reference 3 for Composition B charges ($0.0016 \leq W/V \leq 0.0259$ lb/ft^3) inside a relatively large four-walled cubicle with a circular vent hole in its roof. The curved line in Figure 3 is the predicted peak gas pressures using an NOL computer program [4].

The measured peak gas pressures and NOL predicted values are in excellent agreement for a degree of venting, $A/V < 0.010$ ft^2/ft^3. (Similar agreement was found by Proctor and Filler in comparing NOL predictions with peak gas pressures measured by H.R.W. Weibull for a wide range of charge to volume ratios, $0.00125 < W/V < 0.287$ lb/ft^3, but for relatively small vent areas, $7.6 \times 10^{-6} < A/V < 60 \times 10^{-4}$ ft^2/ft^3) [4]. For larger degrees of venting ($A/V > 0.010$), the data points in Figure 3 fall well below the NOL curve and for a fixed degree of large venting, the difference increases with W/V. For example, for points with $A/V = 0.043$ and 0.031, the measured gas pressures are lower by 27% at $W/V = 0.0069$, 31% at $W/V = 0.069$, 39% at $W/V = 0.145$ and 52% at $W/V = 0.287$. Some of the differences may stem from possible errors in interpreting the measured pressure histories but this source of error could account for no more than perhaps 20% of the difference.

It is concluded from Figure 3 that p_g depends on W/V and to a lesser degree on A/V. For $A/V < 0.010$, venting has no appreciable influence on p_g but for $A/V > 0.010$ the decrease in p_g can be significant,

especially for large values of W/V. Experiments are needed to find the relationship between p_g and W/V for large values of A/V. Until this relationship is found, it is recommended that the NOL curve for gas pressure be used for predicting design loads for $A/V < 0.010$ ft^2/ft^3 and a value 25% less for $A/V > 0.010$ ft^2/ft^3.

Impulse of Gas and Shock Pressures

The scaled peak impulse of the gas pressure measured inside the cubicles is plotted in Figure 4 as a function of the scaled vent area, $A/W^{2/3}$. The unshaded data points denote cases where the total impulse of the gas pressure, i_g, far exceeded the total impulse of the shock pressure, i_s.

The family of solid lines in Figure 4 connect data points having the same value of W/V. The best fit lines are straight and parallel, at least within the range of experimental data. These lines are described by

$$i_g/W^{1/3} = 569\ (A/W^{2/3})^{-0.78}\ (W/V)^{-0.38} \quad \text{for } A/V^{2/3} < 0.21 \qquad (3)$$

Equation 3 has some error because it is derived from impulse data which include the combined impulse from gas and shock pressures. However, any error in Equation 3 from this source is considered insignificant since all data points originate from pressure-time histories which clearly show the shock impulse was insignificant compared to the gas impulse.

There is no experimental data to define the exact shape of the lines in Figure 4 for $0.21 < A/V^{2/3} < 0.60$. To provide compatibility with the impulse curves in the TM5-1300 Design Manual for a fully vented cube, the shapes of the dashed lines in Figure 4 were drawn so that at $A/V^{2/3} = 0.60$, the effective duration of the shock pressure, t'_o, given by Equation 4-1 of the TM5-1300 Design Manual [1] is equal to the effective duration of the gas pressure, $t'_g = 2\, i_g/p_g$. By this scheme, the impulse curves in Figure 4 provide a smooth transition from a partially vented cube to a fully vented cube and are compatible with the pressure loading obtained from the TM5-1300 Design Manual for a fully vented cube.

The instrumentation in the CEL experiments did not allow measurements of the shock pressure impulse. For example, in the partially vented cubicles the shock impulse could not be isolated from the much larger

gas impulse. In the fully vented cubicles, where the gas impulse was insignificant, the shock pressures were too severe for the pressure transducers. However, Figures 4-17 through 4-62 of the TM5-1300 Design Manual already contain curves for predicting the average shock impulse on the wall of a cubicle.

It is recommended for design purposes that Figure 4 be used to predict the gas impulse for $A/V^{2/3} < 0.60$ and Figures 4-17 through 4-62 of the TM5-1300 Design Manual be used to predict the shock impulse for any value of $A/V^{2/3}$. A procedure for predicting i_g for $A/V^{2/3} > 0.60$ is not necessary since one will find in using the above recommendations that for $A/V^{2/3} > 0.60$, $i_g < i_s$, $t'_g < t'_o$ and $p_g < p_r$, i.e. for $A/V^{2/3} > 0.60$, the shock pressure pulse completely masks the gas pressure pulse, and, therefore, dictates the pressure-time design loading for the cubicle.

Duration of Gas and Shock Pressures

The family of straight lines shown in Figure 2 can be expressed in the form

$$t_g/W^{1/3} = 2.26\ [AW^{1/3}/V]^{-0.86} \quad \text{for } A/V^{2/3} < 0.21 \qquad (4)$$

$$t_o/W^{1/3} = 0.664\ [AW^{1/3}/V]^{-1.14} \quad \text{for } A/V^{2/3} > 0.60 \qquad (5)$$

The term $AW^{1/3}/V$ in Equations 4 and 5 is defined as the scaled degree of venting.

Equations 4 and 5 are compared with experimental data in Figure 5. As expected, the unshaded data points ($t_g < t_o$) fall along the solid line (Equation 4) and the shaded data points ($t_g < t_o$) fall along the dashed line (Equation 5). The transition zone, defined in Figure 2 by $0.21 < A/V^{2/3} < 0.60$, falls between these lines and is represented in Figure 5 by a series of reverse curves which are tangent to the solid and dashed lines. Note in Figure 5 that the relative position of the transition lines depends on W/V. For $0.21 < A/V^{2/3} < 0.60$, one must enter Figure 5 with known values of both $AW^{1/3}/V$ and W/V to determine the duration of the positive pressure. It is important to note that the duration obtained from Figure 5 is the duration of the exponentially decaying pressure pulse.

For convenience in design, the exponential pressure pulse is replaced by an equivalent triangular-shaped, pressure-time pulse having the same total impulse. It is recommended that the effective gas duration, t'_g, of the equivalent triangular gas pulse be calculated as

$$t'_g = 2\, i_g / p_g \qquad (6)$$

where i_g = Total gas impulse obtained from Figure 4

p_g = Peak gas pressure obtained from Figure 3

Further, it is recommended that the effective shock duration, t'_o, of the equivalent triangular shock pulse be calculated from Equation 4-1 of TM5-1300 Design Manual [1].

Blast Environment Outside Cubicle

Personnel or frangible buildings may be located in the near vicinity of a cubicle containing explosives. An accidental explosion may produce a blast environment outside the cubicle which constitutes a high hazard to personnel or an unacceptable level of damage to the buildings. In this case, it may be necessary to confine and partially vent the explosion inside a cubicle to reduce the blast environment at some distance from the charge to a safe level. To accomplish this, the designer must know the influence of the size and vent area of the cubicle and the weight and location of the charge on the exterior blast environment at any range from a cubicle.

Peak Positive Pressure

Pressure data from the CEL tests of partially vented cubicles can be described, as shown in Reference 2, by Equation 7.

$$p_{so} = 464 \left(\frac{AW^{1/3}}{V}\right)^{0.37} \left(\frac{R}{W^{1/3}}\right)^{-1.58} \quad \text{for } A/V^{2/3} < 1.0 \qquad (7)$$

Equation 7 describes the leakage pressures from partially vented cubicles ($A/V^{2/3} < 0.60$). However, since data from an open-top cube ($A/V^{2/3} = 1.0$ also fits Equation 7, $A/V^{2/3} < 1.0$) is given as the limit. Note that

leakage pressures depend on the scaled degree of venting, $AW^{1/3}/V$, and the scaled distance from the charge, $R/W^{1/3}$.

Equation 7 indicates that p_{so} is more sensitive to R than A/V. For example, to decrease p_{so} by say 50%, either R must be increased 55% or A/V decreased 84.6%. The important point is that the designer can still "buy considerable distance" by reducing A/V. Where real estate is a premium, controlling p_{so} by adjusting A/V may be the only solution.

Equation 7 was used to construct the design chart shown in Figure 6. The chart is useful in selecting the degree of venting needed to limit the leakage pressure to a safe level at any distance from a partially vented explosion. It is recommended that Figure 6 be used for design purposes provided $A/V^{2/3} \leq 1.0$.

Peak Positive Impulse

Frequently, blast pressures outside a cubicle are very short in duration compared to the fundamental period of vibration of structures located in the near vicinity of the cubicle. In this case, the blast loading is applied very quickly as an impulse which simply imparts an initial velocity to the structure. Resulting peak deflections and the extent of structural damage depend on the peak positive impulse, i_s.

In Reference 2, the impulse data from the CEL cubicles was used to construct the design chart for impulse shown in Figure 7. The chart is useful for selecting the vent area needed to limit the peak positive impulse at any range outside a partially vented explosion. The chart should yield reasonable values of $i_s/W^{1/3}$ within the range of the test data, i.e., $0.072 < W/V < 0.289$ and $0.008 < AW^{1/3}/V < 0.721$. For large values of $AW^{1/3}/V$, Figure 7 indicates that $i_s/W^{1/3}$ is almost independent of $AW^{1/3}/V$ and approaches the value from an unconfined surface burst. As $AW^{1/3}/V$ decreases in value, $i_s/W^{1/3}$ becomes more sensitive to $AW^{1/3}/V$ until for values of $AW^{1/3}/V \lesssim 0.02$, a given change in $AW^{1/3}/V$ produces almost an identical percentage change in $i_s/W^{1/3}$.

It is recommended that Figure 7 be used for design purposes to predict the peak positive impulse outside partially vented cubicles.

Duration of Positive Pressure

Most theoretical procedures for predicting the dynamic response of structures are based on a triangular pressure-time pulse. Consequently, for design purposes, the actual pressure pulse with an exponential decay is approximated by an equivalent triangular pressure-time pulse [1]. The duration of the actual pulse is replaced by a fictitious duration, t'_o, such that the peak pressure, p_{so}, and total impulse, i_s, of the actual and equivalent pulses are identical.

$$t'_o/W^{1/3} = 2\ (i_s/W^{1/3})/p_{so} \qquad (8)$$

Values of $t'_o/W^{1/3}$ from Equation 8 and measured values of $t_o/W^{1/3}$ are plotted versus $R/W^{1/3}$, for several values of $AW^{1/3}/V$, in Reference 2. A smooth curve through the data points is an s-shaped curve, characteristic of the relationship for an unconfined surface burst. Measured values of $t_o/W^{1/3}$ are in fair agreement with Equation 8, except for $R/W^{1/3} < 5$ and very small degrees of scaled venting. In other words, the exponential decay in actual pressure is much greater for very small degrees of venting and scaled distances.

Equation 8 is recommended for design purposes, except for very small scaled degrees of venting ($A/W^{1/3}/V < 0.01$) and scaled distances ($R/W^{1/3} < 5$).

Design Problem

The following problems and their solution serve to illustrate the use of the various charts for constructing the pressure-time loadings (shown in Figure 1) in and around a partially vented cubicle. The first problem illustrates the case where the gas pressures dominate the loading

Problem 1

A four-wall cube with a hole in its roof contains 17 pounds of Composition B explosive located at the geometric center of the cubicle. The length of each wall is 10 feet. The vent hole in the roof is 3.0 feet in diameter. (a) Is the cubicle partially vented? (b) Calculate the pressure-time loading (Figure 1) acting on a wall and (c) Calculate the pressure-time loading outside the cubicle at a point 24 feet from the charge.

Solution

(a) Given W = 17 lb, $A = \pi D^2/4 = \pi(3.0)^2/4 = 7.1$ ft^2 and V = 10 x 10 x 10 = 1,000 ft^3. Therefore, $A/V^{2/3} = 7.1/(1,000)^{2/3} = 0.07$. Since $A/V^{2/3} \leq 0.60$, the cubicle is partially vented and gas pressures must be considered in the loading.

(b) $W/V = 17/1,000 = 0.017$ and $AW^{1/3}/V = 0.018$. From Figure 3, $p_g = 135$ psi. From Figure 5, $t_g/W^{1/3} = 70$ or $t_g = 70(17)^{1/3} = 180$ msec. From Figure 4, $i_g/W^{1/3} = 2,540$ or $i_g = 2,540(17)^{1/3} = 6,530$ psi-mec. For design purposes, the effective duration of the equivalent triangular load pulse from Equation 6 is $t'_g = 2i_g/p_g = 2(6,530)/135 = 97$ msec. From chapter 4 of Reference 1, $i_s/W^{1/3} = 200$ or $i_s = 200(17)^{1/3} = 514$ psi-msec. From Equation 4-1 of Reference 1, $t'_o/W^{1/3} = 1.3$ or $t'_o = 1.3(17)^{1/3} = 3.3$ msec. For design purposes, the fictitious-peak shock pressure is $p_r = 2i_s/t'_o = 2(514)/3.3 = 311$ psi. The calculated pressures, impulses and time durations apply to the load diagram shown in Figure 1a.

(c) Given R = 244 ft and $AW^{1/3}/V = 0.018$. Therefore, $R/W^{1/3} = 24(17)^{1/3} = 9.4$ ft/lb$^{1/3}$. From Figure 6, $p_{so} = 3.0$ psi. From Figure 7, $i_s/W^{1/3} = 2.4$ or $i_s = 2.4(17)^{1/3} = 6.16$ psi-msec. From Equation 8, the effective duration of the equivalent triangular pulse is $t'_o = 2i_s/p_{so} = 2(6.16)/3.0 = 4.1$ msec. The calculated pressures, impulses and time duration apply to the load diagram shown in Figure 1b.

Problem 2

The vent hole in the roof of the cubicle described in Problem 1 is increased to 8.75 feet in diameter. (a) Is the cubicle fully vented? (b) Calculate the pressure-time loading acting on a wall.

Solution

(a) Given D = 8.75 ft. Therefore, $A = \pi D^2/4 = \pi(8.75)^2/4 = 60$ ft^2. V = 1,000 ft^3. Therefore, $A/V^{2/3} = 60/(1,000)^{2/3} = 0.60$. Since $A/V^{2/3} \geq 0.60$, the cubicle is fully vented and no gas pressure must be considered in the design loading, as confirmed by the following calculations.

(b) $W/V = 0.017$ and $AW^{1/3}/V = 60(17)^{1/3}/1,000 = 0.157$. From Figure 3, $p_g = 135$ psi. From Figure 5, $t_g/W^{1/3} = 5.6$ or $t_g = 5.6(17)^{1/3} = 14.4$ msec. From Figure 4, $i_g/W^{1/3} = 87$ or $i_g = 87(17)^{1/3} = 223$ psi-msec. For design purposes, from Equation 6, the effective gas duration is $t'_g = 2i_g/p_g = 2(223)/135 = 3.3$ msec. From Equation 4-1 of Reference 1, $t'_o/W^{1/3} = 1.3$ or $t'_o = 1.3(17)^{1/3} = 3.3$ msec. For design purposes, the fictitious peak shock pressure is $p_r = 2i_s/t'_o = 2(514)/3.3 = 311$ psi. Note that $t_g > t'_o$ but $t'_g \leq t'_o$ and therefore the cubicle is fully vented as indicated by the calculations in (a). The calculated pressures, impulses and time durations apply to the load diagram shown in Figure 1b.

FULLY VENTED EXPLOSIONS

According to the CEL criterion, an explosion is fully vented if $A/V^{2/3} > 0.60$. Within the practical range of aspect rations, three-wall cubicles with or without a roof satisfy this criterion. But the TM5-1300 Design Manual already contains charts for predicting the pressure loading inside three-wall cubicles [1]. Therefore, the following discussion of fully vented explosions is limited to procedures for predicting the blast environment outside three-wall cubicles.

Blast Environment Outside Three-Wall Cubicles

Consider a charge detonated at the geometric center of a three-wall cubicle without a roof. The expanding shock wave and resulting reflected waves eventually produce an erratic train of shock waves escaping to the outside of the cubicle by passing unobstructed through the open front wall and roof and by spilling over the top of the side and back walls.

At points behind the side and back walls, the wave train, by spilling over the back and sidewalls, forms a highly turbulent vortex at the free edges of the walls. At first, the vortex is small but rapidly grows in size with time. Evidence that a vortex indeed forms behind a barrier wall and grows to considerable size is shown in a study by Teel [5]. The vortex apparently distorts the shock front because the peak pressure and impulse at points close-in to the cubicle are much less than those from an unconfined surface burst. A typical relationship found for peak pressures behind a sidewall is shown in Figure 9. Note that at a critical distance from the wall depending on the charge weight and cubicle geometry, the peak pressure

(and impulse) decreases with increasing scaled distance. The pressure corresponding to the peak in the pressure curve (Figure 9) is referred to as p_{so} (max) and the portion of the curve to the right of the peak is referred to as the envelope curve.

Peak Positive Pressure

Envelope curves for the measured peak positive pressure, p_{so}, behind the front, back and sidewalls of the three-wall cubicles, with and without a roof, are shown in Figures 10 and 11, respectively. At all scaled distances, p_{so} is greatest behind the front wall, less behind the sidewalls and least behind the back wall. The curves apply to both cube and rectangular shaped cubicles.

The maximum peak pressure, p_{so} (max) was found to depend on both the cubicle geometry and W/V, as shown in Figure 12. The peak positive pressure, p_{so}, from Figures 10 and 11 must never exceed p_{so} (max) from the appropriate curve in Figure 12. Consequently, Figures 10 and 11 must be used in conjunction with Figure 12, especially for small values of $R/W^{1/3}$ and W/V where one will find that p_{so} (max) from Figure 12 is less than p_{so} from Figures 10 and 11.

It is recommended for design purposes that Figures 10, 11, and 12 be used to predict the peak pressure at any range outside three-wall cubicles with or without a roof.

Peak Positive Impulse

The scaled positive impulse, $i_s/W^{1/3}$, behind the walls of a three-wall cubicle diminishes with increasing $R/W^{1/3}$ in a manner similar to that shown in Figures 8 and 9 for peak pressure. The impulse data shows a clear influence of cubicle geometry and W/V on $i_s/W^{1/3}$. For peak pressures, W/V effected p_{so} only at close-in ranges but for peak impulse, W/V was found to influence $i_s/W^{1/3}$ at all ranges. For both cube and rectangular shaped three-wall cubicles, $i_s/W^{1/3}$ decreases with increasing W/V and $R/W^{1/3}$.

Design curves and equations to predict $i_s/W^{1/3}$ are presented in Reference 2. Typical relationships derived from the data include the following.

Behind the open front wall of a cube shaped cubicle,

$$i_s/W^{1/3} = 110\ (W/V)^{-0.16} (R/W^{1/3})^{-1.05} \qquad (9)$$

for $R/W^{1/3} \geq 7$ and $W/V < 2.1$.

Behind the open front wall of a rectangular shaped cubicle,

$$i_s/W^{1/3} = 96.6\ (W/V)^{-0.15}\ (R/W^{1/3})^{-1.04} \qquad (10)$$

for $R/W^{1/3} \geq 10$ and $W/V < 1.0$.

Behind the sidewalls of both the cube and rectangular shaped cubicles,

$$i_s/W^{1/3} = 71\ (W/V)^{-0.09}\ (R/W^{1/3})^{-0.95} \qquad (11)$$

for $R/W^{1/3} \geq 20$ and $W/V < 1.0$.

Behind the backwall of the cube and rectangular shaped test cubicles there was no clear trend in the impulse data or clear influence of W/V or cubicle geometry.

The lines described by Equations 9, 10, and 11 are nearly parallel to the curve for an unconfined surface burst. Therefore, a critical value of W/V exists, according to the equations, such that $i_s/W^{1/3}$ outside the cubicle is identical to that from an unconfined surface burst. For any W/V greater than this critical value, the line relating $i_s/W^{1/3}$ and $R/W^{1/3}$ should fall, it seems, on the unconfined surface burst curve. For this reason, an upper limit for W/V is given for Equations 9, 10 and 11.

At small scaled distances, the $i_s/W^{1/3}$ curves bend over and peak out in a manner similar to the p_{so} curves. For points close-in behind the open front wall, the curves bend over and tend to merge with the unconfined surface burst curve. This trend is attributed to the shock waves reflecting off the side and back walls which have not yet reached and reinforced the primary shock front. Behind the side and back walls, impulse curves bend over and peak but there appears to be no consistent relationship between the peak and W/V or the cubicle geometry.

It is recommended for design purposes that Equations 9, 10, 11, and similar equations and charts for impulse presented in Reference 2 be used to predict the peak positive impulse outside a three-wall cubicle.

Duration of Pressure

No detailed analysis of $t_o/W^{1/3}$ was made (although the data is tabulated in Reference 2) but a correlation of the data indicates that (1) $t_o/W^{1/3}$ increases with decreasing W/V, (2) the influence of W/V on $t_o/W^{1/3}$ diminishes with increasing $R/W^{1/3}$, and (3) at large $R/W^{1/3}$, the effect of W/V is negligible and $t_o/W^{1/3}$ approaches that from an unconfined surface burst.

It is recommended for purposes of design that the effective duration, t_o', be calculated from Equation 8.

Design Problem

The following problems and their solution serve to illustrate the use of the various charts for constructing the pressure-time loading, shown in Figure 1b, outside a fully vented cubicle.

Problem 1

Design a three-wall cube without a roof to contain 125 pounds of Composition B explosive. The pressures anywhere behind the back and side walls must not exceed 10 psi. (a) What wall dimensions are required? (b) What will the peak pressure be behind the side, back and front walls at a range of 200 feet?

Solution

(a) Given W = 125 lb and p_{so}(max) = 10 psi. From line A in Figure 12 the required W/V = 0.017. From Figure 10, p_{so} = 1.0 psi behind back wall, 1.5 psi behind sidewall and 1.8 psi behind open front wall.

Problem 2

A rectangular-shaped, three-wall cubicle contains 3,375 pounds of Composition B explosive. The ground surface is flush with the floor (h = H) and the walls are 10 feet high. The lengths of the side and back walls are 20 and 40 feet, respectively. Calculate the design loading (p_{so}, i_s, and t'_o) for a point 300 feet from the charge behind the sidewall.

Solution

Given W = 3,375 lb, V = 10 x 20 x 40 = 8,000 ft^3, and R = 300 ft. Therefore, $R/W^{1/3} = 300/(3,375)^{1/3} = 20$ and W/V = 3,375/8,000 = 0.42. From Figure 10, p_{so} = 5 psi. From Equation 11, $i_s/W^{1/3} = 71 (0.42)^{-0.09} (20)^{-0.95} = 4.46$ or $i_s = 4.46(3,375)^{1/3} = 66.9$ psi-msec. For design purposes, the effective duration of the pressure from Equation 8 is $t'_o = 2(66.9)/5 = 26.8$ msec.

PRESSURE DESIGN CRITERIA

Design criteria for predicting the loading in and around fully and partially vented cubicles are summarized in Tables 1 and 2. The design criteria for the loading inside fully vented cubicles are compatible with procedures recommended in the TM5-1300 Design Manual [1]. Design criteria for the loading outside cubicles are limited to h = 0 for four-wall cubicles and h = H for three-wall cubicles. (A semi-empirical procedure is described in Reference 2 for estimating the blast environment for other values of h.)

REFERENCES

1. NAVFAC p-397 Manual; Structures to Resist the Effects of Accidental Explosions. Department of the Army, Navy and Air Force, Washington, D.C., Jun 1969 (also Army TM5-1300 and AFM-88-22).

2. Civil Engineering Laboratory, Technical Reprt R- : Blast Environment from Fully and Partially Vented Explosions in Cubicles, by W. A. Keenan and J. E. Tancreto, Port Hueneme, CA (to be published).

3. Naval Civil Engineering Laboratory, Technical Report R-780, Determination of Blast Leakage Pressures and Fragment Velocity for Fully Vented and Partially Vented Protective Cubicles, by John M. Ferritto, Port Hueneme, CA, Dec 1972

4. J. F. Proctor and W. S. Filler, *A Computerized Technique for Blast Loads from Confined Explosions,* Minutes of the 14th Annual Explosives Safety Seminar, p 99, Nov 1972

5. Ballistics Research Laboratories, BRL Memorandum Report No. 1536: A Study of Flow Patterns in Aircraft Revetments, by George Teel and George Coulter, Aberdeen, MD, Feb 1964

6. Picatinny Arsenal, Technical Report 4168: Full and Model Scale Tests of Bay Structures, by S. Levy, et al, Dover, New Jersey, Feb 1971

LIST OF SYMBOLS

A	Total vent area of the cubicle (ft^2)
D	Diameter of charge or opening in roof (ft)
h	Vertical distance from top of cubicle roof, wall or pipe stack vent down to the ground surface or horizontal plane of interest (ft)
H	Interior height of cubicle wall from floor to roof (ft)
i_s	Unit positive impulse of shock pressure (psi-msec)
i_g	Unit positive impulse of gas pressure (psi-msec)
L	Length (ft)
p_g	Peak positive gas pressure (psi)
p_r	Peak reflected shock pressure (psi)
p_{so}	Peak positive incident pressure (psi)
p_{so}(max)	Maximum peak positive pressure (psi)
R	Horizontal range from charge to point of interest (ft)
R'	Skew range from charge to point of interest (ft)
t_g	Duration of exponential decay in gas pressure (msec)
t_g	Effective duration of gas pressure (msec)
t_o	Duration of exponential decay in shock pressure (msec)
t_w	Thickness of cubicle wall (ft)
V	Internal volume of cubicle (ft^3)
W	Total weight of explosive (lb)

Table 1

Proposed design criteria for loading inside fully and partially vented cubicles

Cubicle	Parameter i_s	t'_o	p_r	i_g	p_g	t'_g
Fully vented $A/V^{2/3} \geq 0.60$	Figures 4-17 through 4-62 of TM5-1300 Design Manual [1]	Equation 4-1 of TM5-1300 Design Manual [1]	$2i_s/t'_o$	a	a	a
Partially vented $A/V^{2/3} < 0.60$			$2i_s/t'_o$	Figure 4	Figure 3	$2i_g/p_g$

[a] Gas pressure not a factor in loading since $t'_g/t'_o \leq 1.0$

Table 2

Proposed design criteria for loading outside fully and partially vented cubicles

Cubicle	Direction	Parameter p_{so}	i_s	t'_o
Four-wall cubicles with $A/V^{2/3} \leq 1.0$	Any	Figure 6[a]	Figure 7[a]	$2i_s/p_{so}$
Three-wall cubicles with $A/V^{2/3} \geq 0.60$	Behind open front wall	Figures 10, 11, and 12	Equations 7, 8, 10 and 11[b] Figures B11, 12, 17 and 18[b]	$2i_s/p_{so}$
	Behind side wall		Equations 9 and 12[b] Figures B13, 14, 19 20[b]	
	Behind back wall		Figures B15, 16, 21, 22[b]	

[a] For h = 0; for h > 0 use semi-empirical procedure described in text

[b] Figure numbers refer to Figures in Reference 2; For h = H; for h > H use semi-empirical procedure described in text

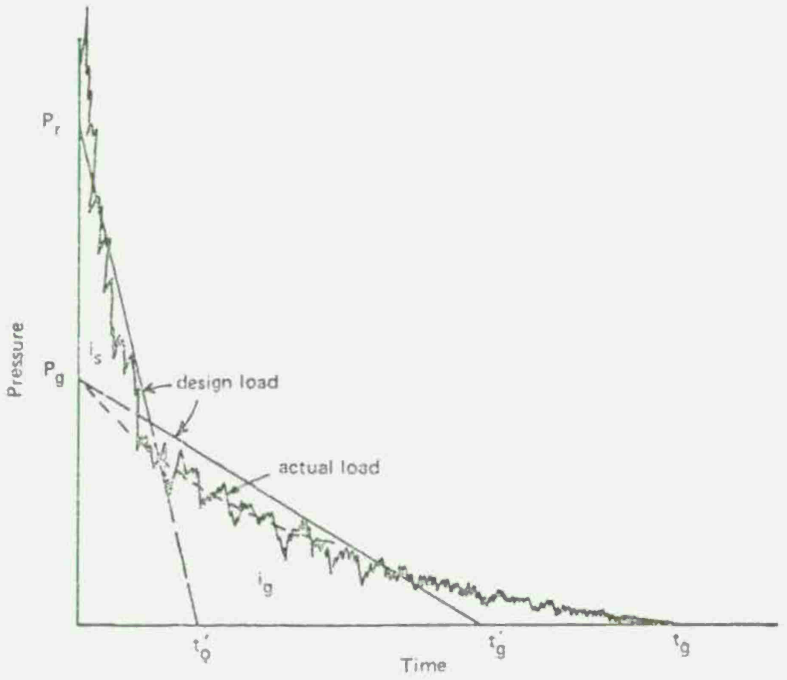

(a) Loading inside partially vented cubicle, $A/V^{2/3} \leqslant 0.60$.

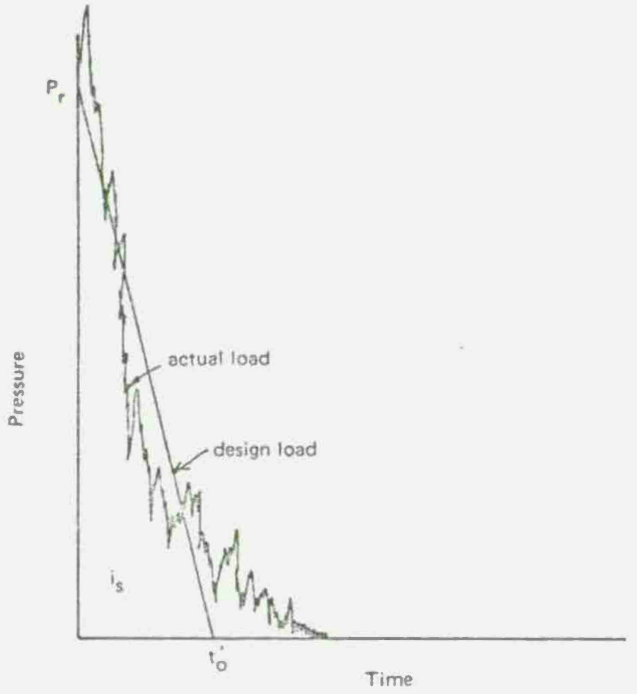

(b) Loading inside full vented cubicle ($A/V^{2/3} \geqslant 0.60$) and outside both fully and partially vented cubicles.

Fig 1 Blast loading from fully and partially vented cubicles

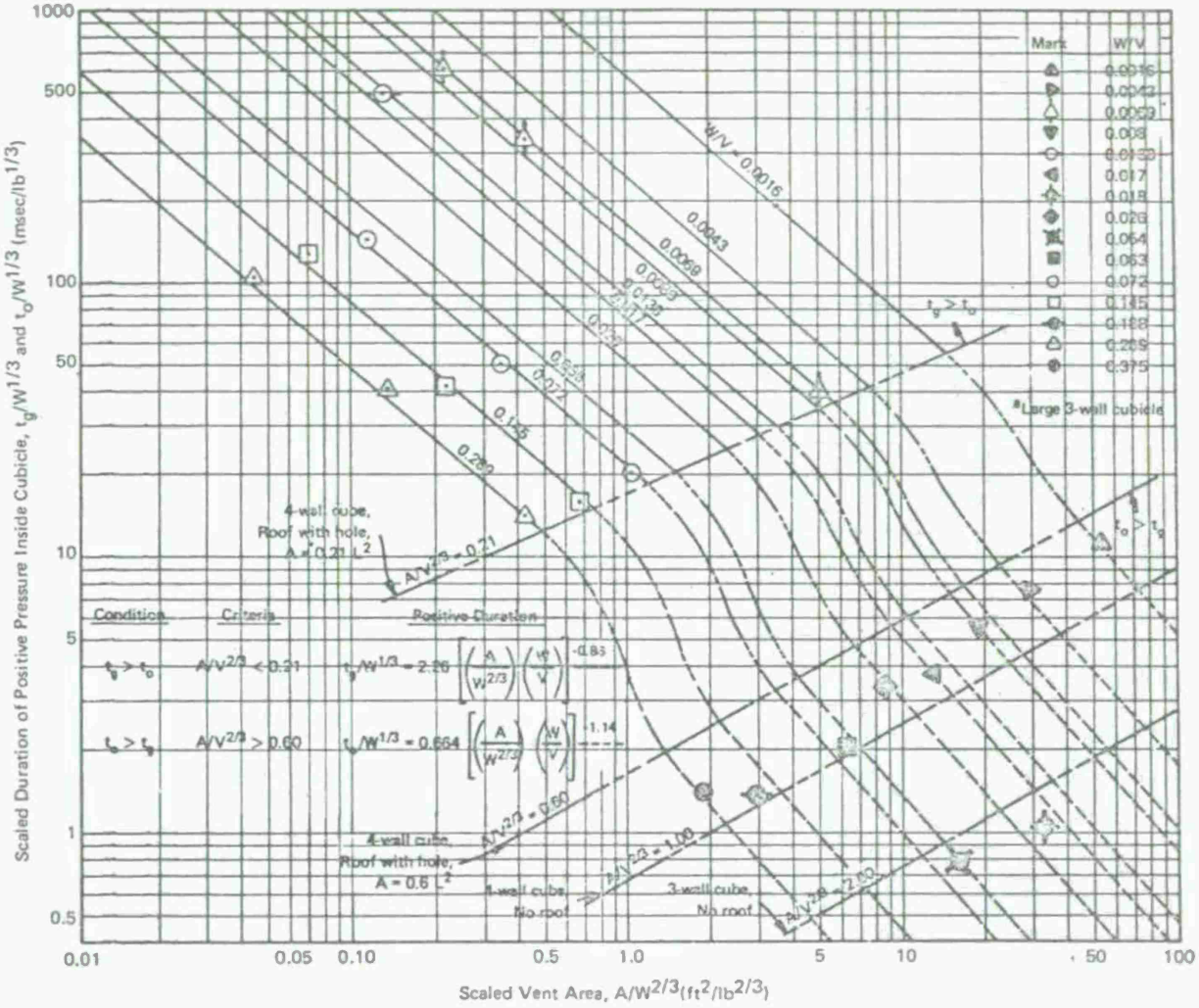

Fig 2 Scaled duration of positive pressure inside four-wall cubicle versus scaled vent area and cubicle volume

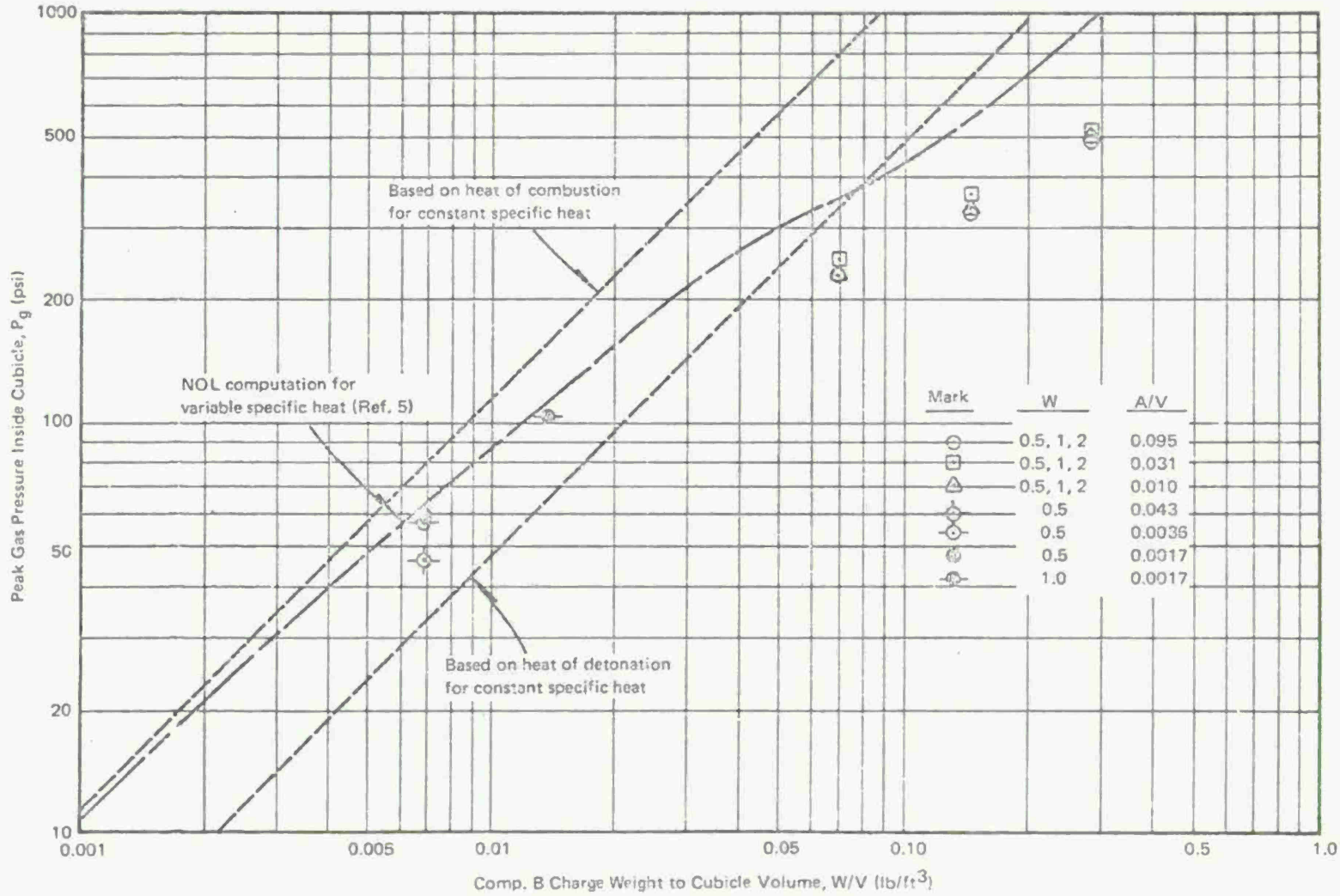

Fig 3 Peak gas pressure from partially vented explosion of Composition B in four-wall cubicle

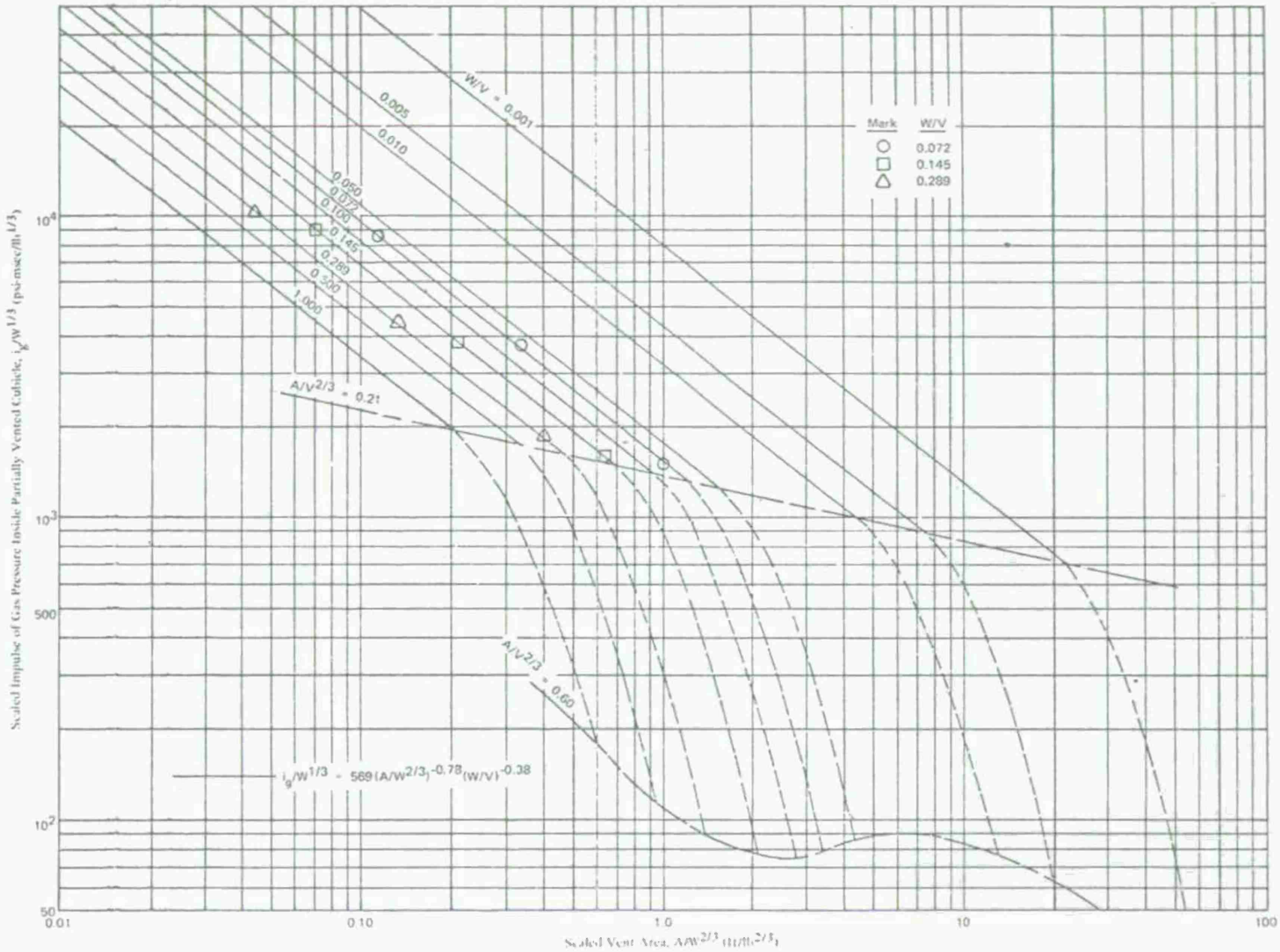

Fig 4 Design chart for scaled impulse of gas pressure inside a partially vented cubicle

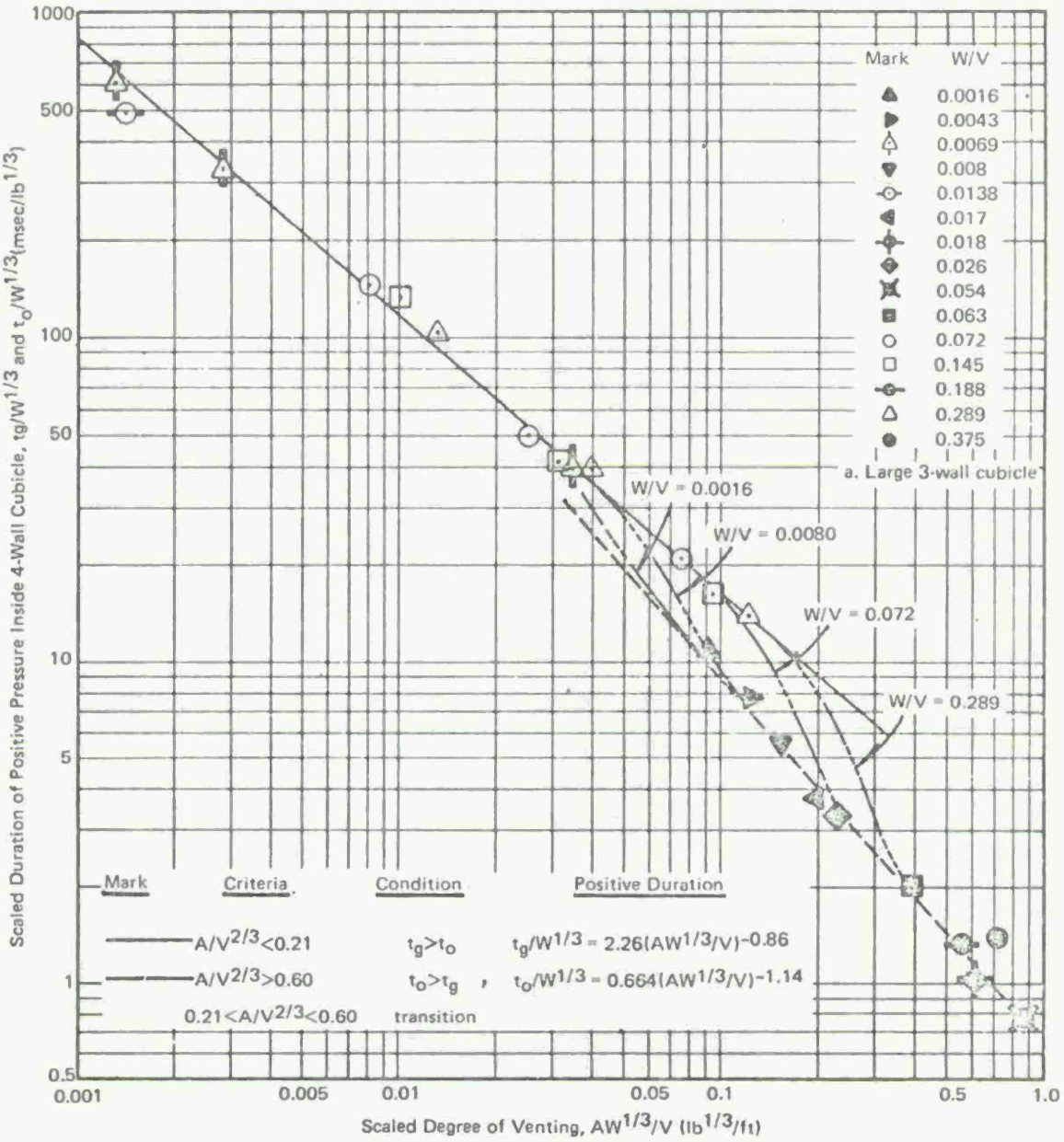

Fig 5 Design chart for scaled duration of positive pressure inside a cubicle versus scaled degree of venting

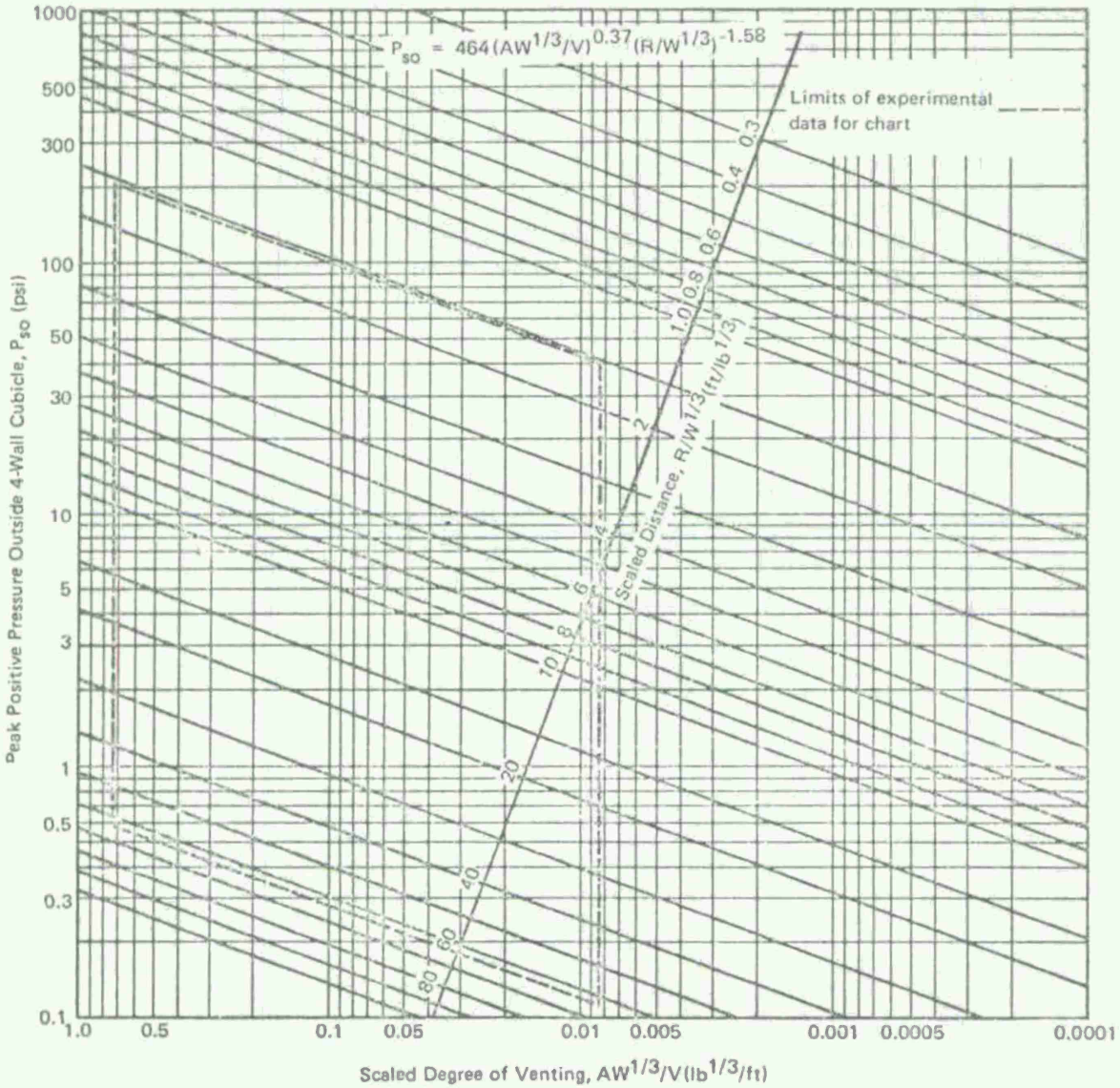

Fig 6 Design chart for vent area required to limit pressures at any range outside a four-wall cubicle

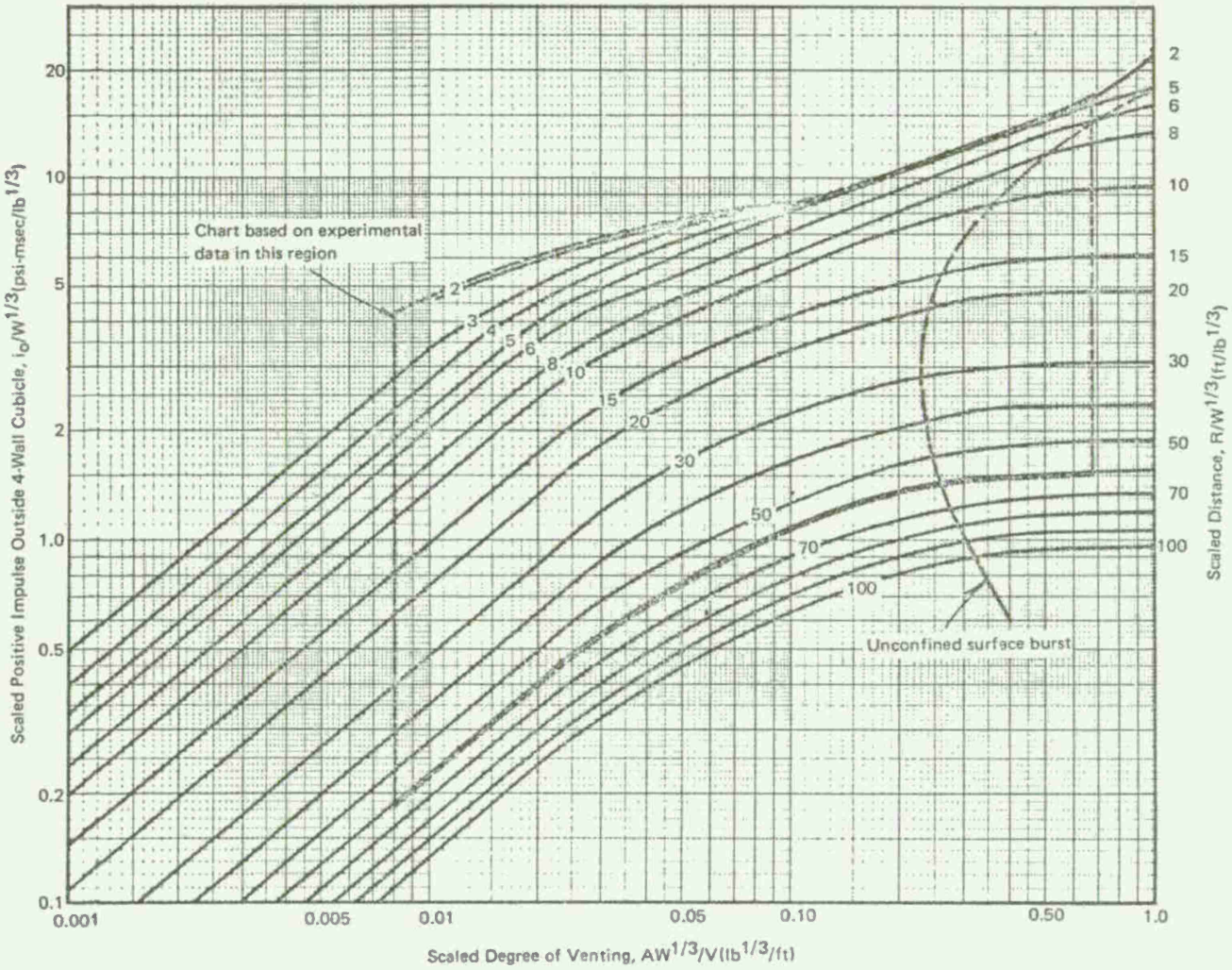

Fig 7 Design chart for vent area required to limit positive impulse at any range outside a four-wall cubicle

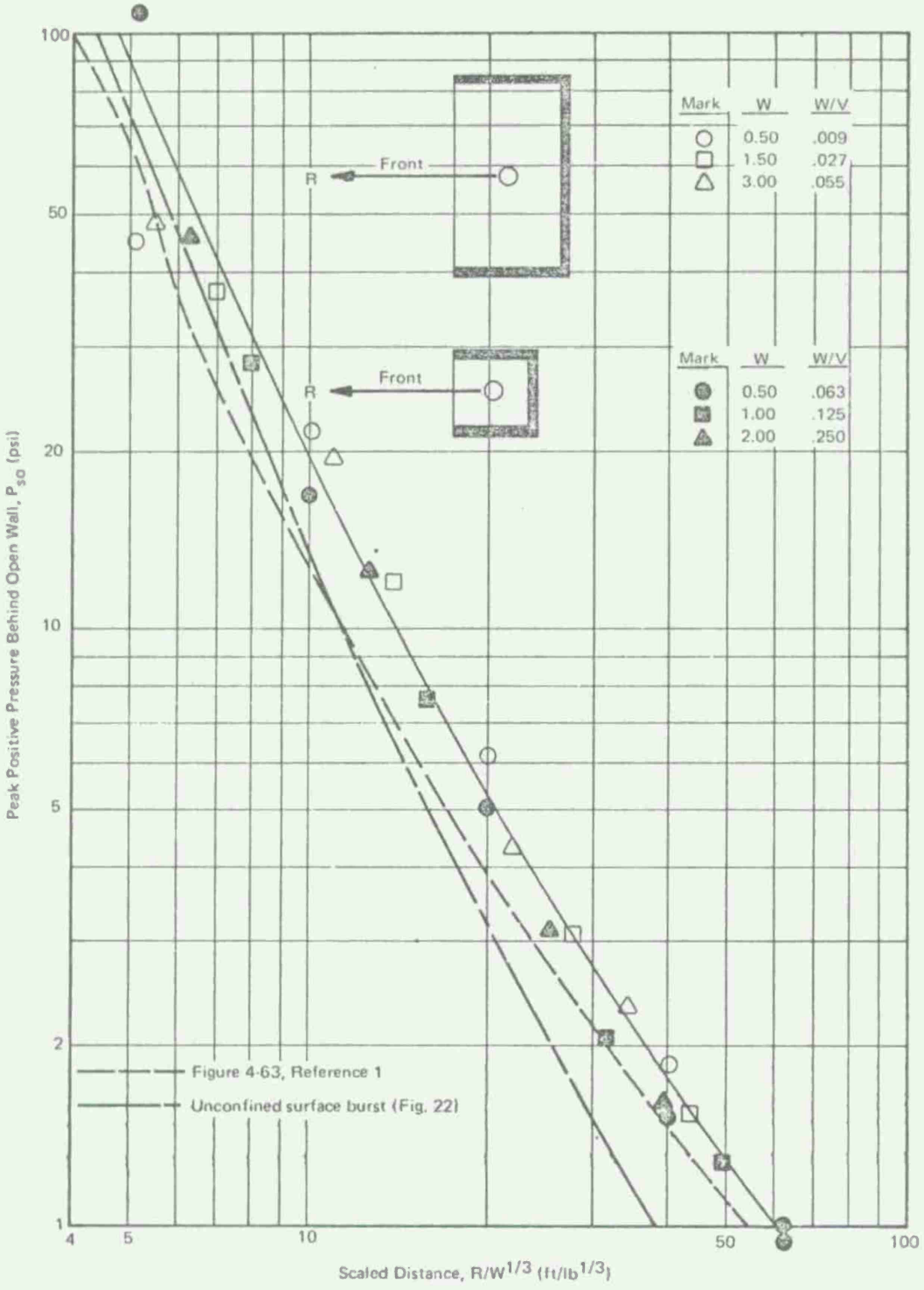

Fig 8 Peak positive pressure behind open wall of three-wall cubicles without a roof

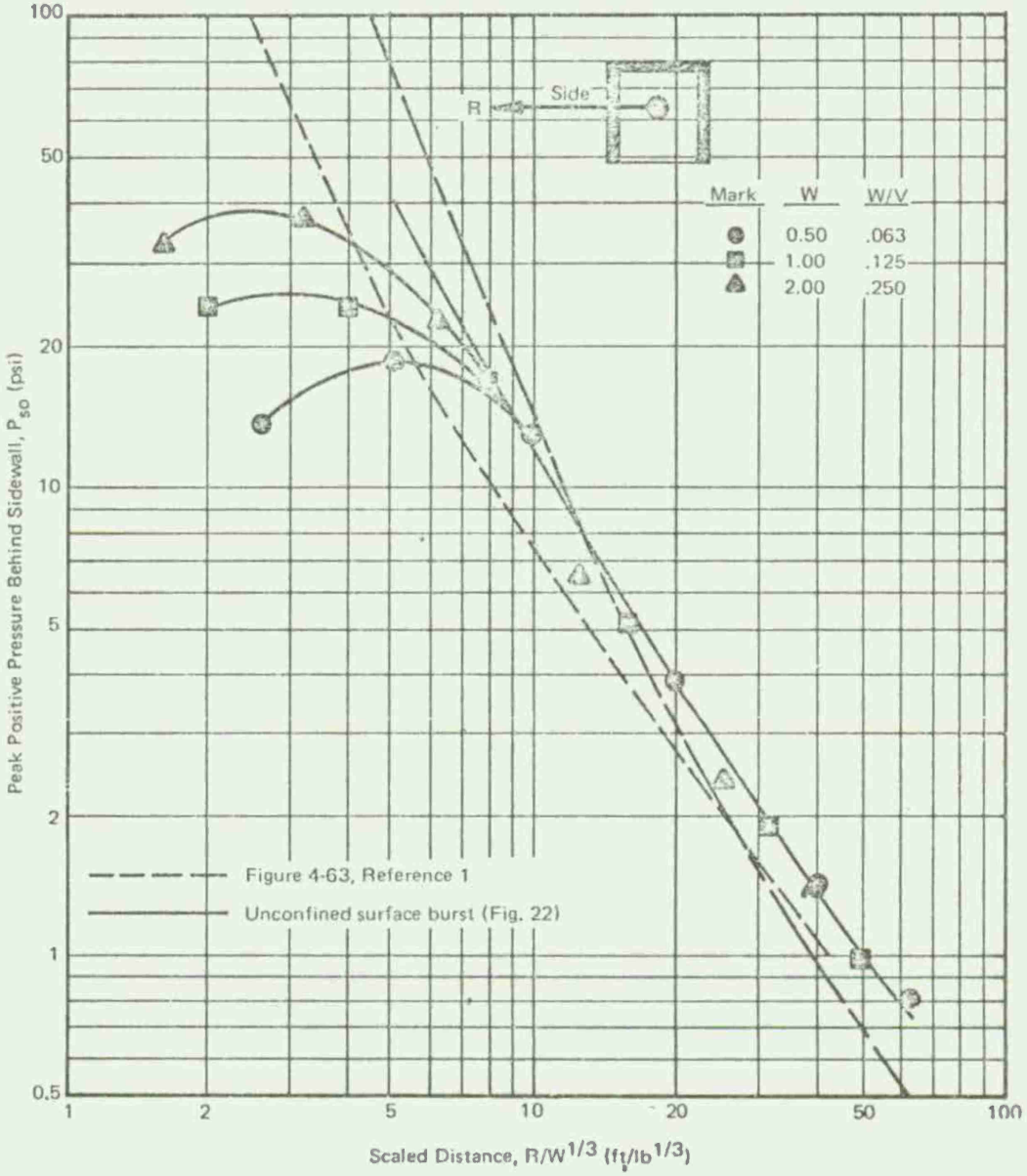

Fig 9 Peak positive pressure behind sidewall of small three-wall cubicle without roof

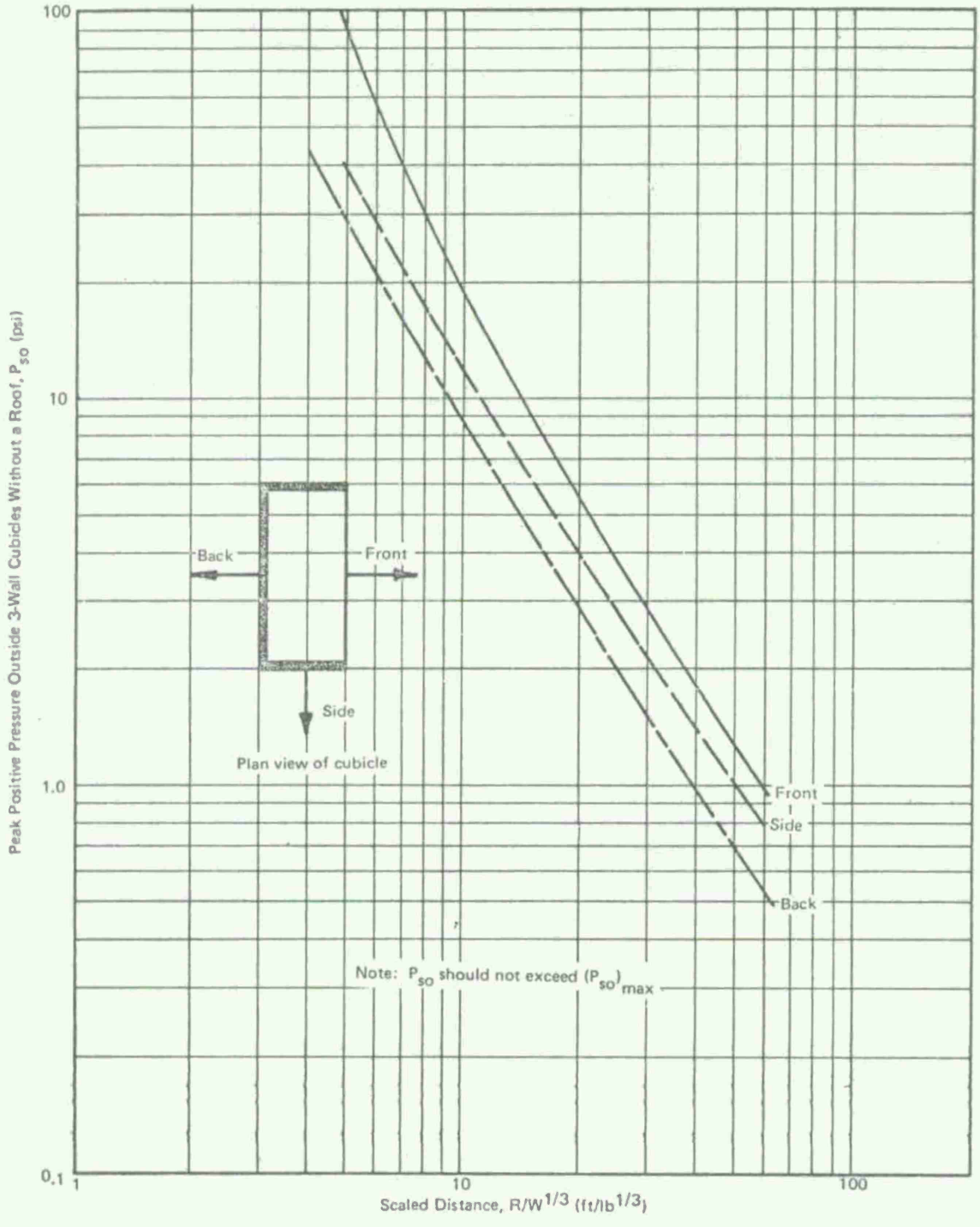

Fig 10 Envelope curves for peak positive pressure outside three-wall cubicles without a roof

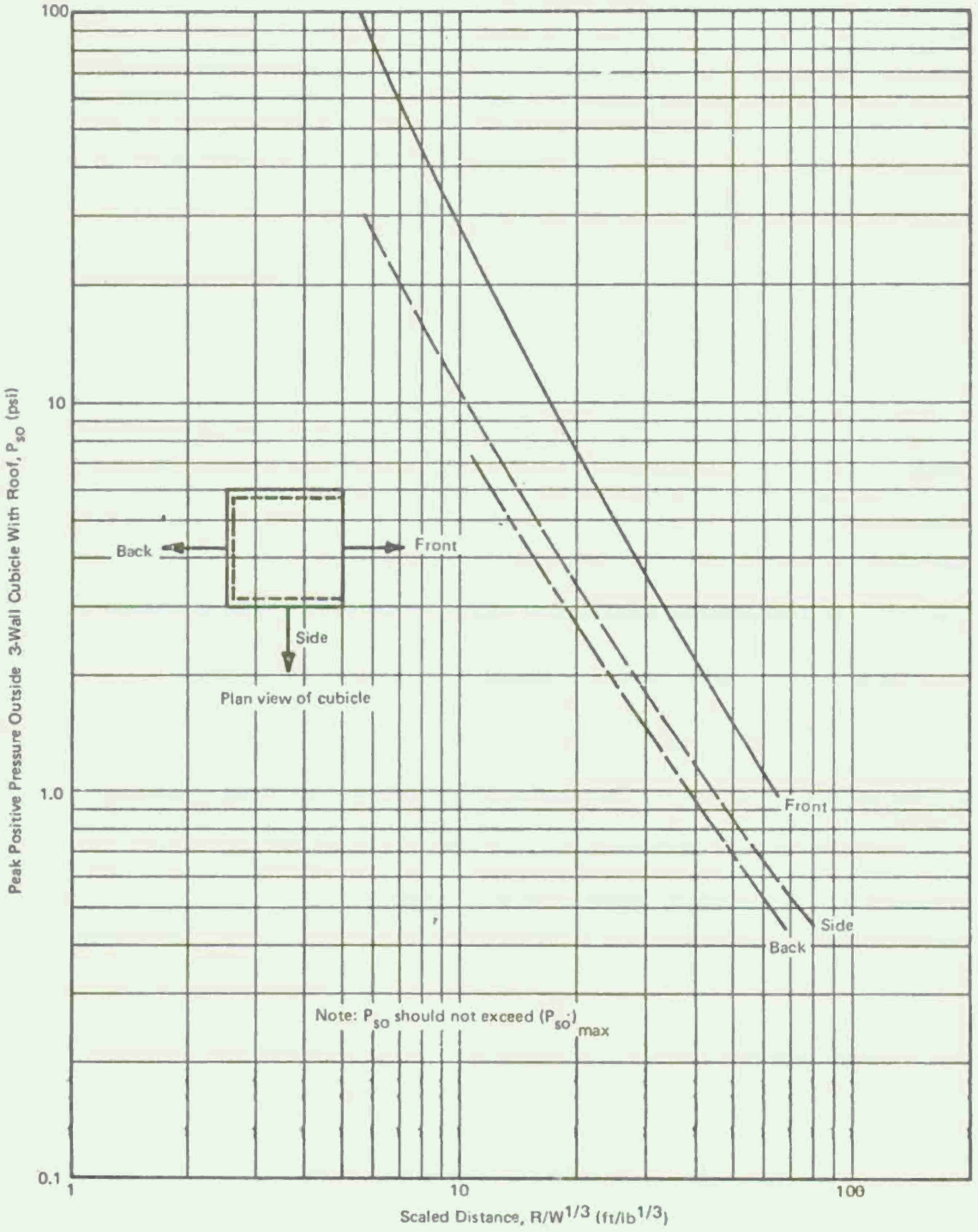

Fig 11 Envelope curves for peak positive pressure outside three-wall cubicles with a roof

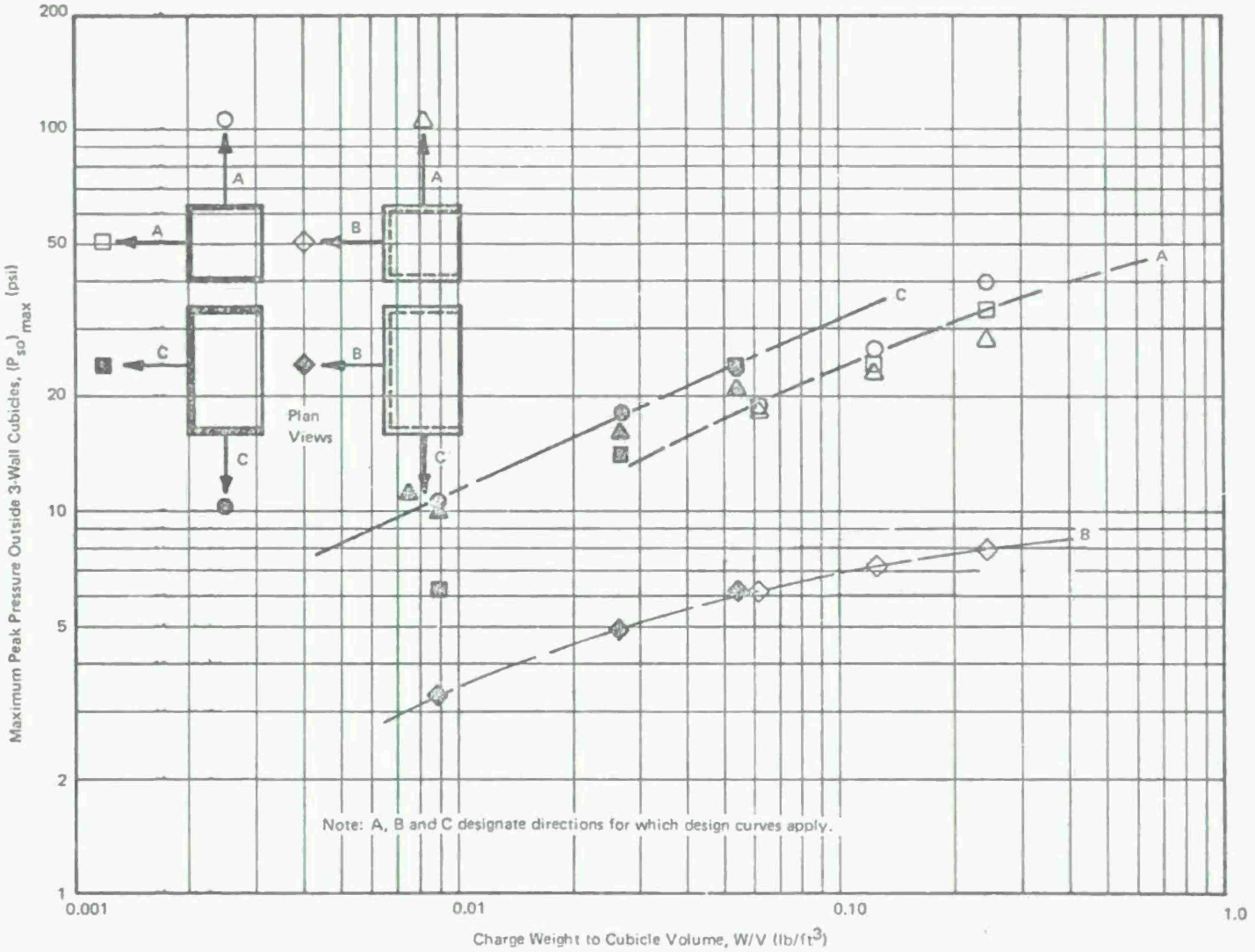

Fig 12 Envelope curves for maximum peak pressure outside three-wall cubicles

EFFECTS OF CHARGE SHAPE, CHARGE COMPOSITION AND SURFACE CONDITIONS ON BLAST ENVIRONMENT

Sixteenth Annual Explosives Safety Seminar
Hollywood, Florida
24-26 September 1974

J. E. Tancreto

CIVIL ENGINEERING LABORATORY
Naval Construction Battalion Center
Port Hueneme, California 93043

INTRODUCTION

The U. S. Army Armament Command (ARMCOM) is modernizing ammunition facilities used in the manufacturing, processing, and storage of conventional munitions. Consistent with new safety regulations, protective structures are being designed to comply with criteria and methods in the TM5-1300 Manual, *Structures to Resist the Effects of Accidental Explosions* (Ref 1). A scale-model cubicle test program to supplement material in TM5-1300 was sponsored by Picatinny Arsenal (Manufacturing Technology Directorate) and conducted by CEL.

The testing described in this paper was conducted to determine the effects of charge shape and composition on the results of the scale model cubicle tests, which would use composition B cylinders. The test site was also utilized for determining the explosive yield of an RDX slurry of the type stored in tanks used in ammunition production facilities.

A more detailed description of the test program and results will be published in a CEL Technical Note (Ref 2).

OBJECTIVE

The primary test objectives were to determine the effects of charge shape and composition on the pressure-time-distance relationships for composition B, TNT, and RDX slurry surface bursts. Results should show the equivalencies of composition B and RDX slurry and the effects of using composition B cylinders in the cubicle test program.

Secondary objectives included a study of the effects of surface conditions and charge elevations on shock wave characteristics. A direct comparison of pressure-time data outside a cubicle from the detonation of cylinders and spheres centered in the cubicle was an additional objective to be accomplished during the cubicle test program.

TEST PROGRAM

Program Development

The original test plan specified a direct comparison of air-blast parameters from detonations of TNT spheres, composition B cylinders, and RDX slurry containers. All charges were slightly elevated over a stiffened

1-inch steel plate to eliminate cratering. Poor detonation of the center-initiated cast TNT spheres precluded use of the TNT test data. Similar problems with small TNT spherical charges have been reported by Fisher and Pitman of NOL (Ref 3).

The test program was then expanded to include surface bursts of composition B hemispheres, spheres, and cylinders. The spherical and hemispherical data would be compared with known TNT surface burst results for determination of TNT equivalency of composition B. Results would also be compared to determine the effect of charge shape.

The hemispherical composition B charges were detonated on sand and on a replaceable 4-inch steel plate to determine which condition produced the most consistent results for surface bursts. The test results indicated that the steel plate should be used for the subsequent surface burst tests of composition B spheres and cylinders.

Spherical composition B charges were also detonated from small elevations so that the effects of small heights of burst could be evaluated for both spheres and cylinders. This information was then used to evaluate the elevated RDX slurry tests. Table 1 summarizes the test program.

Test Site

Testing was conducted at the Pacific Missile Range, Point Mugu, California. Three gage lines, each originating at ground zero, were placed at 90 degrees to each other. The ground surface along each gage line was leveled and covered out to a range of 52 feet. Except for a 4 x 4-foot area centered on ground zero, the first 10 feet of the lines was covered with a steel plate 4 feet wide by 1/4 inch thick. From 10 to 52 feet, the lines were covered with 3/4-inch plywood. Surface conditions at ground zero are summarized in Table 1. Pressure transducers were located on each line at 2, 4, 8, 16, 32, and 50 feet from ground zero. Each transducer was mounted in a steel jacket encased in 1 cubic foot of concrete. The concrete block was buried so that the pressure gage was flush with the ground surface.

Instrumentation

Piezoresistive pressure transducers (HFG series by Tyco Instrument Division, Bytex, Inc.), designed to measure dynamic overpressures, were placed in accordance with the predicted pressure at each gage location.

The pressure-time data was recorded on magnetic tape and then digitized. The digitized data was integrated to obtain an impulse-time record, which was displayed on a hard copy plot with the pressure-time record.

Quick-look data was provided by an oscillograph plotter after each test.

Test Data

A typical computer printout of pressure-time and impulse-time data plots is displayed in Figure 2. Peak pressure and maximum impulse were taken directly from this plot of the digitized data. The end of the positive phase duration was taken at the point of maximum impulse.

Gages at ranges of 16, 32, and 50 feet generally exhibited overshoot due to "ringing" of the gage diaphragm whose natural frequency was nearly that of the peak pressure loading. The positive phase duration at these ranges was long enough so that an exponential curve could be fitted through the average of the data points to obtain the correct peak pressure. Since large segments of the exponentially decaying curve will plot as a straight line on a log pressure versus time plot (Ref 4), these curves were also generated to aid in curve fitting. The log pressure plot expanded, straightened and reduced the slope of the fitted curve and thus allowed for better and more consistent peak pressure analysis of "ringing" gages. Since the "ringing" was balanced around the average pressure-time plot, there was no need to correct the impulse data. Positive phase duration was unaffected.

Pressure and impulse measurements, from repeated tests and multiple gage lines, were averaged and plotted. Table 1 summarizes the number of measurements averaged per plotted value and the figure numbers where the average data points are plotted. Tables of individual measurements are presented in Reference 2. Positive phase durations, not presented here, are also included in Reference 2.

DATA ANALYSIS

The surface burst tests of the spherical and hemispherical composition B charges were conducted for comparison with TNT surface burst data from similarly shaped charges. These tests give the basis for evaluating the cylindrical composition B test data by determining the best surface to

use for the test program, by providing a check on the instrumentation system, and by yielding the equivalency of composition B. The concept of charge weight equivalency is then used to describe the effect of charge shape on air blast parameters.

The surface burst and small height of burst data on cylinders and hemispheres are used to help evaluate the results of the elevated RDX slurry tests. The RDX slurry data is then compared to the hemispherical surface burst curves by using charge weight equivalency.

The effect of charge shape and charge weight on the environment outside a three-wall cubicle is shown by directly comparing peak pressures, scaled impulses, and scaled durations.

Effect of Surface Conditions

The two surface conditions considered to be the easiest to repeat with consistency throughout the test program were a dry sand surface that could be replaced as required. The hemispherical surface bursts were conducted on both of these surfaces to determine the surface effect on pressure and impulse results. The results shown in Figures 3 and 4 from tests on the steel surface agree very well with TNT data while results from tests on the sand surface are significantly lower. Since composition B output is known to be at least equivalent to that of TNT, it was determined that the hard steel surface would best serve the purposes of the test program. As shown in Figures 3 and 4, an extreme difference in surface hardness has a significant effect on blast yield at scaled distances less than about 20 $ft/lb^{1/3}$.

TNT Equivalency of Composition B

The composition B hemispherical and spherical surface burst data are compared to data from similar tests (Ref 5, 6, 7, 8) of larger quantities of TNT in Figures 3, 4, 5, and 6. Differences are small.

Peak pressure from the hemispherical composition B surface burst, detonated on a plate, is virtually the same as that from TNT (see Figure 3). Similar results were obtained with spheres. The spherical composition B peak pressure test values fall on one or the other of the TNT curves (see Figure 5).

Scaled impulses from composition B and TNT hemispherical and spherical surface bursts are compared in Figures 4 and 6. Agreement between the composition B data (on a steel plate) and TNT data is good.

It was anticipated that composition B and TNT charges of the same shape and under similar conditions would have almost identical blast yield. TM5-1300 gives the TNT equivalencies for composition B at pressures between 2 and 50 psi as 1.10 for peak pressure and 1.06 for impulse. In order to experimentally measure these equivalencies, one must be able to measure a ratio in the scaled distances, at the same pressure or impulse, of 1.03 ($1.10^{1/3}$) and 1.02 ($1.06^{1/3}$), respectively. Determining such a low equivalency was not possible because of (1) the magnitude of the standard deviation and (2) the relatively small number of data points. It is important to note that the standard deviation reflects natural differences between identical tests as well as experimental error. The difference between Distant Plain Event 6 (Ref 6) and Prairie Flat (Ref 7, 8) (shown in Figure 5) is an example. At the lower pressure levels the two similar tests differ by more than 10%. This difference can be attributed to many factors including blast anomalies, test site differences, and experimental error.

Shape Equivalency

It is recognized that charge shape has a significant effect on airblast parameters. Results from charges of different shapes are compared in the literature. References 9 through 11 are examples of previous studies. In these references, peak pressure measurements were compared by taking their ratio at given scaled distances. An alternative method would be to show the ratio of equivalent weights that produce the same pressure (or impulse) at the same ground range.

Figures 7 and 8 present composition B cylindrical surface burst test results. These results can now be compared with the spherical and hemispherical results to determine shape equivalency.

Pressure Equivalency

Peak pressures from hemispherical, spherical, and cylindrical surface bursts are compared in Figure 9. The spherical and cylindrical curves are from composition B test results. The hemispherical relationship is taken from TM5-1300 for a TNT surface burst, though composition B results can be considered to be identical for our purpose. Equivalent weight ratios for pairs of charges of different shape are shown in Figure 10.

As expected, equal weights of the sphere and cylinder produce higher pressures than a hemisphere at the smaller scaled distances and lower pressures at the greater scaled distances. The composition B test data was limited to a minimum scaled distance of 2.80 ft/lb$^{1/3}$. Data from Reisler (Ref 6) indicates that the equivalent weight of a hemisphere to that of a sphere has a maximum value of 3.25 lb/lb at a scaled distance of 2 ft/lb$^{1/3}$. Data is not available for cylinders at scaled distances less than about 3 ft/lb$^{1/3}$.

The high equivalency values are not unusual. The basic pressure curves for spheres and hemispheres are well documented but are not usually compared in this manner. Since pressure (and impulse) changes are relatively insensitive to weight changes ($a \propto 1/W^{1/3}$), equivalent weights amplify the pressure (or impulse) differences. Note that at a scaled distance of 2 ft/lb$^{1/3}$, the peak pressure of a sphere is about twice that of a hemisphere, but the equivalent weight of the hemisphere to produce that pressure is 3.25 times the weight of a sphere.

Impulse Equivalency

Scaled unit impulses from hemispherical, spherical, and cylindrical surface bursts are compared in Figure 11. The spherical and cylindrical curves are from the composition B test results. The hemispherical relationship is taken from Kingery's TNT data (Ref 5). The hemispherical composition B results were in good agreement with the TNT results (Fig 4). The TNT data was used since it is a composite of many large scale tests and since the differences between TNT and composition B are not measurable within the accuracy of our recording system. Thus, the effect of charge shape on impulse is the result. Considering the scatter of impulse data, the only significant differences occur at scale distances less than about 6 ft/lb$^{1/3}$. The scaled impulses of the cylinder and sphere peak much higher than those of the hemisphere (42 versus 26 psi-msec/lb$^{1/3}$) and at a slightly larger scaled distance. The data also shows the usual trend of scaled impulse data to fall from the peak value (near 3 ft/lb$^{1/3}$) until it again increases with decreasing scaled distance.

Because of the slope reversal in the impulse data near a scaled distance of 3 ft/lb$^{1/3}$, there is a discontinuity in equivalent weights. (Equal impulse lines are at a 45-degree slope on the scaled impulse versus scaled distance plots. Pairs of scaled distance values that fall on these 45-degree lines describe the weight equivalency. A point-by-point analysis produces a discontinuity when the scaled impulse curve reverses slope to one greater than 45 degrees. This occurs at the peak of the lower curve

when values are being calculated point by point at decreasing scaled distances.) For this reason the impulse equivalency curve in Figure 12 for W_{hem}/W_{cyl} is terminated at 3.2 ft/lb$^{1/3}$. Results for a sphere (W_{hem}/W_{cyl} is terminated at 3.2 ft/lb$^{1/3}$. Results for a sphere (W_{hem}/W_{sph}) would have been similar within the same range of scaled distances. (Figure 11 shows good agreement between the sphere and cylinder for scaled impulses at scaled distances greater than 3 ft/lb$^{1/3}$.)

Effect of Small Heights of Burst

The RDX slurry tests had originally been detonated at small elevations over a stiff steel plate to reduce cratering and to simplify the test setup. They were to be compared directly to TNT spheres at the same elevation, but improper detonation of the TNT charges made that impossible. Composition B cylinders and spheres were detonated at small heights of burst to see how the results differed from those of surface bursts. The cylinders were elevated 3 radii (ground surface to center of gravity of charge) and the spheres were elevated 3 radii of a cylinder of the same weight. Table 1 summarizes the heights of burst for the different charges.

Peak pressures and scaled unit impulses for the elevated spheres and cylinders are compared in Figure 13. Data points from the elevated tests are plotted with the best fit curves from the surface burst tests. Small differences in peak pressure occur at levels above 100 psi with the elevated results being slightly lower. Elevating the charges reduced the peak in the impulse curve near the scale distance of about 3 ft/lb$^{1/3}$.

Equivalency of RDX Slurry

The RDX slurry peak pressure and scaled impulse data are compared to TNT hemispherical results in Figures 14 and 15. The TNT pressure data was taken from TM5-1300 and the impulse data from Kingery (Ref 5). The equivalent weight ratios (W_{TNT}/W_{slurry}) were calculated from these figures and are displayed in Figure 16. The pressure equivalency is highest (1.80 lb/lb) at a scaled distance of 5.2 ft/lb$^{1/3}$. The impulse equivalency peaks at 1.40 lb/lb at a scaled distance of 6 ft/lb$^{1/3}$. The small height of burst of the RDX slurry charges probably reduced the output at scaled distances less than about 4 ft/lb$^{1/3}$ (see previous section). To allow for this height of burst effect, it is recommended that the peak equivalency values be used for decreasing scaled distances as shown by the dashed lines in Figure 16.

Inspection of Figure 15 (with the knowledge that equal impulses occur on 45-degree lines) shows that at a scaled distance near 2.7 ft/lb$^{1/3}$ a discontinuity in impulse equivalency occurs. A dashed vertical line is shown at this scale distance in Figure 16. At scaled distances less than 2.6 ft/lb$^{1/3}$ the equivalency increases substantially to a value of around 5 lb/lb. This high equivalency occurs because the impulse curve for the RDX slurry does not exhibit the trend of other impulse data to turn down at a scale distance around 3 ft/lb$^{1/3}$ before again increasing with decreasing scaled distance.

Three-Wall Cubicle Effects

Peak pressure, scaled impulse, and scaled duration data around a three-wall cubicle were obtained from 1-pound spheres and cylinders and 2.65-pound spheres centered in the cubicle. Gage lines were located along the ground surface perpendicular to the front (open) wall, the sidewall and back wall. The results from the two charge shapes along the three-gage lines are compared for 1-pound charges in Figures 17, 18, and 19. Figures 20, 21, and 22 compare results from spheres of different weight (1.0 and 2.65 pounds). Figure 23 compares results for different directions from 1-pound spherical charges.

Effect of Charge Shape on Leakage Environment

Results from pressure gages outside the open front wall of the cubicle are shown in Figure 17. Charge shape did not affect scaled durations at any scaled distance. At scaled distances greater than 4 ft/lb$^{1/3}$, scaled impulse and peak pressure data showed no charge shape effects. The average peak pressure of the cylinder at 4 ft/lb$^{1/3}$ was 15% higher than that of the sphere and the scaled impulse of the cylinder at 2 ft/lb$^{1/3}$ was 14% higher than that of a sphere.

Cylindrical charge data on a line perpendicular to the open wall of a cubicle produces results that can be used for spherical charges. At worst, the data will be slightly conservative at scaled distances less than 4 ft/lb$^{1/3}$.

Pressure gage measurements along a line perpendicular to the sidewall followed the same trend as found out the front. However, pressures and impulses were affected to a greater scaled distance (8 ft/lb$^{1/3}$).

(Note that the cylindrical pressure at 4 ft/lb$^{1/3}$ is higher than the average of numerous tests run during the subsequent cubicle test program. The average from a larger sampling gives a pressure about 20% higher than that of a sphere. See Reference 12.)

Thus, if data from cylindrical charges is used to design for spherical charges, it would be conservative at scaled distances less than 8 ft/lb$^{1/3}$.

A somewhat different trend is found in comparing results from the sphere and cylinder opposite the back wall of the cubicle. Scaled durations are still the same. However, spherical pressure data is higher at scaled distances less than about 13 ft/lb$^{1/3}$ and cylindrical impulse data is higher over the entire range of measurements. Thus impulse data but not pressure data from cylindrical tests can conservatively be used for a spherical charge. However, more extensive testing from three different cylindrical charge weights (Ref 12) showed that the peak pressure versus scale distance curve of the cylinder has the same maximum pressure value as that of the sphere but at a closer scaled distance. Because the maximum pressure behind the back wall was the same for both shapes, the design method proposed in Reference 12 is applicable to both. That method uses two intersecting straight lines to describe the pressure environment. A horizontal line (dependent on charge density, W/V) limits the maximum pressure and intersects a diagonal line describing the lower pressures at larger scale distances.

Effect of Charge Weight on Leakage Environment

Two spherical charge weights were tested in the cubicle-1.07 pound and 2.65 pounds. Results, plotted in Figures 20, 21, and 22, show considerable differences in the blast environment parameters. This is expected since the size of the cubicle remained constant and was not scaled up for the increased charge weight. Correct scaling requires that the charge density, W/V, remain constant. Therefore, results from different charge weights within a single geometry cubicle are dependent on W/V.

CONCLUSIONS

1. The air-blast environment from composition B charges is essentially equivalent to that from TNT charges of the same shape. The TNT equivalencies in TM5-1300 (1.10 for peak pressure and 1.06 for impulse) should be used in design.

2. The contained RDX slurry is a high explosive with a TNT equivalency that varies with scaled distance and is more indicative of charge shape and containment than charge composition. Peak pressures and impulses for RDX slurry tanks should be obtained directly from the plots of these parameters versus scaled distances (Fig 14 and 15). Since TNT equivalency by weight is not constant, it offers no advantages in design applications.

3. Charge shape effects on the surface burst environment were substantial at scaled distances less than 20 ft/lb$^{1/3}$. Charge shape must therefore be considered at these scaled distances.* Use of data from cylindrical charges at less than 20 ft/lb$^{1/3}$ would be conservative in most cases (i.e., charges approaching spherical, hemispherical, or cylindrical shapes).

4. Charge shape affects the blast environment outside a protective cubicle less than it does in the case of a surface burst. Use of cylindrical charges for the test program described in Reference 12 will produce design curves that will be applicable for most charge shapes.

5. An extreme difference in surface hardness has significant effect on the surface burst environment at scaled distances less than 20 ft/lb$^{1/3}$. A stiff steel plate on sand, for the scale model tests, gave the best agreement with large scale results.

6. Small heights of burst (0.40 ft/lb$^{1/3}$) measurably reduced side-on overpressure and impulse at scaled distances less than 5 ft/lb$^{1/3}$.

---

*The TM5-1300 Design Manual was developed from tests of TNT and composition B charges of both spherical and cylindrical (L/D = 1) configurations. The design data presented reflects this charge shape phenomenon. For charges with L/D greater than one, a procedure whereby the charge is assumed to consist of a series of spherical charges is used. This procedure has produced good agreement with available test data, and a supplement to TM5-1300 is being prepared.

ACKNOWLEDGMENTS

Mr. Richard Rindner of Picatinny Arsenal conceived and administered the study. Mr. Norval Dobbs of Ammann and Whitney provided valuable technical guidance during the program. Testing was conducted at the Pacific Missile Range (PMR), Point Mugu, California. Personnel from the Launching Division at the Operations Department at PMR set up and detonated the explosives. The PMR Data Automation Division digitized and produced hard copy plots of the data.

The author gratefully acknowledges the contribution of these people to the study.

REFERENCES

1. Army, Navy and Air Force, TM5-1300/NAVFAC P-397/AFM 88-22: Structures to Resist the Effects of Accidental Explosions, Washington, D.C., Jun 1969

2. Civil Engineering Laboratory, Technical Note N-1390: Effects of Charge Shape, Charge Composition and Surface Conditions on Blast Environment, by J. E. Tancreto, Port Hueneme, CA (to be published)

3. U.S. Naval Ordnance Laboratory, NAVORD Report 2890: Air Blast Resulting from the Detonation of Small TNT Charges, by E. M. Fisher and J. F. Pittman, White Oak, MD, Jul 1953

4. Aberdeen Proving Ground, Ballistic Research Laboratories, Memorandum Report No. 1691: A Procedure for Reading and Smoothing Pressure-Time Data from H.E. and Nuclear Explosions, by N. H. Ethridge, Aberdeer, MD, Sep 1965

5. Aberdeen Proving Ground, Ballistic Research Laboratories Report No. 1344: Air Blast Parameters Versus Distance for Hemispherical TNT Surface Bursts, by C. N. Kingery, Aberdeen, MD, Sep 1966

6. Aberdeen Proving Ground, Ballistic Research Laboratories Memorandum Report No. 1955: Air Blast Measurements from the Detonation of Large Spherical TNT Charges Resting on the Surface (Operation Distant Plain, Events 6A, 6), by Ralph E. Reisler, Noel H. Ethridge and Louis Giglio-Tos, Aberdeen, MD, Jan 1969

7. Defense Atomic Support Agency, POR-2100: Prairie Flat Event, Fundamental Blast Studies, by L. Giglio-Tos and B. A. Pettot, Washington, D. C., Mar 1971

8. DASA Information and Analysis Center (General Electric), Operation Prairie Flat Symposium Report: Volume 1, Part 1, Santa Barbara, CA, Jan 1970

9. Aberdeen Proving Ground, Ballistic Research Laboratories Interim Memorandum Report No. 42: Air Blast From One Pound Cylindrical Charges Positioned Vertically on the Ground, by R. E. Reisler and D. P. LeFevre, Aberdeen, MD, Apr 1972

10. Aberdeen Proving Ground, Ballistic Research Laboratories Report No. 681: Comparison of the Blast from Explosive Charges of Different Shapes, by C. L. Adams, J. N. Sarmousakis, and J. Sperrazza, Aberdeen, Md, Jan 1949

11. John Wisotski and William H. Snyer, *Characteristics of Blast Waves Obtained From Cylindrical High Explosive Charges*, Denver Research Institute, Denver, CO, Nov 1965

12. Civil Engineering Laboratory, Technical Report R- : Blast Environment From Fully and Partially Vented Explosions in Cubicles, by W. A. Keenan and J. E. Tancreto, Port Hueneme, CA (to be published)

Table 1

Summary of test program[a]

Explosive		Conditions				
Composition	Shape	Weight (lb)	Elevation[b]	Surface	Number of Gage Measurements per Plotted Value	Figure Numbers
Composition B	Cylinders (L/D = 1)	0.5	3.3	Stiffened steel plate	4	9
		1.00	4.0		4	
		1.49	4.8		4	
		2.01	5.2		4	
		3.03	6.0		4	
RDX slurry	Encased disc	2.1[c]	5.8		18	10,11
		3.7[c]	6.6		20	
Composition B	Hemispheres	1.0	Surface burst	4-in. Steel plate and sand	6	3,4
		2.95			6	5,6,9
Composition B	Spheres	1.07	Surface burst and 4.1	4-in. Steel plate	6	5,6,9
		2.67	Surface burst and 5.9		6	
Composition B	Cylinders	1.49	Surface burst and 4.8	4-in. Steel plate	6	7,8,9
		3.03	Surface burst and 6.0		6	
Composition B	Spheres	1.07	1.83	Three-wall cubicle without roof	3	17,18,19
		2.67	1.83		2	20,21,22
Composition B	Cylinders	1.00	1.83		2	17,18,19

[a] Shown in sequence of testing

[b] Elevations from ground to c.g. of charge except for slurry which was measured to bottom of container

[c] Includes weight of 100-gram booster

Hemispherical Charges – Composition B

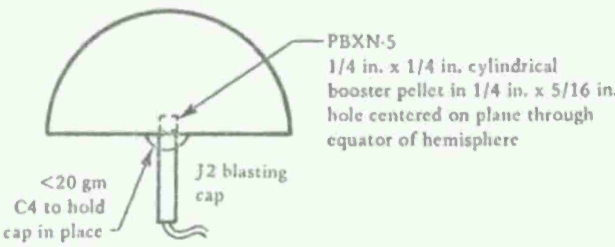

Avg. Charge Weight (lb)	Nominal Diameter (in.)
1.00	4.00
2.95	5.75

Spherical Charges – Composition B

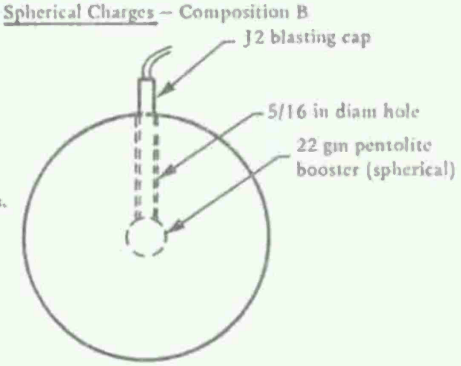

Avg. Charge Weight (lb)	Nominal Diameter (in.)
1.07	3.25
2.69	4.38

Cylindrical Charges – Composition B

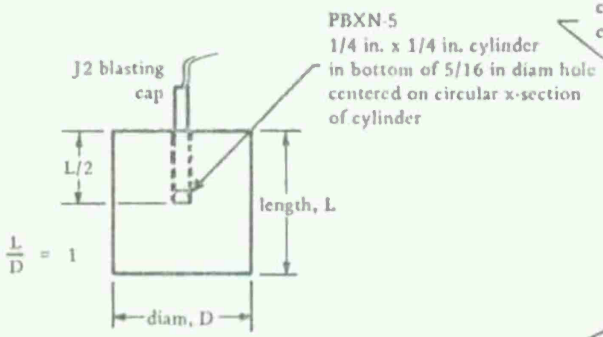

Avg. Charge Weight (lb)	Avg. Diameter (in.)
0.49	2.2
1.00	2.7
1.49	3.2
2.01	3.5
3.03	4.0

Encased RDX Slurry Charges*

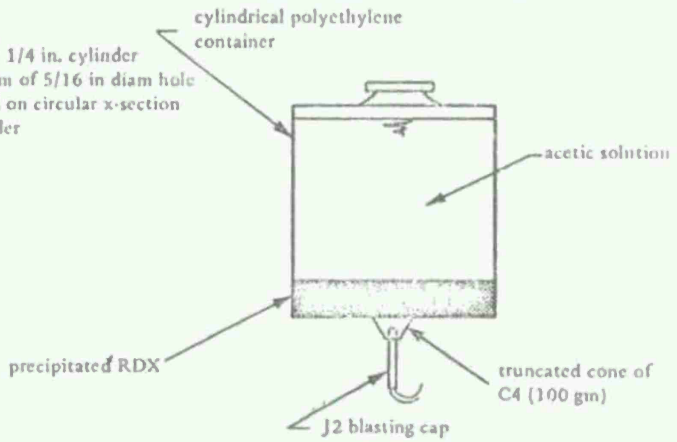

Avg. Charge Weight (lb)	Container Diameter (in.)
1.9	7
3.5	8.5

* See Table 1 for detailed listing of RDX slurry specimen dimensions

Fig 1 Charge dimensions

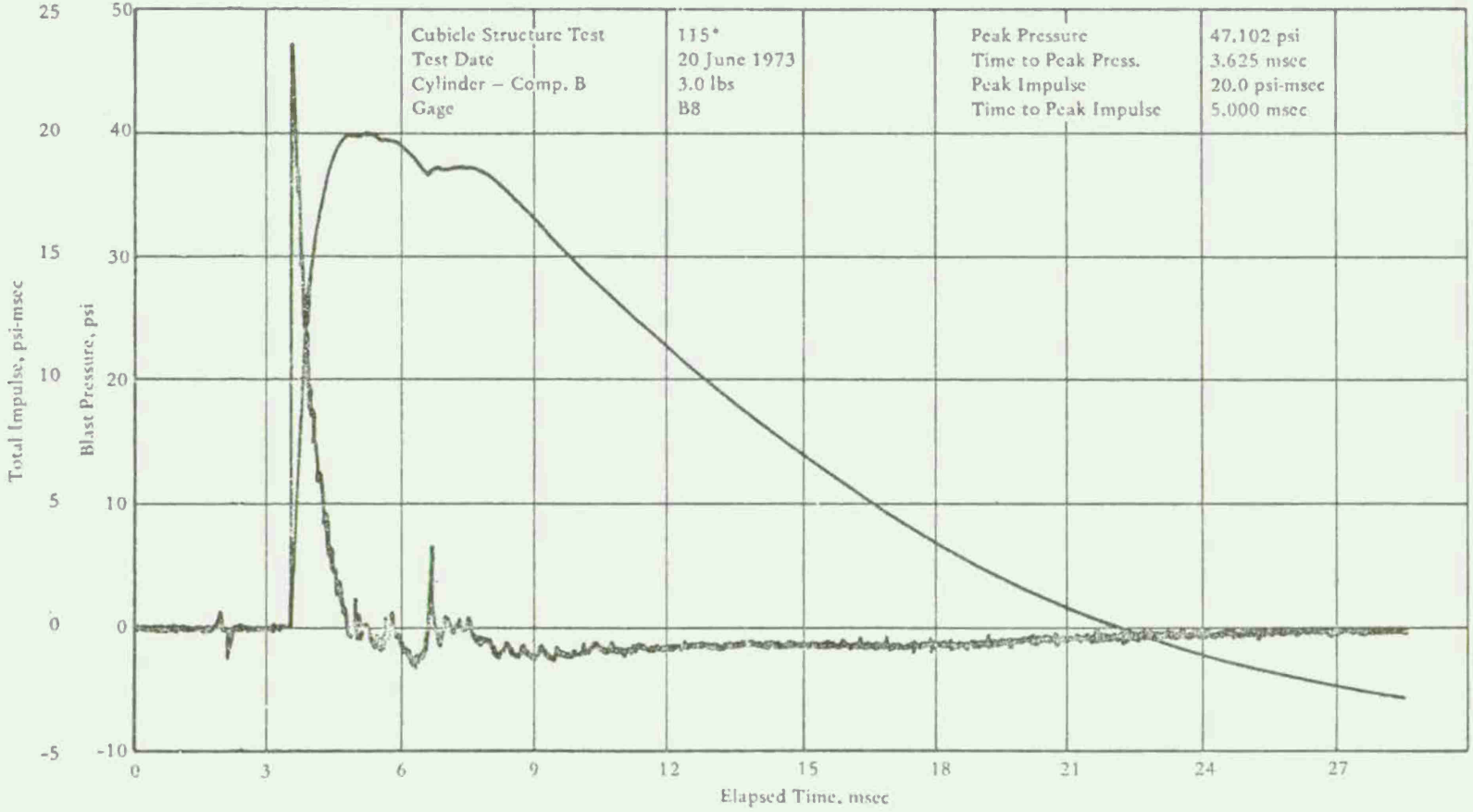

Fig 2 Typical plot of digitized pressure-time data

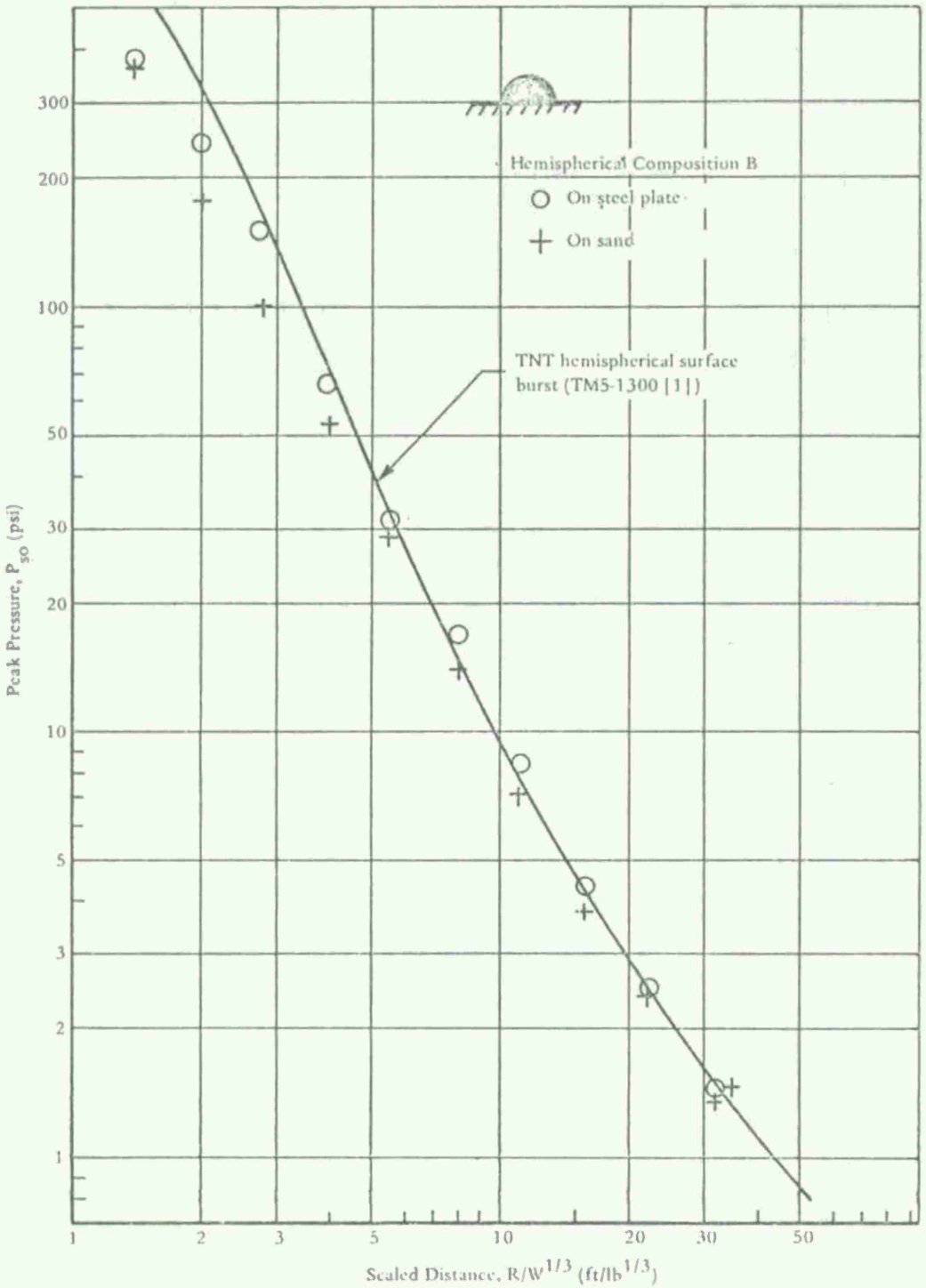

Fig 3 Peak pressure from hemispherical surface bursts on sand and on steel plate

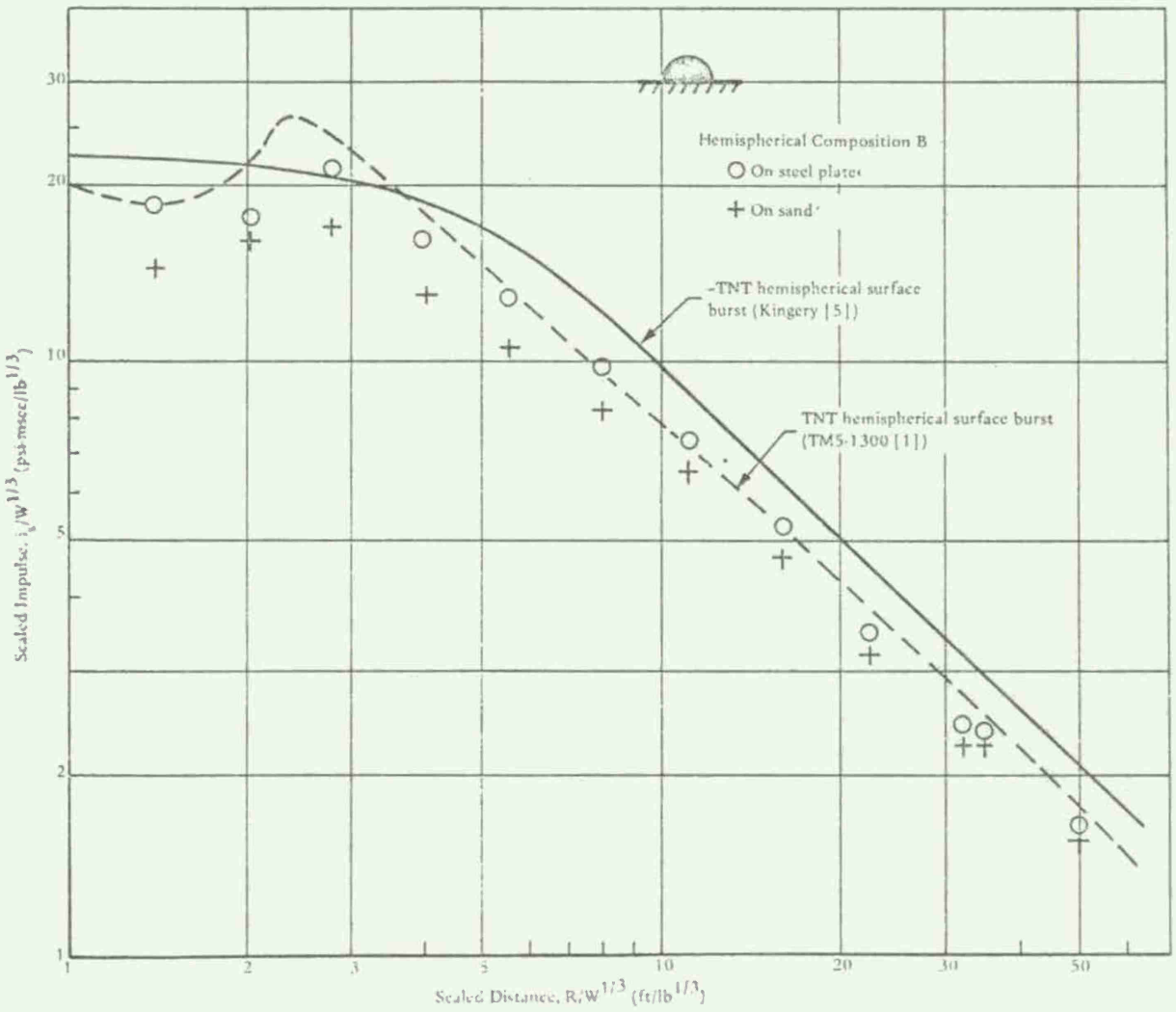

Fig 4 Scaled impulse from hemispherical surface bursts on sand and on steel plate

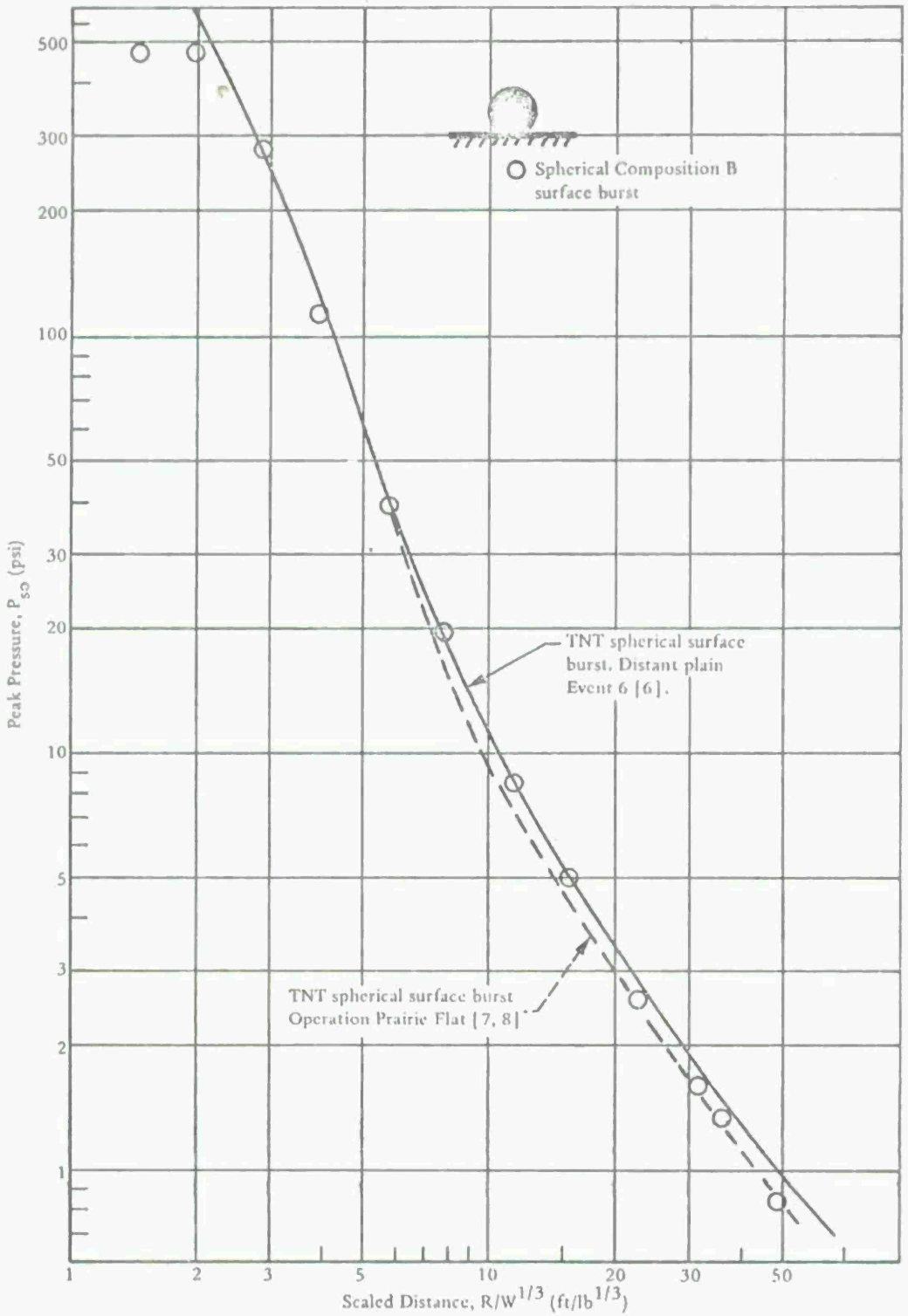

Fig 5 Peak pressure from spherical surface bursts

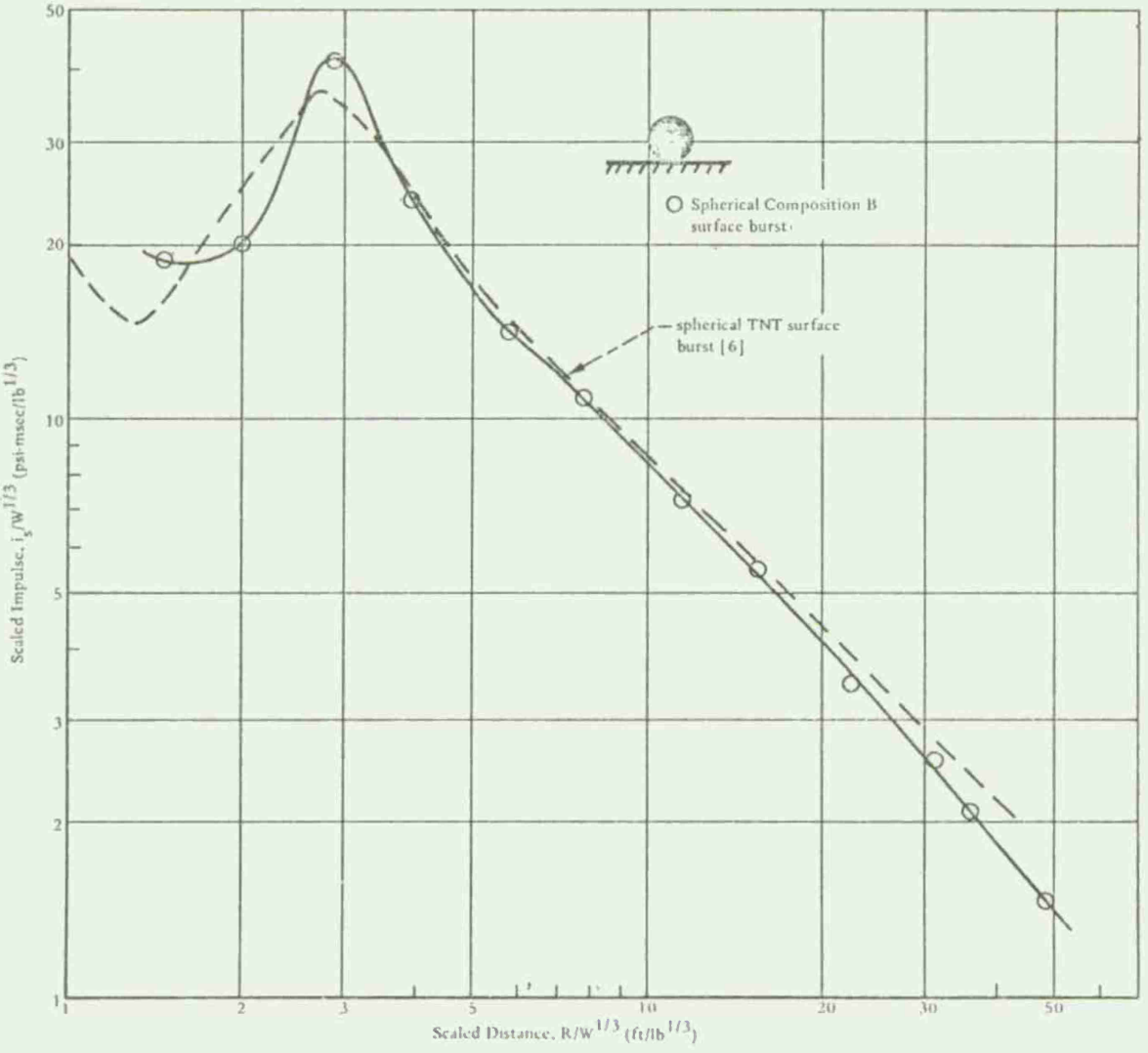

Fig 6 Scaled impulse from spherical surface bursts

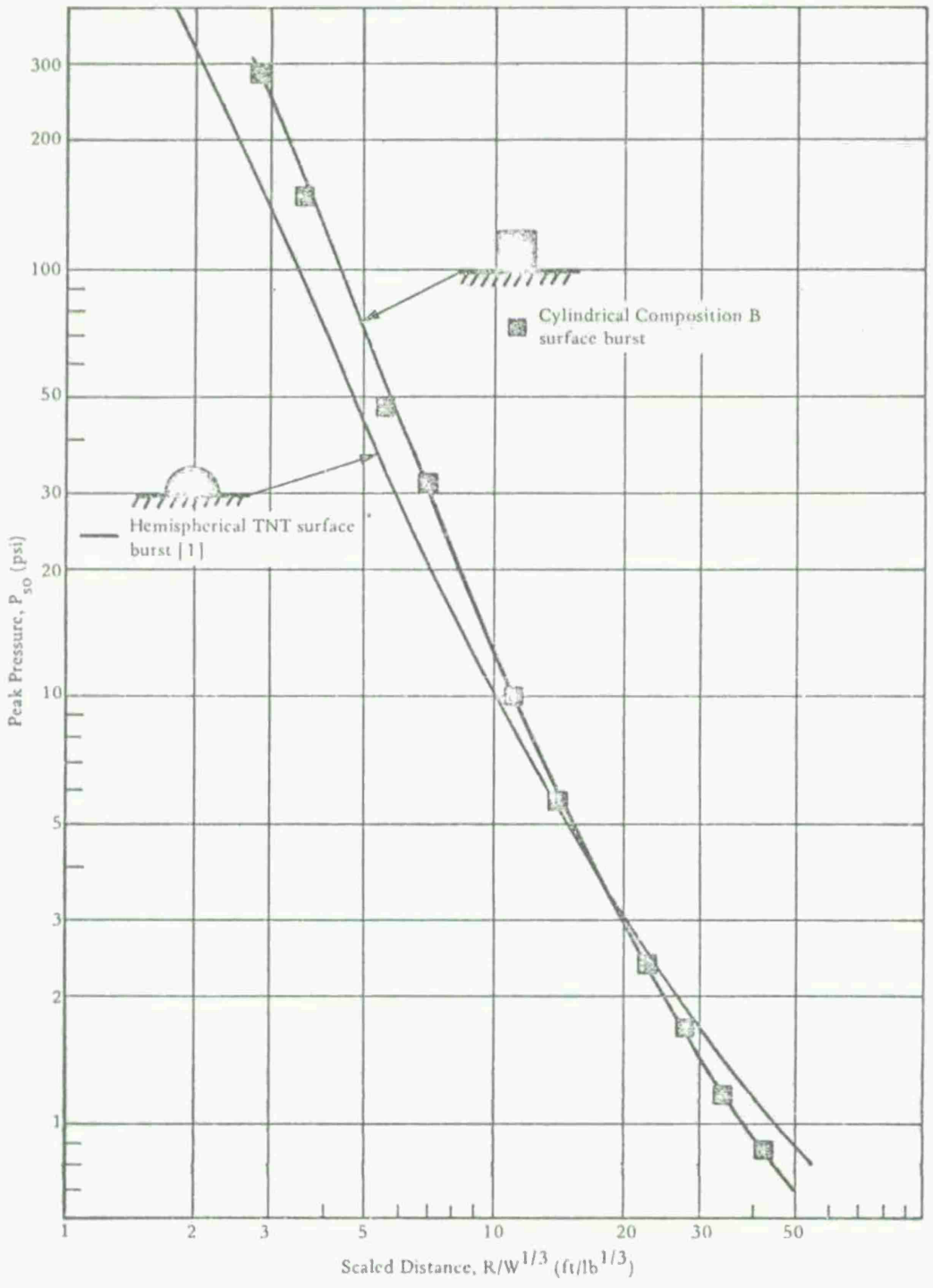

Fig 7 Peak pressure from cylindrical composition B and hemispherical TNT surface bursts

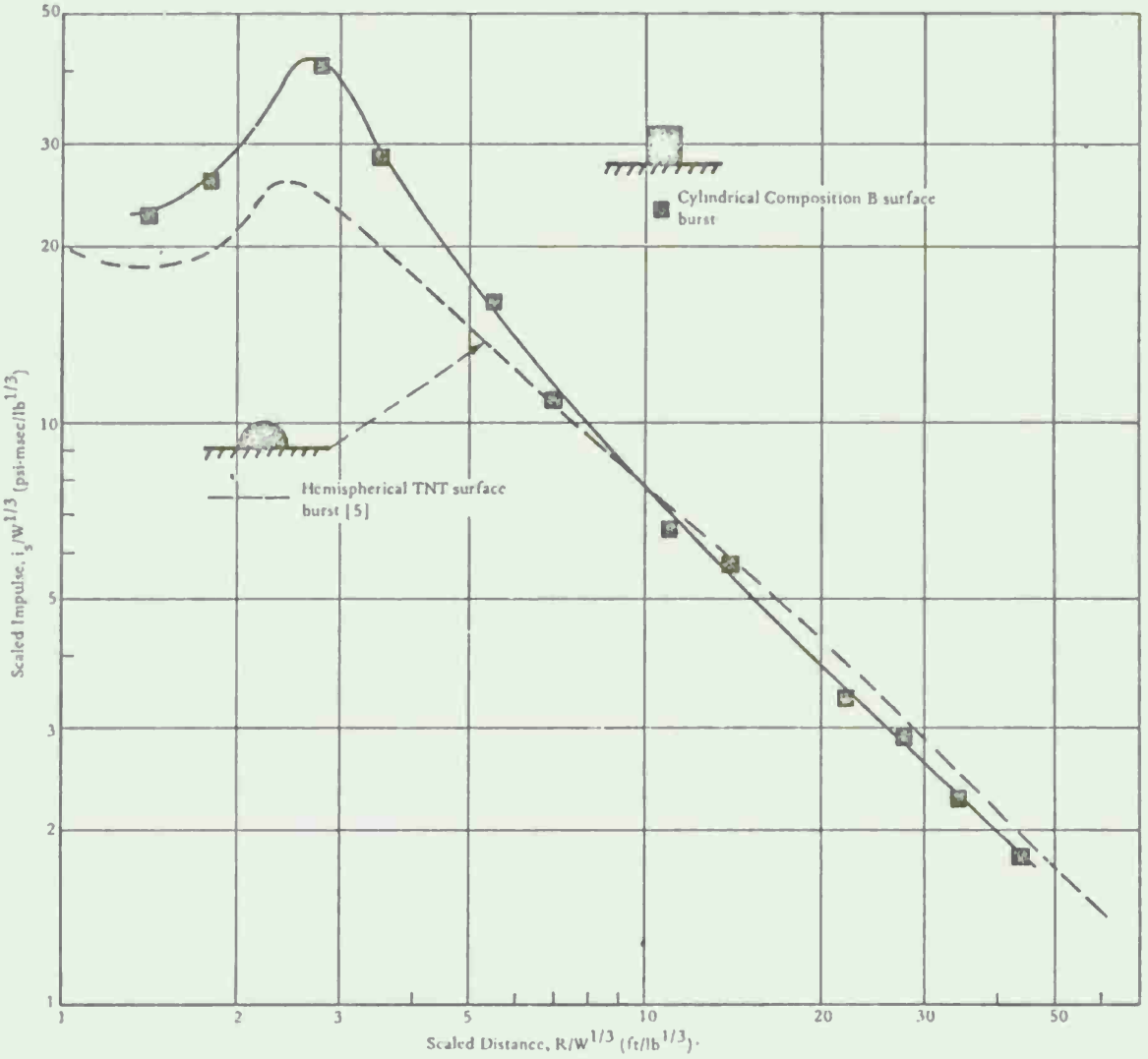

Fig 8 Scaled impulse from cylindrical composition B and hemispherical TNT surface bursts

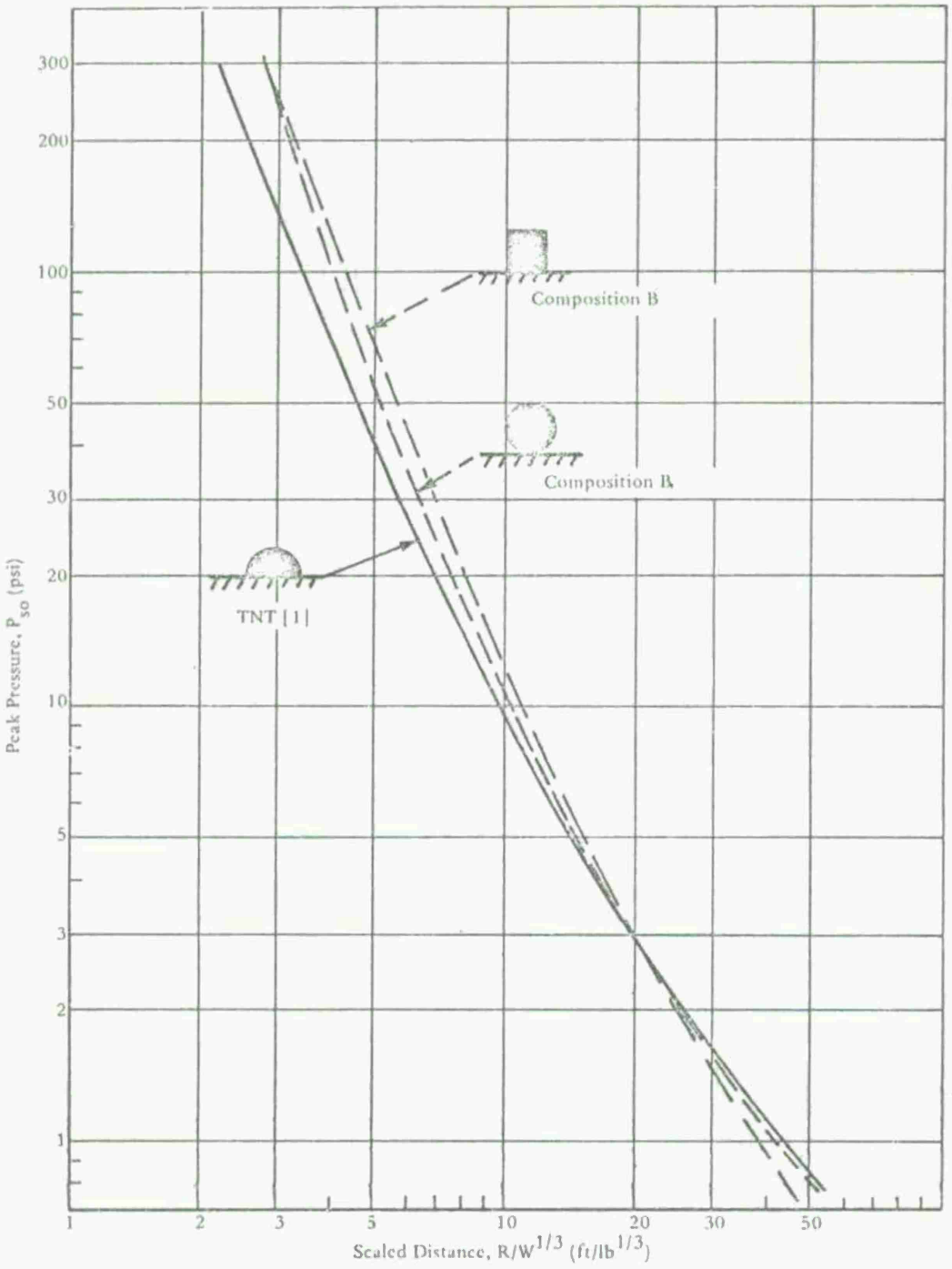

Fig 9 Peak pressure from spherical, hemispherical, and cylindrical surface brusts

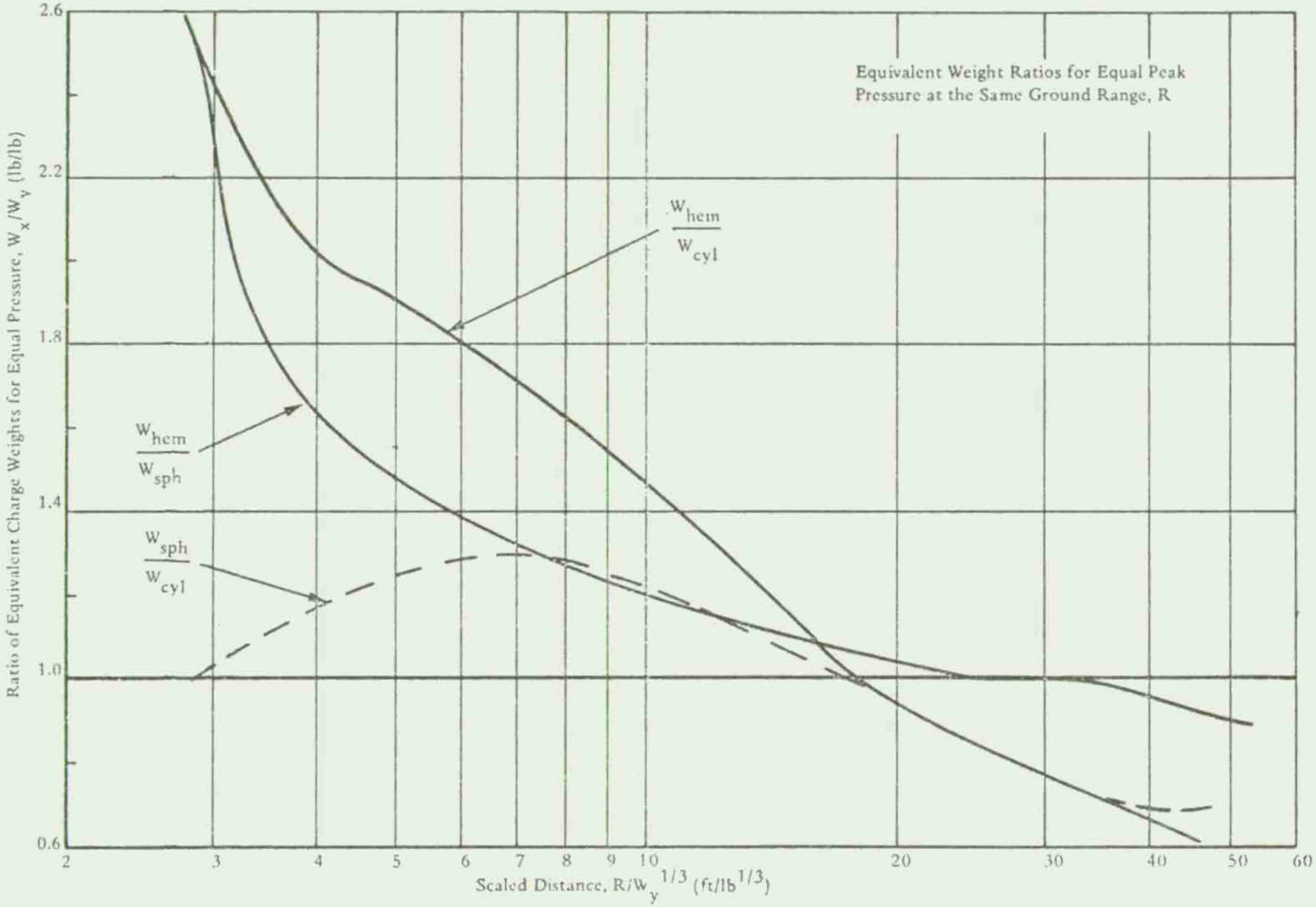

Fig 10 Equivalent weight ratios for equal pressures from charges of different shape

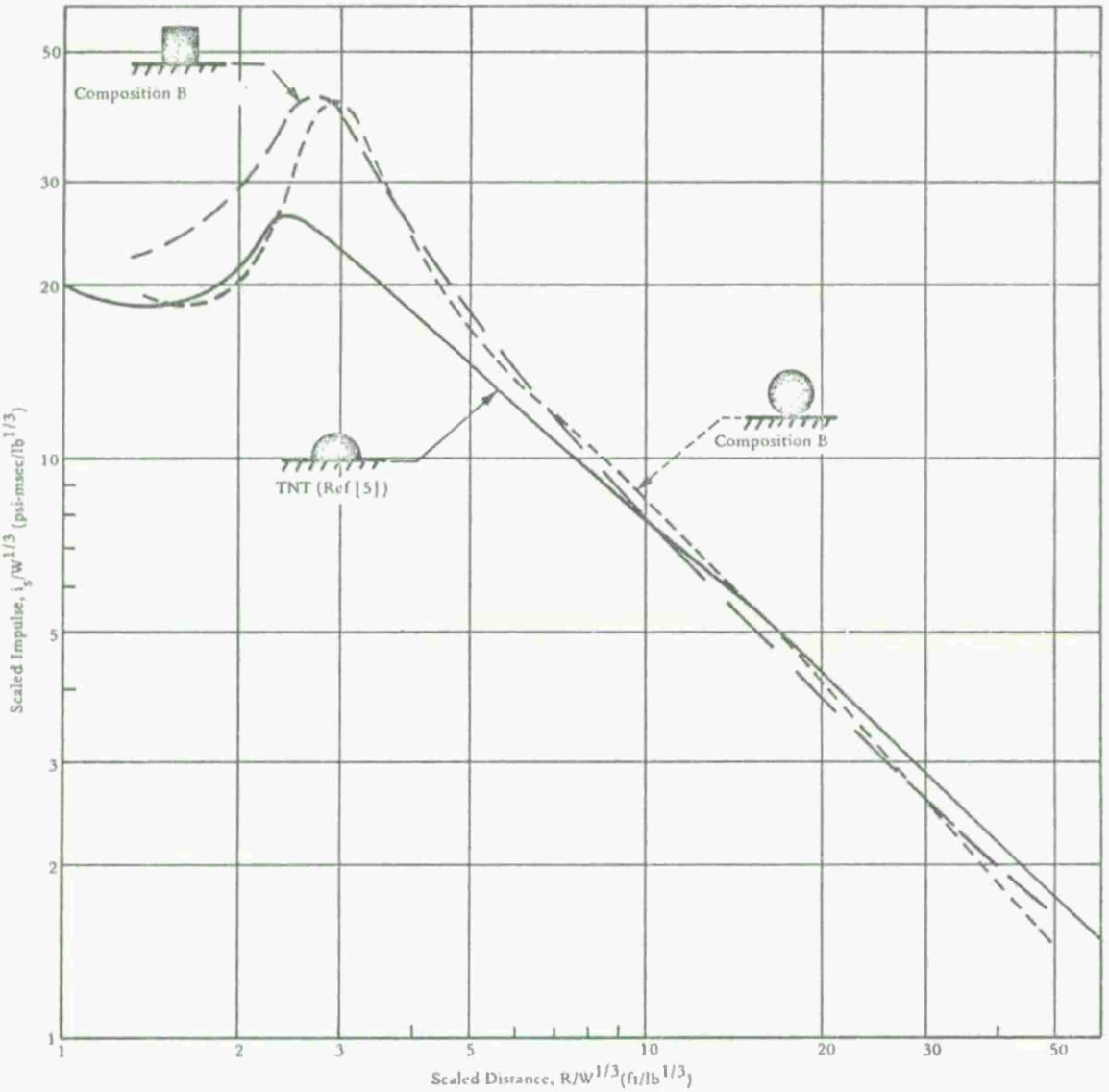

Fig 11 Scaled impulse from spherical, hemispherical, and cylindrical surface bursts

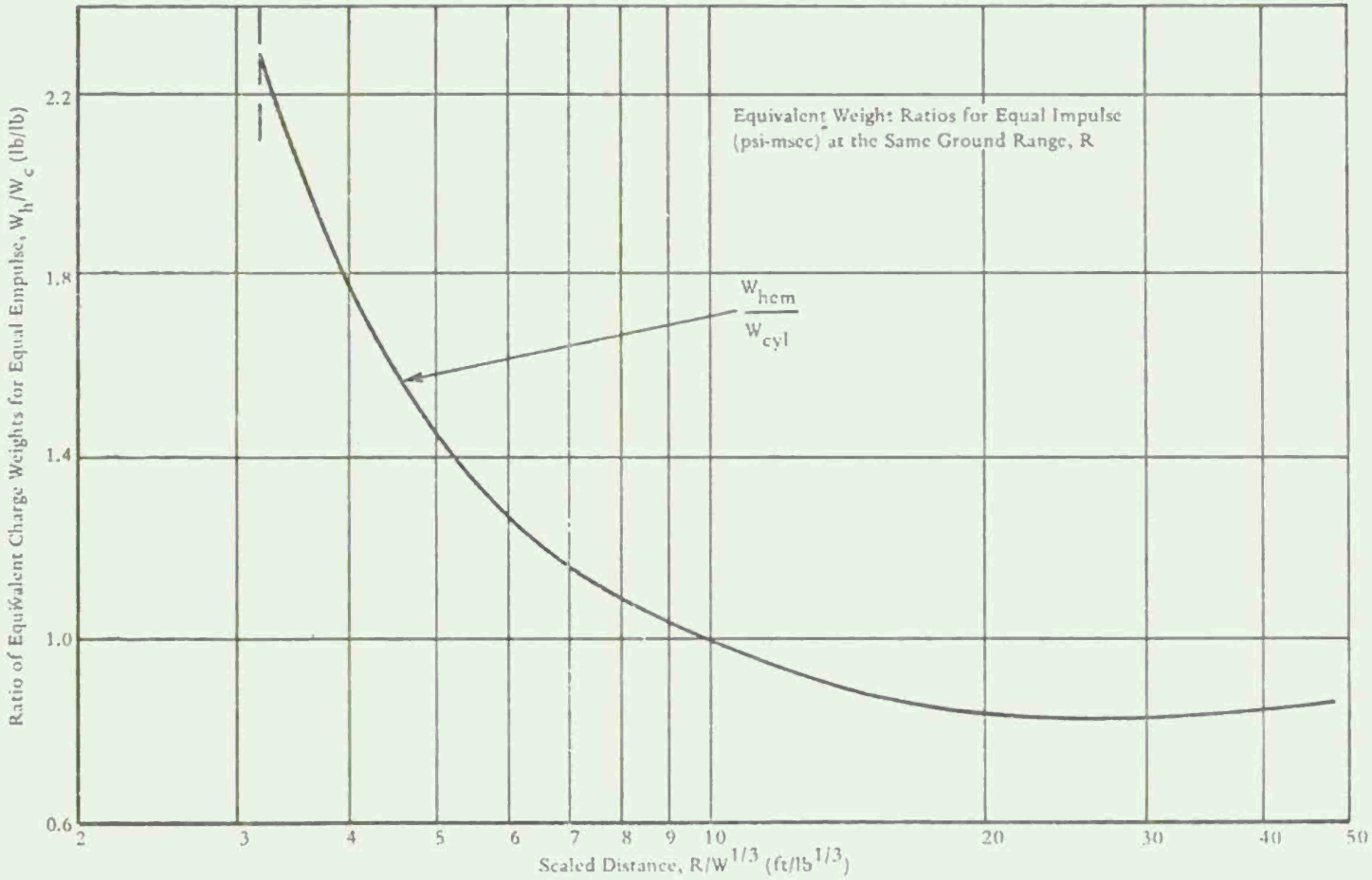

Fig 12 Equivalent weight ratios for equal impulse from hemispherical and cylindrical surface bursts

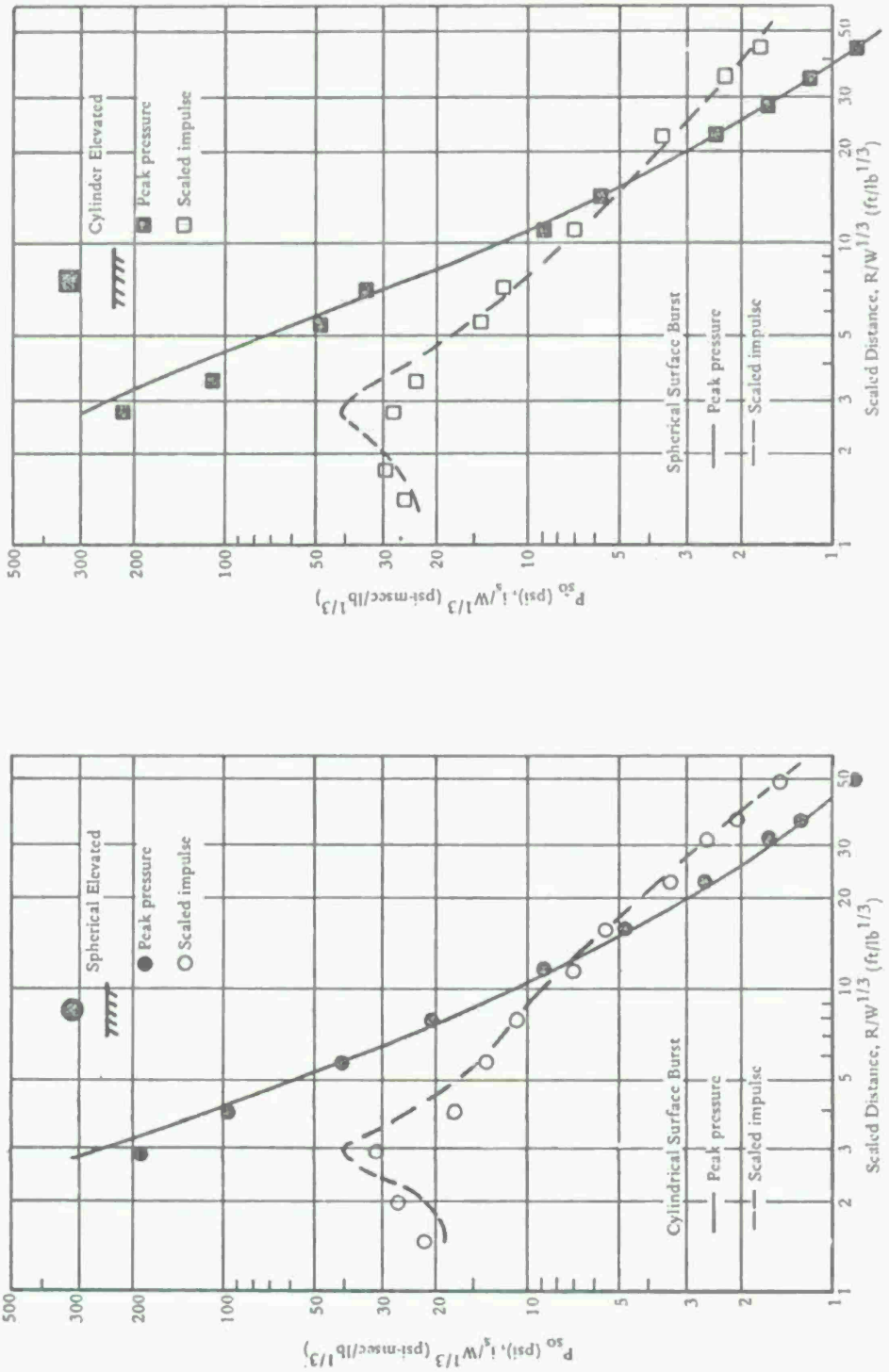

Fig 13 Peak pressures and scaled impulses for surface bursts and elevated cylindrical and spherical composition b charges

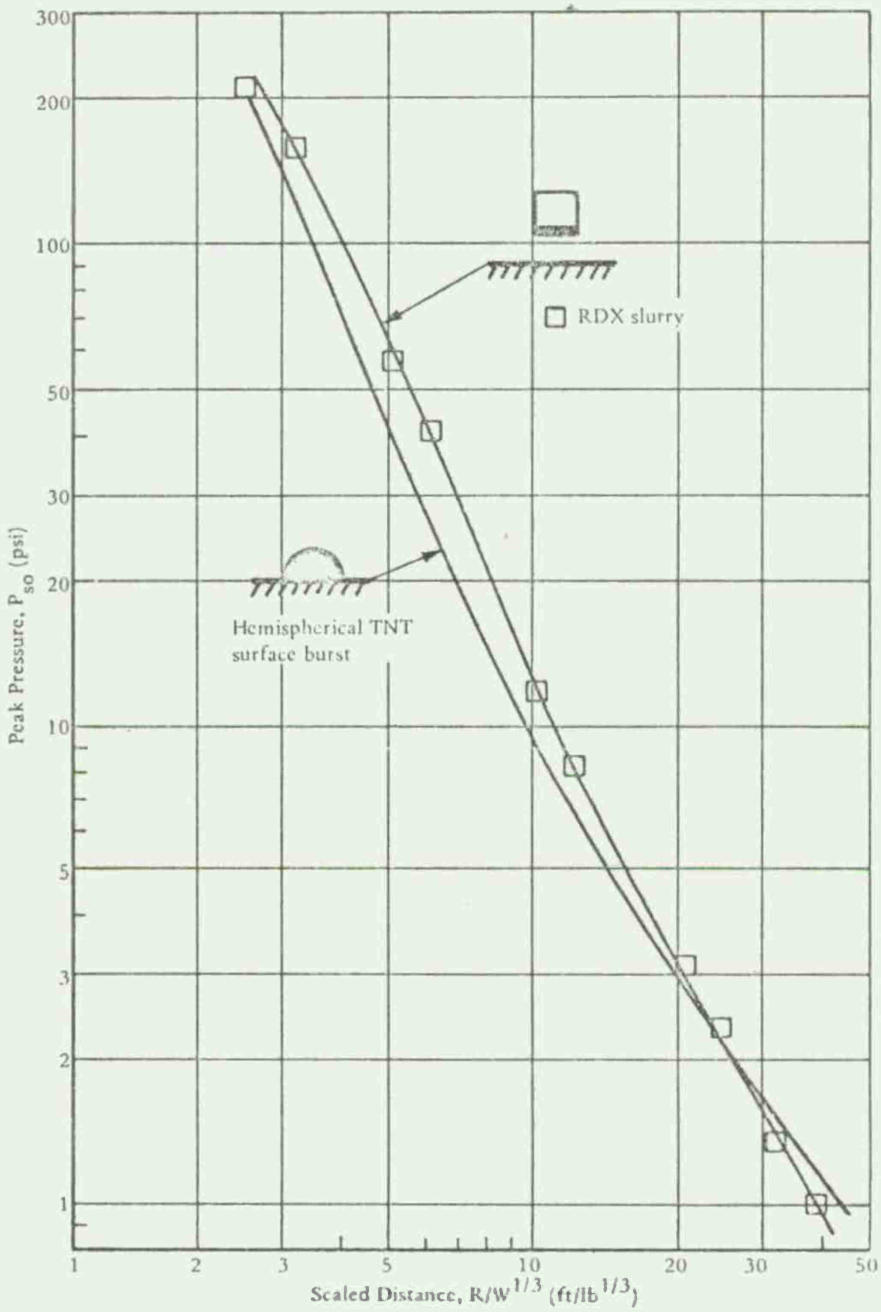

Fig 14 Peak pressure from RDX slurry and hemispherical TNT

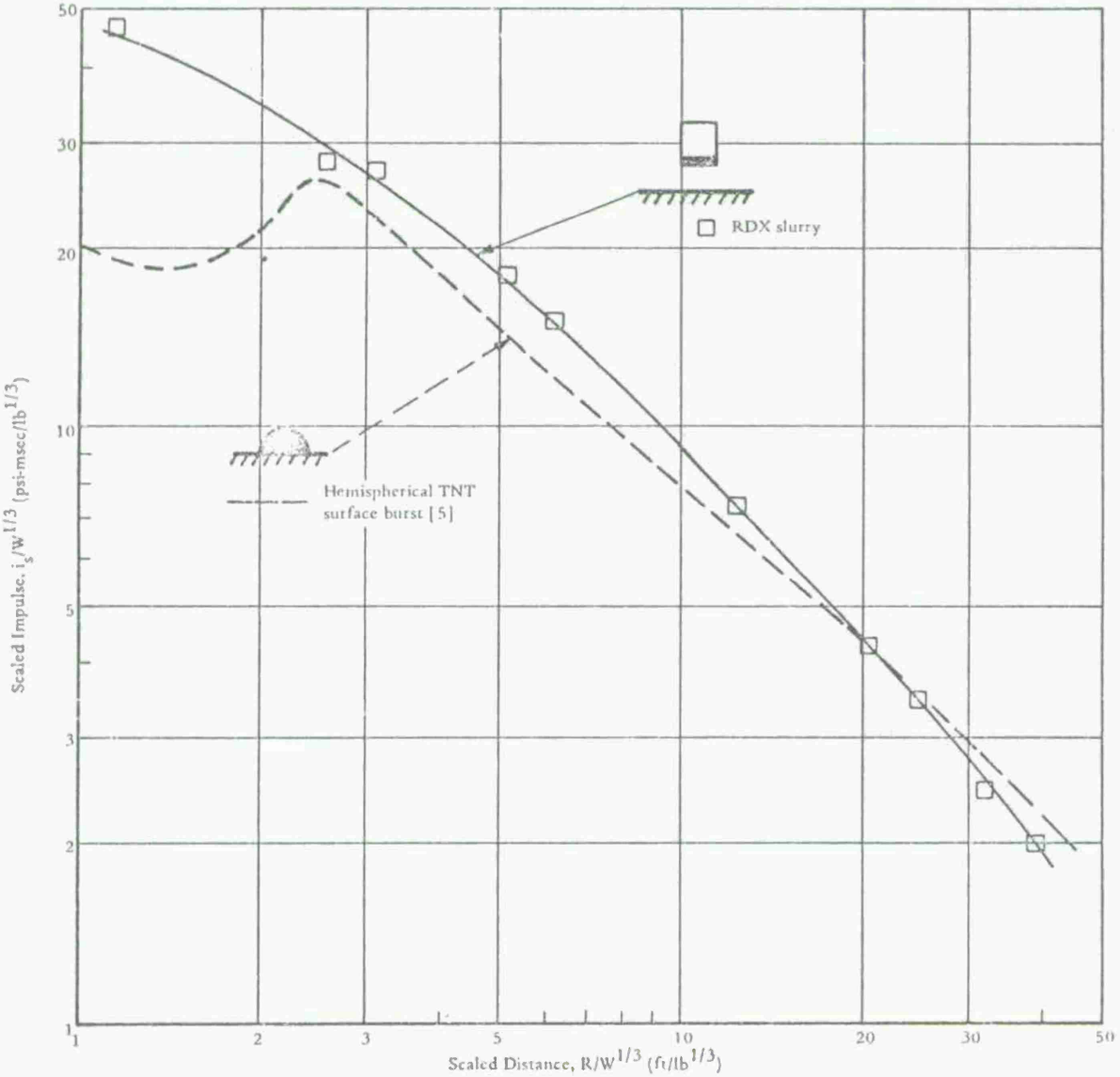

Fig 15 Scaled impulse from RDX slurry and hemispherical TNT

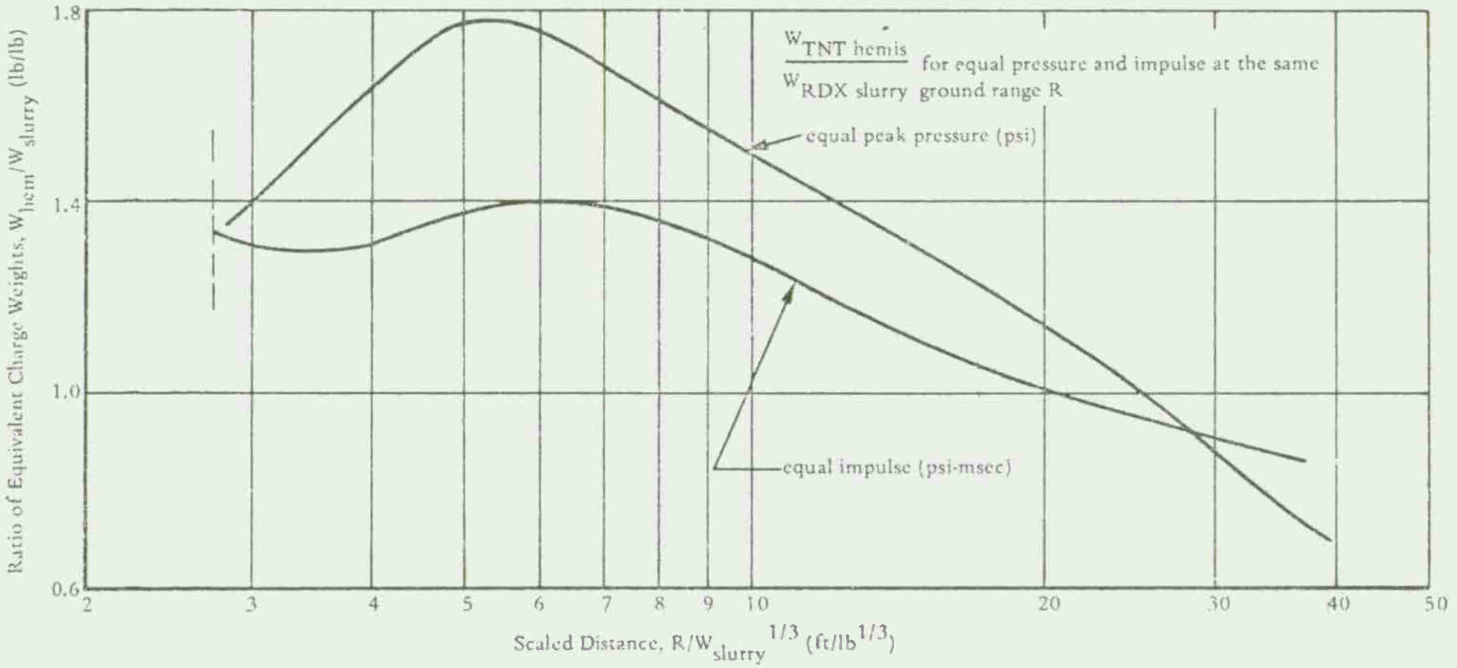

Fig 16 Equivalent weight ratios for equal peak pressure and impulse from cylindrical RDX slurry and TNT hemispheres

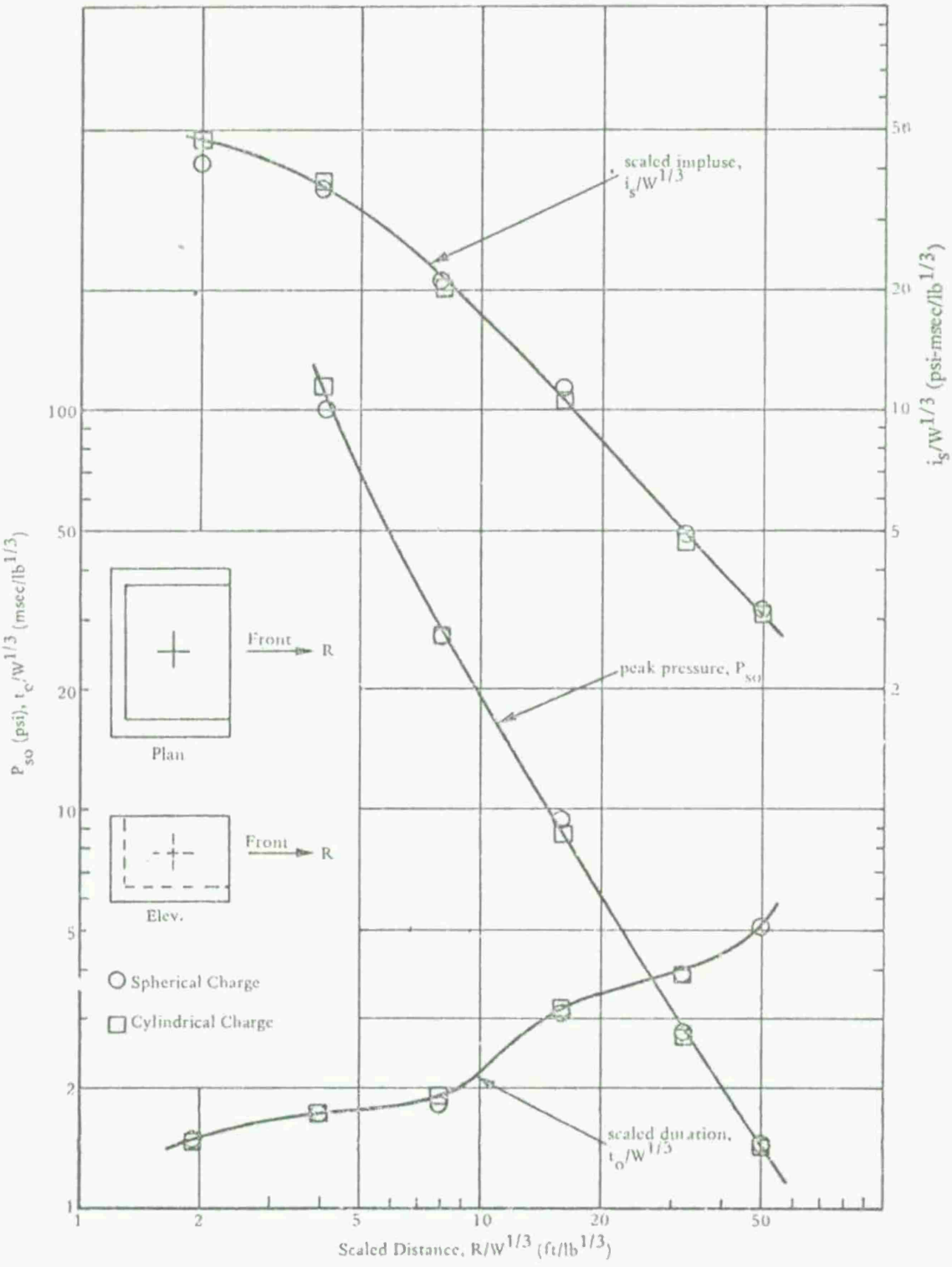

Fig 17 Blast environment out open wall of cubicle for spherical and cylindrical charges (W = 1.0 pound)

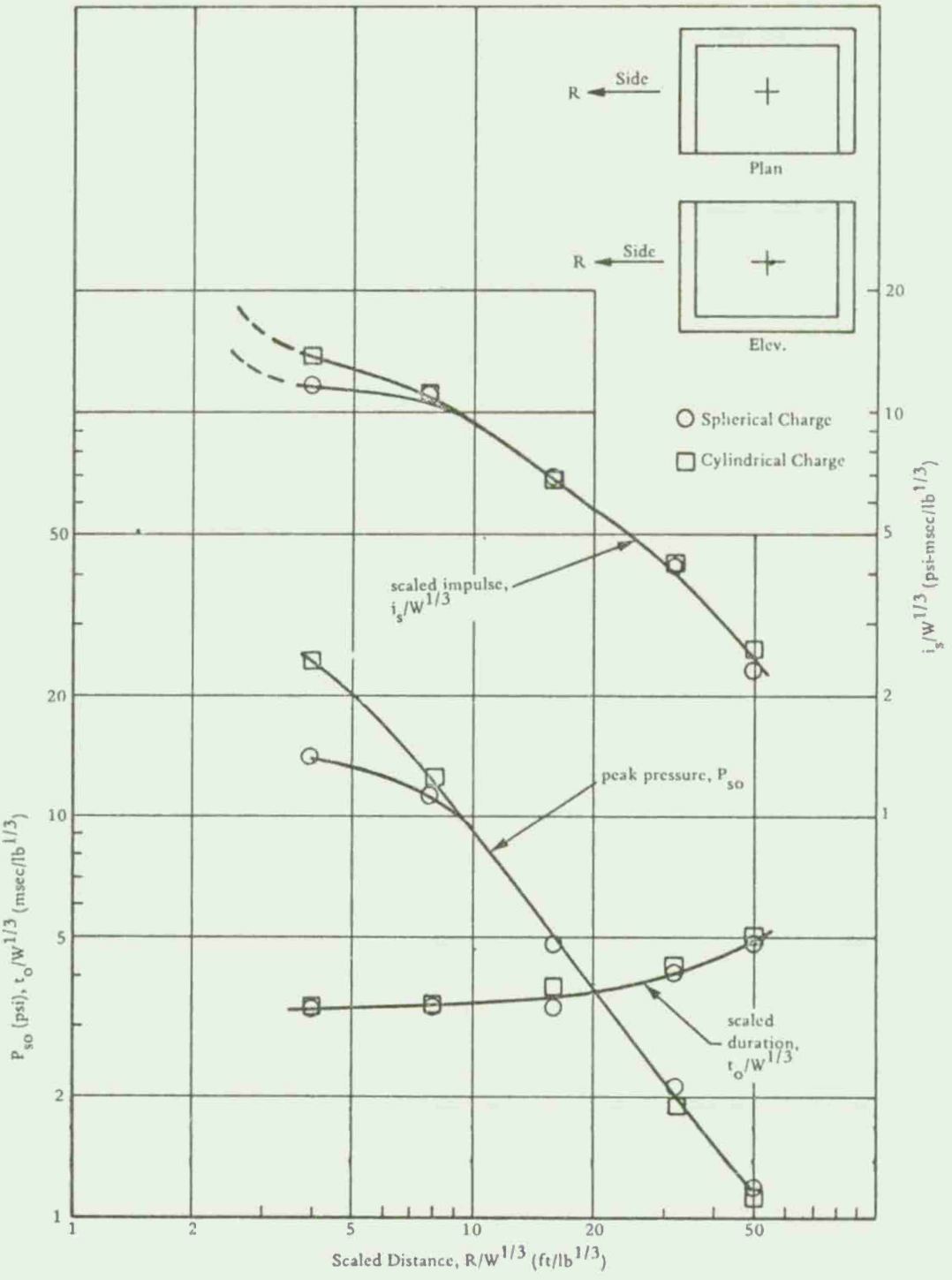

Fig 18 Blast environment behind sidewall of cubicle for spherical and cylindrical charges (W = 1.0 pound)

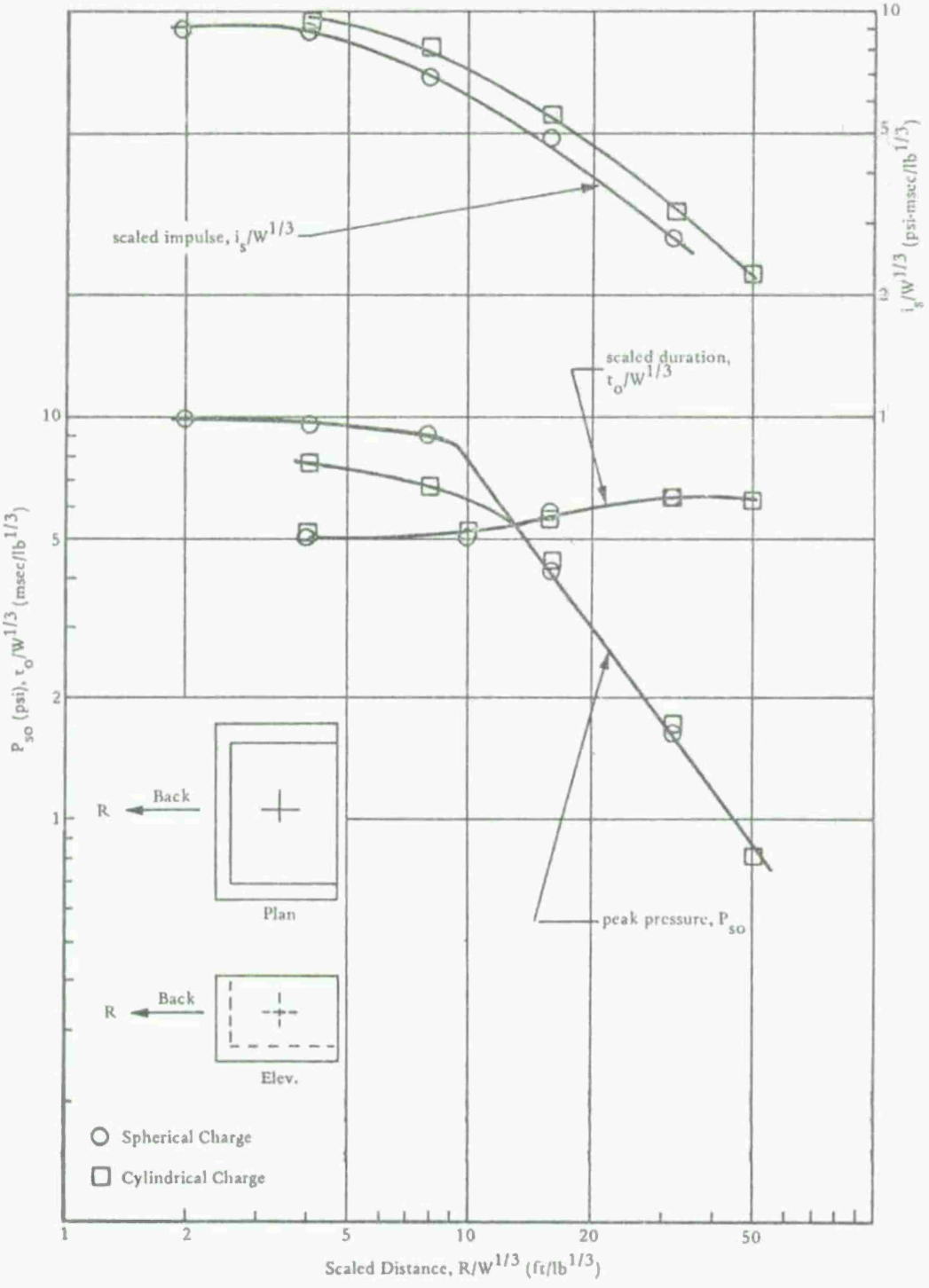

Fig 19 Blast environment behind backwall of cubicle for spherical and cylindrical charges (W = 1.0 pound)

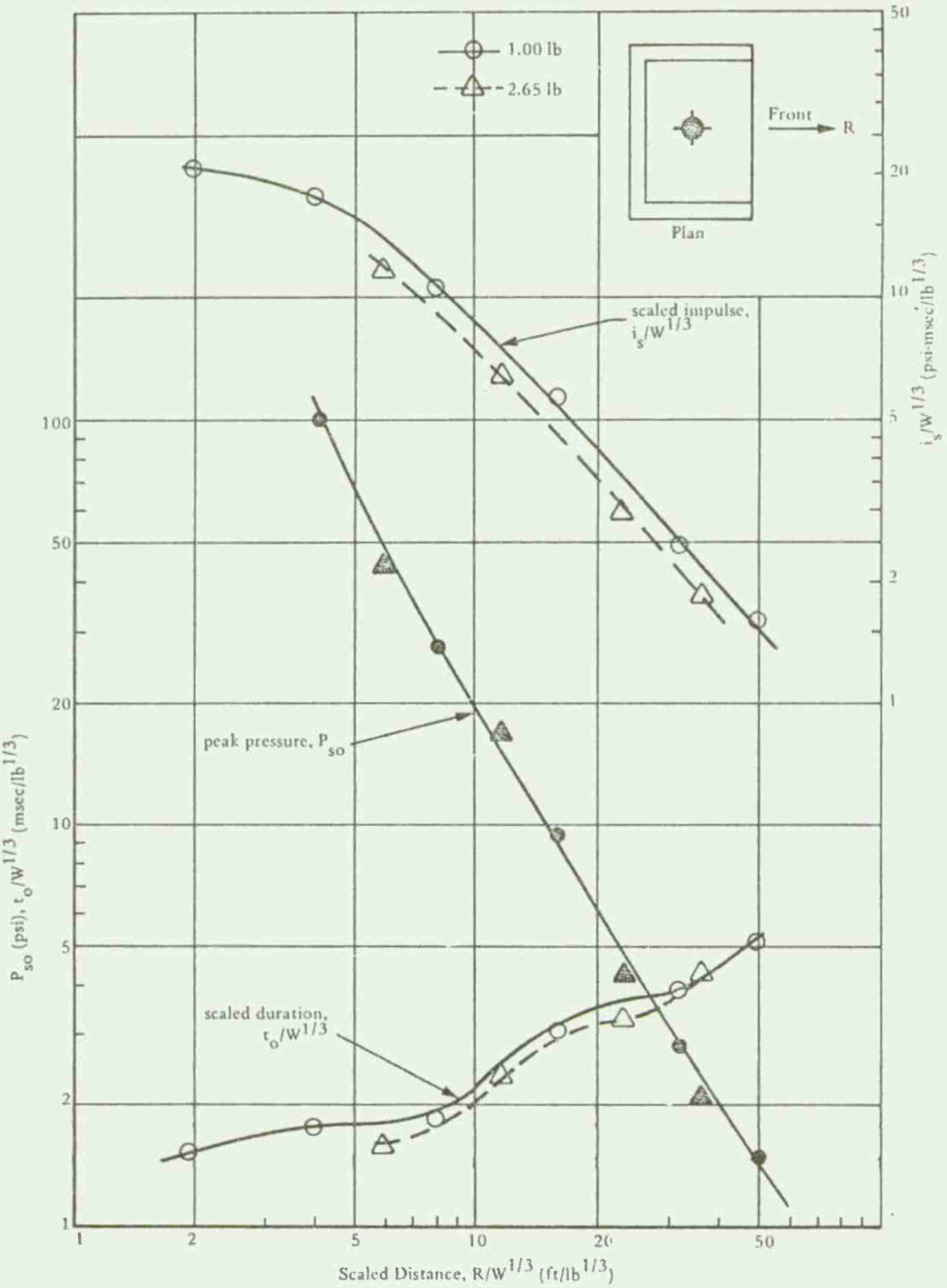

Fig 20 Blast environment out open wall of cubicle for 1.00- and 2.65-pound spherical charges

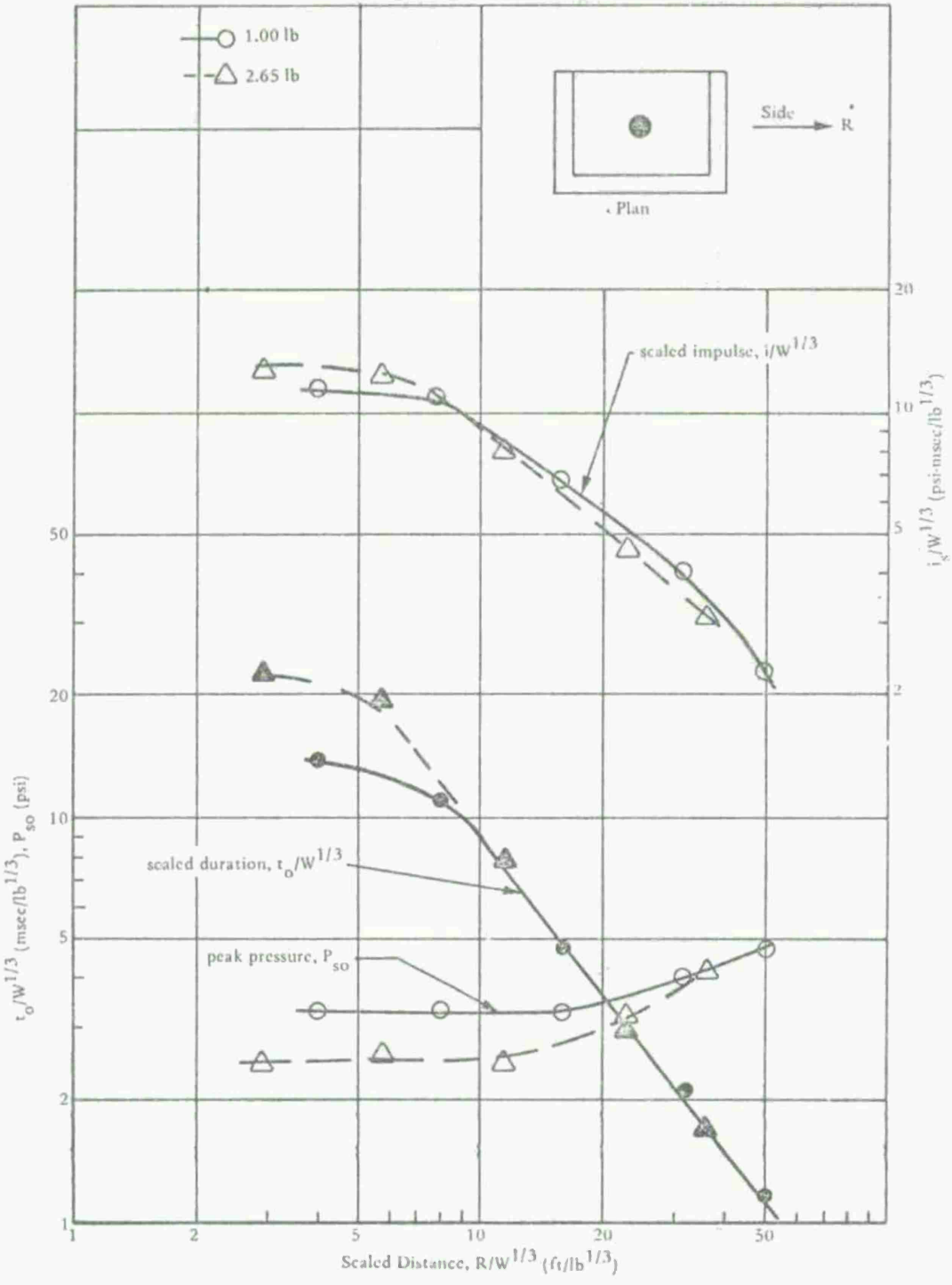

Fig 21 Blast environment behind sidewall of cubicle for 1.00- and 2.65-pound spherical charges

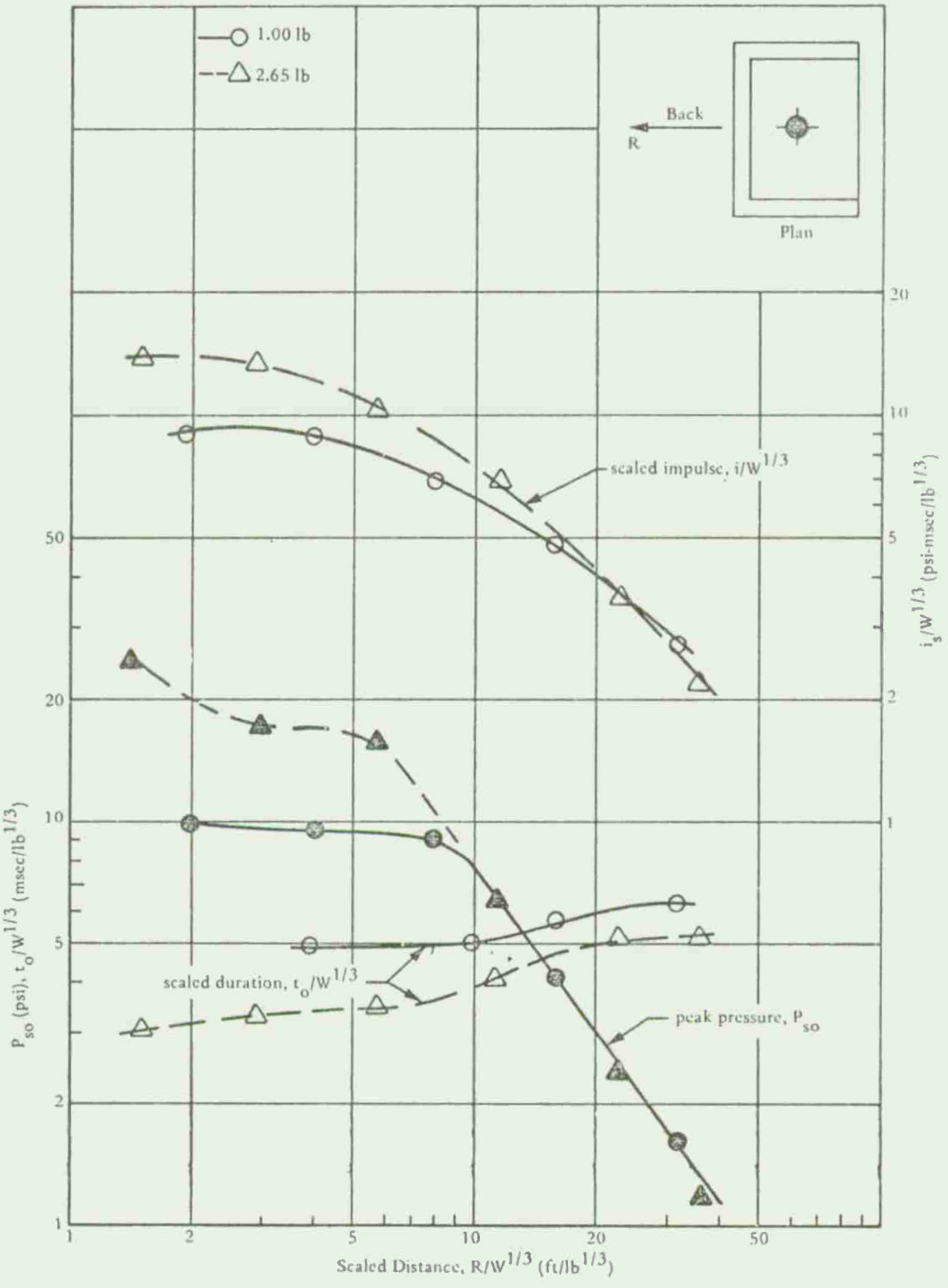

Fig 22 Blast environment behind backwall of cubicle for 1.00- and 2.65-pound spherical charges

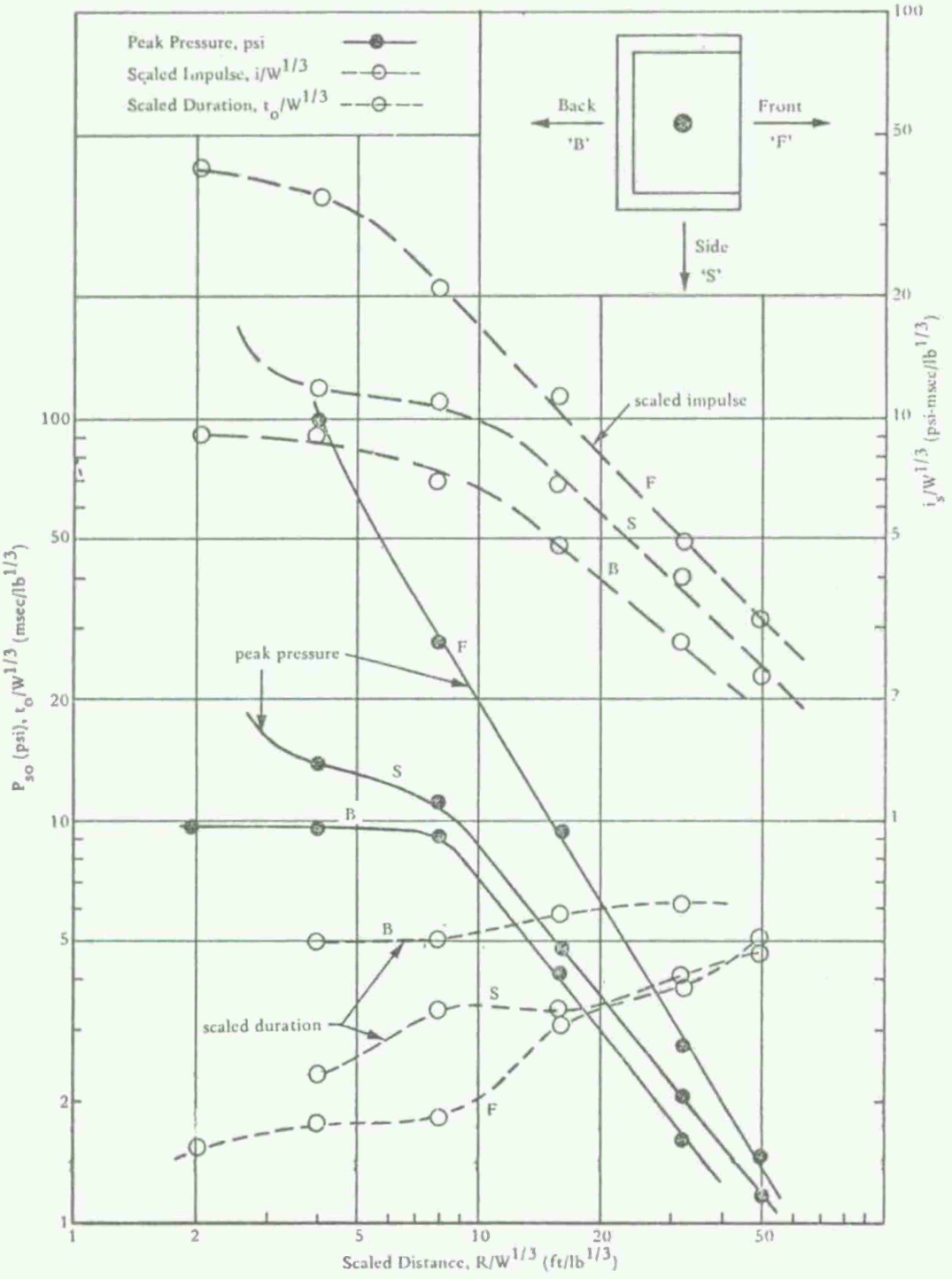

Fig 23 Blast environment outside three-wall cubicle (1.00-pound spherical charge)

AN ANALYTICAL MODEL TO PREDICT EXPLOSION PROPAGATION

James M. Dobbie and Donald S. Allan

Arthur D. Little, Inc.
Cambridge, Massachusetts 02140

ABSTRACT

This paper describes an analytical model for predicting the spacing required between adjoining explosive projectiles to obtain a high probability that a detonation will not propagate from one to another. It also describes experiments that were conducted to obtain data for comparing with the analytical model.

The general procedure is as follows: from fragmentation data and empirical equations obtained from such tests estimate the mass and spatial distributions of fragments relative to the donor. Also, estimate the initial velocities of the fragments issuing in various polar zones. Use geometrical relationships and drag laws, if the spacings are large, to estimate the distribution of mass and striking velocity of fragments on various zones of the receptor. Next, use sensitivity data and empirical equations obtained from such tests to determine the effects of fragment impacts, in particular the probability of high-order detonation. Finally, use simple probability arguments to compute the probability that the receptor will receive at least one high-order impact, thereby obtaining the probability of propagation as a function of the spacing. Then solve the set of equations, by iteration if necessary, to obtain the spacing required for a given probability of propagation.

The purpose of this presentation is to describe the model, summarize the results of the experiments that were made to develop and test the model, and to indicate analytical and experimental work that is needed to improve the model.

1. The Propagation Model

1.1 Background

The spacing necessary to prevent the propagation of an explosion between two or more adjoining projectiles is of prime concern in the design and layout of ammunition plants. Knowledge of the required spacing may also aid in achieving improved safety both in the storage and field use of projectiles.

The usual method of determining "safe" separation distances between explosive items is to conduct propagation tests at selected spacings, using sufficient receptors to obtain a small confidence interval for the confidence level of interest. This method is slow and expensive. Also, it yields little insight into the propagation process and the factors that are critical.

Recently Arthur D. Little, Inc., under a contract with Picatinny Arsenal, undertook the development of an analytical model with which to predict the probability of detonation for a given spacing and orientation of the donor and receptor, and to estimate the spacing required to obtain a given probability of propagation. Such a model can be used not only for determining safe separation distances of current projectiles, but also for estimating the effects of shields and deflectors, and the effects of changes in case thickness, charge composition, charge-to-metal weight ratio, etc.

The type of detonation of primary interest is a high-order detonation, similar to that produced by the firing of a fuze. If detonation of this type is initiated at one or more positions along the lateral surface of the receptor, it is expected that the detonation wave will propagate throughout the charge and the receptor will detonate high-order. This type of detonation might be called domino detonation, since fragments from the receptor could detonate a third projectile at the same spacing. Low order detonations, while not negligible, are of secondary interest.

The basis for the model is the knowledge that propagation of a detonation between explosive projectiles of interest is caused by primary fragment impact. The sensitivity of the acceptor projectile to detonation is determined by the presented area of the fragment, its velocity at impact, the angle at which it impacts, the casing thickness, and the explosive loading of the acceptor. Some sensitivity data and empirical relationships are given by Slade and Dewey (Ref 1). The sensitivity results and analyses that have

been performed by Picatinny Arsenal (Ref 2) and by Arthur D. Little, Inc. (Ref 3) for both the Arsenal and the Department of Defense Explosives Safety Board (Ref 4) provide a reasonable basis for the development of an analytical model.

1.2 Fragment Properties and Distributions

Data have been obtained on the properties of fragments that are produced in the detonation of projectiles. These properties include initial velocities and various measures of fragment size. Measurements have been made of the distribution of fragment mass, the spatial distribution of ejected metal, and the variation of mass distribution with the polar angle measured from the nose of the projectile. Measurements have been made of the initial velocity of fragments and the variation of velocity with polar angle. The results of these measurements have been used to obtain various empirical equations from which the fragment properties can be estimated from the dimensions of the projectile, the composition of the charge, and the composition of the case. References 5, 6, and 7 contain equations of this type and discussions of other properties for which empirical equations have not yet been developed.

From scaled drawings of the donor estimate the average outside diameter and case thickness over the middle third of the projectile. From these quantities and the densities of the charge and metal compute the corresponding charge-to-metal ratio, the initial velocity V_o, and the average mass m_o of fragments from well-known equations. The one-third rule has been observed to yield accurate estimates of V_o for the central 10 degree polar zone. Accurate estimates of m_o for the central zone required a change in a parameter K_o from the value that applied to all fragments to a smaller value.

In general, the maximum initial velocity is obtained in the central polar zone. The variation of the initial velocity with polar angle depends on the projectile. Let the initial velocity at polar angle φ be $V_o F_v(\varphi)$. The values of $F_v(\varphi)$ for a typical nose-fuzed projectile are approximately as follows:

φ (degrees):	60	70	80	90	100	110	120
$F_v(\varphi)$	9,6	0.7	0.9	1.0	0.7	0.6	0.5

The distribution of fragments with polar angle also depends on the projectile. For a typical nose-fuzed projectile the fraction $F_M(\varphi)$ of the fragment mass that is ejected in a polar zone of 10 degrees centered at polar angle φ varies as follows:

φ (degrees):	60	70	80	90	100	110	120
$F_M(\varphi)$:	0.05	0.10	0.10	0.15	0.45	0.05	0.05

The accuracy needed for the $F_v(\varphi)$ and $F_M(\varphi)$ factors depends on the particular application of the model. The spacing required for a small probability of a high-order detonation of a receptor is small enough that the fragments that can strike the receptor are limited to those that issue from the donor in a small polar zone. Hence, only the factors that apply to that zone are needed. For example, when the receptor and donor are parallel, as in Load-Assembly-Pack operations, only the factors for the 10 degree zone centered at $\varphi = 90$ degrees are needed. On the other hand, spacings that yield propagation probabilities near 50 percent are small enough that several 10 degree polar zones are involved.

We also need the distribution of fragment sizes in the relevant polar zone. Here we used an empirical distribution function that has been found to yield a fair fit to the observed distribution of all fragments. The fit is good for small and medium sizes, but not for large sizes. The critical fragment size for explosive propagation is in the region where the fit is good when the spacing is small. For small probabilities of propagation the spacings may be large enough for some projectiles that the assumed distribution function is not adequate. When work on the model is resumed we expect to re-examine this question in an attempt to obtain a more appropriate distribution function, one that applies to fragments in the relevant polar zones and to all critical sizes.

At large spacings the striking velocity may be significantly less than the initial velocity. We estimated striking velocities from the square drag law, using a shape factor for random steel fragments. The drag factor depends on the fragment mass, as well as the spacing.

1.3 Sensitivity Properties

The sensitivity equation gives an estimate of the striking velocity that is required for high-order detonation of the receptor. This critical striking velocity depends on the sensitivity of the charge, the thickness of the casing, the size of the fragment, and the impact angle θ to the normal.

Most of the available data consist of the critical (50 percent) detonation velocities obtained in sensitivity tests with cylindrical fragments of known size, orientation, and impact angle. Slade and Dewey (Ref 1) give results and empirical equations for tetryl and Composition B with bare charges and with charges covered by plates.

Most of the data for cylindrical fragments were obtained at zero impact angle, with the circular face parallel to the surface of the charge or plate. To use the corresponding sensitivity equations it is necessary to change from cylindrical fragments to irregularly shaped fragments and from zero impact angle to the variations of impact angle that occur on the receptor.

The results reported in Reference 1 and in some classified reports indicate that the critical measure of fragment size for cylindrical fragments in the orientation described above is the area of the striking face. We used the shape factor for irregularly shaped fragments to make the conversion from average presented area to the mass m. Since an irregularly shaped fragment of given presented area will not be as effective in producing detonation as a cylindrical fragment of the same presented area, we introduced a factor F_A to account for this difference. This factor is the fraction of the presented area of the irregularly shaped fragment that is as effective in producing detonations as a cylindrical fragment having a circular face equal to that area. The value F_A is not known; it probably lies in the interval (0.5, 1.0).

When the transformation described above has been made the sensitivity equation gives the striking velocity V required at normal impact in terms of the mass m, for a given explosive composition and case thickness. It also may be regarded as an equation that determines the critical mass as a function of striking velocity. If the drag is significant, the relationship is complicated, since the drag factor also depends on the mass.

In practice it was found that the drag factor could be handled by iteration, starting with the assumption that the drag is negligible. After the critical mass and corresponding spacing are computed, the drag factor can be estimated and new values computed for the critical mass and spacing, etc. It was found that only a few iterations are needed to obtain the spacing to within one percent.

The sensitivity equation was solved for the critical mass m in terms of the striking velocity V, which is determined from the initial velocity V_o in the central zone, the $F_V(\varphi)$ factor in the relevant φ direction, and the drag factor. The mass distribution function and geometric relationships then were used to estimate the number of fragments with more than critical mass that would strike the receptor.

1.4 Effect of Non-Normal Impact

Since most fragments will not strike at normal impact, the computed number of supercritical fragments for normal impact is multiplied by an impact factor F_I. Its value depends on how the effective component of striking velocity varies with the impact angle. The value of F_I is not known accurately and probably depends on the charge composition. For composition B it is estimated to be in the interval (0.2, 0.4), as described below.

Relatively few sensitivity tests have been made at impact angles different from zero. Results of some tests at small angles from the normal are reported in Reference 1 for tetryl and composition B. We used three results to get a rough estimate of the effect of non-normal impact.

We assumed that the effective velocity at impact angle θ is $V(\cos\theta)^j$, where V is the striking velocity. Figures 8 and 9 of Reference 1 indicate that j is at least 2 for $\theta \leq 30$ degrees. For bare Comp B there is an anomalous value at θ=8 degrees, while the critical velocity at θ=20 degrees is approximately 1.45 times the critical velocity at θ=0, which corresponds to a value of j of approximately 6. For convenience, we used j=2 and j=5 as limiting values.

We replaced V in the sensitivity equation by $V(\cos\theta)^j$, computed the corresponding critical mass $m(\theta)$ and the fraction $f(\theta)$ of the fragments that are supercritical. From geometric relationships we determined the range of θ and computed the average $\bar{f}$ of $f(\theta)$. The factor F_I is the ratio $\bar{f}/f_i(0)$ of the average to the value at impact angle θ=0. For typical projectiles the value of F_I was found to be approximately 0.4 for j=2 and 0.2 for j=5.

1.5 Probability of Detonation for a Given Spacing

We assume that the donor and receptor are parallel with center-to-center spacing S, the bases of the projectiles are in the same plane, and no shielding is between them. The probability P that the receptor will detonate (high-order) was computed from the following steps:

a. On a scaled drawing with the donor and receptor spaced S inches center-to-center lay off the dividing rays for polar zones of 10 degrees. Determine the polar zones in which fragments from the donor can strike the receptor. For each zone estimate the average outside diameter and case thickness and the fraction of the zone over which the vulnerable section of the receptor extends.

b. For each zone estimate the striking velocity from V_o and the $F_v(\varphi)$ factors; then compute the corresponding critical mass for normal impact.

c. Estimate the fraction of the striking fragments in each zone that have sufficient mass to produce detonation of the receptor charge. This quantity is the product of two factors. The first factor is the fraction of fragments that have mass exceeding the critical mass for normal impact. The second factor is the impact-angle factor F_I.

d. Estimate the total number of fragments in each zone. Use geometric probability to estimate the fraction of these fragments that strike the receptor.

e. Combine the results from c and d to obtain the expected number of fragments that strike the receptor and have sufficient mass and velocity to detonate the receptor.

f. Compute the probability that the receptor receives at least one supercritical hit. This is the probability P that explosive propagation will occur when the donor detonates at spacing S from the receptor.

1.6 Computation of the Required Spacing

The spacing S for a given probability P is obtained by solving the equations described in Section 1.5 for S when P is given. The solution is difficult to obtain directly. Iterative procedures have been developed for two important cases, while trial values and interpolation can be used in all cases. The procedures are described below.

a. Procedure for Large spacings

This procedure is based on the assumption that S is large enough that all fragments that can strike the receptor are in the central 10 degree zone. The assumption is valid for all the projectiles involved when P is small and is valid for projectiles larger than 155 mm when P=0.5.

At the large spacings for which the assumption is valid the air drag on the fragments decreases the striking velocity significantly. Except for this fact the relevant equations can be solved analytically for S in terms of P. Hence, S can be computed by an iteration that starts with the estimate S_1 obtained by ignoring the drag. Then S_1 can be used to estimate the drag for the second estimate, which usually is accurate to the nearest inch. Another iteration yields a very accurate estimate of S.

b. Procedure for Small Spacings

This procedure is based on the assumption that the receptor is close enough to the donor to subtend the entire polar zone over which supercritical fragments may issue, except for the base and nose fragments. Then the drag can be ignored and the spacing S can be computed by another iterative procedure. This procedure starts with an estimate S_1 that is obtained by using the average case thickness and outside diameter over the entire vulnerable section of the receptor for all polar zones. With the initial value S_1 estimates are made of the average case thickness and outside diameter for each zone, which yields a more accurate value S_2. Iteration is continued until a stable value is obtained.

c. Procedure for Intermediate Spacings

If neither of the above assumptions is found to be valid, the spacing S can be found by using trial values and linear interpolation until a value of S is obtained that yields the probability P by the method described in Section 1.5 above.

2. Description of Experimental Tests

2.1 General

Two types of tests were performed, the first being the primary tests to establish projectile separation distances over which an explosion would propagate 50 percent of the time, and the second being tests to obtain information on the fragmentation characteristics of the three projectile designs employed in the explosive propagation experiments. All of the experimental work was conducted by the Space Research Corporation (SRC), North Troy, Vermont under the supervision of ADL personnel.

2.2 Explosive Propagation Tests

Three series of tests were conducted to obtain data on the spacing which would result in a 50 percent probability of propagation of an explosion between the donor and receptor projectiles. Each series of tests was devoted to a different projectile design. That is, three different projectiles were employed, 81 mm, 105 mm, and 175 mm, all Comp B loaded.

The test arrangement was essentially the same for each series of tests. Three projectiles were used in each test; one, the donor, was placed between two receptors. They were placed side by side so that their longitudinal axes were parallel to the ground and their bases located all in the same plane. The projectiles were held at the same height above the ground by individual wooden supports. The spacing between the donor and each receptor was the same in each test but was varied from test to test according to a specific test design.

A number of possible test designs described in Reference 9 were carefully reviewed and a modification of the Kesten design, which is a variation of the Robbins-Monro design, was selected. In the Kesten design the spacing between projectiles is changed in the appropriate direction by a fixed amount until a straddle is obtained. The amount by which the spacing is changed is reduced each time a straddle is obtained, thereby generating a sequence of spacings converging to the 50 percent spacing.

We modified the Kesten design in two ways. First, we adjusted the procedure to account for the fact that two receptors are used in each trial, rather than the one receptor assumed in the Kesten design. Second, we changed the assumption of a normal distribution for the initial estimate of S, on which the Kesten design is based, to the more reasonable assumption that this estimate is lognormally distributed. We believe that the modified design is significantly better than the Kesten design, particularly in tests for which the initial estimate may contain a large error.

An initial estimate of the 50 percent spacing is used on the first trial. The spacing on a subsequent trial depends on the outcomes on the preceding trials. If no detonation is obtained on a trial, the spacing on the next trial is reduced by a fraction of the previous spacing. If two detonations are obtained, the spacing on the next trial is increased by a fractional amount. If one detonation is obtained, no change is made in the spacing.

The fraction that is used to change the spacing initially depends on a measure of the errors that are likely to occur in the initial estimate of the 50 percent spacing. This fractional change is used until a straddle or a match is obtained. A match is defined to be the outcome on a single trial in which one receptor detonates and the other receptor does not. A straddle is defined to be the outcome on two consecutive trials in which opposite results are obtained, that is, two detonations followed by no detonations, or conversely. At the first occurrence of a match or straddle, the fractional change is reduced to half the initial fraction; at the second occurrence it is reduced to one-third; etc.

In the conduct of the tests the detonation of the receptors was established by observing their condition after the test was completed. There were three primary cases observed: one in which no reaction of the explosive was observed (no detonation); the second in which reaction of the explosive was noted, but either or both unreacted explosive or very large fragments were observed (low-order detonation); or the third in which the projectile was completely fragmented and all of the explosive was consumed (high-order detonation). All projectiles that did not detonate (either high or low order) were photographed on the side exposed to fragments from the donor.

2.3 Results of Propagation Tests

It was necessary to make initial estimates of the 50 percent spacings to start the test procedure described above. These estimates were made from a preliminary model early in the development, since the test program could not start without them. The preliminary model did not contain the factor F_A for the effective area of irregularly shaped fragments, and the impact factor F_I was chosen before the analysis described in Section 1.4 had been made. For these and other reasons the initial estimates were much too large.

TABLE 1

SPACINGS FOR 50 PERCENT PROBABILITY OF DETONATION

	Spacings in Inches		
	81mm	105 mm	175 mm
Initial Estimates	24	38	155
Experimental Values	10.5	10.5	80.5

The initial estimates and the experimental values are listed in Table 1. Despite the fact that the initial estimates were much too large, the test procedure described in Section 2.2 converged rapidly towards the final values. For all three projectiles the test spacings had converged to values within about 10 percent of the final values in eight tests, and then made small oscillations during the remaining eight tests.

2.4 Fragmentation Tests

Two fragmentation tests were conducted with each of the projectile designs used in the propagation tests. The purpose of these tests was to obtain data on the spatial distribution of the fragments of the donor projectile. The number and size of the fragments projected in angular zones around the projectile were determined.

In each test the projectile was held with its long axis parallel to and about four feet above the ground. Plywood panels placed vertically in a semicircle around the projectile with a radius of from 10 to 35 feet (increasing with projectile size) were used to intercept the fragments projected by the projectile.

After each test the plywood panels were photographed and the photgraphs analyzed to provide data on the spatial distribution of the fragments.

3. Estimates of Required Spacings

3.1 Parameter Values

Average values of case thickness and outside diameter were obtained by measurement from the drawings listed in Reference 10. Additional measurements were made for particular spacings. Also, the length of the vulnerable section of the receptor and the total weight of metal fragments from the donor were obtained.

Two parameters that have a large effect on the estimates of spacings are F_A and F_I. The area factor F_A is the fraction of the average presented area of the irregularly shaped fragment that is effective in producing high order detonations. It was omitted in our initial computation of the 50 percent spacings, which is equivalent to using $F_A=1.0$. We have no data from which to estimate the value of F_A. Sensitivity tests with irregularly shaped fragments are needed for this purpose.

The impact-angle factor F_I accounts for non-normal impacts. It can be interpreted as the fraction of the area presented by the charge of the receptor to the fragment stream that is vulnerable to attack. The value of F_I is approximately 0.4 if the effective component of striking velocity varies as $(\cos\theta)^2$, where θ is the impact angle; and is approximately 0.2 if the effective component varies as $(\cos\theta)^5$. For composition B, values near 0.2 appear to be more likely for F_I than values near 0.4, from the meager data available on non-normal impacts.

3.2 Estimates of 50 Percent Spacings

Estimates of spacings required for P=0.50 and for P=0.02 for projectiles that are loaded with composition B explosive are listed in Table 2 in the order in which they were obtained. The original 50 percent spacings were made early in the development of the model, since they were needed to start the experimental tests. The value of $k_o = 5500$ used there applies to all fragments, whereas the value $k_o = 4500$ used in later computations yields a more accurate estimate of the average mass for those fragments that strike the receptor. As stated above in Section 3.1, the area factor F_A was omitted from the original model and added later in refining it.

The impact-angle factor $F_I = 0.4$ was chosen before the analysis of the effects of the impact angle was made. At that time it was little more than a guess, based on the estimate in Figure 34 of Reference 8, that the width of the effective strip for the 155 mm projectile is about two inches.

The experimental results listed in Table 2 were obtained by a procedure described in Section 2.2. Since the estimates from the experiments are much smaller than the original estimates from our model, the model was reexamined and some revisions were made. In addition to changing K_o to 4500 and F_I to 0.2, for reasons given above, the area factor F_A was introduced. The value $F_A = 0.75$ used in the revised parameters is a fortuitous guess that happened to yield estimates of S that are very close to the experimental values when used with the revised values of K_o and F_I.

The fitted parameter values, $F_A = 0.58$ and $F_I = 0.38$, were obtained by finding the values of F_A and F_I that would yield estimates of S = 10.5 inches for both the 81 mm and 105 mm projectiles, as had been obtained in the experimental tests. The corresponding value of 84 inches for the 175 mm projectile is close to the experimental value of 80.5 inches, although not as close as that obtained with the revised parameter values.

3.3 Comparison of 50 Percent Spacings

The experimental values listed in Table 2 are those obtained for the 50 percent spacing with composition B loaded projectiles by an efficient test design described in Section 2.2, using approximately 32 receptors for each of the three projectiles listed. The corresponding spacings that are obtained for composition B by computation from our model when the revised parameter values are used are almost equal to the experimentally determined values. Thus, the experimentally determined spacings are 10.5, 10.5, and 80.5 inches for 81 mm, 105 mm, and 175 mm projectiles respectively, while the computed spacings are 9.9, 11.1, and 80 inches respectively.

We have also examined experimental data reported in Reference 8 for the 155 mm (M107) projectile. In these tests the projectiles were mounted either vertically or horizontally on test stands. The results are reported in terms of the case-to-case separation distance, which is S-D in our notation. Hence, we add D, which is approximately 6 inches, to obtain the

corresponding center-to-center spacing. In the vertical orientation four of four receptors detonated (high-order) at S=30 inches, 3 of 4 at 54 inches, 2 of 4 at 78 inches, 0 of 12 at 90 inches, and 0 of 4 at 102 inches. In the horizontal orientation 1 of 2 detonated at 54 inches, 2 of 8 at 66 inches, and 0 of 2 at 78 inches.

Unfortunately there were insufficient experimental data to allow a reasonable statistical estimate to be made for the 50 percent spacing. Our model, however, using the revised parameter values, predicts a 50 percent spacing of approximately 42 inches. The experimental data for the 90 inch spacing does allow a limited statistical comparison to be made with model predictions. For the 0 out of 12 detonations a confidence interval on the true probability, p, for 95 percent confidence probability is, from the theory of Bernoulli trials used to obtain Figure 31 of Reference 8, $0<p\leq 0.27$. The probability of detonation at S=90 inches computed from the model described in Section 2 is p=0.14, which is approximately at the midpoint of the confidence interval. The estimated p falls within the confidence interval for all values of the confidence probability greater than 0.67.

A total of 12 detonations were obtained with the 38 receptors positioned at different spacings and orientations. Taking the spacings into account our model predicts 10 detonations for 38 receptors, which is in good agreement with the observed number.

3.4 Predicted Spacings for Small Probabilities

As indicated above, the spacings required for small probabilities of detonation can be predicted from the model described in Section 1. The accuracy of these predictions depends upon the validity of the model, particularly on the variation of the probability of detonation with the spacing.

The spacings required for 2 percent probability of detonation were computed by using the revised parameter values and by using the fitted parameter values. These estimates are listed in Table 2. For a given projectile the required spacing for 2 percent probability is much larger than that for 50 percent probability.

3.5 Some Limitations on the Model

More experimental data are needed to test the model before it can be used with confidence to predict required spacings for small probabilities of detonations. We have examined potential areas of uncertainty in our model in terms of its ability to accurately predict spacings for small probabilities.

Some possible sources of error are: (a) uncertainties concerning the parameter values, such as F_A and F_I; (b) validity of the empirical equations used in the derivation, such as the fragment distribution and the drag law; and (c) possible discrepancies between the conditions that existed in the propagation tests and the corresponding assumptions made in developing the model. These likely sources are discussed briefly below.

The model predicts that the expected number of supercritical hits decreases as the inverse square of the spacing from geometric considerations, and also decreases in a complex way from the decrease in striking velocity, as the spacing increases. We assumed the usual square drag law in computing the striking velocity. The corresponding effect on the expected number of supercritical hits depends on the variation of the required mass with striking velocity from the sensitivity equation, and the fragment mass distribution. The empirical equations involved here are open to question. The transformation of the sensitivity equation to make it applicable to irregularly shaped fragments needs to be checked. Also, the empirical distribution function for fragment mass is questionable, especially the tail of the distribution for large masses in the central 10 degree zone. We used the usual exponential distribution function for the probability that a fragment has mass exceeding m. This distribution appears to be good for small values of m, but not for large values of m. Since one dimension of a fragment is limited to the case thickness and the total amount of metal in the central 10 degree zone is limited, a distribution with an upper limit is more appropriate.

Another possible source of error is that some of the assumptions made in developing the model are not in agreement with the conditions that existed in the experiment. For example, the fragment distribution of the 155 mm projectile may have been distorted by the supports.

The ultimate objective of the experimental tests and model construction is to obtain a procedure for estimating separation distances for a given probability of explosive propagation under the conditions that exist in Load-Assembly-Pack (LAP) operations. If the conveyors that support the projectiles in LAP operations distort the fragment distributions and velocities, as appears likely, the distributions and velocities in our models should be modified accordingly when information on these effects becomes available.

REFERENCES

1. Slade, D.C. and Dewey, J., *High Order Initiation of Two Military Explosives by Projectile Impact,* BRL Report No. 1021, July 1957, UNCLASSIFIED

2. Rindner, R.M., *Response of Explosives to Fragment Impact,* Annals of New York Academy of Sciences, Vol 152 Art 1, Oct 28, 1968

3. McLean, D.G. and Allan, D.S., *An Experimental Program to Determine the Sensitivity of Explosive Materials to Impact by Regular Fragments,* Final Report to Picatinny Arsenal by Arthur D. Little, Inc., Contract DA-19-020-ORD-5617, Dec 26, 1965

4. Allan, D.S. and Meyers, S., *Development of a Weapons' Sensitivity Handbook (U),* Final Report (Phase I and II) to Department of Defense Explosives Safety Board by Arthur D. Little, Inc. Contract DAH-C04-70-C-0042, Feb 28, 1971

5. Gurney, R.W., *The Initial Velocities of Fragments from Bombs, Shells, and Grenades,* BRL Report No. 405, September 1943 UNCLASSIFIED

6. Heppner, L.D., *Fragmentation Test Design, Collection, Reduction and Analysis of Data,* APG Misc Report No. 306, September 1959, UNCLASSIFIED

7. Giere, A.C., *Calculating Fragment Penetration and Velocity Data for Use in Vulnerability Studies,* Naval Ordnance Report No. 6621, Oct 1, 1959, UNCLASSIFIED

8. Anderson, C. and Rindner, R., *Separation Distance Tests of 155 mm (M107) Projectiles,* Picatinny MTD Technical Report No. 4425, Jan 1973, UNCLASSIFIED

9. Rocketdyne Report R-6152, *The Design and Analysis of Sensitivity Experiments,* NASA CR-62026, May 1965, UNCLASSIFIED

10. Specification Drawings of Part No. 10543028 (81 mm M374 Projectile), Part No. 1053878 (105 mm MI projectile), Part No. 75-4-99 (155 mm M107 projectile), Part No. 10520195 (175 mm M437), and Part No. 10534911 (8 inch M106), UNCLASSIFIED

Table 2

Estimates of required spacings for projectiles with Comp B loading

No.	Conditions	P	81 mm	105 mm	155 mm	175 mm	8 in.
1	Original parameters	0.5	24	38	90	155	160
2	Experimental values	0.5	10.5	10.5	--	80.5	---
3	Revised parameters	0.5	9.9	11.1	41.5	80	73
4	Fitted parameters	0.5	10.5	10.5	--	84	---
5	Revised parameters	0.02	75	105	208	349	333
6	Fitted parameters	0.02	79	104	212	360	343

Original parameters: $K_o = 5500$, $F_A = 1.0$, $F_I = 0.4$

Revised parameters: $K_o = 4500$, $F_A = 0.75$, $F_I = 0.2$

Fitted parameters: $K_o = 4500$, $F_A = 0.58$, $F_I = 0.38$

HAZARDOUS WASTE DISPOSAL THROUGH FLUIDIZED BED INCINERATION

Joseph S. Santos
John J. Canavan

Facilities and Protective Technology Division
Manufacturing Technology Division
Picatinny Arsenal

ABSTRACT

Picatinny Arsenal has the responsibility for developing the technology and equipment necessary for the elimination of the pollutants generated by the Army's government owned, contractor operated (GOCO) plants manufacturing munitions. One of the major problems at all of these plants is the disposal of explosive and propellant waste material. The current method of "open burning" is unacceptable from safety and environmental aspects. Therefore, it was decided that incineration appeared to be the best approach to eliminate open burning. The feasibility of incinerating explosives in a water slurry was accomplished at Picatinny Arsenal. Concurrently, Radford Army Ammunition Plant evaluated an off-the-shelf rotary kiln incinerator. The nominal feed rate for these systems was 250 lb/hr of waste explosives and propellants. Typical wastes were TNT, Comp B, RDX and HMX explosives; single, double and triple base propellants. In addition to the incineration effort, the ancillary processes of grinding, slurry preparation and pumping, and injection techniques were fully demonstrated. To meet future requirements, an advanced incineration technique, the fluidized bed combustor, was selected for investigation. This system successfully demonstrated the disposal of explosives and propellants in a small scale pilot plant. During the course of this effort, a catalyst was found that reduced the NO_x concentration in the stack gas to virtually zero. In support of the incineration efforts, a pilot plant hazards analysis on the rotary kiln, an engineering development hazards analysis on the fluidized bed and detonation propagation tests on aqueous slurries of explosives and propellants have been accomplished.

INTRODUCTION

The U. S. Army is a major producer of munitions for the United States. In the course of the manufacturing and load assembly pack operations conducted at the GOCO plants throughout the United States, nonrecoverable and nonrecyclable waste propellants and explosives are accumulated. The current method of disposing of this waste is by open burning. Here the material is spread on concrete pads and remotely initiated. Stock piling of hazardous waste materials, air and water pollution, personnel exposure, and inefficiency characterize the problems associated with open burning and emphasize the need for a safe, reliable, pollution free alternative.

Controlled combustion is the most logical, technical solution, but little information of an engineering nature is available on this subject. Therefore, the objective of this study was to develop the necessary engineering technology for a total system (Fig 1) and to test and evaluate the systems, developed as pollution abatement vehicles, to eliminate the open burning disposal practice. Three incinerator designs, vertical induced draft, rotary kiln and fluidized bed were operated on a pilot and laboratory scale. The feasibility of this concept was shown by successfully destroying TNT, Composition B, RDX and HMX in the vertical induced draft unit. The rotary kiln incinerator was successfully piloted, at 250 lb/hr, and the results of the pilot plant effort were incorporated into a Design Criteria Package for implementation of a full scale (1350 lb/hr) complex. Studies on a laboratory scale fluidized bed incinerator were extremely interesting. The combustion of the explosives and propellants was rapid and a catalyst was uncovered that drastically reduced the NO_x in the exhaust gas. In addition to the incineration techniques, the ancillary processes of grinding, slurry preparation, pumping and injection were fully demonstrated. In the hazards analysis area, each system was analyzed for normal operations and for abnormal conditions or malfunctions. It was found that for normal operations there are no serious hazards. However, the addition of tramp metal, loss of water, poor housekeeping or operation could lower the safety margin to zero. Hazards analyses identified the potential hazards and operational procedures were then developed that minimized the hazards.

TECHNOLOGY DEVELOPMENT

Three incinerator designs, a vertical induced draft, rotary kiln, and fluidized bed were selected for investigative studies to determine their applicability to explosive and propellant waste disposal.

Vertical Incinerator

Initial work was accomplished in an existing vertical induced draft incinerator designed and built in 1957 for liquid explosive waste disposal (Fig 2). It is a cylindrical steel furnace lined with firebrick. Inside dimensions are 8 feet diameter and 30 feet high. The upper zone contains the oil burners and auxiliary equipment to produce the heat necessary to evaporate the water and bring the temperature of the solid explosive waste up to the ignition point. Introduction of the explosive waste occurs just under the oil burners. An induced draft fan, with a capacity of 10,000 cubic feet per minute, and a cyclone dust collector are the other main elements of the plant, with the combustion gases exiting via the flue to a 125 foot stack. The furnace is provided with 3 oil burners operating on #2 fuel oil supplied from a 7,500 gallon underground storage tank.

After the furnace is brought up to operating temperature, about 1500°F in the combustion zone, temperature may be controlled by the use of one or two burners as desired. The furnace generally operates under a negative pressure due to operation of the induced draft fan and the natural draft in the stack. About 30% of combustion air is taken in by induction with additional atomizing and combustion air provided by the controllable turbo-blower capable of furnishing 1150 cubic feet per minute maximum. Instrumentation and control equipment are provided for temperature control and automatic shut-down if incinerator equipment malfunction occurs. In addition, 10 explosion blow-out doors are provided as an additional safety measure.

This incinerator was modified to accept solid waste explosives in water slurries. Feasibility and safety requirements, particle size reduction, suspension, injection, combustion and baseline gaseous emission data were established and evaluated. The explosive was ground to a uniform particle size using a rubber-lined steel jar mill and bronze balls. Water was added to the explosive in the grinder in the ratio of 3:2 by weight, respectively. The resulting slurry was sieved through a 20 mesh screen and water added to achieve a water/explosive ratio of 6.7/1 prior to incineration for a disposal rate of 250 pounds per hour equivalent dry explosive. The feed system employed is depicted in Figure 3. Suspension was maintained by a pneumatic agitator and the slurry transferred into the incinerator through a water cooled injection tube. Two means of slurry transfer were evaluated: a steam ejector and a diaphragm pump, both of which performed satisfactorily. The end of the injection tube was equipped with a spray nozzle to disperse the slurry upward into the combustion chamber.

A summary of materials incinerated with the combustion conditions for the initial testing in the vertical induced draft incineration is shown in Figure 4. A total of 49 tests were completed with explosive slurries. Duration of tests ranged from thirty seconds to twenty minutes. Temperature and photographic data showed controlled, rapid combustion occurring in the injection and combustion zones with only an occasional flaming particle visible. An analysis of the exhaust gases emitted is shown in Figure 5. It is apparent that while the feasibility of the concept was proven, the environmental aspects still required some work. Visual observation indicated that the unsightly dense smoke associated with open burning was eliminated; however, small amounts of NO_x fumes were visible.

The instrumentation and control systems installed on the incinerator performed as required and resulted in the program being completed with no serious incidents. Preliminary hazards analyses identified the potential hazards and operational procedures were then developed that minimized the hazards. This includes the processes of grinding, pumping, injection and incineration of the explosive and propellant/water slurries.

Rotary Kiln Incinerator System

An important task in the overall program to develop an acceptable incineration system was to select an off-the-shelf unit and adapt it to meet immediate needs. The unit selected for this purpose was the rotary kiln incinerator. This system was designed for nominal feed rate of 250 lb/hr of propellant or explosive. It was installed and operated at Radford AAP concurrently with the vertical incinerator effort at Picatinny Arsenal.

The rotary kiln used (Fig 6) was approximately five feet in diameter and eight feet long. The cylinder is lined with alumina fire brick, which can withstand temperatures to 2400°F, and has a variable speed of 0-6 rpm. No. 2 fuel oil or butane can be used for the burner which fires countercurrent to the material and exhaust gas flow. The afterburner is a refractory lined cylinder located above and downstream of the incinerator. A precooler quenches the hot exhaust gases to 600°F prior to entrance into the wet scrubber. The marble bed scrubber washes out particles and water-soluble chemicals in the exhaust stream. The exhaust gases then pass through an induced draft fan and up the stack where they are characterized for CO, CO_2 NO, NO_2, SO_2, HC, H_2S and particulates.

The waste explosive or propellant was ground by a rotating knife grinder with water added. The resulting slurry is immediately discharged through an eight mesh screen in the bottom of the grinder to a slurry tank. Here the proper slurry ratio is maintained, transferred by centrifugal pump from the tank to the incinerator where a metering pump (peristaltic type) delivers the slurry to the combustion chamber. The unmetered slurry is returned to the storage tank at velocities high enough to maintain suspension integrity. Incineration tests have been successfully accomplished on single, double and composite base propellants, HMX, TNT, and RDX-based explosive compositions. Water to explosive ratios and feed rates were varied from 19:1 to 3:1 and from 40 to 440 pounds per hour respectively, with chamber temperatures varied from 1600-2000°F. A summary of materials tested is shown in Figure 7. Representative emission data for single and double base propellant-water slurries is shown in Figure 8. Propellant/water ratios were 1:3 by weight respectively, with a main burner temperature of 1400-1800°F. The results of the rotary kiln pilot plant effort were used to prepare a Design Criteria Package for implementation of a full scale incineration complex to meet the immediate needs of the Army Ammunition Plant at Radford, Virginia.

Hazard evaluation studies were made of the pilot-scale automated incinerator for assessing the initiation, flame transition, and explosive propagation hazard potential for incineration of propellants and the high explosives, TNT, HMX, RDX, and Composition B. The material preparation, grinding and feeding operational phases were assessed. The studies to date support strongly that the potential hazards associated with the incineration of propellant wastes are minimized by use of water as a coolant/diluent. Under normal operating conditions, quantitative hazards analyses of the drum dumpers, conveyor feed hopper, and transfer pumps show safety margins ranging from 1.1 to 4460. The low safety margin of 1.1 was found for impact and friction initiation stimuli applied to nitroglycerin films which are unlikely to be present. Similar analyses of abnormal events such as operator error, entry of hard foreign objects and absence of water coolant show safety margins ranging from none to 61.0. The absence of safety margins in some cases emphasizes the importance of maintaining operator reliability, safety interlocks, the assurance of continuous coolant supply, and good housekeeping in minimizing localized initiation of waste materials.

Normal grinding of propellant and explosive material < 0.1 inch to permit slurry suspension for fully dispersed pumping to the incinerator is shown to supply energy levels sufficiently high to induce initiation reactions in the combustibles. These initiations are kept localized by the continuous presence of water as a coolant at a ratio of 10:1 water: waste. In the abnormal situations of coolant supply failures or excessive grinder vibration, e.g., from broken blades, system safety is maintained by an interlock stopping the propellant feed to the grinder by interrupting power to the conveyor and valving-off sluicing water. The grinder was shown to present no critical shaft speed hazards at rotor unbalances up to ten percent.

Under normal agitation there is no metal-to-metal contact between impeller and suspension tank wall, and hence, no hazard from impact or friction initiation energy. Critical shaft speed analysis shows the design is fully adequate over the operating range to preclude any friction or impact hazard arising from shaft whip. Abnormal conditions arising from loss of the impeller or bending and set of the shaft can release sufficient energy to induce initiation in all combustibles to be incinerated. Again the presence of excess water coolant inhibits growth of the localized initiation into sustained burning. Material bypassing the grinder could permit inadvertent entry of foreign objects capable of damaging pumps and plugging flow lines; this entry should be avoided by screening all materials entering the agitation tank.

The Galligher Vac-Seal centrifugal pump used to transfer the propellant/water suspension poses no hazard in transfer of the dispersed combustibles to the incinerator kiln feed pump line under normal conditions, fully suspended in water. The Tri-Clover incinerator feed pump has adequate safety margins under normal conditions. An initiation hazard is introduced in the event this pump is run with dry Sprint propellant present.

Likewise, engineering hazard analyses have shown that the solid explosives and propellants can be processed safely in the present prototype incinerator. No transition from slow burning to an explosive reaction is predicted for 1:3 solids-to-water dispersions and expected settled material heights for explosive and/or propellant mixtures. Under normal operating conditions, these combustibles are fully suspended as a solids diluent system at a weight ratio of 1:3. This is assured by pumping at high enough rates to secure turbulent flow Reynolds numbers. In the

suspended condition, each combustible particle is well surrounded by copious water coolant which prevents any localized initiations from becoming self-sustaining by both heat sink action and thermal insulation effects.

Fluid Bed Incinerator

An advanced incineration technique investigated for future application was the fluidized bed combustor (Fig 9). The ultimate goal for this investigation is to convert the vertical induced draft incinerator to a fluidized bed system to fully demonstrate this technique.

The fluidized bed reactor concept is well-known and has been found to offer economic advantages for many chemical industrial reactions. Gas flows through the distributor plate and can be controlled to any desired rate. At low rates the bed remains in its original "settled" state with the pressure drop across the bed increasing with flow rate until it is equal to the downward force exerted by the solids resting on the plate. The bed begins to expand at this point which is called incipient fluidization, allowing more gas to pass through the bed at the same pressure drop. The bed is now fluidized and has all the properties of a fluid.

Application of this concept to incineration of propellants and explosives offers several advantages over conventional incineration. The violent agitation of the bed particles causes rapid mixing and acts as a large heat reservoir. Their movement throughout the bed keeps it at a constant temperature eliminating the development of hot zones in the bed. When a combustible particle is added to the bed, transfer of energy is rapid and the particle quickly reaches its ignition temperature. The heat of combustion is then rapidly transferred back to the bed. Contact between the burning particle and the oxygen in the gas is excellent reducing the excess air requirements. Combustion can be closely controlled by altering the hazardous waste residence time which is accomplished by increasing or decreasing the fluidizing gas flow. The bed particles can be of any material that will promote chemical or catalytic reactions. For clarification, the introduction of secondary air embraces a technique called two stage combustion. This concept requires that the total amount of air supplied be broken into two streams and introduced at two separate locations in the reactor. Less than stoichiometric primary air entered the fluid bed at the base of the reactor, and passed up through the distributor grid, while the secondary air entered the bed proper at a point above the distributor grid. This modification for meeting the air requirements of the incinerator had a very significant bearing on the emissions from the incineration process.

To exploit the above fluidized bed characteristics, a small scale unit was designed, constructed and tested* (see Fig 9). The diameter of the fluidized bed was six inches with an overall height of 10 feet constructed of a high temperature alloy. Bed material was tabular alumina (Al_2O_3) having a particle size of 500 microns. Combustion air was preheated and propane utilized as fuel. A peristaltic pump was employed to transfer the explosive slurry from a recirculating line to the combustor. A sampling train downstream of the cyclone particulate collector was used to record flue gas analysis for CO, CO_2, NO, NO_x, HC, and O_2. A summary of materials incinerated in water slurry form is shown in Figure 10. Average operating conditions were as follows: (1) a fluidized bed temperature of 1600-1800°F, (2) a settled bed height of two feet and a fluidized bed height of five feet, (3) an explosive feed slurry concentration of 10 weight percent, (4) a superficial bed velocity of three to six feet per second, and (5) theoretical air required to stoichiometrically combust fuel and explosive was varied from 90 to 120 percent.

During the course of the test program, a catalyst was uncovered that drastically reduced NO_x concentrations in the flue gas. It was extensively demonstrated that NO_x emissions could be driven to virtual extinction using the catalyst in the alumina bed while burning in a two-stage mode.

Figure 11 shows the results obtained in the combustion of a 10 weight percent TNT water slurry during one-stage and two-stage catalytic and non-catalytic combustion. Of particular interest is the progression that was evident in the exhaust gas analysis as the study progressed through the four combustion modes. The introduction of a catalyst in the single-stage mode had a detrimental effect on NO-NO_x emissions; however, when catalyst was used in conjunction with two-stage burning, a startling reduction in NO-NO_x, CO and HC concentrations was experienced. Present indications are that the reducing atmosphere created in the fluidized bed by two-stage combustion in conjunction with the catalyst accelerated the reaction of $2NO + 2CO \rightarrow 2CO_2 + N2$. NO_x emissions without the catalyst range from 1200 to 3500 ppm by volume depending upon the material incinerated in single-stage combustion. Reductions of NO_x emissions of fifty percent could be accomplished by employing the two-stage technique. Using two-stage combustion and the catalyst, representative emission data for explosive slurries were as follows: NO - 47 ppm, NO_x - 57 ppm, CO - 40 ppm, CO_2 - 12%, O_2 - 4% and hydrocarbons - 10 ppm.

*Esso Research & Engineering Company, Linden, New Jersey

In addition to these dramatic results, it was also shown that a soluble form of the catalyst could be transmitted to the combustor via the slurry tank and could be used to remotely activate the bed resulting in immediate NO_x reduction. This could prove invaluable as a means of overcoming any catalyst inhibition without interruption of operations.

To explore these important developments, the vertical induced draft incinerator at Picatinny Arsenal is being converted to a full-scale (eight feet diameter) fluidized bed unit. Figure 12 shows this conversion schematically, in which maximum use will be made of the existing system hardware. Major additions will encompass the compressor, air preheater, plenum chamber and cyclone separator. Revisions to exhaust piping, slurry injection and heat input from the oil burner will be made to effect the changeover to fluid bed operation.

To insure a safe system an engineering development hazards analysis is currently underway. Data available from the rotary kiln incinerator system processes will be used where applicable. In addition, detonation propagation tests of aqueous slurries of explosives and propellants are in progress. This effort was initiated to determine the maximum slurry concentrations, both in suspended and settled conditions, that would not support the propagation of a detonation wave, should one be initiated. Initial test results (Fig 13) indicate that slurries of TNT, Composition B, and M-9 propellant at concentrations of 30% (by weight of solids) and below will not support a detonation propagation. This effort has been expanded to include other explosives and propellants.

CONCLUSIONS

The explosive and propellant incineration program has shown that it was possible to safely and cleanly destroy waste explosive material under controlled thermal conditions. The rotary kiln incinerator with scrubbing of exhaust gases can be used to meet immediate needs but has attendant problems of scrubber water treatment. The fluid bed incinerator appears to be a superior system because:

a. NO_x emission levels significantly below 200 ppm can be achieved without scrubbing.

b. There are fewer moving parts, and no requirement for a pre-cooler or separate after burner.

c. Bed may be readily activated by inclusions of solid catalyst with the solid bed material or by addition of the catalyst in a soluble form in the slurry feed system.

In addition, ancillary procedures of particle size reduction, slurry preparation and transfer and injection have been positively demonstrated with no serious incidents. It is apparent that a safe solution to the problem of open burning waste hazardous materials is attainable.

REFERENCES

1. Santos, Heidelberger, Antman and Bhute, *Design Guide for Explosive Waste Incineration*, Manufacturing Technology Directorate, Picatinny Arsenal, Dover, New Jersey, Technical Report 4577, October 1973

2. Kalfadelis, C.D., *Development of a Fluidized Bed Incinerator for Explosives and Propellants*, Esso Research and Engineering Company, Government Research Laboratory, Linden, New Jersey October 1973

3. Petino, Westover, *Detonation Propagation Tests on Aqueous Slurries of TNT, Composition B, M-9 and M-10*, F & PTD, MTD, Picatinny Arsenal, Dover, New Jersey, Technical Report 4584, November 1973

4. Carter, *Hazards Evaluation of the Prototype Automated Waste Propellant Incineration System Report 3*, Hercules Incorporated, Radford Army Ammunition Plant, Radford, Virginia June 1973

5. Carter, *Hazards Evaluation Summary of the Prototype Automated Waste Propellant Incineration System*, Hercules Incorporated, Radford Army Ammunition Plant, Radford, Virginia, March 1973

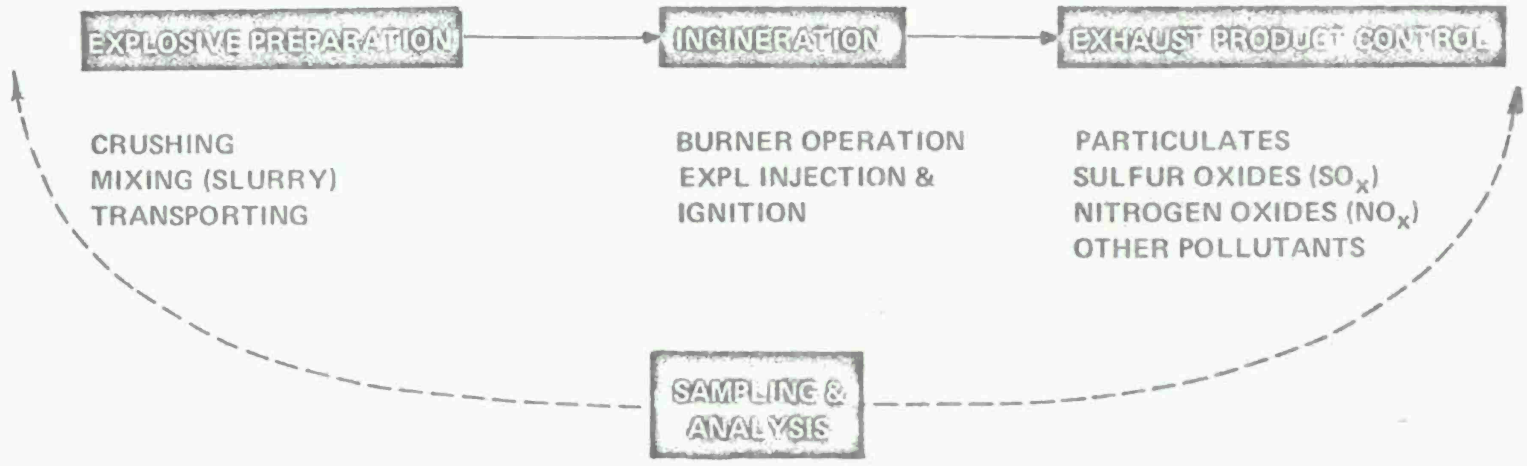

Fig 1 Explosive waste incineration as a system

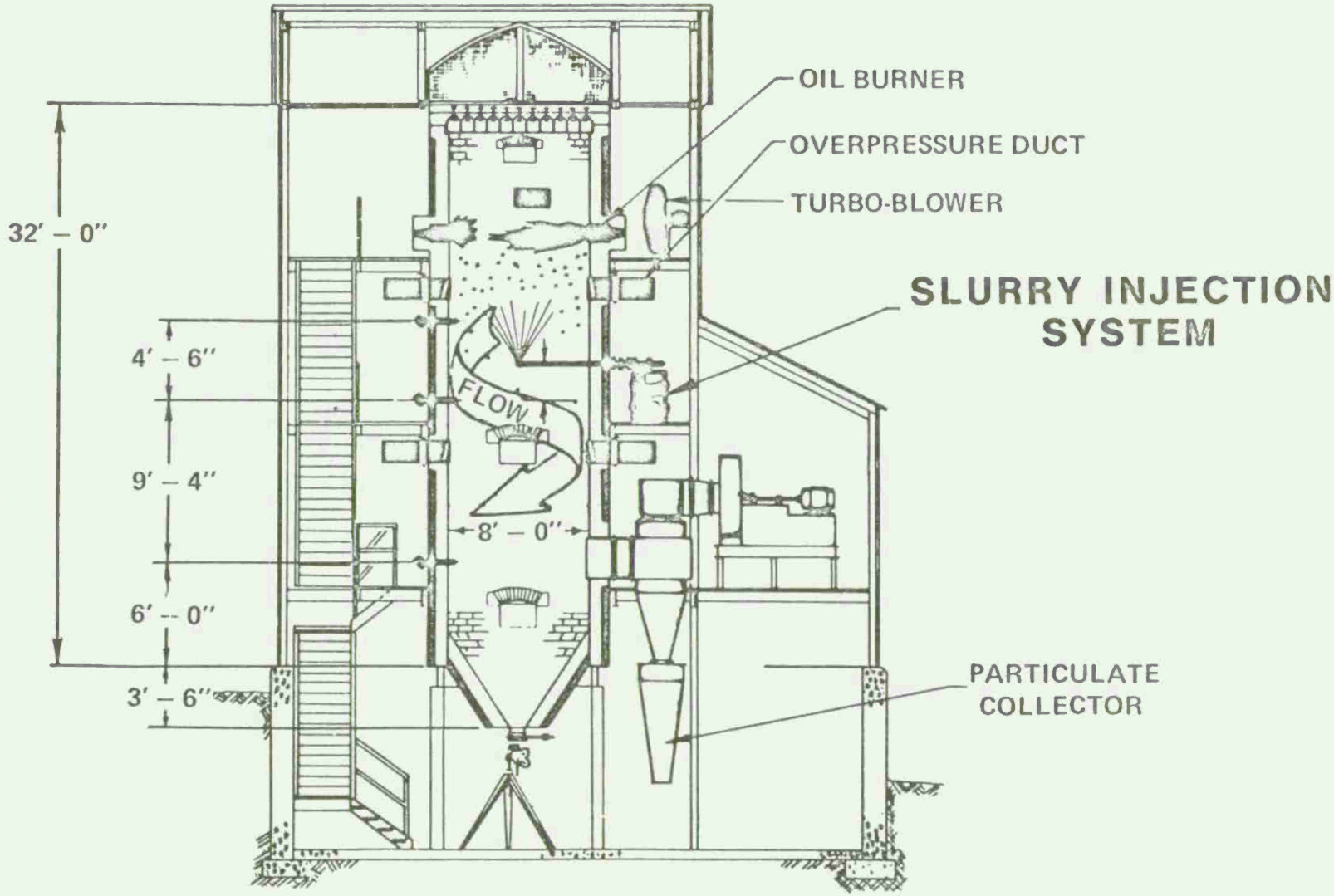

Fig 2 Picatinny Arsenal vertical induced draft incinerator

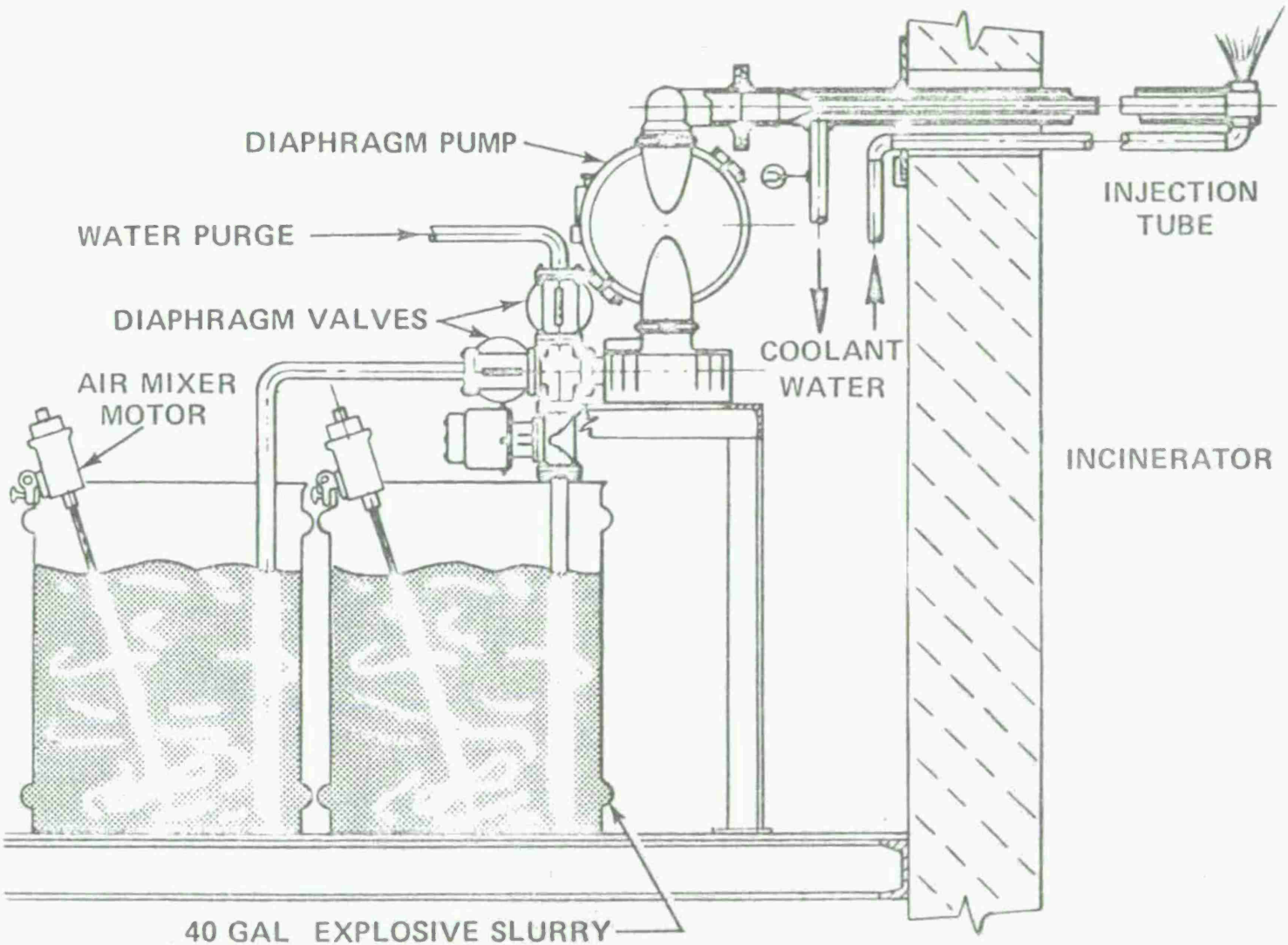

Fig 3 Explosive slurry pump feed system

VERTICAL INDUCED DRAFT INCINERATOR

NOMINAL OPERATING PARAMETERS

- BURNING RATE: 250 LB/HR
- DURATION: 21 MIN
- TEMPERATURE: 1600°F – 1800°F
- SLURRY RATIO: 19:1 ⟶ 7:1

MATERIAL	NO. TESTS	DURATION
TNT	20	2.5 HR
COMP B	19	2.6HR
HMX	6	3.5 MIN
RDX	4	2.0 MIN

Fig 4 Summary of incineration tests

MATERIAL	PARTICULATE 12%CO_2 GR/SCF	%CO_2	%O_2	%CO	NO_x (PPM)
BLANK	.0052	2.6	18.0	.001	33.8
TNT	.081	4.0	16.0	.0075	1110
COMP B	.10	3.4	16.6	.005	1030

Fig 5 Flue gas analysis vertical induced draft incinerator

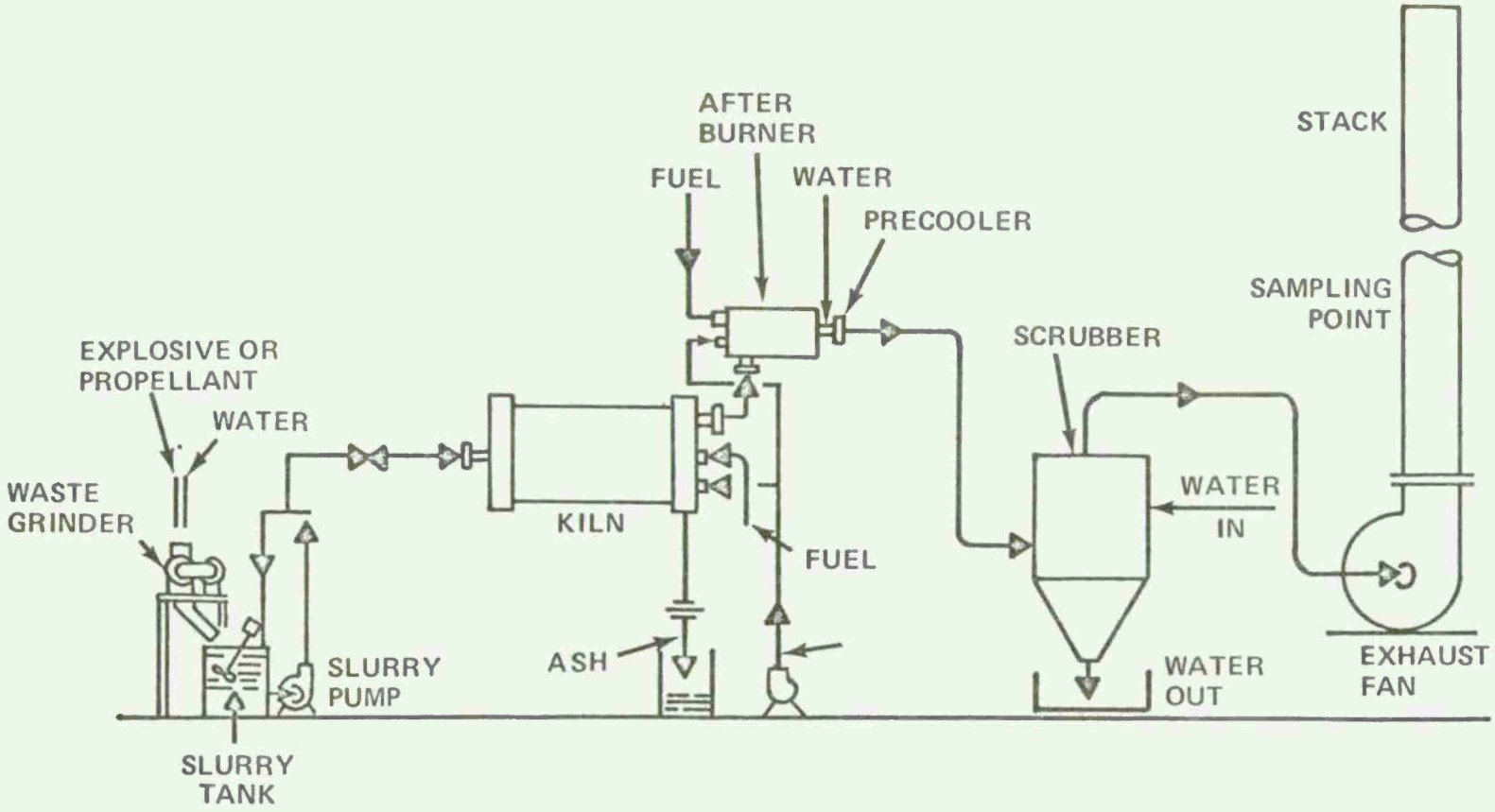

Fig 6 Rotary kiln incinerator

TYPE	LIQUID TO SOLID RATIO	FEED RATE (gpm)	NO. OF RUNS	TOTAL TIME (HRS)	TOTAL BURNED (LBS)
IMR	19:1 TO 3:1	1.78 - 2.0	>15	62.4	15600
IMR/EDB	19:1 TO 3:1	1.78 - 2.0	>50	180	45000
EDB	19:1 TO 5.6:1	1.78 - 2.0	>100	120	30000
M1 + INERT	5:8:1	1.78 - 2.0	1	0.88	220
M8	7:5:1	1.78 - 2.0	>4	0.80	200
M8/EDB	7:1 TO 5:1	1.78 - 2.0	3	3.4	855
TNT	12:1 TO 10:1	1.78 - 2.0	10	8.0	2000
2056D	4:1	1.78 - 2.0	3	1.0	250
HMX	10:1 TO 3:1	1.78 - 2.0	15	24.0	6000
COMP A5	3:1	1.78 - 2.0	13	18	4500
COMP B	3:1	1.78 - 2.0	13	18	4500
COMP C - 3	3:1	1.78 - 20	13	16	4500
BS - NACO	3:1	1.78 - 2.0	1	1.2	300
HOOIE/TOW GR.	3:1	1.78 - 2.0	2	0.4	75/25
M7 LAW STICK	3:1	1.78 - 2.0	1	1.2	300

Fig 7 Summary of rotary kiln incineration tests

TYPE	TEMP	HC	H_2S	GASES ANALYZED IN PPM NO	NO_2	SO_2	CO_2(%)
EDB–IMR	1400	26	32	265	0	6	1.2
	1600		35	208	11	2	1.5
	1600	43	0	198	0	268	2.8
	1800	21	65	205	0	15	2.0
	1400	0	13	146	24	71	2.1
	1600	5	20	190	9	3	2.5
	1800	8	32	101	10	123	2.8
	1500		8	91	0	7	2.1
	1600	0	5	110	4	8	2.6
EDM–IMR	1600	0	2	180	31	13	1.6

Fig 8 Rotary kiln incineration test results

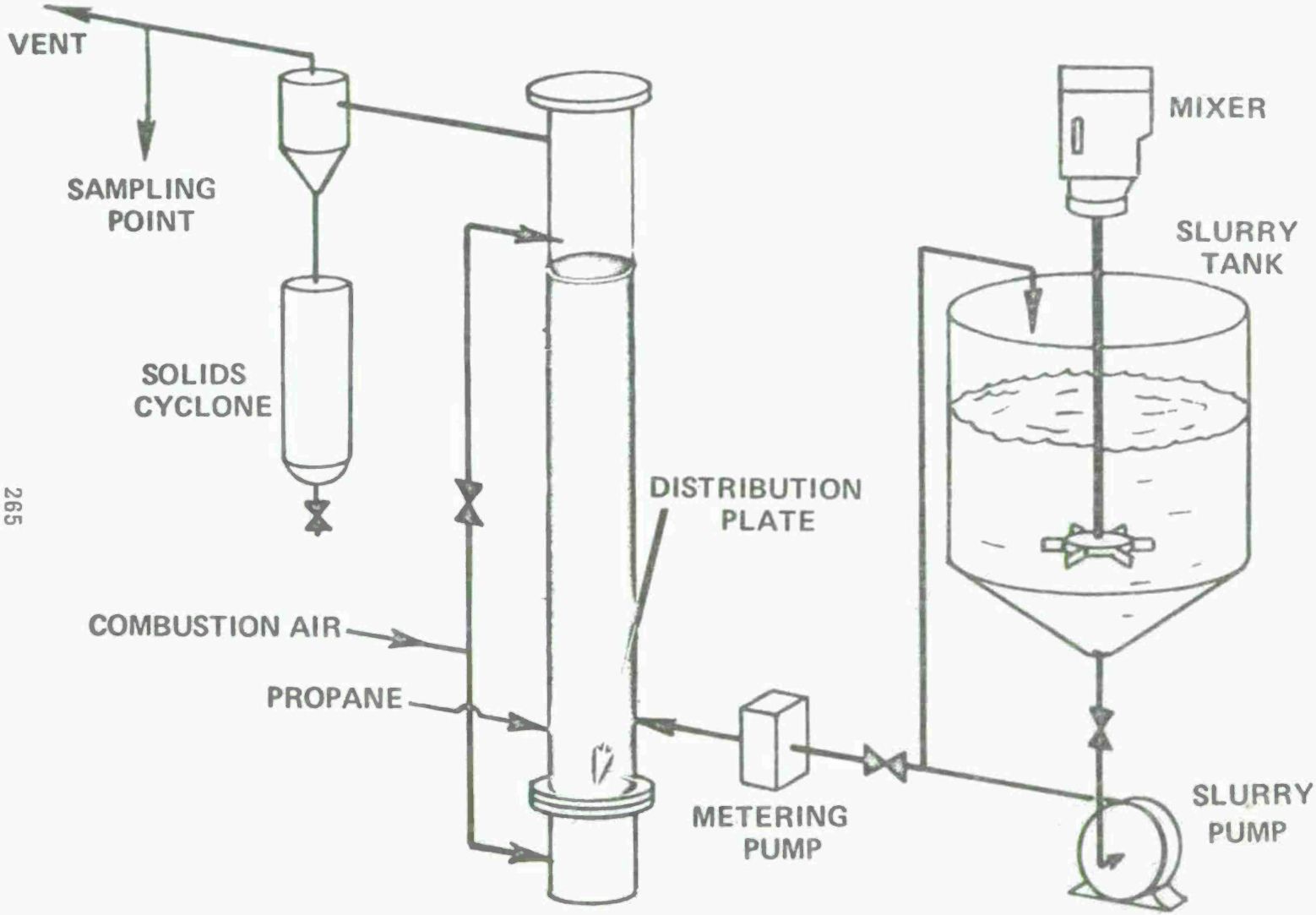

Fig 9 Lab scale fluidized bed combustor

MATERIAL	NO. OF TESTS	TOTAL DURATION (HRS)
TNT	16	60
COMP B	2	12
RDX	6	20
HMX	7	24
NH_4NO_3	1	6
HNO_3	1	6
CBI (98%NC)	4	22

Fig 10 Summary of fluidized bed test program

PARAMETERS:

- TEMPERATURE: 1600 - 1850°F
- FEED RATE: 7 lb/HR 10% TNT/WATER SLURRY
- VELOCITY: 4.8 - 5.5 FT/SEC
- THEORETICAL AIR: 1 STAGE 2 STAGE
  - PRIMARY 120% 63%
  - SECONDARY 57%

	CATALYTIC		NON CATALYTIC	
	1 STAGE	2 STAGE	1 STAGE	2 STAGE
NO (ppm)	2500	47	1650	800
NO_x(ppm)	2900	57	1750	840
CO (ppm)	250	40	640	650
HC (ppm)	100	10	290	350
CO_2%	12.1	12	12	12
O_2%	3.8	3.7	5.5	4.0

Fig 11 Fluidized bed combustion emission data

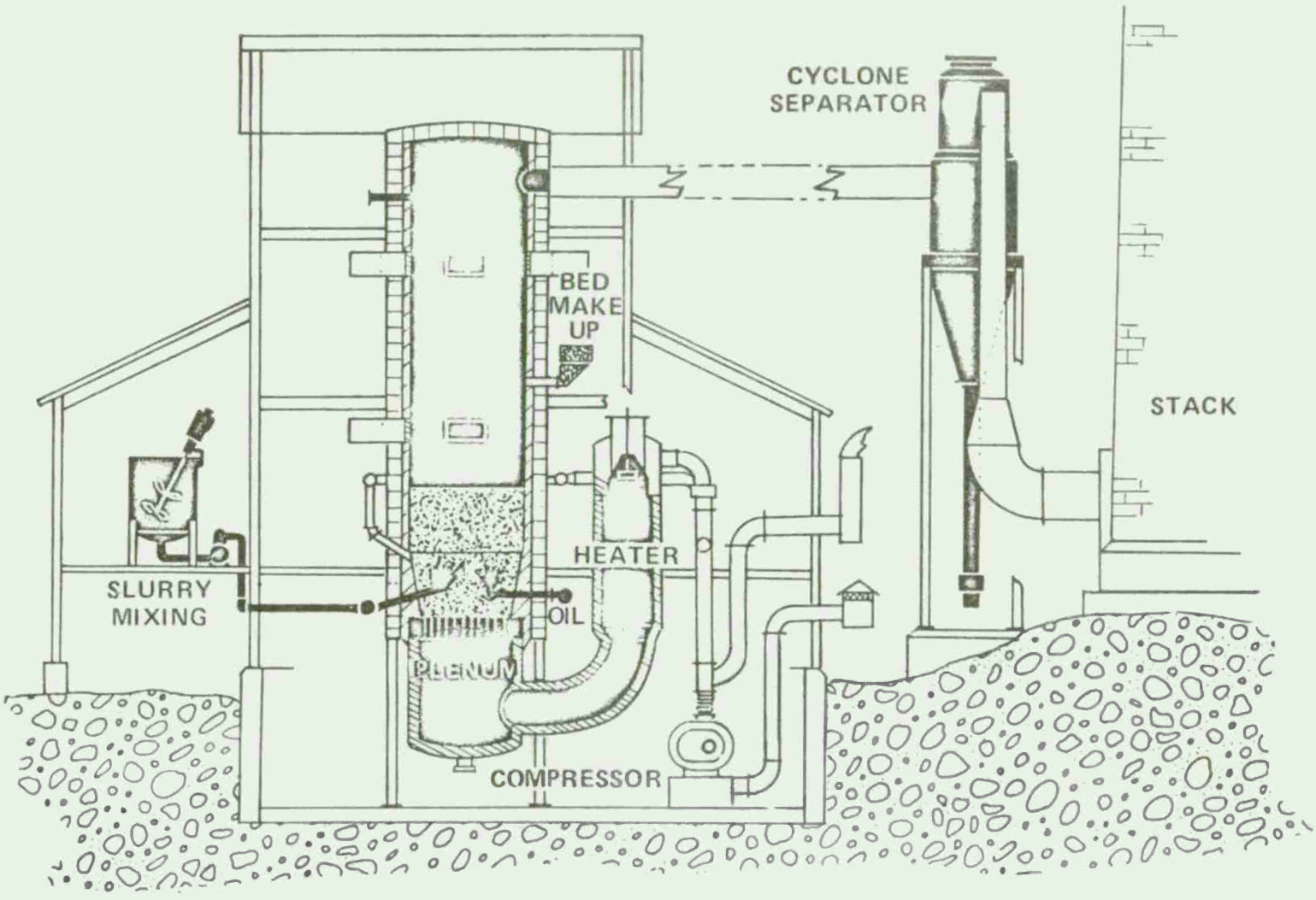

Fig 12 Fluidized bed conversion of PA incinerator

MATERIAL	SLURRY	CONCENTRATION (WT %) PROPAGATION NONE	HIGH ORDER
TNT	GELLED	30–40	60
TNT	SETTLED	40	55–60
COMP B	GELLED	30	40
COMP B	SETTLED	30–35	45–50
M–9	GELLED	20–40	50
M–9	SETTLED	35–40	50
M–10	GELLED	50	70*
M–10	SETTLED	10–12.5	15–35

* LOW ORDER

Fig 13 Summary of detonation propagation tests

DISTRIBUTION LIST

	Copy No.
Commander Picatinny Arsenal ATTN: SARPA-CO	1
SARPA-MT; MT-C; MT-M; MT-T	2-5
SARPA-MT-F	6-18
SARPA-S	19
SARPA-TS-S Dover, New Jersey 07801	20-24
Chairman Department of Defense Explosive Safety Board Forrestal Building, GB-270 Washington, D. C. 20314	25
Administrator Defense Documentation Center ATTN: Accessions Division Cameron Station Alexandria, Virginia 22314	26-37
Commander Department of the Army Office, Chief Research, Development & Acquisition ATTN: DAMA-CSM-P Washington, D. C. 20310	38
Office, Chief of Engineers ATTN: DAEN-MCZ Washington, D. C. 20314	39
Commander U. S. Army Materiel Command ATTN: AMCSF	40
AMCRD	41
AMCRP	42
AMCIS 5001 Eisenhower Avenue Alexandria, Virginia 22333	43

Commander
USAMC Installations & Services Agency
ATTN: AMCIS-RI 44
Rock Island, Illinois 61201

Commander
U. S. Army Procurement Equipment Agency
ATTN: AMX-PE-MT 45
Rock Island, Illinois 61201

Project Manager for Munition Production Base
Modernization and Expansion-USAMC
ATTN: AMCPM-PBM 46
AMCPM-PBM-S 47
AMCPM-PBM-L 48
Dover, New Jersey 07801

Commander
U. S. Army Armament Command
ATTN: AMSAR-SF 49
AMSAR-SC 50
AMSAR-EN 51
AMSAR-PPI 52
AMSAR-RD 53
AMSAR-IS 54
AMSAR-ASF 55
Rock Island, Illinois 61201

Commander
Edgewood Arsenal
ATTN: SAREA-TD 56
SAREA-MTD 57
Aberdeen Proving Grounds, Maryland 21010

Commander
Frankford Arsenal
ATTN: SARFA-T 58
Philadelphia, Pennsylvania 19137

Commander
U. S. Army Engineer Division
ATTN: HNDED 59
P.O. Box 1600-West Station
Huntsville, Alabama 35809

District Engineer
U. S. Army Engineering District, Ft. Worth
Corps of Engineers
P.O. Box 17300
Fort Worth, Texas 76102 60

District Engineer
U. S. Army Engineering District, Mobile
Corps of Engineers
P.O. Box 2288
Mobile, Alabama 36628 61

District Engineer
U. S. Army Engineering District, Omaha
Corps of Engineers, 6014 US PO & Courthouse
215 N. 17th Street
Omaha, Nebraska 68102 62

District Engineer
U. S. Army Engineering District, Baltimore
Corps of Engineers
P.O. Box 1715
Baltimore, Maryland 21203 63

District Engineers
U. S. Army Engineering District, Norfolk
Corps of Engineers
803 Front Street
Norfolk, Virginia 23510 64